

**Colony stimulating factor 1 receptor (CSF1R) blockade of microglia reactivity in
the light-damage model of retinal degeneration**

Inaugural Dissertation

zur

Erlangung des Doktorgrades

Dr. nat. med.

der Medizinischen Fakultät

und

der Mathematisch-Naturwissenschaftlichen Fakultät

der Universität zu Köln

vorgelegt von

Nils Laudenberg

aus Köln

Hundt Druck, Köln

Köln 2023

Betreuer/Betreuerin: Prof. Dr. Thomas Langmann

Referent/Referentin: Prof. Dr. Elena Rugarli
Prof. Dr. Christian Pallasch

Datum der mündlichen Prüfung: 12.09.2023

"Would you tell me, please, which way I ought to go from here?"

"That depends a good deal on where you want to get to."

Lewis Carroll

Table of contents

Summary	IV
Zusammenfassung	V
List of figures	VII
List of tables	IX
List of abbreviations	IX
1. Introduction	1
1.1 The mammalian retina.....	1
1.2 Age-related macular degeneration.....	3
1.2.1 Age-related macular degeneration associated risk factors.....	4
1.3 Microglia – the resident immune cells of the retina.....	6
1.3.1 Origin and self-maintenance of microglia.....	6
1.3.2 Role of microglia in the developing and adult retina.....	7
1.3.3 Microglia in the retina under disease condition.....	9
1.3.4 Light damage model mimics features of AMD in rodents.....	10
1.3.5 Microglia depletion as therapeutic strategy in neurodegenerative diseases.....	11
1.4 Colony stimulating factor 1 receptor signaling pathways.....	13
1.4.1 Colony stimulating factor 1 receptor structure and its ligands.....	14
1.4.2 Early phosphorylation events in signal transduction of CSF1R.....	14
1.4.3 Downstream signaling pathways of CSF1R.....	15
1.5 Microglia depletion.....	17
1.5.1 Conditional genetic depletion of microglia.....	18
1.5.2 Pharmacological depletion of microglia.....	18
1.6 Microglia repopulation.....	20
1.7 Aims of the study.....	21
2. Material and Methods	22
2.1 Cell culture.....	22
2.1.1 Maintaining and subculturing of cell lines.....	22
2.1.2 PLX3397 stimulation.....	22
2.1.3 Cell viability assay.....	23
2.1.4 Cell death assay.....	23
2.1.5 Morphological analysis.....	24
2.2 Mouse experiments.....	24
2.2.1 Mouse husbandry.....	24
2.2.2 Mouse strain.....	24

2.2.3 PLX3397 administration.....	25
2.2.4 Light exposure regime.....	25
2.2.5 Experimental setup.....	25
2.2.6 <i>In vivo</i> imaging.....	28
2.3 Molecular biology.....	28
2.3.1 Genotyping.....	28
2.3.2 Quantification of PLX3397 in the retina.....	30
2.3.3 Immunohistochemistry.....	31
2.3.4 Cell death detection assay.....	31
2.3.5 RNA isolation, cDNA synthesis, and qRT-PCR.....	31
2.4 Data analysis.....	33
2.4.1 Image analysis.....	33
2.4.2 Statistical analysis.....	34
2.5 Chemicals, buffers, kits, devices, and software.....	34
3. Results.....	38
3.1 Potency of PLX3397 in different cell lines.....	38
3.1.1 PLX3397 treatment reduces the metabolic activity in different cell lines.....	38
3.1.2 PLX3397 treatment increases death rate in different cell lines.....	39
3.1.3 PLX3397 treatment leads to an altered morphology in different cell lines.....	40
3.2 PLX3397 can be detected in the retina after oral administration.....	44
3.3 Effect of preventive microglia depletion in the light damaged retina.....	45
3.3.1 Preventive PLX3397 treatment does not affect the extend of retinal degeneration.....	45
3.3.2 Absence of microglia triggers astrocytic and Müller cell reactivity...	47
3.3.3 Absence of microglia cannot prevent photoreceptor cell death.....	50
3.3.4 Absence of microglia increase the amount of TUNEL ⁺ cells.....	51
3.3.5 PLX3397 prevents the expression of pro-inflammatory markers....	52
3.4 The nature of retinal microglia repopulation.....	54
3.4.1 Microglia repopulate after 7 days with a few changes in morphology.....	54
3.4.2 Repopulated microglia show altered pro-inflammatory marker expression.....	55
3.5 Progression of retinal degeneration after low intensity light exposure.....	59
3.5.1 Retinal degeneration reaches its maximum 7 days after light exposure.....	59

3.5.2	Reactivated microglia recover after retinal degeneration has reached its peak.....	59
3.5.3	Pro-inflammatory marker expression progressively declines, after retinal degeneration peaks.....	60
3.6	Effect of curative microglia depletion in the light damaged retina.....	65
3.6.1	The timing of microglia depletion has no effect on the extent of retinal degeneration.....	65
3.6.2	Repopulated microglia are reactivated by a damaged environment.....	67
3.6.3	Microglia that removed all cell debris undergo re-ramification and return to the plexiform layers.....	68
3.6.4	Curative microglia depletion and repopulation cannot prevent photoreceptor cell death.....	68
3.6.5	Curative microglia depletion and repopulation triggers astrocytic and Müller cell reactivity.....	72
3.6.6	Repopulated microglia show increased pro-inflammatory marker expression.....	73
3.7	Effects of microglia depletion in a model of acute retinal degeneration.....	75
4.	Discussion.....	76
4.1	PLX3397 allows specific and rapid depletion of microglia populations.....	76
4.2	Microglia show content dependent and region-specific responses.....	78
4.3	Astrocytes might contribute to retinal degeneration.....	80
4.4	Müller cells might contribute to retinal degeneration.....	81
4.5	Microglia develop tolerance to repeated or persistent inflammatory stimuli...	81
4.6	Microenvironment influences the response of repopulated microglia to stimuli.....	82
4.7	Microglia depletion does not reduce the extend of light-induced retinal degeneration.....	85
5.	Conclusion.....	87
6.	References.....	88
7.	Attachments.....	108
8.	Acknowledgements.....	117
9.	Eidesstattliche Erklärung.....	118
10.	Curriculum Vitae.....	119

Summary

Reactive microglia are commonly present in retinal degenerative diseases. They can secrete neurotoxic substances, which contribute to photoreceptor cell death, and cause vision loss in the elderly. However, as a fundamental part of the regulatory immune system they also possess supportive effects. In this present study, we aimed at studying the effects of complete microglia depletion and repopulation in a mouse model of acute retinal degeneration that mimics some features of dry AMD using the CSF1R-antagonist PLX3397. Here, we want to elucidate, whether the absence of microglia or repopulated microglia associated with being unprimed would reduce the extend of retinal degeneration. *CX3CR1^{GFP/+}* reporter mice that carried the light sensitive RPE65 Leu450 variant received PLX3397 or control diet prior or after white light-exposure to induce retinal degeneration. Microglia were efficiently depleted with PLX3397 under normal and light damage conditions. We demonstrated microglia depletion could stop excessive pro-inflammatory marker expression. However, the extent of retinal degeneration could not be reduced when microglia were absent. In this condition, PLX3397 treatment failed to reduce the rate of photoreceptor loss. Here, we showed that dead cell debris remained in the ONL when microglia where depleted because they were unable to be phagocytosed. Furthermore, the absence of microglia increased the expression of GFAP and genes linked to Müller cells and astrocytes reactivity, like *Ccl2* and *Il-6*. Discontinuation of PLX3397 resulted in rapid renewal of microglia. We demonstrated that the reactivity of newly repopulated microglia could not be dampened in any case. Microglia were instantly reactivated, assumed an amoeboid shape, and migrated into the nuclear layers as they repopulated in an already damaged environment, which was combined with an increased expression of pro-inflammatory markers. In addition, increased astrocyte and Müller cell reactivity was also associated with the newly repopulated microglia. Our study demonstrated that the model of light-induced retinal degeneration does not benefit from microglia depletion and repopulation. In fact, the opposite was true, as the loss of positive effects outweighs the negative effects. Since photoreceptors are on the verge between function and cell survival and dysfunction and death, literally any defect could shift them toward cell death. We assume that one strategy by which microglia might prolong photoreceptor survival is the clearing of dead photoreceptors to prevent bystander cell damage. We demonstrated that astrocytes and Müller cells are likely to become reactive when microglia are absent and contribute to photoreceptor cell death. However, they were unable to constitute for the microglia's phagocytic activity, which was reflected in increased numbers of TUNEL⁺ cells. Our findings imply that the development of the pro-inflammatory phenotype of microglia in the condition of retinal degeneration was influenced by the microenvironment. We conclude that the microenvironmental impacts of degenerative diseases are likely to have an impact on the repopulation of microglia in a way that restores their initial over-reactive phenotype.

Zusammenfassung

Überreaktive Mikroglia sind bei degenerativen Erkrankungen der Netzhaut häufig anzutreffen. Sie können neurotoxische Substanzen ausschütten, zum Absterben der Fotorezeptorzellen beitragen und bei älteren Menschen häufig zur Blindheit führen. Als wichtiger Bestandteil des Immunsystems haben sie jedoch auch unterstützende Effekte. In dieser Studie haben wir die Auswirkungen einer vollständigen Depletion und Repopulation der Mikroglia in einem Mausmodell der akuten Netzhautdegeneration untersucht, dass einige Merkmale der trockenen AMD aufweist. Depletiert wurden die Mikroglia durch den CSF1R-Antagonisten PLX3397. Wir wollten herausfinden, ob das Fehlen oder die Repopulation der Mikroglia, die mit einem nicht reaktiven Phänotyp assoziiert ist, das Ausmaß der Netzhautdegeneration verringern könnte. *CX3CR1^{GFP/+}* Reportermäuse, die die lichtempfindliche RPE65 Leu450 Variante trugen, erhielten PLX3397 oder eine Kontrolldiät vor oder nach Licht-Exposition. Die Licht-Exposition wurde durchgeführt um eine retinale Degeneration zu verursachen. Die Mikroglia wurden durch PLX3397 sowohl unter normalen als auch unter lichtgeschädigten Bedingungen depletiert. Wir konnten nachweisen, dass eine Depletion der Mikroglia eine übermäßige Expression von pro-inflammatorischen Markern stoppen konnte. Das Ausmaß der Netzhautdegeneration wurde in Abwesenheit der Mikroglia jedoch nicht verringert. Auch konnte eine PLX3397 Behandlung die Zahl der toten Fotorezeptoren nicht reduzieren. Hier konnten wir zeigen, dass tote Zellreste in der ONL zurückblieben, wenn Mikroglia abwesend waren, da keine Phagozytose stattfinden konnte. Darüber hinaus erhöhte das Fehlen der Mikroglia die Expression von GFAP und Genen, die mit der Aktivität von Astrozyten bzw. Müllerzellen in Verbindung stehen, wie *Ccl2* und *Il-6*. Das Absetzen von PLX3397 führte zu einer schnellen Repopulation der Mikroglia. Wir konnten zeigen, dass die Reaktivität der neu repopulierten Mikroglia in keinem Fall gedämpft werden konnte. Sie wurden sofort reaktiviert, nahmen eine amöboide Form an und wanderten in die nukleären Schichten ein, da sie sich in einem bereits geschädigten Milieu neu ansiedelten, was mit einer erhöhten Expression pro-inflammatorischer Marker einherging. Zusätzlich wurde eine erhöhte Astrozyten und Müllerzellen Reaktivität mit repopulierten Mikroglia assoziiert. Unserer Studie hat gezeigt, dass das Modell der lichtinduzierten Netzhautdegeneration nicht von der Depletion und Repopulation der Mikroglia profitierte. Das Gegenteil war der Fall, denn der Verlust an positiven Effekten überwiegt den der negativen Effekte. Da sich Fotorezeptoren an der Schwelle zwischen Funktion und Überleben und Dysfunktion und Tod befinden, könnte jeder Defekt sie in Richtung Zelltod leiten. Wir gehen davon aus, dass eine Strategie, mit der Mikroglia das Überleben von Fotorezeptoren verlängern könnten, darin besteht, tote Fotorezeptoren zu beseitigen, um Schäden an Zellen in der näheren Umgebung zu verhindern. Wir konnten nachweisen, dass Astrozyten und Müllerzellen in Abwesenheit von Mikroglia reaktiv werden und zum Tod von Fotorezeptoren beitragen könnten. Sie waren jedoch nicht in

der Lage, die phagozytotische Aktivität der Mikroglia zu kompensieren, was sich in einer erhöhten Anzahl an TUNEL⁺ Zellen zeigte. Unsere Ergebnisse deuten darauf hin, dass die Entwicklung des pro-inflammatorischen Phänotyps der Mikroglia in einem degenerativen Milieu durch die Mikroumgebung beeinflusst wird. Wir kommen zu dem Schluss, dass die Auswirkungen degenerativer Erkrankungen auf die Mikroumgebung, die Repopulation der Mikroglia in einer Weise beeinflusst, die ihren ursprünglich überreaktiven Phänotypen wiederherstellen.

List of figures

Figure 1: Anatomy of the human eye and retina.....	2
Figure 2: Clinical stages, signs and symptoms of AMD.....	5
Figure 3: Microglia location and morphology in healthy and diseased retinas.....	10
Figure 4: Schematic overview of microglia activation in retinal degenerative diseases...	12
Figure 5: CSF1R structure and signaling.....	17
Figure 6: Effects of PLX3397 in different cell lines on morphology and viability.....	23
Figure 7: PLX3397 concentration determination.....	26
Figure 8: Preventive microglia depletion in the light damage model of retinal degeneration.....	26
Figure 9: Documentation of retinal microglia repopulation.....	27
Figure 10: Development of retinal degeneration in a low light exposure regime.....	27
Figure 11: Curative microglia depletion in a low light exposure regime.....	28
Figure 12: Identification points of the analyzed morphological parameters.....	33
Figure 13: Effect of PLX3397 on metabolic activity in different cell lines.....	39
Figure 14: Effect of PLX3397 on cell death rate in different cell lines.....	40
Figure 15: Effect of PLX3397 on morphology in BV-2 cells.....	42
Figure 16: Effect of PLX3397 on morphology in 661W cells.....	43
Figure 17: Effect of PLX3397 on morphology in HEK293 cells.....	44
Figure 18: LC-MS determination of PLX3397 in the retina.....	46
Figure 19: SD-OCT analysis on the effect of preventive microglia depletion on retinal degeneration.....	48
Figure 20: Cryosection analysis on the effect of preventive microglia depletion on retinal degeneration.....	49
Figure 21: Flat mount analysis on the effect of preventive microglia depletion on retinal degeneration.....	49
Figure 22: GFAP staining analysis in the context of preventive microglia depletion in retinal degeneration.....	50
Figure 23: Cone arrestin staining analysis in the context of preventive microglia depletion in retinal degeneration.....	51
Figure 24: TUNEL staining analysis in the context of preventive microglia depletion in retinal degeneration.....	52
Figure 25: Pro-inflammatory marker expression in the context of preventive microglia depletion in retinal degeneration.....	53
Figure 26: Investigation of microglia repopulation in retinal flat mounts.....	56
Figure 27: Investigation of microglia repopulation in retinal cryosections.....	57

Figure 28: Investigation of pro- and anti-inflammatory marker expression in repopulated microglia.....	58
Figure 29: SD-OCT analysis of retinal degeneration after low intensity light exposure...	61
Figure 30: Investigation of microglia morphology after low light intensity light exposure in retinal flat mounts.....	62
Figure 31: Investigation of microglia location after low intensity light exposure in retinal cryosections.....	63
Figure 32: Investigation of pro- and anti-inflammatory markers after low intensity light exposure.....	64
Figure 33: SD-OCT analysis on the effect of curative microglia depletion on retinal degeneration.....	66
Figure 34: Investigation of microglia morphology in a curative setting of early, late, and no microglia depletion on retinal degeneration.....	69
Figure 35: Investigation of microglia location in a curative setting of early, late, and no microglia depletion on retinal degeneration.....	70
Figure 36: TUNEL staining analysis in a curative setting of early, late, and no microglia depletion on retinal degeneration.....	71
Figure 37: Cone arrestin staining analysis in a curative setting of early, late, and no microglia depletion on retinal degeneration.....	71
Figure 38: GFAP staining analysis in a curative setting of early, late, and no microglia depletion on retinal degeneration.....	72
Figure 39: Investigation of pro- and anti-inflammatory markers in a curative setting of early, late, and no microglia depletion.....	74
Supplementary figure 1: Pro-inflammatory marker expression the context of preventive microglia depletion in retinal degeneration.....	108
Supplementary figure 2: Investigation of microglia repopulation in retinal flat-mounts...	109
Supplementary figure 3: Investigation of microglia repopulation in retinal flat-mounts...	110
Supplementary figure 4: Investigation of pro- and anti-inflammatory marker expression in repopulated microglia.....	111
Supplementary figure 5: Investigation of microglia morphology after low intensity light exposure in retinal flat mounts.....	112
Supplementary figure 6: Investigation of microglia morphology after low intensity light exposure in retinal flat mounts.....	113
Supplementary figure 7: Investigation of microglia morphology in a curative setting of early, late and no depletion on retinal degeneration.....	114
Supplementary figure 8: Investigation of microglia morphology in a curative setting of early, late and no depletion on retinal degeneration.....	115

Supplementary figure 9: Investigation of pro- and anti-inflammatory markers in a curative setting of early, late and no depletion on retinal degeneration.....	116
--	-----

List of tables

Table 1: List of genotyping primer used in this study.....	29
Table 2: List of genotyping PCR programs used in this study.....	30
Table 3: List of antibodies used for immunohistochemistry.....	31
Table 4: List of SYBR® Green qRT-PCR primer used in this study.....	32
Table 5: qRT-PCR program used in this study.....	32
Table 6: List of chemicals and reagents used in this study.....	34
Table 7: List of buffers and solutions used in this study.....	35
Table 8: List of kits used in this study.....	36
Table 9: List of devices used in this study.....	36
Table 10: List of software used in this study.....	37

List of abbreviations

A2E	N-retinylidene-N-retinylethanolamine
Abi	Actin-binding and interacting protein
AD	Alzheimer's disease
AIF-1	Allograft inflammatory factor 1
AL	Activation loop
AMD	Age related macular degeneration
AP-1	Activator protein 1
ARMS2	Age-related maculopathy susceptibility 2 gene
ATP	Adenosintriphosphate
Atp5b	ATP synthase, H ⁺ -transporting, mitochondrial F1 complex, β polypeptide
BAF	BluePeak laser autofluorescence
BBB	Blood-brain barrier
BDNF	Brain-derived neurotrophic factor
BM	Bruch's membrane
bp	Base pair
BRB	Blood-retina barrier
BSA	Bovine serum albumin
Ca ²⁺	Calcium
c-Cbl	Casitas B-cell-lymphoma

CCL2	CC-chemokine ligand 2
CD11b	Cluster of differentiation molecule 11b
CD200	Cluster of differentiation 200
Cdc42	Cell division control protein 42
cDNA	Complementary DNA
CFH	Complement factor H
cGMP	Cyclic guanosinemonophosphate
c-Kit	Knirps im Thorax (mammal equivalent)
CL	Chlodronate liposomes
CNS	Central nervous system
Crb1 ^{rd8}	Crumbs family member 1, photoreceptor morphogenesis associated; retinal degeneration 8
Cre	Causes recombinase
cRGD	Cyclic arginine-glycine-aspartate
CSF1	Colony stimulating factor 1 (ligand)
CSF1R	Colony stimulating factor 1 receptor
CT	Cycle threshold
CX3CR1	Fractalkine
D	Domain
DAMP	Damage-associated molecular pattern
DAPI	4',6-diamino-2-phenylindole
DBI	Diazepam binding inhibitor
DHA	Docosahexaenoic acid
DMEM	Dulbecco's Modified Eagle Medium
DMSO	Dimethyl sulfoxide
DNA	Deoxyribonucleic acid
dNTP	Dinucleotid triphosphate
DT	Diphtheria toxin
DTR	Diphtheria toxin receptor
DUSP1	Dual specificity phosphatase 1
EC ₅₀	Excitatory concentration
EDTA	Ethylenediaminetetraacetic acid
EGFP	Enhanced green fluorescent protein
ERK	Extracellular signal-regulated kinases
F4/80	Marker of murine macrophages
FCS	Fetal calf serum
FIMP	Fms-interacting protein

FIRE	Fms-intronic regulatory element
FMS	Feline McDonough sarcoma
g	gram
GA	Geographic atrophy
Gab3	Grb2 associated binder 3
GCL	Ganglion cell layer
GCV	Ganciclovir
GFAP	Glial fibrillary acidic protein
GPCR	G protein-coupled receptors
Grb2	Growth factor receptor-bound protein 2
h	Hour/hours
HCL	Hydrochloric acid
HEK293	Human Embryonic Kidney 293 cells
HET	Heterozygous
His	Histidine
HOM	Homozygous
HSVTK	Herpes simplex virus-derived thymidine kinase
Iba1	Ionized calcium binding adapter molecule 1
IC ₅₀	Inhibitory concentration
IFN	Interferon
Ig	Immune globulin
IHC	Intracerebral hemorrhage
IL	Interleukin
INL	Inner nuclear layer
iNOS	Inducible nitric oxide synthase
IPL	Inner plexiform layer
IRF8	Interferon regulatory factor 8
IRSp53	Insulin receptor substrate protein 53 kDa
IS	Inner segments of photoreceptors
IVC	Individual ventilated cages
JMD	Juxtamembrane domain
kDa	Kilodalton
KO	Knockout
LC-MS	Liquid chromatography - mass spectrometry
LDH	Lactate dehydrogenase
Leu	Leucine
LoxP	Locus of X-over P1

LPS	Lipopolysaccharide
MACRO	Macrophage receptor with collagenous structure
MAP	Mitogen activated protein kinase
MEK	MAP/ERK kinase
Met	Methionine
MgCl ₂	Magnesium chloride
MHCII	Major histocompatibility complex class II
min	Minute/minutes
MIP	Mean intensity projection
mm	Milimeter
MPEG1	Macrophage expressed 1
mRNA	Messenger ribonucleic acid
MS	Multiple sclerosis
NaCl	Sodium chloride
NaOH	Sodium hydroxide
NDS	Normal donkey serum
NF-κB	Nuclear factor κB
NGFR	Nerve growth factor receptor
NK cells	Natural killer cells
nm	Nano meter
NO	Nitric oxygen
O.C.T. TM	Optimal Cutting Temperature medium
OC	Osteoclasts
ONL	Outer nuclear layer
OPL	Inner plexiform layer
OS	Outer segments of photoreceptors
P/S	Penicillin-Streptomycin
PAMP	Pathogen-associated molecular pattern
PBS	phosphate-buffered saline
PCR	Polymerase chain reaction
PD	Parkinson's disease
PDGF	Platelet-derived growth factor
PFA	Paraformaldehyde
pH	Potential Hydrogenii, negative decadic logarithm of the H ₃ O ⁺ concentration
PI3K	Phosphoinositide-3-kinase
PKB	Protein kinase B
PKC1	Protein kinase C 1

PLC	Phospholipase C
PLX	Pexidartinib
ppm	Parts per million
PRR	Pattern recognition receptor
PTK	Protein tyrosine kinase
PU.1	Purine-rich box 1
qRT-PCR	Quantitative real-time PCR
RAC1	Ras-related C3 botulinum toxin substrate 1
rd	Retinal degeneration
RNA	Ribonucleic acid
ROS	Reactive oxygen species
RPE	Retinal pigment epithelium
RPE65	RPE-specific protein (65 kDa)
RPMI	Park Memorial Institute
RT	Room temperature
SD-OCT	Spectral-domain optical coherence tomography
sec	Second/seconds
Ser	Serine
SRS	Subretinal Space
T	Trophoblasts
TBE	Tris-borate-EDTA buffer
TGF β	Transforming growth factor β
TLR	Toll-like receptor
TNF α	Tumor necrosis factor α
TRIS	Tris (hydroxymethyl) aminomethane
TSPO	Translocator protein 18 kDa
TUNEL	Terminal deoxynucleotidyl transferase dUTP nick end labeling
Tyr	Tyrosine
U	Units
UV	Ultra violet
V	Volt
WASP	Wiskott-Aldrich syndrome protein
WAVE2	Wiskott-Aldrich syndrome protein 2
WT	Wild type

1. Introduction

1.1 The mammalian retina

Vision means quality of life and is by far the most frequently used of the five senses. With the eye, we gather information from our environment, thus we are able to move safely, overcome obstacles and navigate through rough terrain. Visual information makes up more than 75% of the information we receive about the world. The eye converts light into nerve impulses that are transmitted to the brain for processing by focusing it onto a specialized layer of cells called the retina. It develops from the embryonic diencephalon and is a component of the central nervous system (CNS) along with the brain and spinal cord (Varga, Wegner et al. 1999). The eye can only be stimulated by the visible spectrum of light, which ranges from 400 to 750 nm wavelength (Sloney 2016). To reach the light sensitive photoreceptors, light enters the eye through the cornea and travels through the aqueous humor, pupil, lens and entire retina (Figure 1). Both the cornea and the lens are crucial for directing incoming light onto the center of the retina with the greatest visual acuity called the *fovea centralis* located within the macula (Chader and Taylor 2013). Rods and cones are the two types of photoreceptors within the retina. About 95% of the rods in the retina are located in the periphery, whereas the *fovea centralis* is abundant in cones. Prior to sending the visual information to the brain, the retina starts rudimentary visual processing. It transforms the light it receives into electrical and chemical signals that are sent to the brain via the optic nerve. The retina is extremely complex, as evidenced by the more than 55 unique, highly specialized cell types that compose its distinctive cellular structure. It is subdivided into three distinct cellular layers by synaptic layers. Incoming light must pass through every layer of the retina due to its inverse construction in order to excite the light-sensitive photoreceptors (Masland 2001).

Initiating the first event in light perception is the retina's translation of a single photon's energy into an electrical signal. G protein-coupled receptors (GPCR) known as opsins are responsible for this signal transduction. Cone and rod photoreceptors contain these opsins in their membranous outer segments (OS) (Arshavsky, Lamb et al. 2002, Moiseyev, Chen et al. 2005). Cones cover daytime and color vision with excellent visual acuity (photopic vision) while rods are in charge of seeing in low light (scotopic vision) (Sakurai, Onishi et al. 2007). The absorption of a photon by an opsin induces the chromophore photoisomerization from 11-*cis*-retinal to all-*trans*-retinal. This changes the opsin GPCR's conformation and initiates a signaling cascade that closes cyclic guanosine monophosphate (cGMP)-gated cation channels, which hyperpolarizes the photoreceptor cell (Muñiz, Greene et al. 2014). Our brain interprets the nerve impulses that are triggered by the combined change in the rods and cones receptor potentials as vision. All-*trans*-retinal is reduced to all-*trans*-retinol and subsequently transported to the nearby retinal pigment epithelium (RPE) after isomerization and release

Introduction

from opsin (Muniz, Villazana-Espinoza et al. 2007). Lecithin-retinol acyltransferase converts it to retinylester, which the isomerohydrolase RPE65 subsequently converts to 11-*cis*-retinol (Moiseyev, Chen et al. 2005). When it returns to the photoreceptors, it is oxidized to 11-*cis*-retinal and then it combines with opsin to generate rhodopsin.

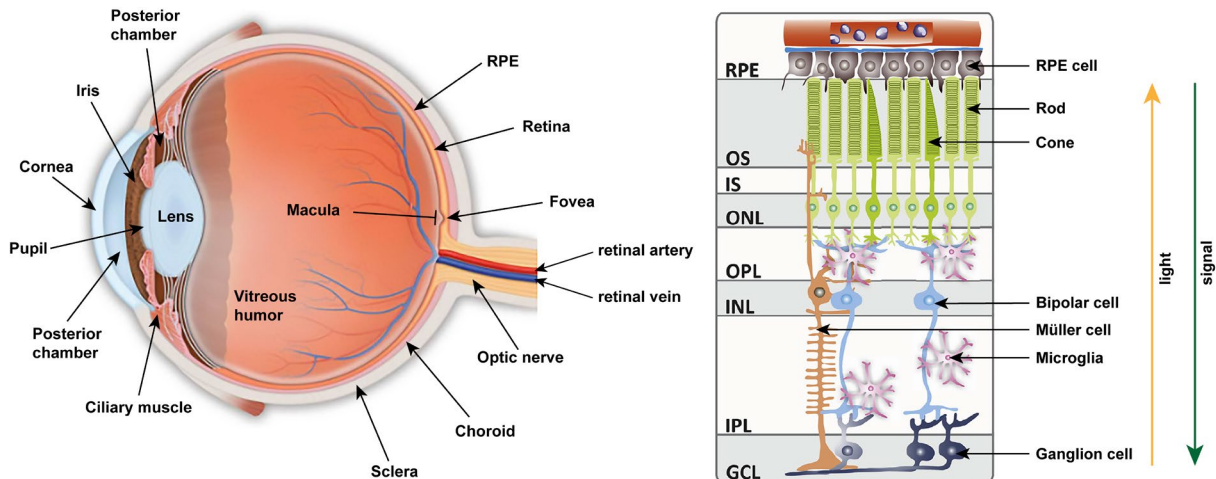


Figure 1 Anatomy of the human eye and retina. Schematic overview of the anatomy of the eye (left). Schematic cross section of the retinal layers (right). Ganglion cells build up the GCL, Müller cell nuclei, amacrine cells, bipolar cells, and horizontal cells build up the INL, Photoreceptor nuclei build up the ONL. Microglia reside in both plexiform layers and scan their environment for DAMPs and PAMPs. GCL: ganglion cell layer, IPL: inner plexiform layer, INL: inner nuclear layer, OPL: outer plexiform layer, ONL: outer nuclear layer, IS: inner segment of photoreceptors, OS: outer segment of photoreceptors, RPE: retinal pigment epithelium. Modified from Eye Anatomy | glaucoma.org and Karlstetter et al. 2015.

A connecting cilium combines the OS and inner segment (IS) of the photoreceptor, which together compose up the outer nuclear layer (ONL) (Horst, Johnson et al. 1990). Through synapses in the outer plexiform layer (OPL), the signal is subsequently sent to inner retinal cells, including bipolar cells which cell bodies constitute the inner nuclear layer (INL). Horizontal and amacrine cells are two more varieties of neurons with INL-based cell bodies. While amacrine cells control transmission to ganglion cells, horizontal cells influence synaptic transmission of photoreceptor and bipolar cells. The bipolar cells have connections in the inner plexiform layer (IPL) that connect them to ganglion cells further. The ganglion cells' axons constitute the optic nerve, and their nuclei make up the ganglion cell layer (GCL), which carries chemotactic signals to the brain where they are processed into images (Purves). Three different forms of glia cells, including astrocytes, microglia, and Müller cells are also present in the retina. The blood-retina barrier (BRB) is built by astrocytes, which are only present in vascular zones (Kautzman, Keeley et al. 2018). The resident immune cells in the retina are called microglia. They are situated in both plexiform layers and use their protrusions to keep an eye on their surroundings (Karlstetter, Scholz et al. 2015). Müller cells are the main glia cells that act as support structures. They connect the inner and outer retina surfaces by extending radially throughout the retina. Their cell bodies are found in the INL, and their terminations comprise the inner and outer limiting membranes. They serve as optic fibers that

carry the light from the retinal surface to the photoreceptors and support neuronal cell survival by preserving the retinal extracellular environment, including the BRB (Cunha-Vaz 2007, Franze, Grosche et al. 2007).

The RPE, a monolayer of pigmented cells that is a component of the BRB, is responsible of absorbing the light energy that is focused on the retina by the lens. Ions, water, and metabolic waste products are transported from the subretinal space (SRS) to the blood by the RPE. The RPE is in constant exchange with the photoreceptors and recycles their metabolic products produced during the visual cycle. All-*trans*-retinal, which is created upon photon absorption, cannot be isomerized back into 11-*cis*-retinal by photoreceptors. All-*trans*-retinal is carried to the RPE, isomerized to 11-*cis*-retinal, and then transported back to the photoreceptors to maintain photoreceptor excitability. RPE dysfunction is a significant pathologic alteration seen in a variety of retinal degenerative disorders, leading to blindness, including age-related macular degeneration (AMD). It develops from the malfunction and death of RPE cells, whether or not there is choroidal neovascularization, to the loss of photoreceptors and consequent central vision loss (Strauss 2005, Cho, Kim et al. 2012).

1.2 Age-related macular degeneration

Our vision typically deteriorates with time as we age. Additionally, some people have health issues that might further impair their vision or possibly cause blindness. AMD is one potential factor contributing to impaired eyesight. It is one of the leading causes to central vision loss among the elderly in industrialized countries. The accumulation of acellular, polymorphous deposits in one area of the eye, between the RPE and Bruch's membrane (BM) is one change that happens as we age. These focal deposits, also known as drusen, are the initial clinical signs of AMD, serving as a hallmark for this condition (Jager, Mieler et al. 2008). There are three identified clinical stages of AMD (Figure 2). Few, medium-sized drusen or anomalies in the pigmentation of the retina are the hallmarks of early AMD. Indicators of intermediate AMD include at least one large druse, multiple medium-sized drusen, or geographic atrophy that does not reach the center of the macula. Advanced AMD may be neovascular (wet or exudative) or non-neovascular (dry or atrophic) (Figure 2). Advanced neovascular AMD is characterized by subretinal hemorrhage driven by compromised BM and choroidal neovascularization. Geographic atrophy (GA) and drusen that extend to the macula's center are signs of advanced non-neovascular or dry AMD, which causes a progressive degeneration of the photoreceptors in this region (Gass 1967, Jager, Mieler et al. 2008). Visual loss in early AMD is often modest and frequently asymptomatic. Nevertheless, some symptoms, such as impaired vision, diminished contrast sensitivity, inappropriate dark adaption and the requirement for brighter light may manifest. In patients with advanced non-neovascular AMD,

gradual vision loss with central or pericentral visual scotomas commonly occurs over months to years (Sunness, Rubin et al. 1997). On the contrary hand, subretinal hemorrhage or fluid accumulation secondary to choroidal neovascularization can cause rapid and severe visual loss within days to weeks in patients with neovascular AMD (Ferris, Fine et al. 1984).

1.2.1 Age-related macular degeneration associated risk factors

Due to intricacy of the retina, complicated interplay of environmental and genetic factors, a variety of risk factors, and molecular mechanisms that affect disease development and progression, AMD's etiology is still not completely understood. Advanced age, white race, hereditary characteristics, and a history of smoking are among the many unmistakable risk factors for the onset and progression of AMD (VanNewkirk, Nanjan et al. 2000, Augood, Vingerling et al. 2006). Growing older is linked to dramatic increases in AMD incidence, prevalence, and progression. The retina and RPE are more susceptible to damage as we age because of increased oxidative stress, declining photoreceptor performance, and changes in RPE cell activity. This causes RPE cells and photoreceptors to reduce mitochondrial activity with age. Additionally, as people grow older, the choroidal layer becomes thinner, loses some of its flexibility, and has a reduced capacity to handle metabolites. The result is impaired BM function, which further results in the development of drusen by ongoing debris deposition (Curcio, Johnson et al. 2009, Lambert, ElShelmani et al. 2016, Heesterbeek, Lorés-Motta et al. 2020). A person's lifestyle can also affect how quickly AMD develops. High-fat, refined carbohydrate diets that are hyperglycemic are positively linked to an increased incidence of AMD. It has been demonstrated that consuming many calories might cause intestinal dysbiosis, which is linked to excessive choroidal neovascularization (Morris, Imrie et al. 2007, Andriessen, Wilson et al. 2016). Smoking is a significant additional risk factor for AMD that is known to enhance oxidative stress and decrease the retina's and RPE's antioxidant defense (Velilla, García-Medina et al. 2013). Furthermore, AMD shows significant variations in the prevalence among racial or ethnic groups. AMD affects more white people than black people. Chinese and Hispanic people appear to have a higher prevalence of AMD than black people do but a lower prevalence than white people (Klein, Klein et al. 2006, Bressler, Muñoz et al. 2008).

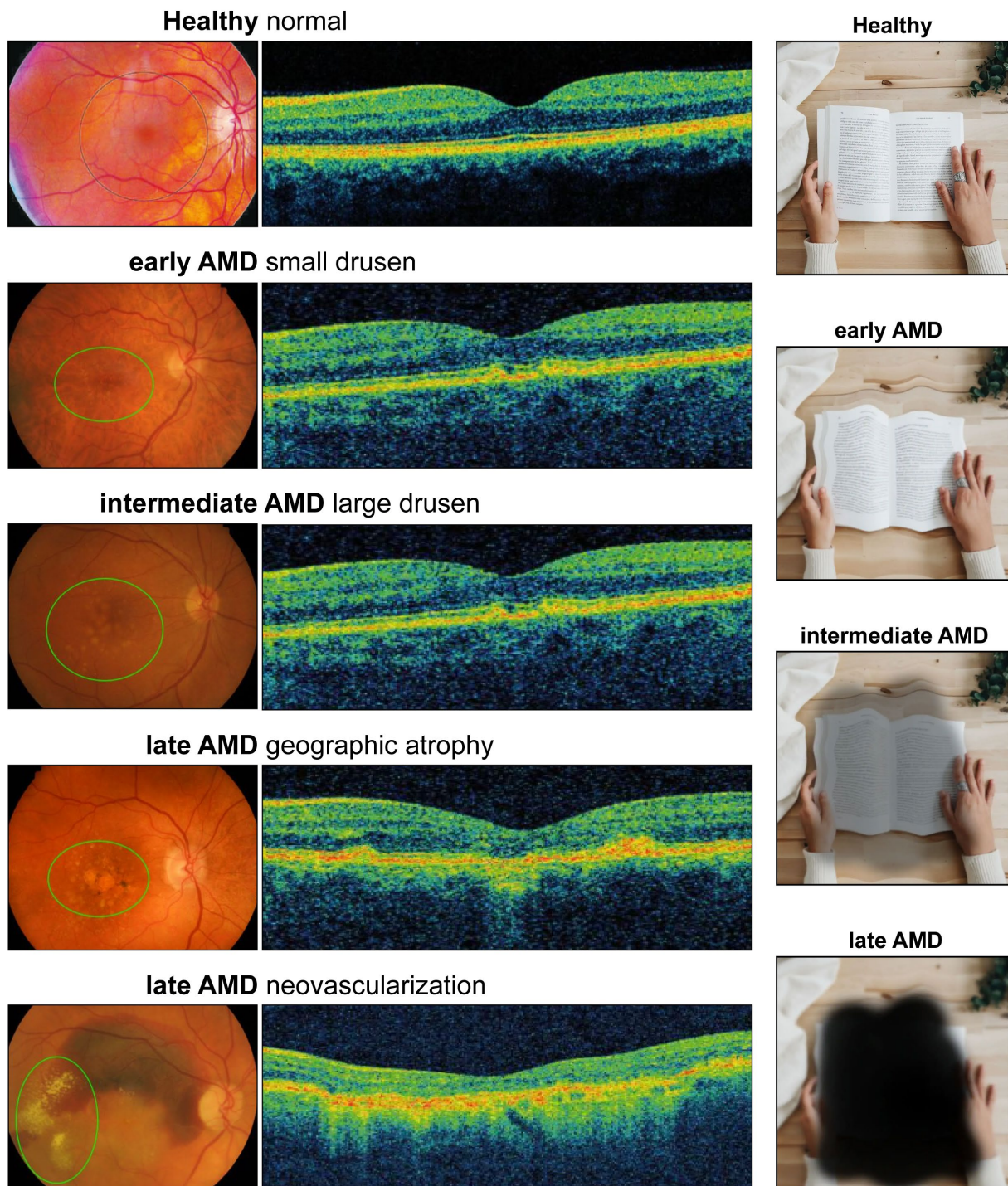


Figure 2 Clinical stages, signs and symptoms of AMD. Fundus images from healthy patients and patients with early, intermediate and late AMD (left side). The late stage is divided in geographic atrophy and neovascularization. Yellow acellular drusen deposits are present around the macular region in early AMD. They are growing larger in the intermediate stage. Large drusen and confluent RPE and photoreceptor degeneration regions centered on the macula are characteristics of GA. Choroidal neovascularization, which causes vascular leakage and macular edema, is a characteristic of neovascular AMD. SD-OCT showing the retinal layers and their degeneration with drusen formation and vascular leakage (middle). Early indicators of vision loss include a little center distortion; as the disease advances, this area enlarges, causing blind patches and subsequently making it harder to perceive colors and fine details under total central vision loss (left side). Fundus and SD-OCT images are adapted from: Stages of age-related macular degeneration | Macular Disease Foundation (mdfoundation.com.au), Optical Coherence Tomography in Age-related Macular Degeneration | www.amdbook.org and schematic illustrations adapted from: Simulation – PRO RETINA (pro-retina.de).

Although twin studies and familial aggregation analyses have clearly shown that AMD is heritable, genetic studies of AMD have generally been difficult. AMD appears relatively late in life and is characterized by a variety of diverse phenotypes. Because patients' children are often too young to exhibit disease symptoms and that parents of patients are frequently deceased, this can only allow for the study of one generation of patients in clinical research (Seddon, Ajani et al. 1997, Hammond, Webster et al. 2002, Seddon, Cote et al. 2005). According to DNA-sequence data from the "Human Genome Project", genetic variants in immune system genes are strongly linked to AMD (Klein, Zeiss et al. 2005). To date more than 30 loci with 50 common and uncommon genetic variants have been associated with AMD. Many of these offending genes regulate inflammation, the homeostasis of the retina, and different elements of the complement system pathway (DeAngelis, Owen et al. 2017, Geerlings, de Jong et al. 2017). The incidence of AMD in whites is markedly increased by a polymorphism (Tyr402His) in the complement factor H (*CFH*) gene, which is found on chromosome 1 (1q31). *CHF*, which is synthesized in the macula and found in drusen, is a significant inhibitor of the complement system (Hageman, Anderson et al. 2005, Haines, Hauser et al. 2005). In addition to *CFH*, the Ala69Ser polymorphism of age-related maculopathy susceptibility 2 gene (*ARMS2*), found on chromosome 10 (10q26), has also been substantially linked to AMD development. The protein that *ARMS2* encodes for has been localized in mitochondria and is expressed in the retina, although its function is yet unknown (Kanda, Chen et al. 2007). Despite the fact that these complement components are present throughout the body, there is now convincing evidence that AMD also probably be caused by an innate immune system disturbance involving reactive mononuclear phagocytes, particularly microglia (Anderson, Radeke et al. 2010, Madeira, Boia et al. 2015).

1.3 Microglia – the resident immune cells of the retina

The CNS' tissue macrophage population is represented by microglia cells. Microglia serve as both a friend and a foe, contributing to the maintenance of retinal integrity in healthy retinas while also causing auto-destructive responses in diseased retinas (Thanos, Kacza et al. 1994). They regulate neuronal excitability, synaptic pruning, neurogenesis, and the removal of dead cells debris from the brain while continuously monitoring the environment in order to react to precisely calibrated CNS activities (Karlstetter, Scholz et al. 2015).

1.3.1 Origin and self-maintenance of microglia

Del Rio-Hortega first identified microglia in the brain parenchyma as cells with small cell bodies, long cellular processes, and phagocytic capability. Microglia are a unique cellular entity, which have a rudimentary erythromyeloid origin. They are derived from simple hematopoietic

progenitors found in the yolk sac. On day 9.5 of the mouse embryo's development, these cells produce macrophages that cross the BRB and enter the brain while it is still open (Alliot, Godin et al. 1999, Ginhoux, Greter et al. 2010). The morphology of early microglia is amoeboid, with large, rounded cell bodies and short, dense branching. Even while the morphology gradually changes during brain development to a branching and ramified appearance, this amoeboid profile is seen in adult brains exposed to pro-inflammatory stimuli (Ashwell 1990, Milligan, Cunningham et al. 1991, Chan, Kohsaka et al. 2007). These progenitors represent a self-maintaining and long-lived cell population that endures for month or even throughout the lifespan of the organism (Ajami, Bennett et al. 2007, Askew, Li et al. 2017). Healthy adult mice and the human brain both have slow turnover rates of microglia (Réu, Khosravi et al. 2017). However, colony stimulating factor 1 receptor (CSF1R) signaling, PU box binding 1 (PU.1)- and interferon regulatory factor 8 (IRF8)-dependent pathways are crucial for microglia development and self-maintenance (Kierdorf, Erny et al. 2013). CSF1R is also crucial for microglia development (Stanley and Chitu 2014). It was demonstrated that microglia were depleted in the CNS whether CSF1R was blocked or the factors PU.1 and IRF8 were absent (Mezey, Chandross et al. 2000, Elmore, Najafi et al. 2014). CSF1R signaling and microglia depletion is explained in detail in chapter 1.4 and 1.5.

1.3.2 Role of microglia in the developing and adult retina

It has been demonstrated that on the neonate ganglion cell layer, a substantial number of F4/80 immunoreactive cells co-localize with a large number of apoptotic neurons (Hume, Perry et al. 1983). Around embryonic day 16, these cells begin to infiltrate the retina and are found near blood vessels on the vitreo-retinal surface (Perry and Gordon 1988). This was validated by retrograde labeling of retinal ganglion cells, which allowed for the discovery of amoeboid phagocytic microglia around postnatal day 5, the time when ganglion cell death peaks in the retina. This suggested that retinal microglia are engaged in the phagocytosis of dying neurons before they establish their strategic places in both plexiform layers of the adult retina (Thanos, Pavlidis et al. 1992). Recent microglia ionized calcium binding adaptor molecule 1 (Iba1) stainings showed that microglia first reside in the nerve fiber layer and GCL before progressively colonizing the plexiform layers (Santos, Calvente et al. 2008). Homeostatic microglia have a role in sculpting neuronal connections, regulating embryonic apoptosis, phagocytosing cell debris, and directing the development of primary retinal vessels (Provis 2001, Bessis, Béchade et al. 2007, Schafer, Lehrman et al. 2012). The control of synaptogenesis is yet another key role for microglia in the maturing retina. Microglial phagocytosis also regulates synaptic pruning, which modifies the neuronal network in the early postnatal retina. Since changes in retinal ganglion cell activity have a direct impact on how

synaptic inputs are engulfed by microglia, neuronal activity plays a significant regulatory role in this process (Roumier, Béchade et al. 2004, Paolicelli, Bolasco et al. 2011, Schafer, Lehrman et al. 2012).

Microglia enter the plexiform layers of the retina after their developmental processes are finished and exhibit a highly ramified morphology with small cell bodies and long cellular protrusions that may cover the entire nuclear layers (Figure 3.A). Ramified microglia, which continually moving their processes to scan the surface of retinal neurons in a specific region around each individual cell, collectively form an orderly territorial network (Figure 3.C) (Damani, Zhao et al. 2011, Karlstetter, Scholz et al. 2015). When damage-associated molecular patterns (DAMPs) or pathogen-associated molecular patterns (PAMPs) are recognized by microglia via pattern recognition receptors (PRRs), both the migration to the site of damage and a graded shift in morphology from ramified to amoeboid follow (Figure 3.B; D) (Kreutzberg 1996, Kettenmann, Hanisch et al. 2011). The expression of multiple cell surface receptors, such as Iba1, major histocompatibility complex class II (MHCII) proteins, and cluster of differentiation molecule 11b (CD11b), as well as the mobilization of immune cells from the periphery to the site of damage (or pathogen detection) are all increased in this reactivated state of microglia (Dick, Ford et al. 1995, Xu, Chen et al. 2007). Reactivated microglia are a double-edged sword in situations of CNS injury. On one side, they release neurotoxic substances like nitric oxide (NO) and reactive oxygen species (ROS) to fight infectious particles but might also affect healthy tissue (Figure 3.E) (Langmann 2007). On the other side, they facilitate neuronal renewal and synaptic stripping in order to restore homeostasis. Moreover, microglia request support in form of interleukin 6 (IL-6) and interleukin 1 β (IL-1 β) activated mononuclear phagocytes, by releasing the attractant cytokine CC-chemokine ligand 2 (CCL2) (Kradky, Lin et al. 2008, Ferreira, Santos et al. 2012). The removal of debris and preservation of retinal homeostasis depend heavily on the interactions between microglia and other retinal neurons and macroglia (Nimmerjahn, Kirchhoff et al. 2005). Several surface proteins on microglia, including receptors for cytokines, chemokines, complement system subunits, antibodies, and DAMPs, allow them to sense their surroundings. Due to the microglia's high sensitivity, the healthy retina's inhibitory mechanisms must be very strict in controlling the microglia's activation (Dick, Carter et al. 2003). As transforming growth factor β (TGF β) secreted by the RPE causes microglial interleukin 10 (IL-10) to be released, which in turn suppresses the production of antigen-presenting proteins, the RPE appears to be a key player in this process. According to a global gene expression analysis, TGF β can also directly rewire microglia to have an anti-inflammatory phenotype (D'Orazio and Niederkorn 1998, Paglinawan, Malipiero et al. 2003). Another controlling mechanism of microglia reactivity is mediated by cluster of differentiation 200 (CD200). CD200 binds to its receptor on microglia cells and elicits a signaling cascade to block pro-inflammatory activation (Hoek, Ruuls et al.

2000, Wright, Puklavec et al. 2000). Another microglial regulator to inhibit neurotoxicity is the fractalkine (CX3CR1) signaling pathway (Cardona, Pioro et al. 2006). To keep levels of neurotrophic factors crucial for retinal function constant, microglia actively cross-talk with Müller cells. Therefore, Müller cells can release a number of neurotrophic factors, all of which increase photoreceptor survival in stressful situations or encourage the healing process after injury, when microglia are present (Harada, Harada et al. 2003, Wenzel, Grimm et al. 2005, Joly, Lange et al. 2008). Müller cells can reduce microglia reactivity by constitutively secreting the translocator protein 18 kDa (TSPO) -ligand diazepam binding inhibitor (DBI) during development, and they may even be able to switch active microglia that are already present into their ramified surveillance state. The same process is at work in Müller cell gliosis during retinal degeneration, where DBI release acts as a checkpoint against excessive microglia activation (Wang and Neumann 2010). To summarize, controlled microglia activation is thought to be neuroprotective, whereas persistent activation can end up in retinal degenerative diseases.

1.3.3 Microglia in the retina under disease condition

When microglia enlarge, retract their branches and express pro-inflammatory associated genes accompanied by migration from the plexiform layers towards the damaged area is a clear sign for many retinal degenerative diseases (Figure 4) (Tang and Kern 2011, Karlstetter, Scholz et al. 2015). One of the most common diseases, which contribute to vision loss in elderly, is AMD (Jager, Mieler et al. 2008). The relationship between AMD and an innate immune system dysregulation, primarily involving complement system components and reactive macrophages and microglia is nowadays sufficiently supported by genetic and immunohistochemical data (Fritsche, Fariss et al. 2014). Large amoeboid macrophages and microglia, which are strongly co-located with the drusen in early AMD, were found in patient's tissue upon examination (Figure 4). In early AMD, the presence of drusen is probably what causes a strong pro-inflammatory stimulus and triggers macrophages and microglia to congregate around the BM and choroid (Cherepanoff, McMenamin et al. 2010). The age-dependent increase of intracellular N-retinylidene-N-retinylethanolamine (A2E) a component of lipofuscin, may be also a significant driver of subretinal microglia migration (Ma, Coon et al. 2013). Retinas from patients with GA show reactive microglia in the ONL, where they phagocytose both apoptotic and stressed but living photoreceptors (Figure 4) (Gupta, Brown et al. 2003, Zhao, Zabel et al. 2015). Human AMD donor eye transcriptome analysis revealed that *macrophage receptor with collagenous structure (MACRO)* and *macrophage expressed 1 (MPEG1)*, as well as other complement system components and chemokine mRNAs, were strongly overexpressed, indicating that microglia are reactivated and play a key role in the

pathogenesis of AMD (Newman, Gallo et al. 2012). This suggests that the death of photoreceptors, retinal degeneration and progression of AMD are all influenced by microglia reactivity. Microglia are therefore not only a spectator, but rather a key factor of AMD progression.

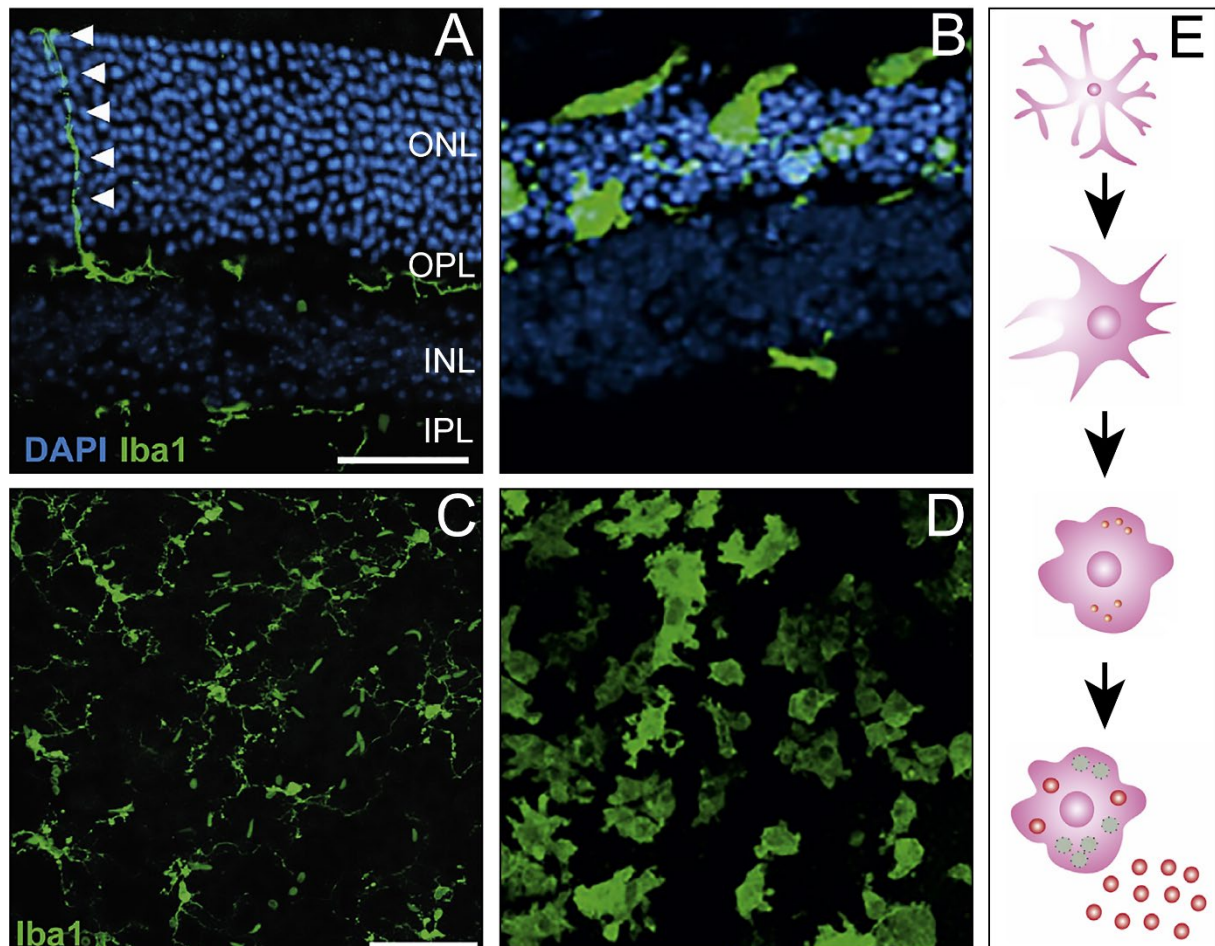


Figure 3 Microglia location and morphology in healthy and diseased retinas. Iba1 stainings in healthy (A; C) and degenerative (B; D) retinal cryosections (A; B) and flat mounts (C; D). Illustration showing the progression of morphological changes in activated microglia from ramified to amoeboid. In a healthy retina, ramified microglia are dispersed evenly across the plexiform layers in a non-overlapping network and use their protrusion to maintain a watchful eye on their surroundings. Microglia migrate to the ONL and subretinal space during retinal degeneration, changing their morphology from ramified to amoeboid, increasing their phagocytic activity, and releasing pro-inflammatory cytokines. As a result, they actively contribute photoreceptor loss and retinal degeneration. ONL: outer nuclear layer, OPL: outer plexiform layer, INL: inner nuclear layer, IPL: inner plexiform layer. Modified from Karlstetter, Scholz et al. 2015.

1.3.4 Light damage model mimics features of dry AMD in rodents

The majority of AMD mouse models are limited to the study of particular traits of human pathology like retinal degeneration and immune cell activation because rodents lack a macula. A well-established paradigm for stimulating the photooxidative stress and retinal degeneration found in atrophic AMD is intense white light exposure (Karlstetter, Scholz et al. 2015). Photoreceptor loss is typically present in light-damaged retinas, and microglial cells are highly

reactive. Only a few hours after light damage, these microglia showed a robust pro-inflammatory response, according to transcriptomic analyses utilizing DNA microarrays (Combadière, Feumi et al. 2007, Joly, Francke et al. 2009, Ebert, Walczak et al. 2012). In white light damage, migration to the outer retina is preceded by early events such as alterations in microglial morphology and polarization of processes towards the ONL. All of these pathologies have also been demonstrated in patients with AMD, making the light damage model a very suitable one for non-vascular AMD reenactment in mice to develop further details of the progression and possible treatments. Greater susceptibility to light damage was associated to an allele expressing leucine than methionine at amino acid 450 of the RPE65 protein. Mice with the RPE65 Leu450 polymorphism had higher RPE65 protein levels and regenerate rhodopsin more rapidly after exposure to light. The retina's resistance to light is decreased by the higher amounts of regenerated rhodopsin, which increases photon absorptions and makes the retina more prone to light damage (Grimm and Remé 2013). This shows that mice carrying the light sensitive RPE65 Leu450 variant are best suited for the light damage model.

1.3.5 Microglia depletion as therapeutic strategy in neurodegenerative diseases

The foregoing sections clarified how synaptic pruning by microglia supports neuronal health by encouraging proper neuron connections and development. Additionally they support CNS homeostasis by phagocytosing dead cell debris. However, microglia over-reactivity is a characteristic found in many neurodegenerative diseases and is generally unrelated to the underlying genetic flaw or etiology. In order to slow the progression of a number of neurodegenerative diseases, microglia specific immunotherapy may be a promising and sustainable approach (Spangenberg, Lee et al. 2016, Jin, Shi et al. 2017, Spangenberg, Severson et al. 2019). In order to mitigate the negative effects of microglia in a diseased status, it is helpful to target the onset of a destructive microglia response or to deactivate excessively reactive microglia.

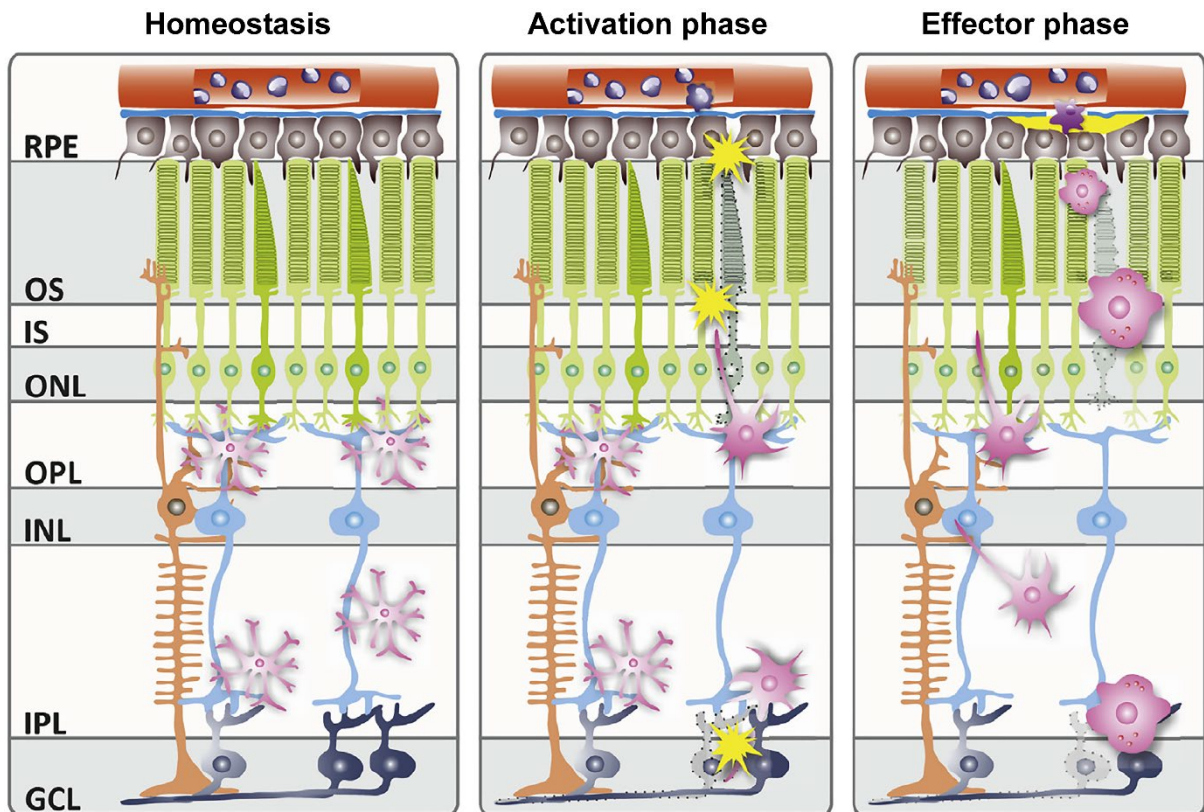


Figure 4 Schematic overview of microglia activation in retinal degenerative diseases. Under homeostatic conditions, resident and activated microglia are located in both plexiform layers, while scanning their environment with their protrusions for pathogens, cell debris and antigen presenting cells. Here microglia exhibit a ramified phenotype. The activations phase follows in early stages of AMD, which is characterized by RPE dysfunction and small drusen formation between BM and RPE. Thus, microglia rapidly reactivate and change gradually into an amoeboid phenotype whilst migrating towards the damaged area (mainly subretinal space). In the effector phase, large drusen accumulate which in turns to fully reactivated and phagocytosing microglia. Here they exhibit a highly amoeboid phenotype, releasing pro-inflammatory cytokines and cytotoxic substances, which contribute to retinal degeneration. RPE: retinal pigment epithelium, OS: outer segment of photoreceptors, IS: inner segment of photoreceptors, ONL: outer nuclear layer, OPL: outer plexiform layer, INL: inner nuclear layer, IPL: inner plexiform layer, GCL: Ganglion cell layer (Karlstetter, Scholz et al. 2015).

Minocycline, an antibiotic is able to reduce the pro-inflammatory response of microglia. It significantly reduces the amount of phagocytic microglia in the subretinal space and attenuates photoreceptor cell loss in a mouse model of subretinal hemorrhage (Yang, Kim et al. 2009, Zhao, Ma et al. 2011). Moreover, minocycline reduces the expression of pro-inflammatory cytokines in mouse models of diabetic retinopathy (Kradny, Basu et al. 2005). Docosahexaenoic acid (DHA) is a well-known powerful immunomodulatory molecule that suppresses microglia's pro-inflammatory reactivity and aids in the survival of RPE and photoreceptor cells (Bazan, Calandria et al. 2010, Antonietta Ajmone-Cat, Lavinia Salvatori et al. 2012). In X-linked retinoschisis mouse models, DHA supplementation dramatically reduced retinal degeneration and microglial reactivation (Dornstaedter, Suh et al. 2012). Another molecule known as chondroitin sulfate proteoglycan-disaccharide is able to modulate microglia to stay in their regulatory phenotype with increased phagocytic capability in models of neurodegenerative diseases (Ebert, Schoeberl et al. 2008).

Not only the modulation of microglia reactivity but also their complete depletion has been reported to minimize neuroinflammation in several diseases. The absence of microglia could prevent the breakdown of the BRB in retinopathy-connected diseases (Kokona, Ebnetter et al. 2018). After intracerebral hemorrhage, the advantage of microglia depletion was associated with decreased leukocyte infiltration in the brain and enhanced blood-brain barrier (BBB) integrity (Li, Li et al. 2017). Furthermore, microglia depletion could prevent neuronal loss and improved recovery of motosensory abilities after induction of hippocampal lesions (Rice, Spangenberg et al. 2015). It is also important to note that microglia are able to repopulate after depletion. This repopulated microglia also show a reduced reactivity and positive effects on neurodegenerative diseases (Szalay, Martinecz et al. 2016, Coleman, Zou et al. 2020). Since CSF1R signaling is crucial for microglia survival and proliferation, inhibiting this signaling pathway may be an efficient strategy to deplete chronically reactivated microglia (Stanley and Chitu 2014). However, depletion of microglia in neurodegenerative diseases is highly controversial since the CNS needs the beneficial homeostatic functions of microglia, such as the ability to phagocytose dead cell debris.

1.4 Colony stimulating factor 1 receptor signaling pathways

The development and survival of microglia highly depend on CSF1R signaling. At three weeks of age, the *Csf1^{-/-}* mouse brain has essentially no microglia left (Chitu and Stanley 2017). In rats lacking CSF1R, resident macrophages, including brain microglia, are lost globally (Erblich, Zhu et al. 2011). Hematopoietic stem cells express the CSF1R at low levels, whereas tissue-resident macrophages, osteoclasts, myeloid cells, and microglia express it at higher levels, and it regulates the development of these cell types (Guilbert and Stanley 1980, MacDonald, Rowe et al. 2005, Sarrazin, Mossadegh-Keller et al. 2009, Nandi, Gokhan et al. 2012). The widespread pattern of CSF1R expression is consistent with the pleiotropic effects of this receptor on tissue repair, inflammation, innate immunity and tumor environment (Stanley and Chitu 2014). CSF1R expression can be regulated with two separate promotor regions. The first is the T/OC promotor, which regulates expression in trophoblasts and osteoclasts, and the second is the macrophage *Csf1r* promotor, which has regulatory components that enhance expression during macrophage differentiation (Bonifer and Hume 2008, Ovchinnikov, DeBats et al. 2010). Maximum CSF1R expression in differentiated monocytes/macrophages depends on the *Fms*-intronic regulatory element (FIRE), a highly conserved sequence enhancer region that also possesses reverse promoter activity. Because FIRE encodes an antisense CSF1R transcript, it may be able to prevent overexpression (Himes, Tagoh et al. 2001, Sasmono, Oceandy et al. 2003).

1.4.1 Colony stimulating factor 1 receptor structure and its ligands

The CSF1R belongs to the platelet-derived growth factor (PDGF) receptor family or receptor tyrosine kinases class III which also includes Knirps im Thorax (c-Kit) and Feline McDonough sarcoma (Fms) -like tyrosine kinase 3 (Rönnstrand 2004). It was shown that the murine CSF1R is a single glycosylated polypeptide chain of about 165 kDa with a tyrosine kinase activity that is activated by binding to the ligands interleukin 34 (IL-34) and CSF1 (Sherr, Rettenmier et al. 1985, Liu, Leo et al. 2012). The receptor has an intracellular domain made up of a juxtamembrane domain (JMD), an intracellular tyrosine kinase domain that is interrupted by a kinase insert domain. CSF1R also possesses a transmembrane domain as well as an extracellular region that is glycosylated and contains five immunoglobulin domains (D1 – D5) (Figure 5) (Coussens, Van Beveren et al. 1986, Rothwell and Rohrschneider 1987, Hampe, Shamoon et al. 1989, Stanley and Chitu 2014). CSF1 or IL-34 ligand binding results in the homodimerization of CSF1R, which allows autophosphorylation and the activation of downstream signaling pathways (Figure 5) (Stanley and Chitu 2014). Both are expressed *in vitro* as well as *in vivo* under the control of the CSF1R promotor. The two ligands have complementary functions in regulating the proliferation, maintenance and activity of the various cell types because of their different spatiotemporal expression (Wei, Nandi et al. 2010). CSF1 in circulation exhibits humoral regulation, and its transmembrane and proteoglycan isoforms have local effects (Cecchini, Dominguez et al. 1994, Dai, Zong et al. 2004). IL-34 on the other hand cannot be found in the circulation, meaning that its effects are probably limited to the local microenvironments where it is expressed (Hwang, Choi et al. 2012, Tian, Shen et al. 2013). It was also shown that CSF1 expression is found in the cerebellum and the spinal cord, whereas IL-34 expression is restricted to the neocortex, olfactory bulb, and striatum (Nandi, Gokhan et al. 2012). This may allow a regionally restricted fine-tuning of the cells dependent on CSF1R signaling.

1.4.2 Early phosphorylation events in signal transduction of CSF1R

Both ligands, CSF1 and IL-34, bind to the concave surface created by the D2 and D3 domains of the CSF1R, however the IL-34:CSF1R complex is different from the CSF1:CSF1R complex (Chen, Liu et al. 2008, Elegheert, Desfosses et al. 2011). Basically, CSF1R binds more strongly to the D2 and D3 domains, which IL-34 compensates for by forming amino- and carboxy-terminal extensions to D2 and D3 (Liu, Leo et al. 2012, Ma, Lin et al. 2012). Despite the differences between both complexes, the D3 – D4 junction distance is crucial for D4 interactions and signal transduction, which is equivalent in this case (Elegheert, Desfosses et al. 2011, Felix, Elegheert et al. 2013). The CSF1R kinase domain activation loop (AL) is folded back into the ATP-binding cleft in its inactive conformation, with AL tyrosine 807 functioning as

a pseudosubstrate and preventing substrate binding. JMD tyrosine 559 is phosphorylated to alleviate inhibition. This tyrosine, which is the initial residue to undergo phosphorylation in response to ligand binding, functions as a switch that is inactive in the absence of a ligand and active when phosphorylation occurs in reaction to a ligand (Rohde, Schrum et al. 2004, Yu, Chen et al. 2008). This is followed by phosphorylation of AL tyrosine 807 and JMD tyrosine 544. These three phosphorylations are essential and sufficient for the complete CSF1R kinase activity and recruitment of the c-Cbl complex. CSF-1R multiubiquitination, conformational alterations, elevated phosphorylation, and internalization of receptor-ligand complexes are driven on by c-Cbl activation (Wilhelmsen and van der Geer 2004, Xiong, Song et al. 2011). In order to activate different regulatory pathways individual CSF1R tyrosines can be phosphorylated to produce docking sites for a number of signaling molecules (Figure 5) (Pixley and Stanley 2004).

1.4.3 Downstream signaling pathways of CSF1R

Phosphorylation of tyrosine 721 leads to the activation of the protein kinase B/phosphoinositide-3-kinase (PKB/PI3K) pathway that is a crucial factor in the macrophage lineage's capacity to survive (Lee and States 2000, Sampaio, Yu et al. 2011). Phospholipase C (PLC) and Fms-interacting protein (FIMP) are involved in PKB/PI3K independent pathways of CSF1R mediated survival. The PI3K and the PLC pathway work separately to improve survival by regulating glucose uptake (Mancini, Koch et al. 2004, Chang, Hamilton et al. 2009). A dose dependent increase in the rate of protein synthesis by CSF1 is linked to macrophage proliferation. Both the MAP/ERK kinase (MEK) and PI3K pathways are activated by tyrosine 807 signaling, which separately support macrophage proliferation (Tushinski and Stanley 1983, Munugalavadla, Borneo et al. 2005). MEK inhibition suggest that many extracellular signal-regulated kinases (ERKs) are involved in the regulation of macrophage proliferation. For efficient proliferation, ERK5 must be activated in a Src family kinase (SFK)-dependent manner by CSF1. ERK1/2 phosphorylation might serve as a CSF1 concentration sensor. The CSF1R promotes increases in dual specificity phosphatase 1 (DUSP1) expression by activating membrane associated protein kinase C 1 (PKC1) which in turn inhibits prolonged ERK1/2 activation, which would otherwise result in a cell cycle arrest (Suzu, Hiyoshi et al. 2007, Wilhelmsen, Mesa et al. 2012). The ERK1/2 pathway mostly mediates the CSF1R-controlled myeloid differentiation process. Early and sustained waves of phosphorylation of MEK and ERK1/2 are induced by CSF1. The late wave, which is not dependent on PI3K activity, is the only one needed for macrophage differentiation. Adaptor protein Mona interacts with Grb2 associated binder (Gab3) and the tyrosine 697 site to promote late ERK1/2 phosphorylation. The Mona and Gab complex interact together, causing ERK1/2 to be activated downstream

from growth factor receptors (Nishida, Yoshida et al. 1999, Bourgin, Bourette et al. 2002, Meng, Chen et al. 2005). Several additional regulators of macrophage progenitor differentiation and proliferation are also brought on by CSF1R. These include interferon-inducible gene 204 (Ifi204), which decreases proliferation and prefers differentiation, and DUSP5, a negative feedback regulator of ERK1/2 that inhibits macrophage differentiation and induces granulocytic differentiation (Dauffy, Mouchiroud et al. 2006, Grasset, Gobert-Gosse et al. 2010). CSF1 triggers chemotaxis and the associated cell spreading and polarization processes including the dynamic reorganization of the actin cytoskeleton and focal adhesions. This is done by two waves of actin polymerizations. Wiskott-Aldrich syndrome protein (WASP) and WASP-family activation, which is dependent on cell division control protein 42 (Cdc42) and tyrosine 721, triggers the initial wave of actin polymerization (Papakonstanti, Zwaenepoel et al. 2008, Cammer, Gevrey et al. 2009). Actin polymerization in the second wave that causes membrane ruffling is independent of tyrosine 721 and involves Rac1/IRSp53 activation of the WAVE2/Abi complex (Kheir, Gevrey et al. 2005, Abou-Kheir, Isaac et al. 2008). Inhibitory proteins locally block the development of adhesion structures during cell migration, and actomyosin-dependent contractility is required to retract the outer parts. The Ca^{2+} and myosin IIA-binding protein S100A4 prevents actomyosin assembly. Due to decreased persistence and magnitude of membrane protrusions linked to persistent and accelerated actomyosin-IIA assembly, hyperphosphorylation, and mislocalization of paxillin, S100A4 loss impairs the CSF1 chemotactic response (Li, Spektor et al. 2003, Li, Dulyaninova et al. 2010).

Altogether, CSF1 signaling serves significant regulatory roles throughout the entire immune system, which may have an impact on neurodegenerative diseases. It was shown that mutations in CSF1R contribute to neurodegenerative diseases like Parkinson's disease (PD), or Multiple sclerosis (MS) (Beckmann, Giorgetti et al. 2018, Chang, Wu et al. 2019). In PD related mouse models, dopamine neuron loss and motor behavioral impairments are significantly reduced by pharmacological microglia depletion using a CSF1R inhibitor (Neal, Fleming et al. 2020). Furthermore, CSF1R inhibitor treatment improved remyelination by reducing neuroinflammation, which in turn stopped the progression of MS and dramatically decreased its severity (Beckmann, Giorgetti et al. 2018, Tahmasebi, Pasbakhsh et al. 2019). In-depth mechanistic studies on the various roles represented by CSF1R in these diseases are required given the recent and continuing expanding of neurological diseases linked to microglia dysfunction. Specifically treating CSF1R associated neurodegenerative diseases may be made possible by CSF1R inhibitor mediated microglia regulation or depletion. As a result, microglia CSF1R is emphasized as one of the newer targets for neurodegenerative diseases modifying therapy (Hu, Duan et al. 2021).

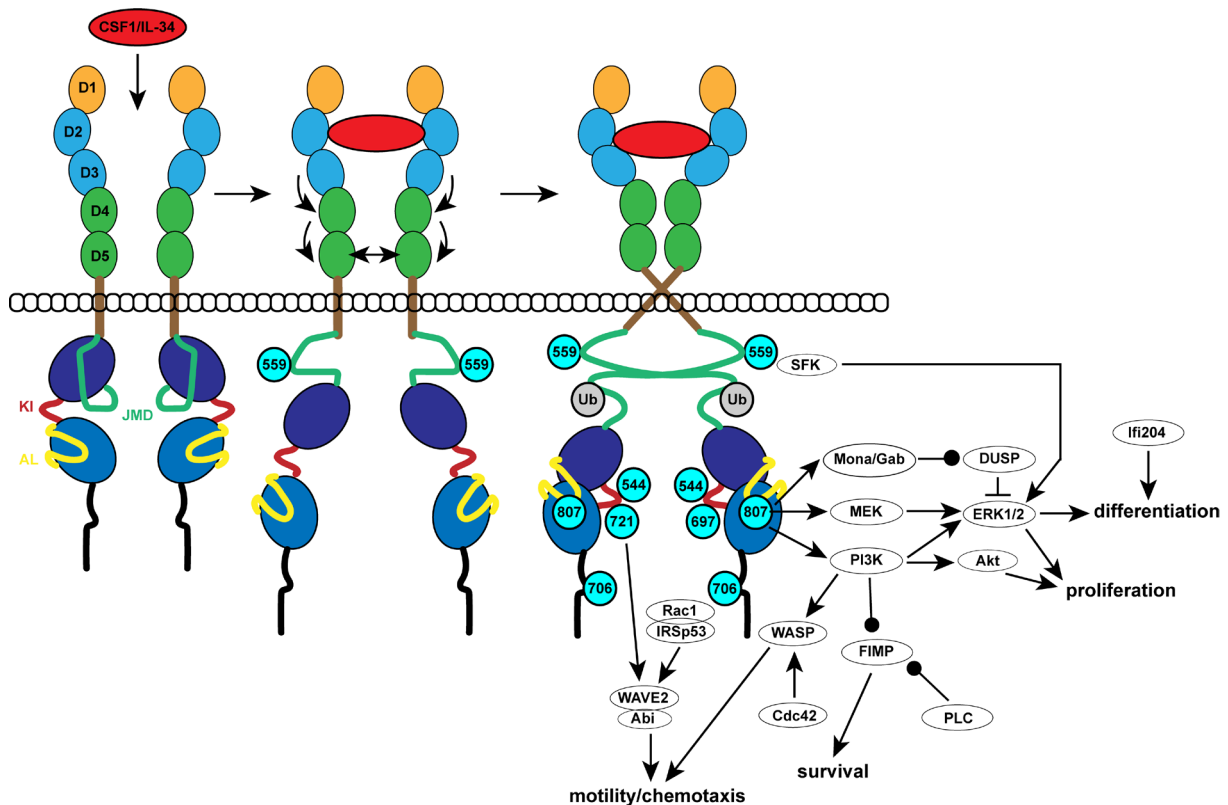


Figure 5 CSF1R structure and signaling. Structure of CSF1R ligand - receptor complex. Light blue spheres, phosphotyrosines; gray spheres, ubiquitination. It should be noted that full receptor activation and subsequent signaling depends on the phosphorylation of CSF1R tyrosine residue 559 and intracellular domain ubiquitination. Pathways mediating macrophage proliferation, differentiation, survival and chemotaxis are illustrated. AL: activation loop, JMD: juxtamembrane domain, KI: kinase domain. Black arrows indicate activation; black capped arrows indicate inhibition; round capped arrows indicate increased expression (Stanley and Chitu 2014).

1.5 Microglia depletion

Microglia ablation systems enable the investigation of their growth and function during CNS homeostasis as well as in neurodegenerative and neuroinflammatory diseases. A possible attempt to deplete microglia are genetic mouse models in which essential genes for microglia development and differentiation carry a mutation. One method is gene targeting in embryonic stem cells to create mice with a PU.1 locus mutation, a transcription factor specific for the development of hematopoietic tissue (Scott, Simon et al. 1994). Mice lacking PU.1 expression barely have any microglia. Another method is the production of knockout mice using the CRSPR method. Here, it was shown that no microglia could be detected in *Cx3cr1*^{-/-} mice (Fuhrmann, Bittner et al. 2010). CX3CR1 is highly expressed in microglia. The fact that these mice rarely reach adulthood and have pleiotropic impairments in organs that go beyond the CNS renders these techniques ineffective (McKercher, Torbett et al. 1996). For instance, mice are born alive but perish within 48 hours from severe septicemia. CSF1R knockout mice not only lack microglia but also have drastically reduced macrophage numbers and critical developmental flaws such as osteoporosis. Another example involves mice devoid of

microglia, which not only exhibit severe alternations in the development of macrophages but also manifest autoimmune diseases at a young age (Shull, Ormsby et al. 1992, Butovsky, Jedrychowski et al. 2014).

1.5.1 Conditional genetic depletion of microglia

For this reason, there is a strong demand for alternative methods of microglia depletion. This demand can be satisfied by conditional genetic deletion models. A mouse line that overexpresses a herpes simplex virus-derived thymidine kinase (HSVTK) under the myeloid specific promotor CD11b allows the depletion of myeloid cells including microglia when ganciclovir (GCV) is injected. Here, microglia did not die afterwards but instead showing a “frozen” phenotype in which microglial reactivation was completely suppressed (Heppner, Greter et al. 2005). A further development of the CD11b system by direct intracerebroventricular GCV injections lead to a 95% depletion of microglia after 4 weeks of treatment. However, it also results in mouse deaths, possibly because of the GCV’s myelotoxicity (Grathwohl, Kälin et al. 2009). Use of diphtheria toxin (DT)-based models provides an alternate conditional genetic strategy for depleting myeloid cells, including microglia. These pairs transgenic mice with genes for the diphtheria toxin receptor (DTR) loxP-flanked stop sequences, which are eliminated upon Cre recombination to drive gene expression in myeloid cells, with myeloid promotor-driven Cre recombinase mouse lines (Buch, Heppner et al. 2005). In myeloid cells that express DTR, subsequent delivery of DT results in acute cell death. *CX3CR1^{creER/+}* mouse lines are the most frequently used to achieve inducible DTR expression and cell depletion (Waisman, Ginhoux et al. 2015, Kaiser and Feng 2019). Importantly, inducible *CX3CR1^{creER/+}* animals require tamoxifen treatment for recombination and expression of DTR in *CX3CR1⁺* cells, offering more temporal control than inherent Cre lines (Parkhurst, Yang et al. 2013, Lund, Pieber et al. 2018). However, DTR models only provide temporary microglia depletion (5 days), provoke a cytokine storm and rely on toxic Cre recombinase (Bruttger, Karram et al. 2015). Therefore, care must be taken when performing a detailed functional investigation of microglia, especially when utilizing knockout mice that affect both peripheral and CNS myeloid cells (Locatelli, Wörtge et al. 2012, Gritsch, Lu et al. 2014).

1.5.2 Pharmacological depletion of microglia

Administration of chlodronate liposomes (CL) or CSF1R inhibition are two extremely popular and feasible methods of microglia depletion. CL’s, however, have proven to be comparatively nonspecific, and the medication has negative side effects (Bader, Enos et al. 2019). It was demonstrated that CL therapy increased adipose tissue mRNA expression of pro-inflammatory cytokines and caused neutrophilia and anemia. Furthermore, chlodronate liposomes in animal

models must be surgically infused directly into the CNS since they cannot penetrate the blood-brain barrier. For these reasons, depleting microglia should be accomplished through CSF1R inhibition. According to in situ hybridization, CSF1R is primarily confined to macrophage and microglia populations (Hume, Monkley et al. 1995). The analysis of osteopetrotic *Csf1^{op}/Csf1^{op}* mice, which have a spontaneous mutation in the *Csf1* gene and a resulting lack of Csf1, led to the discovery of the essential role of Csf1 signaling in macrophage biology (Wiktor-Jedrzejczak, Bartocci et al. 1990, Yoshida, Hayashi et al. 1990). Thus, these mice exhibit significant lower levels of macrophages and microglia in the bone, blood and CNS (Wiktor-Jedrzejczak, Ratajczak et al. 1992). There were also a number of other phenotypic alterations, including as osteoporosis, brain abnormalities such slower neuronal processes outgrowth, and aberrant auditory and visual evoked potentials (Michaelson, Bieri et al. 1996). It is noteworthy that conditional knockout mice with a loxP-flanked exon in the *Csf1r* gene have enabled spatial and temporal control of microglia when combined with driving Cre expression under a promoter for a microglia specific transcription factor, leading to transient elimination of microglia with tamoxifen (Buttgereit, Lelios et al. 2016, Cronk, Filiano et al. 2018).

Although the CSF1-associated knockout mice demonstrated that CSF1R signaling is important for the early formation of microglia, research on the significance of this signaling in age-related diseases in the adult mouse CNS were limited since these animals rarely survive to adulthood. Pexidartinib (PLX3397 or PLX5622) is a commonly used CSF1R inhibitor that can pass the blood brain barrier, which is proven to deplete approximately 90% microglia (Spangenberg, Severson et al. 2019). Subsequent oral administration of PLX3397 provided an approach for non-invasive microglia depletion at any age. PLX3397 directly engages the JMD region and binds the autoinhibited state of CSF1R. Tyrosine 546 and tryptophan 550 are used to create the essential hydrogen bonds that bind the inhibitor molecule to the receptor (Tap, Wainberg et al. 2015). Consequently, CSF1 and IL-34 binding sites are blocked, which prevents signaling and causes microglia to die (Gelderblom and de Sande 2020). Cessation of the medication led to a rapid repopulation of microglia from CNS-resident and nestin-expressing cells within 5 days (Elmore, Najafi et al. 2014). Wide ranges of mouse models of CNS disease or damage have been treated with CSF1R inhibitors. Eliminating microglia with PLX3397 can alleviate Alzheimer's disease by restoring dendritic spine loss, preventing neuronal loss, lowering overall neuroinflammation and improving contextual memory according to behavioral testing (Spangenberg, Lee et al. 2016). Post hippocampal lesion treatment with PLX3397 resulted in improved recovery in terms of motosensory capacities, along with a decrease in pro-inflammatory cytokine expression and a normalization of lesion-induced alternations in synaptophysin (Rice, Spangenberg et al. 2015). Additionally, in two experimental models of intracerebral hemorrhage driven on by injection of collagenase or autologous blood, microglia depletion reduced neurodeficiencies and brain edema. It was also possible to establish a

connection between the absence of microglia and enhanced blood-brain barrier integrity after intracerebral hemorrhage (Li, Li et al. 2017). These results show that CSF1R inhibition in mice has enabled researchers to explore adult microglia's critical role in CSF1R signaling as well as the impact of microglial depletion on CNS development, homeostasis, and diseases. Here, microglia depletion occurs without subsequent cytokine storm, or blood-brain barrier disruption, and had no discernible deleterious effects on behavior and cognition (Elmore, Najafi et al. 2014, Hillmer, Holden et al. 2017). Although pharmacological CSF1R inhibition is a highly effective and flexible technique to deplete microglia, treatment relies on peripheral administration of a tiny molecule that, like any exogenously delivered medication, may have off-target consequences. Additionally, because CSF1R is expressed on every myeloid cell, inhibiting CSF1R can also prevent peripheral myeloid cell populations from signaling through this receptor. However, myeloid cell populations in the blood and spleen did not show any appreciable changes during trials (Mok, Koya et al. 2014, Hilla, Diekmann et al. 2017, Merry, Brooks et al. 2020).

1.6 Microglia repopulation

Depleted microglia are able to repopulate *in vivo*, albeit there is controversy over where the repopulated microglia originated from (Elmore, Lee et al. 2015). Among other things, it was proposed that peripheral macrophage infiltration in the brain aids in the development of new microglia (Varvel, Grathwohl et al. 2012). In terms of density, morphology, gene expression and immune response, these repopulating microglia finally resemble their original counterparts in every way. In contrast, it has been demonstrated that residual microglia proliferate and refill the entire brain (Huang, Xu et al. 2018). Another study revealed that microglia repopulation is done by a combination of local proliferation of residual microglia and infiltration of macrophages (Lund, Pieber et al. 2018). Nevertheless, experiments concerning the repopulation in the retina have shown that they migrate back from two different origins (Huang, Xu et al. 2018). On one hand, it was found that some microglia in the optic nerve survived after CSF1R inhibition. Therefore, these microglia were stained with dtTomato and it was shown that dtTomato⁺ microglia first appeared in the central region of the retina, close to the optic nerve head, before spreading radially towards the periphery. These findings strongly imply that the newly repopulated microglia in the center originate from residual microglia in the optic nerve. On the other hand, the majority of repopulated microglia in the periphery of the retina were dtTomato⁻, suggesting a distinct origin from the center-emerging cells. In order to identify the origin, the ciliary body and iris were examined in detail because these tissues are linked to the peripheral retina. For that reason, retinas lacking microglia were cultivated with or without the ciliary body and iris. Here, only ciliary body / iris-connected retinal explants showed peripheral

microglia. These microglia migrate from the periphery to the central region of the retina. These results indicate that the periphery-emerging microglia derived from ciliary body and iris macrophages. Repopulated microglia have a distinctive gene expression pattern and morphological markers that may result in a particular functional profile (Lund, Pieber et al. 2018). However, it has been demonstrated that low doses of lipopolysaccharide (LPS) can induce an inflammatory response in newly repopulated microglia, indicating that these cells are just as susceptible as resident microglia (Elmore, Lee et al. 2015).

1.7 Aims of the study

The CNS' resident immune cells are identified as microglia. Chronic activation of microglia causes excessive phagocytosis of stressed but still viable photoreceptors as well as persistent release of neurotoxic substances. Thus, in retinal degenerative diseases, over-reactive microglia play a significant role in retinal degeneration and vision loss. For these reasons microglia offer themselves as a perfect target for the treatment of retinal degenerative diseases like AMD. The survival of microglia depends strongly on CSF1R signaling. Blocking of CSF1R signaling with the potent inhibitor PLX3397 leads to a rapid and complete depletion of microglia. Moreover, it has been shown that after cessation of PLX3397, microglia repopulate within a few days. Here, we proposed that, in a light damage paradigm that simulates some aspects of dry AMD, microglia depletion with PLX3397 probably reduces the extent of retinal degeneration. On one hand, we wanted to investigate the effects of preventive microglia depletion in a mouse model acute retinal degeneration. In this instance, photoreceptor phagocytosis and associated retinal degeneration should be reduced since microglia are no longer present. It should also be understood that the complete depletion of microglia results in the loss of all beneficial homeostatic properties, rendering microglia depletion a double-edged sword. On the other hand, we wanted to examine the effects of curative microglia depletion after the onset of retinal degeneration. In this context, we focused on the differences in reactivity between naïve microglia and newly repopulated microglia. We predicted that depletion followed by repopulation would activate a reset mechanism that would sensitize microglia and attenuate their over-reactivity, preventing them from causing retinal degeneration and the accompanying phagocytosis of photoreceptors.

2 Material and Methods

2.1. Cell culture

2.1.1 Maintaining and subculturing of cell lines

661W photoreceptor cells (Department of Cell Biology, University of Oklahoma Health Science Center, USA) were maintained at 37°C in a humidified atmosphere with 5% CO₂ as they were cultured in a monolayer in Dulbecco's Modified Eagle Medium (DMEM) high glucose supplemented with 10% fetal calf serum (FCS) and 1% Penicillin-Streptomycin (P/S). Cells were washed with 1x phosphate-buffered saline (PBS) and then treated with 1x trypsin-EDTA for one minute at 37°C to detach adherent cells once they had reached around 90% confluence. By adding an equal proportion of DMEM high glucose medium supplemented with 10% FCS and 1% P/S, the process was stopped. A Neubauer chamber was used to count the cells for further processing after they had been collected, centrifuged at 300 x g for 5 min, and then resuspended in DMEM high glucose medium supplemented with 10% FCS and 1% P/S. BV-2 murine microglia cells (Blasi, Barluzzi et al. 1990) from passages 8 through 15 were utilized and grown at 37°C with a humidified 5% CO₂ atmosphere. FCS at 5%, P/S at 1%, L-Glutamine at 3 mM, and 50 µM β-Mercaptoethanol were all included in the Roswell Park Memorial Institute (RPMI) 1640 medium, in which BV-2 cells were cultured. Cells were split with a cell-scraper for further processing when they were at 90% confluence, and the medium was changed every three days. The same medium that was utilized in the earlier approach to grow 661W photoreceptor cells was employed to cultivate Human Embryonic Kidney (HEK) 293 cells. In the further course, the HEK293 cells received the same treatment that was necessary for the cultivation of BV-2 microglia cells, the only difference being the culture medium, which was described in the upper section.

2.1.2 PLX3397 stimulation

The CSF1R inhibitor PLX3397 was purchased from MedChemExpress, diluted in dimethyl sulfoxide (DMSO) to a stock solution of 10 mM and stored at -80°C until further use. Cells were cultivated in 96-well or 12-well plates, with 8,000 or 150,000 cells per well. After overnight attachment, cells were treated with PLX3397 diluted to the desired concentrations in a culture medium suited for the cell line. The following course was stimulated for either 24 or 48 h (Figure 6).

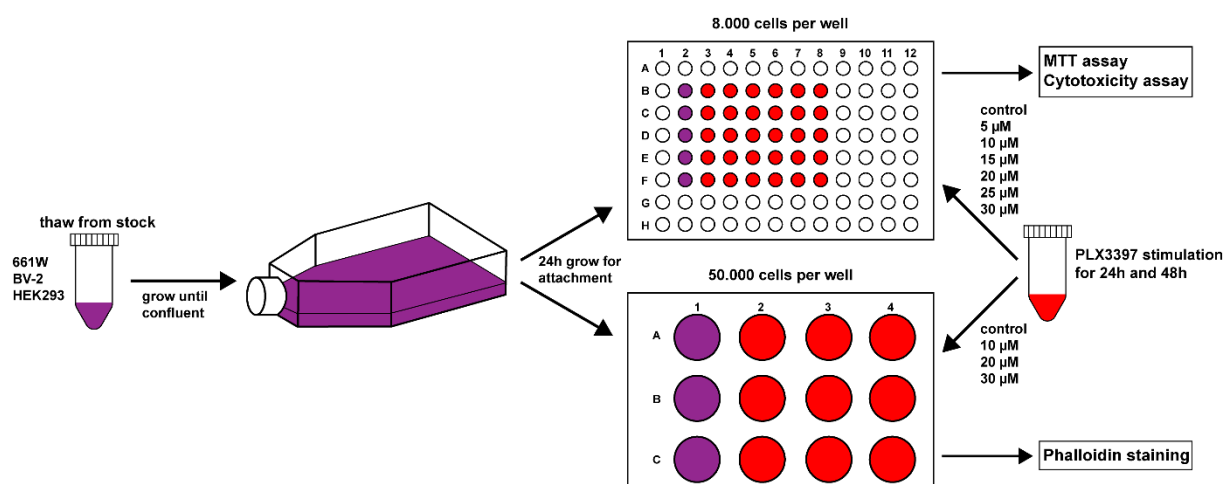


Figure 6 Effects of PLX3397 in different cell lines on morphology and viability. 661W, BV-2 and HEK293 cells were thawed from liquid nitrogen stock and cultivated in T75 flasks. For PLX3397 stimulation, they were seeded in 96-well plates (cytotoxicity and MTT assay) or in 12-well plates (phalloidin stainings). PLX3397 concentrations ranged from either 5 µM to 30 µM (in steps of 5 for cytotoxicity and MTT assay) or from 10 to 30 (in steps of 10 for phalloidin stainings).

2.1.3 Cell viability assay

The CellTiter 96® assay from Promega measures the reductive activity of the tetrazolium molecule as it is enzymatically converted to water-insoluble formazan crystals by dehydrogenases found in the mitochondria of living cells. Cells were adjusted to the target concentration and then 100 µl were added to a 96-well plate. The cells were given 24 h to attach. Subsequently, each well received 100 µl of PLX3397 concentrations that have been serially diluted. 15 µl of the Dye Solution were added to each well after the allotted PLX3397 incubation time. The plate was then placed in a humidified CO₂ incubator and kept at 37°C for one hour. Each well received 100 µl of Stop Solution when the incubation time had ended. Finally, the absorbance was measured at 570 nm. The IC₅₀ value was determined from these data.

2.1.4 Cell death assay

The purpose of Promega's CellTox™ Green Cytotoxicity assay was to evaluate cytotoxicity in cell culture following experimental treatment. The assay utilizes an asymmetric cyanine dye that selectively stains the DNA of dead cells while excluding living cells. CellTox™ green dye was transferred to the assay buffer bottle and diluted in a 1:500 ratio to create the CellTox™ green reagent. To guarantee homogeneity, the combined solution of assay buffer and CellTox™ green dye was blended in a vortex mixer. 50 µl of cells were added to a 96-well plate after cells had been adjusted to the target concentration. Cells were allowed to adhere for 24 h. Then, in a 96-well configuration. 50 µl of serially diluted PLX3397 concentrations were added to each well. Following the specified PLX3397 incubation period, 100 µl of the CellTox™ green

reagent were applied to each well. To achieve homogeneity, the plate was then shaken orbitally for one minute at 700-900 rpm. After that, it was incubated at room temperature for 15 min while being protected from light. The fluorescence was measured at 485-500 nm_{Ex} and 520-530 nm_{Em}. The EC₅₀ value was determined from these data.

2.1.5 Morphological analysis

The cells were sown on coverslips in 12-well plates at the desired density. Cells were treated with serially diluted PLX3397 after 24 h of attachment and incubated for either 24 or 48 h. Afterwards, cells were fixed for 20 min with 4% paraformaldehyde (PFA) and then rinsed with PBS after receiving PLX3397 treatment. Subsequently the cytoskeleton was labeled for an hour while being protected from light with 0.01 g/ml Phalloidin-TRITC (Sigma-Aldrich). The cells were washed with 1x PBS before being put on microscope slides with a mounting medium that contained 4',6-diamino-2-phenylindole (DAPI). Before analyzing cell morphology under a microscope, the slides must finally dry.

2.2 Mouse experiments

2.2.1 Mouse husbandry

The National Institute of Health and the local government committee's (Tierschutzkommission acc. §15 TSchG des Landesamt für Natur, Umwelt und Verbraucherschutz Nordrhein-Westfalen) criteria were followed in all mouse experiments. The animals were kept in a system of individually ventilated cages (M 500, Tecniplast® Greenline) with a maximum of five animals per cage under SPF conditions. The temperature and relative humidity were set to 22±2°C and 45-65% relative humidity, respectively, while the light was adjusted to a 12h/12h light/dark cycle. Acidified water and irradiated phytoestrogen-free standard rodent diet (Altromin 1314) were accessible *ad libitum*.

2.2.2 Mouse strain

Experiments were carried out on 8 to 12 week old male and female mice. Throughout the work heterozygous *CX3CR-1^{GFP/-}* reporter mice were used, which were kindly provided by Deniz Hos (Ophthalmology, University Hospital of Cologne). Here, coding exon 2 of the *chemokine (C-X3-C motif) receptor 1 (Cx3cr1)* gene in mice has the first 390 base pairs replaced with an enhanced green fluorescent protein (EGFP) sequence. Therefore, monocytes dendritic cells, NK cells, brain and retinal microglia express EGFP. The first 390 base pairs of exon 2 were disrupted using a targeting vector including an EGFP cDNA sequence, *loxP*-flanked neomycin

Material and Methods

resistance gene, herpes simplex virus thymidine kinase gene, and simian virus 40 polyadenylation site sequence. To remove the selection cassette, the construct was electroporated into 129P2/OlaHsd derived E14.1 embryonic stem cells that had previously been transiently transfected with a Cre recombinase vector. Blastocyst recipients received injections of embryonic stem cells that had undergone Cre-mediated recombination successfully. The resulting chimeric mice were backcrossed to C57BL/6 (Jung, Aliberti et al. 2000). These *CX3CR-1^{GFP}* reporter mice could be helpful for investigations on macrophage migration and trafficking. The light-sensitive RPE-specific protein (65 kDa) (RPE65) Leu450 variant and the wildtype *Crb1^{rd8}* (retinal degeneration 8) were genetically inherited in all of the animals utilized in this study from the BALB/cJ strain.

2.2.3 PLX3397 administration

The CSF1R inhibitor PLX3397 hydrochloride was obtained from MedChemExpress and added by Altromin to the standard rodent diet at a rate of 1.2 g or 0.15 g per kilogram of diet. Depending on the experimental design, the mice received the PLX3397 diet for a maximum of 14 days.

2.2.4 Light exposure regime

Prior to being exposed to light, mice were dark adapted for 16 hours. Immediately prior to the exposure to light, pupils were dilated with 2.5% phenylephrine and 0.5% tropicamide (Pharmacy, University Hospital Cologne) under diffuse red light. To avoid covering, mice were put into separate cages with reflective aluminum foil coating. The mice were exposed to bright white light for an hour at an intensity of 15,000 or 5,000 lux, which had a blue peak in its spectrum. The mice were returned to their regular light cycle after being exposed to light pending further investigations.

2.2.5 Experimental setup

The following provides an overview of the different experimental investigations. In the first experimental setup, the orally administered CSF1R inhibitor will be shown to cross the BRB into the central nervous system. For this reason, two distinct concentrations of PLX3397 (1200 and 150 ppm) formulated in standard rodent diet were provided and evaluated in comparison to the standard rodent diet (Figure 7). Subsequently, the concentration in the retina was determined by liquid chromatography - mass spectrometry (LC-MS).

Material and Methods

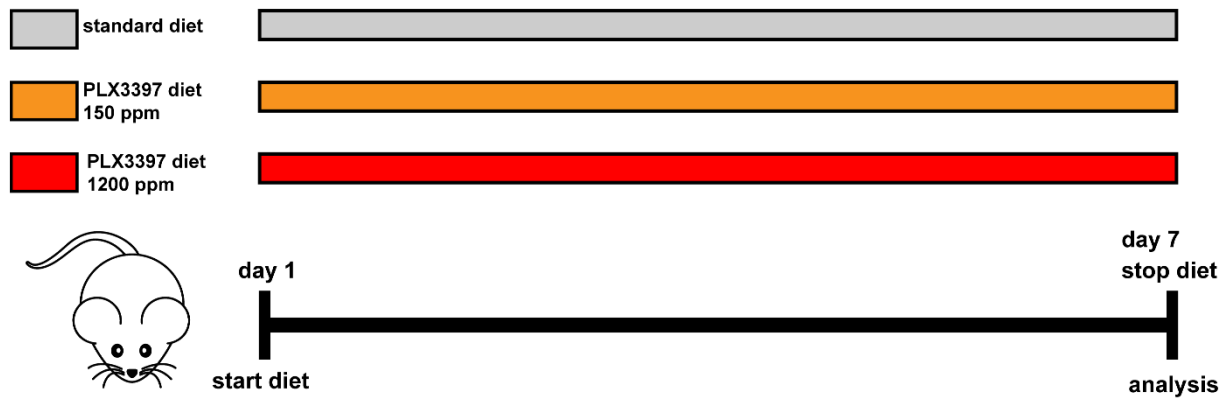


Figure 7 PLX3397 concentration determination. For 7 days, the *CX3CR-1^{GFP/-}* reporter mice were fed diets containing 1200 and 150 ppm of PLX3397, whereas the control group was given the standard rodent diet. The eyes were taken out after 7 days of dieting, and the retina was used for LC-MS analysis.

The second experimental setup is preventive and will be investigating the effects of microglia depletion in a mouse model of acute retinal degeneration. In order to induce retinal degeneration, two groups of mice were exposed to 15,000 lux of white light for one hour. Group four received PLX3397 diet beginning 7 days prior to the light exposure to ensure that microglia were depleted before the onset of retinal degeneration and continued until the time of analysis, whereas group three received a control diet. Groups one and two, in contrast, were not exposed to light, and group two again received PLX3397 diet for the entire duration of the experiment while group one received the standard rodent diet (Figure 8). 4 days after being exposed to light, mice were sacrificed and the eyes were retrieved and processed for further examinations.

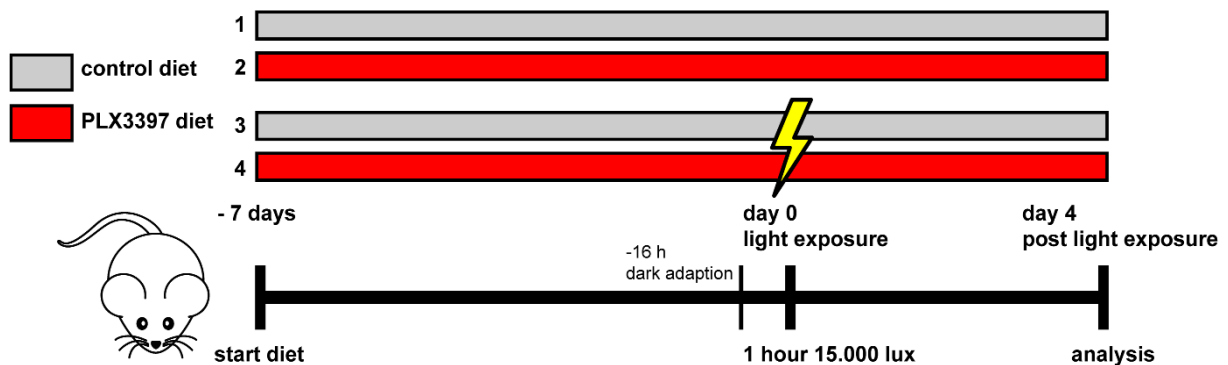


Figure 8 Preventive microglia depletion in the light damage model of retinal degeneration. *CX3CR-1^{GFP/-}* reporter mice were fed PLX3397 diet 7 days before being exposed to white light with an intensity of 15,000 lux in order to make sure that microglia were absent when retinal degeneration was induced. In contrast, in another group microglia were present. As a baseline, there were two other groups that had not been exposed to white light. In this case, one group was given PLX3397 diet, and the other the standard rodent diet.

Material and Methods

The third experimental setup aimed to discover more about the timespan and progression of retinal microglia repopulation. Consequently, mice received a 7-day PLX3397 diet to completely deplete microglia. Afterwards, PLX3397 diet was switched to the standard rodent diet, followed by analyses 4, 7 and 10 days after cessation of PLX3397 diet (Figure 9).

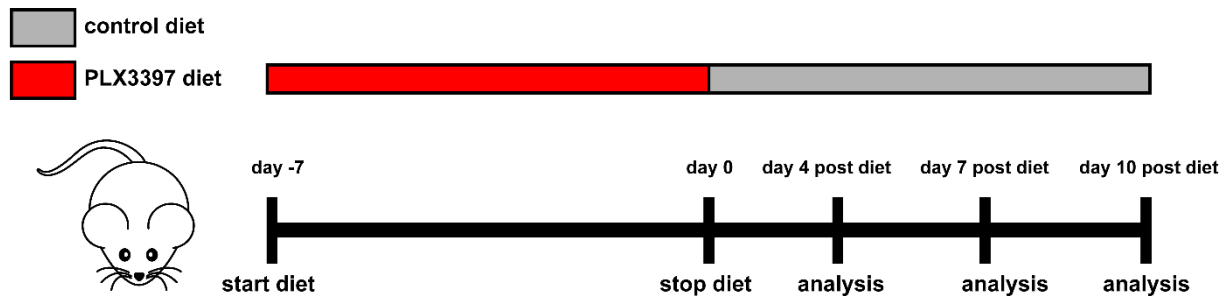


Figure 9 Documentation of retinal microglia repopulation. *CX3CR-1^{GFP/-}* reporter mice were fed with PLX3397 diet for 7 days to ensure all microglia were absent. Then PLX3397 diet was stopped and switched to the standard rodent diet. The eyes were collected and prepared for further examination 4, 7 and 10 days after ceasing PLX3397 diet.

The fourth experimental setup was designed to look at how retinal degeneration develops and progresses in a 5,000 lux low light exposure regime for one hour, with analysis taking place up to 14 days later. Eyes were taken out and prepared for further examinations at 4, 7, 10 and 14 days that followed light exposure in order to get a thorough overview (Figure 10).

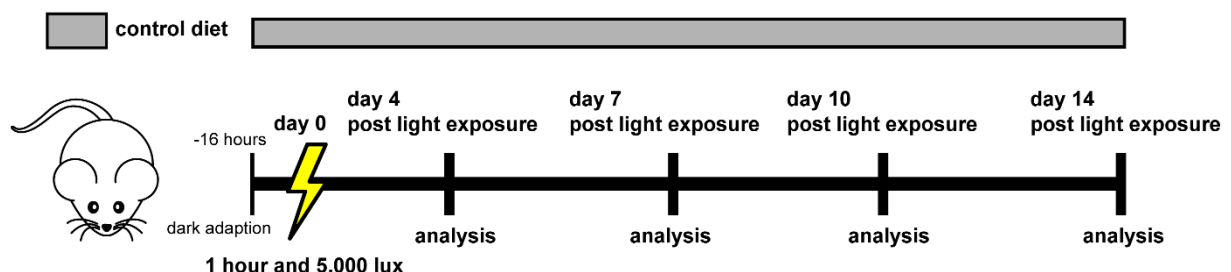


Figure 10 Development of retinal degeneration in a low light exposure regime. *CX3CR-1^{GFP/-}* reporter mice were exposed to 5,000 lux of white light. 4, 7, 10 and 14 days after light exposure, retinal degeneration was analyzed.

The fifth experimental setup was curative and was designed to investigate the effect of microglia depletion 14 days after the onset of retinal degeneration. Therefore, all groups were exposed to white light with an intensity of 5,000 lux for one hour. Because the analysis was conducted 14 days after the commencement of retinal degeneration and 15,000 lux would be excessively intense throughout this time, this intensity was chosen. In addition, it was investigated whether early or late depletion made a difference in the progression of retinal degeneration. Early depletion resulted in repopulation of microglia. Here, the effect of newly repopulated microglia on the course of retinal degeneration will be investigated and compared

Material and Methods

to naïve microglia. Group one was given the standard rodent diet all through the entire period, while group two was provided PLX3397 diet immediately upon light exposure until analysis. Among groups three and four, there was a diet switch. Group three was given standard rodent diet from day 0 to day 7 following light exposure and was subsequently switched from day 7 to day 14 to PLX3397 diet. Group four received PLX3397 diet at first and then switched to the standard rodent diet from days 7 to 14 after being exposed to light (Figure 11).

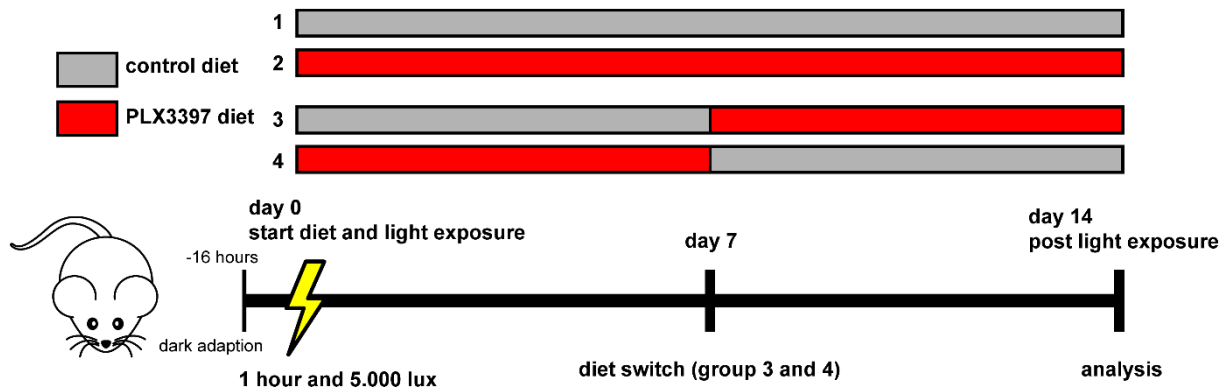


Figure 11 Curative microglia depletion in a low light exposure regime. *CX3CR-1^{GFP/-}* reporter mice were exposed to 5,000 lux of white light. Dieting begun as soon as mice were exposed to light. Group 1 was given the standard rodent diet until 14 days following light exposure, while group 2 was given PLX3397 diet. Group 3 started with the standard rodent diet and was switched to PLX3397 diet from day 7 to day 14, while group 4 was fed the opposite way.

2.2.6 In vivo imaging

For imaging, mice were administered with ketamine (Ketavet, 100 mg/kg) and xylazine (Bayer, 2% Rompun, 5 mg/kg) in order to anesthetize them. 2.5% phenylephrine and 0.5% tropicamide were used to dilate their pupils. Spectral-domain optical coherence tomography (SD-OCT) and BluePeak laser autofluorescence (BAF), were used with the Spectrails™ HRA/OCT instrument to measure retinal thickness and fundus autofluorescence, respectively, at the time points explained in the upper section. Software from Heidelberg called Heidelberg Eye Explorer (HEYEX) was used to construct retinal thickness heatmaps. The average of four segments surrounding the optic nerve were accounted for one n throughout analysis utilizing 3 mm and 6 mm diameter values.

2.3 Molecular biology

2.3.1 Genotyping

Using the HotSHOT technique (Truett, Heeger et al. 2000), genomic DNA was extracted from ear punches taken between P18 and P21. The samples were first processed for 15 min at 95 °C in alkaline lysis buffer, then for 5 min on ice. Subsequently, the DNA was diluted to a

Material and Methods

concentration of 25 ng/μl after being combined with an equivalent amount of neutralizing buffer. Using a NANODrop 2000 (Thermo Fischer Scientific) Spectrophotometer, the purity of DNA was evaluated. Pure was defined as having a 260/280 nm absorbance ratio between 1.8 and 2.0. Polymerase chain reaction (PCR), based on genotyping techniques from Jackson Laboratories, were used to establish the genotyping of *CX3CR-1^{GFP/-}* mice. The customized primer (purchased from IDT) were used together with Taq-S PCR kit (Genaxxon). Each amplification was carried out in a reaction volume of 25 μl that contained 50 ng of DNA, 25 pmol of each primer, 25 μM of dNTP mix, 1x reaction buffer S, and one unit of Taq polymerase. Following amplification, Tyrosinase samples were digested with 1 unit of HpyF3I enzymes and RPE65 samples were digested with 1 unit of HpyF10VI in 1x Buffer Tango at 37°C for 2 h, respectively. The samples were then thermally inactivated at 65°C or 80°C for 20 min. Genotyping-derived amplified DNA was examined using gel electrophoresis. DNA samples were combined with loading dye and electrophoresed at 120 V in a 2% agarose gel. The size of amplicons was identified under UV light (Gel iX20 Imager, Intrax). Primer and PCR programs are listed in table 1 and 2, respectively.

Table 1 List of genotyping primer used in this study.

Gene	Primer	Sequence 5' - 3'	Amplicon size [bp]
<i>Cx3cr1</i>	Forward wildtype	gtcttcacgttcggtctggt	Wildtype: 410
	Forward mutant	ctccccctgaacctgaaac	Mutant: 500
	Reverse common	cccagacactcgttgctctt	Heterozygous: 410 and 500
<i>RPE65</i>	Forward	cactgtggtctctgctatcttc	Met: 674
	Reverse	ggtgcagttccattcagtt	Leu: 437; 236 (after digest)
<i>Crb1^{rd8}</i>	Forward wildtype	gtgaagacagctacagtctgatc	Wildtype: 220
	Forward mutant	gcccctgttgcatggaggaaactggaagacagctacagtctctctg	Mutant: 244
	Reverse common	gccccattgcacactgatgac	
<i>Tyrosinase</i>	Forward	aagaatgctgccaccatg	Cys: 165; 110; 73; 12 (after digest)
	Reverse	gacatagactgagctgatagtatgtt	Ser: 130; 110; 73; 35; 12 (after digest)

Table 2 List of genotyping PCR programs used in this study

Gene	Step	Temperature [°C]	Time	Cycles
<i>Cx3cr1</i>	Initial denaturation	94	2 min	x1
	Denaturation	94	20 sec	x10
	Annealing	65	15 sec	
	Elongation	68	10 sec	
	Denaturation	94	15 sec	x28
	Annealing	60	15 sec	
	Elongation	72	10 sec	
	Final elongation	72	2 min	x1
<i>RPE65</i>	Initial denaturation	95	2 min	x1
	Denaturation	95	20 sec	x35
	Annealing	56	15 sec	
	Elongation	72	20 sec	
	Final elongation	72	2 min	x1
<i>Crb1^{rd8}</i>	Initial denaturation	95	2 min	x1
	Denaturation	95	20 sec	x35
	Annealing	58 (WT) ; 65 (MUT)	15 sec	
	Elongation	72	20 sec	
	Final elongation	72	2 min	x1
<i>Tyrosinase</i>	Initial denaturation	95	2 min	x1
	Denaturation	95	20 sec	x40
	Annealing	58	15 sec	
	Elongation	72	20 sec	
	Final elongation	72	2 min	x1

2.3.2 Quantification of PLX3397 in the retina

Retinas of enucleated eyes were cut open and homogenized with 80 µl ethanol. After centrifuging the samples at 16.000 x g at 4°C for 15 min, the supernatant was then transferred into a separate tube. The supernatant from the preceding pellet was added to the remaining pellet after it had been washed twice with 40 µl of ethanol. After that, the samples were kept at -80°C for processing. The LC-MS facility (Dr. Sabine Metzger, Methodenentwicklung LC-MS, Department für Biologie, Universität zu Köln) then carried out the analysis.

2.3.3 Immunohistochemistry

Enucleated eyes were fixed in 4% PFA at room temperature (RT) for 2 h. For flat mounts, retinas were cut open, permeabilized, and unspecific antigen binding sites were then blocked using Perm/Block Buffer overnight at 4°C. Subsequently, retinal flat mounts were incubated with the primary antibody diluted in Perm/Block (1:500) for 24 h at 4°C. Following incubation of the secondary antibody diluted in PBST-X (0.3% Triton X-100 in PBS) (1:800) for one hour at RT. Finally, retinal flat mounts were embedded with Vectashield® HardSet™ fluorescence mounting medium, placed on microscope slides and allowed to dry thoroughly until examination under the microscope. For immunohistochemical analysis of cryosections, after fixation in 4% PFA, they were incubated stepwise with increasing concentration in sucrose (10%, 20% and 30%) for dehydration. They were then embedded in Optimal Cutting Temperature (O.C.T.™) medium and placed on dry ice. Subsequently, sections with a thickness of 10 µm were prepared in a cryostat (Leica, CM3050 S) and stored at -20°C until further processing. Unspecific antigens were blocked with BLOTTO Buffer for 30 min at RT after frozen slides were thawed and rehydrated in PBS for 10 minutes. Then an overnight incubation at 4°C with primary antibody diluted in BLOTTO Buffer (1:500) followed. Cryosections were incubated with a secondary antibody for an hour at RT before being covered with a DAPI-containing mounting medium. Slides must finally dry before examination under a microscope.

Table 3 List of antibodies used for immunohistochemistry

Antibodies	Species	Dilution	Manufacturer, Cat. No
anti-GFAP	Rabbit, polyclonal	1:500	Sigma-Aldrich; G9269
anti-cone arrestin	Rabbit, polyclonal	1:500	Sigma-Aldrich; 32160702
Alexa Fluor® 594	Donkey anti-rabbit IgG	1:800	Invitrogen; A11007
Alexa Fluor® 647	Donkey anti-rabbit IgG	1:800	Invitrogen; A-31573

2.3.4 Cell death detection assay

The in situ cell death detection kit RED (Roche) was used in accordance with the manufacturer's instructions to detect and quantify retinal cell death on cryosections using terminal deoxynucleotidyl transferase dUTP nick end labeling (TUNEL).

2.3.5 RNA isolation, cDNA synthesis, and qRT-PCR

RNA was extracted from retinal and RPE/choroidal tissue in line with the manufacturer's instructions using the Qiagen RNeasy® Micro Plus kit. Thermo Fischer's reverse transcriptase

Material and Methods

kit was used as directed by the manufacturer to create cDNA. The RevertAid First Strand cDNA Synthesis kit was used to synthesize first-strand cDNA from whole mRNA. Quantitative real-time PCR was used to determine the transcript levels of pro- and anti-inflammatory markers using the primers specified in table 5 respectively, and was carried out in a LightCycler® 480 II with SYBR® Green detection in accordance with the manufacturer's instructions. The housekeeping gene *ATP synthase, H⁺-transporting, mitochondrial F1 complex, β polypeptide* (*Atp5b*) was employed. Technical duplicate measurements were made, and the relative quantification of the results was done using the $\Delta\Delta$ CT threshold computation.

Table 4 List of SYBR® Green qRT-PCR primer used in this study

Gene	Forward primer (5'-3')	Reverse primer (5'-3')	NM accession number
<i>Atp5b</i>	ggcacaatggaggaaagg	tcagcaggcacatagatagcc	NM_016774.3
<i>Aif-1</i>	ggatttgcagggaggaaaag	tgggatcatcgaggaattg	NM_019467.4
<i>Il-1β</i>	tgtaatgaaagacggcacacc	tcttcttgggtattgcttg	NM_008361.4
<i>Il-6</i>	gctaccaaactggatataatcagga	ccaggtagctatggtactccagaa	NM_001314054.1
<i>Tspo</i>	ggaacaaccagcgactgc	gtacaaagtaggctcccatgaa	NM_009775.4
<i>Tnfa</i>	ctgtagcccacgtcgtagc	ttgagatccatgccgttg	NM_001278601.1
<i>Ccl2</i>	catccacgtgttggtca	gatcatcttgcgttggaatgagt	NM_011333.3
<i>Bdnf</i>	ggctgacacttttgagcacgt	ctccaaaggcacttgactgctg	NM_001048141.1
<i>Ngfr</i>	ggagagaaaactgcacagcgaca	caggctactgtagaggttgcca	NM_033217.3
<i>Synaptophysin</i>	ttggcttcgtgaaggtgctgca	actctccgtctgttggcacac	NM_009305.2

Table 5 qRT-PCR program used in this study

Target °C	Acquisition mode	Hold (h:mm:ss)	Ramp rate (°C/s)	Acquisition (per °C)
Pre-incubation 1 cycles				
95	none	00:05:00	4.8	none
Amplification 45 cycles				
95	none	00:00:10	4.8	none
60	none	00:00:10	2.5	none
72	single	00:00:10	4.8	none
Melting curve 1 cycle				
95	none	00:00:05	4.8	none
65	none	00:01:00	2.5	none
97	continuous		0.57	1
Cooling 1 cycle				
40	none	00:00:30	2.5	none

2.4 Data analysis

2.4.1 Image analysis

Morphological analysis of microglia in retinal flat mounts was done with a Java plugin for FIJI is just ImageJ (FIJI) called MotiQ (version 3.1.1), a public and fully automated analytical program. For this MotiQ was provided two-dimensional images with mean intensity projection (MIP). Here, six morphological parameters were analyzed. First, the ramification index is a unitless value that describes the segmentation and morphology of the cells. With a high ramification index, the cells have long, branched processes and occupy a large area. With a low ramification index, they are small, roundish and have few to no branched processes (Figure 12.A). Second, the spanned area is the region that is bounded by the polygonal object created by connecting the outer points of the dendritic arborizations (Figure 12.A). Third, the entire tree length is the sum of all dendritic segments defined in the skeletonized cell body (black) (Figure 12.B). Fourth, the number of junctions is defined as the point where more than two branches meet (red dots). The fifth and sixth parameters analyzed are the number of branches (black lines) and end-points (blue dots) identified in the arborization's skeletonized representation (Figure 12.C). In addition, the outline of the cell lines in the in vitro experiments was determined, which corresponds to the length of the skeletonized cell body. Here high values indicate that the cell is in a ramified shape, while a low value indicates an amoeboid shape.

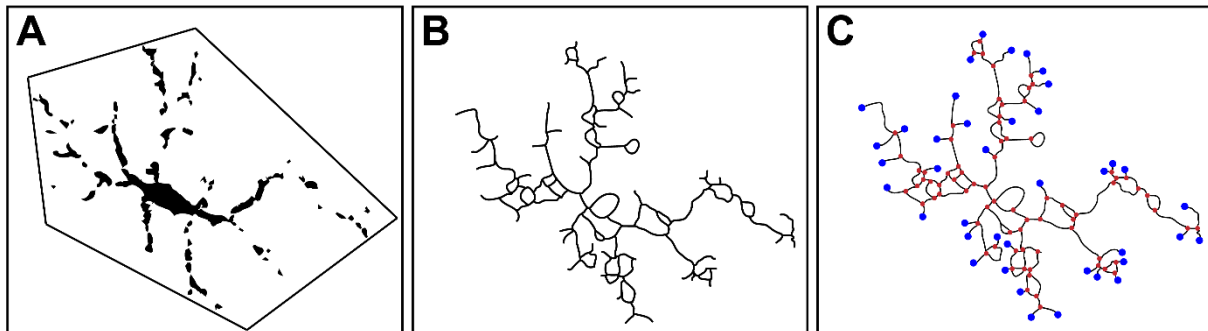


Figure 12 Identification points of the analyzed morphological parameters. Throughout the study, six morphological parameters were analyzed: Ramification index (black, skeletonized cell body), spanned area (area circumscribed by the polygonal object), tree length (sum of all dendritic segments; black lines), number of junctions (where more than two branches meet; red dots), number of branches (amount of dendritic segments; black lines), and number of end-points (blue dots).

The amount of cone-arrestin⁺ cells in retinal flat mounts was counted with the particle analyzer tool from ImageJ.

The percentage of TUNEL⁺ cells in ONL was calculated to assess the cell death rate. The total number of ONL and both TUNEL⁺ cells were counted for this purpose with ImageJ's multi-pointer tool.

Material and Methods

In order to analyze microglial migration, *CX3CR-1^{GFP/-}* cells in the ONL, OPL, INL, and IPL were also counted using the multi-pointer tool.

2.4.2 Statistical analysis

Throughout the study, all data were analyzed and plotted with GraphPad Prism (version 8.4.3). Both *in vitro* and *in vivo* data were subjected to a normality test prior to statistical analysis. For the *in vitro* data, an ordinary one-way ANOVA was used followed by Dunnett's multiple comparison test. Here, all micrographs shown are representative images of at least three independent experiments with biological triplicates. IC₅₀ and EC₅₀ values were calculated by generating a spline curve from the plotted data. For the *in vivo* data, a two-way ANOVA was used followed by Tukey's multiple comparison test (*p < 0.05, **p < 0.01, ***p ≤ 0.001). n-numbers represent one retina or one RPE, respectively, from at least three independent experiments. Graphs show the mean and error bars show the standard deviation.

2.5 Chemicals, buffers, kits, devices, and software

Table 7 has a list of all the chemical compounds, whereas tables 8 and 9 contain lists of the buffers and kits used in this study, respectively. Furthermore, all devices (Table 10) and software (Table 11) used throughout the study are also listed.

Table 6 List of chemicals and reagents used in this study

Name	Manufacturer, Cat. No.
Agarose	Biozym; 84004
Artelac® Splash	Bausch & Lomb; PZN 07706996
Bovine serum albumin (BSA)	Sigma-Aldrich; A9418
Bromophenol blue	Sigma-Aldrich; B-6131
Ethanol absolute	AppliChem; A3678
Ethanol, 70%	Carl Roth; T868.1
Ethidium bromide	Sigma-Aldrich; 46067
Ethylenediaminetetraacetic acid (EDTA)	Sigma-Aldrich; E9884
Fetal calf serum (FCS)	Gibco; 10270
Fluoromount-G with DAPI	Invitrogen; 00-4959-52
GeneRuler 100 bp plus	Thermo Scientific; SM0332
Glycerol	Sigma-Aldrich; 49781
HpyF10VI (Mvol)	Thermo Scientific; ER1731
HpyF3I (Ddel)	Thermo Scientific; ER1881
Hydrochloric acid (HCl), 37%	Carl Roth; X942.1
Ketaset 100 mg/ml	Zoetis; PZN 12467832

Material and Methods

Name	Manufacturer, Cat. No.
L-Glutamine, 200mM	Gibco; 25030
Milk powder (low fat)	Roth; T145.3
Normal donkey serum (NDS)	Linaris; ADI-NDKS-10
Penicillin/Streptomycin	Gibco; 15140
Pexidartinib 3397	MedChemExpress; HY-16749
Pexidartinib 3397 hydrochloride	MedChemExpress; HY-16749A
Phalloidin-TRITC	Sigma-Aldrich; P1951-.1MG
Phenylephrine 2.5% / Tropicamide 0.5%	University Hospital Cologne; Pharmacy
Rompun 2% (Xylazine)	Bayer; PZN 1320422
Roti Histofix 4%	Roth; P087.4
Sodium Chloride (NaCl) 0.9%	Fresenius Kabi; PZN 06605514
Sodium hydroxide (NaOH)	Merck; 1.06462
Sucrose	Roth; 4621.1
Tissue-Tek® optimal cutting temperature (O.C.T.™) compound	Sakura Finetek; 4583
TRIS	Carl Roth; 4855.3
Tri-Sodium citrate dihydrate	Roth; 3580
Triton X-100	Sigma-Aldrich; X100
Trypan Blue 0.4%	Thermo Scientific; 15250061
Vectashield® HardSet™ Mounting Medium	Vectashield®; H1400
β-Mercaptoethanol	Sigma-Aldrich; M-7154

Table 7 List of buffers and solutions used in this study

Buffer / Solution	Chemical composition / Manufacturer, Cat. No.
10x Buffer Tango	Thermo Scientific; BY5
Alkaline lysis buffer	25 mM NaOH 200 mM EDTA pH 12 in ddH ₂ O
Antibody solution	2% BSA 0.3% Triton X-100 in 1x PBS
BLOTTO	1% milk powder 0.3% Triton X-100 in 1x PBS
DMEM-high glucose	Sigma; D0819-500ML
DNA loading dye (6x)	30% Glycerol 0.25% bromophenol blue in ddH ₂ O
DNase I dilution buffer	50 mM TRIS-HCL 1 mg/ml BSA 10 nM MgCl ₂
Neutralization buffer	40 mM TRIS-HCL pH 5 in ddH ₂ O

Material and Methods

Buffer / Solution	Chemical composition / Manufacturer, Cat. No.
PBST-X	0.3% Triton X-100 in PBS
Perm / Block buffer	5% NDS 0.2% BSA 0.3% Triton X-100 in 1x PBS
Permeabilization Solution	0.1% Sodium Citrate 0.1% Triton X-100
Phosphate buffered saline (DPBS)	Gibco; 14190-094
Rosewell Park Memorial Institute (RPMI) medium	Gibco; 31870-025
TBE buffer (10x)	1 M Boric acid 1 M Tris pH 7.5 20 mM EDTA pH 8.0 in ddH ₂ O
Trypsin-EDTA (0.05 % phenol red)	Thermo Scientific; 25300054

Table 8 List of kits used in this study

Kit	Manufacturer, Cat. No
CellTiter 96 [®] Cell Proliferation Assay	Promega; G4000
CellTox Green Cytotoxicity Assay	Promega; G8741
In situ Cell Death Detection Kit, TMR red	Roche; 12156792910
RevertAid RT Kit	Thermo Scientific; K1691
RNeasy [®] Micro Kit	Qiagen; 74004
RNeasy [®] Micro Plus Kit	Qiagen; 74136
Takyon [™] No ROX Probe MasterMix blue dTTP	Eurogentec; UF-NPMT-B0701
Taq-S PCR Kit	Genaxxon Bioscience; M3313

Table 9 List of devices used in this study

Device	Manufacturer
Adventurer Pro Balance	Ohaus [®]
BlueMarine [™] 200 Electrophoresis Unit	SERVA Electrophoresis GmbH
Centrifuge 5415 R	Eppendorf
Centrifuge Mini Star	VWR International
Cryostat CM3050 S	Leica Biosystems
Explorer R Ex 124 Balance	Ohaus [®]
Galaxy 170S CO ₂ Incubator	Eppendorf
Heraeus Megafuge 40R Centrifuge	Thermo Scientific
Intas Gel iX20 Imager	Intas
LightCycler [®] 480 Instrument II	Roche Applied Science
Matrix [™] Multichannel Pipette	Thermo Scientific

Material and Methods

Device	Manufacturer
MSC-Advantage Hood	Thermo Scientific
NanoDrop 2000 Spectrophotometer	Thermo Scientific
Neubauer counting Chamber	OptikLabor
PeqSTAR 2x Cycler	Peqlab
See-saw rocker SSL4	Stuart®
Spectralis™ HRA+OCT	Heidelberg Engineering
Thermomixer Compact	Eppendorf
Vibracell 75115 Sonicator	Fisher Bioblock Scientific
Vortex-Genie™	Scientific Industries
Zeiss Imager M.2 with ApoTome.2	Zeiss
Zeiss Stemi 508 Stereo Microscope	Zeiss

Table 10 List of software used in this study

Software	Manufacturer
Adobe Illustrator	Adobe Systems
Adobe Photoshop	Adobe Systems
EndNote X9	Clarivate Analytics
GraphPad Prism 8 (v8.4.3)	GraphPad Software; Inc.
Heidelberg Eye Explorer (HEYEX)	Heidelberg Engineering
FIJI (v1.53v)	Wayne Rasband; NIH
Intras Gel Documentation Software	Intras Science Imaging
Light Cycler® 480 Software (v1.5.1)	Roche Applied Science
Microsoft Office 2016	Microsoft Corporation
NanoDrop 2000 Software	Thermo Scientific
Zen Blue Edition (v3.1)	Zeiss

3 Results

3.1. Potency of PLX3397 in different cell lines

In order to determine the potency of the CSF1R inhibitor PLX3397 in the following *in vitro* part of this study, the IC_{50} value was calculated in the course of the cell viability assay, since the metabolic activity decreases with increasing PLX3397 concentration. In contrast, the EC_{50} value had to be calculated when determining the cell death rate, since the amount of free DNA increased in the course of cell death with increasing PLX3397 concentration.

3.1.1 PLX3397 treatment reduces the metabolic activity in different cell lines

Initially, we wanted to investigate the effect of PLX3397 on metabolic activity in three different cell lines. Murine BV-2 microglia cells, whose proliferation and survival is strongly dependent on the CSF1R signaling pathway express CSF1R at high levels (Stanley and Chitu 2014). In further *in vivo* experiments, a complete microglia depletion was targeted. Therefore, a preliminary investigation of the effects of PLX3397 on microglia and photoreceptors in the retinal milieu was useful. 661W photoreceptor cells, which are an important component of the retina were also exposed to PLX3397 in the later course of the *in vivo* experiments with oral supplementation. These are known to express the CSF1R at very low levels (Cömert et al., unpublished). HEK293 cells were chosen as the last cell line because they do not possess the CSF1R and therefore non-specific binding and cytotoxicity of the inhibitor could be investigated on them (Cömert et al., unpublished). Metabolic activity after PLX3397 treatment was evaluated using a cell viability assay and the IC_{50} was determined (Figure 13). After 24 h, only the IC_{50} value for the BV-2 cells could be determined, which was 14.399 μ M (Figure 13.A), but not for the 661W photoreceptor and HEK293 cells (Figure 13.B; C). After 48 h, it was possible to determine the IC_{50} value for the BV-2 and 661W cells as well as for the HEK293 cells. These values were 17.550 μ M, 26.933 μ M and 27.838 μ M (Figure 13.D – F). Here it could be seen that although IC_{50} values were available for all cell lines, the IC_{50} value for the 661W and HEK293 cells was higher compared to the BV-2 cells and was only slightly lower than the 30 μ M PLX3397 treatment. This attests to the high specificity of the inhibitor, as only extremely high concentrations had any discernible effect on the metabolism of cells that lack the receptor entirely or only minimally.

Results

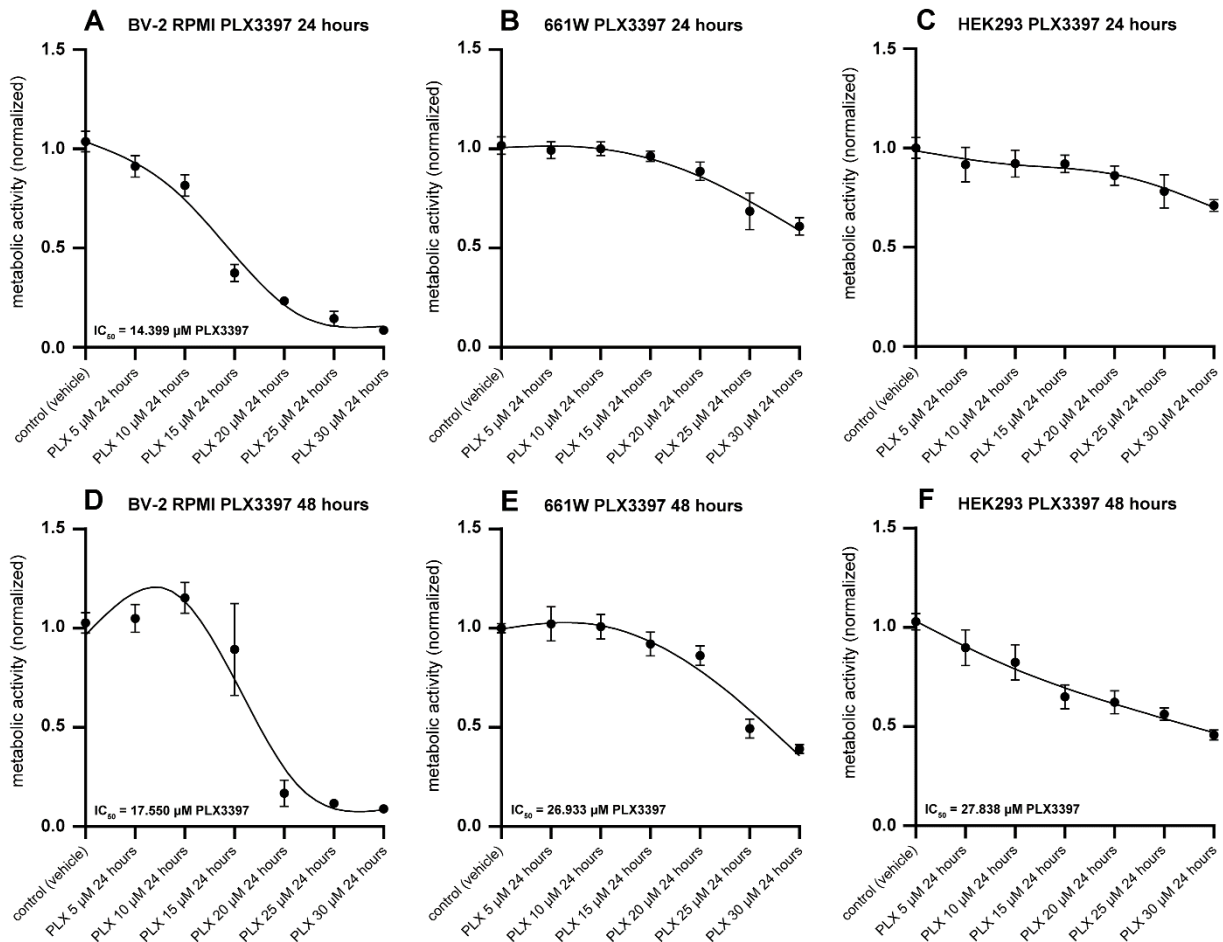


Figure 13 Effect of PLX3397 on metabolic activity in different cell lines. PLX3397 was used to treat BV-2, 661W and HEK293 cells for 24 or 48 h at concentrations ranging from 5 μM to 30 μM in 5 μM increments. After 24 h, it was only feasible to determine the IC_{50} value in BV-2 cells, where it is 14.399 μM (A); it was not possible to do so in 661W and HEK293 cells (B and C). Only after 48 h, the effect of PLX3397 on 661W and HEK293 cells was sufficient to determine an IC_{50} value. For BV-2, 661W and HEK293 cells, they are 17.550 μM , 26.933 μM and 27.838 μM , respectively (D – F) ($n = 10$).

3.1.2 PLX3397 treatment increases death rate in different cell lines

In a subsequent course, we sought to look into the connection between metabolic activity and the cell death rate following treatment with PLX3397. With the BV-2, 661W, and HEK293 cells, a cytotoxicity experiment was carried out for this aim (Figure 14). Because an EC_{50} value could only be determined for the BV-2 cells after 24 h of PLX3397 treatment, the cell death rate trend was similar to that of the metabolic activity (Figure 14.A). This value, which was 8.413 μM , was much lower than the IC_{50} value for the metabolic activity that was ascertained previously. An EC_{50} value for each of the three cell lines could be determined after 48 h of PLX3397 treatment. For the BV-2 cells, this was 4.464 μM , for the 661W cells it was 18.583 μM , and for the HEK293 cells it was 21.259 μM (Figure 14.D – F). The half-maximum effectiveness of PLX3397 was also obtained in this scenario at lower concentrations. However, PLX 3397 was shown to have the strongest effect on mortality rate in BV-2 cells, followed by photoreceptors and HEK293 cells.

Results

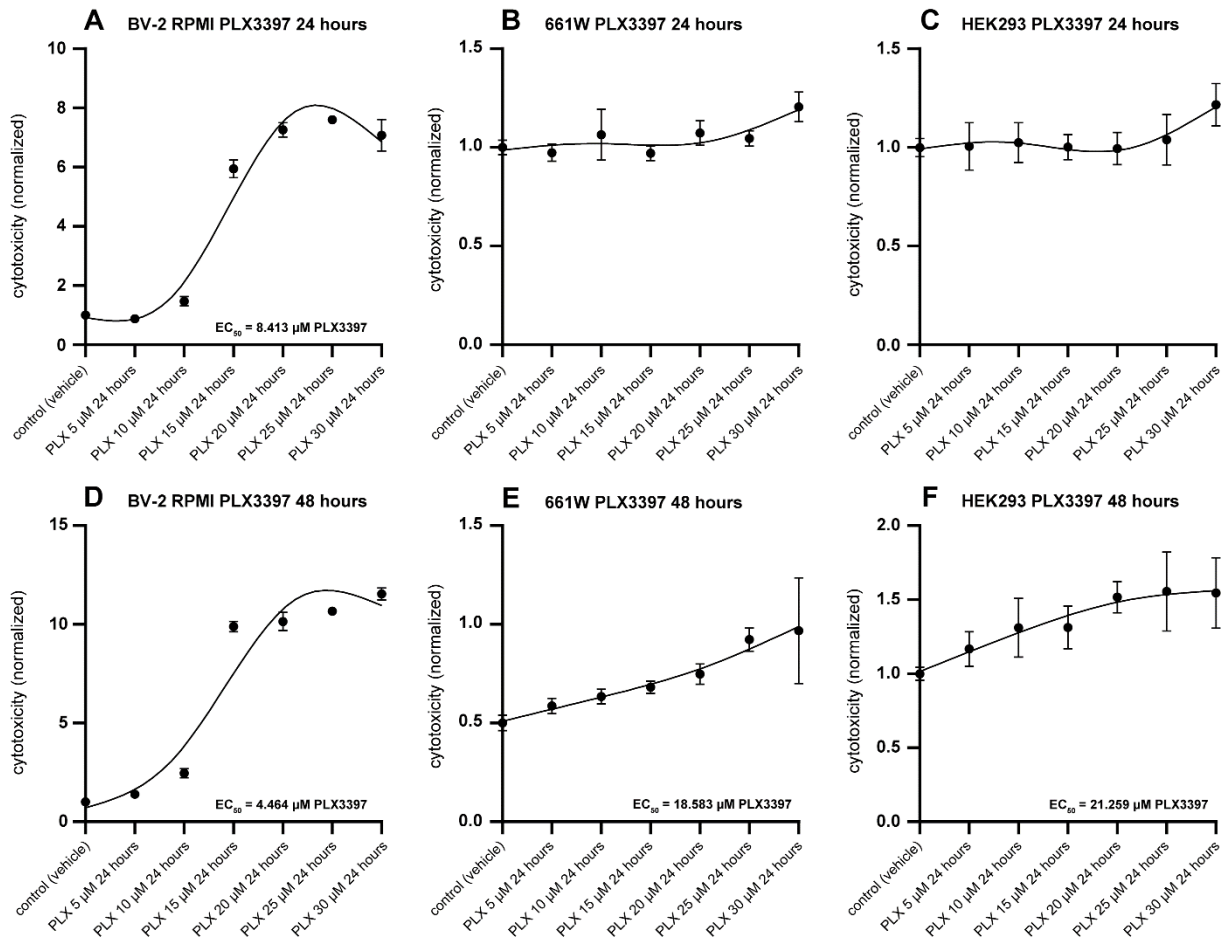


Figure 14 Effect of PLX3397 on cell death rate in different cell lines. PLX3397 was used to treat BV-2, 661W and HEK293 cells for 24 or 48 h at concentrations ranging from 5 μM to 30 μM in 5 μM increments. After 24 h, it was only possible to calculate the EC_{50} value in BV-2 cells, here it was 8.413 μM (A), in 661W and HEK293 cells this was not possible (B and C). The effect of PLX3397 on 661W and HEK293 cells was not sufficient to determine an EC_{50} value until 48 h had passed. For BV-2, 661W and HEK293 cells, they are 4.464 μM , 18.583 μM and 21.259 μM , respectively (D – F) ($n = 10$).

3.1.3 PLX3397 treatment leads to an altered morphology in different cell lines

After studying the effect of PLX3397 on cell viability and mortality, we were now interested in the effects of CSF1R inhibition on cell morphology and shape. For this purpose, BV-2, 661W and HEK293 cells were treated with different PLX3397 concentrations from 10 μM to 30 μM in 10 μM steps. The analysis was performed after 24 h, because a longer incubation time would have resulted in a too strong washing off of the cells in the course of the phalloidin staining. Nevertheless, a clear effect can already be determined after 24 h. In order to describe the cell morphology in the best possible way, the following parameters were investigated: ramification index, spanned area, and the outline of the cell. The PLX3397 treatment had a greater effect on the cell morphology the lower the values of the morphological parameters are.

Results

Investigating the BV-2 cells, it was shown that the cell number decreased with increasing PLX3397 concentration (Figure 15.A – D). This trend was most pronounced in the BV-2 cells compared to the other tested cell lines. Furthermore, a significant decrease in the measured morphological parameters and thus a strong change to an amoeboid phenotype could be already observed with 10 μ M PLX3397 treatment (Figure 15.E – J). This was anticipated given how strongly BV-2 cells express CSF1R.

Inspecting the 661W cells revealed that their phenotype changed significantly and their number only marginally declined with increasing PLX3397 concentrations (Figure 16.A – D). A distinct pattern could be seen for each parameter that was examined. When PLX3397 was present in concentrations of 20 μ M and 30 μ M, the morphological parameters significantly decreased (Figure 16.E – J). Here, in the wake of increasing PLX3397 concentrations, the photoreceptors became smaller and their processes regressed. This is most likely caused by the low level CSF1R expression in the 661W cells.

Finally, yet importantly, the morphological parameters of the HEK293 cells following treatment with PLX3397 were also investigated. There were no alterations in cell quantity or morphology because these cells do not express CSF1R (Figure 17). Even in the control condition (Figure 17.A), the HEK293 cells had a small, rounded and compact phenotype that presumably allows for little alteration, so it is crucial to highlight this.

Results

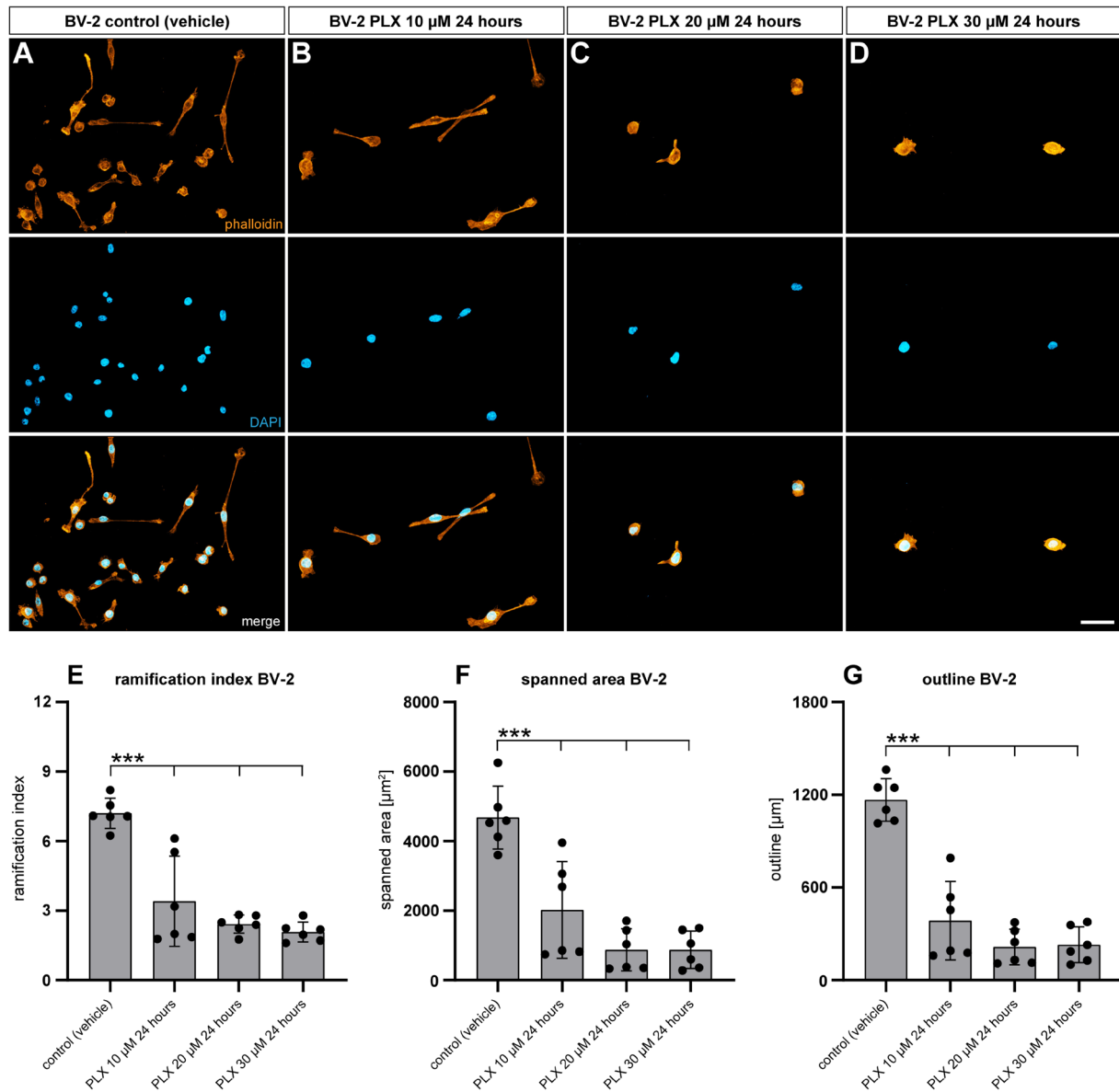


Figure 15 Effect of PLX3397 on morphology in BV-2 cells. For 24 and 48 h, PLX3397 was used to treat BV-2 cells at concentrations ranging from 10 μ M to 30 μ M in 10 μ M increments. Using phalloidin stainings, cell morphology was examined (A – D). A drop in the number of cells could also be seen in addition to a visible change in cell morphology. 3 different parameters were carefully investigated to see which ones would best convey the morphology (E – G). With increasing PLX3397 concentration, all of the parameters evaluated experienced the same trend, which was a significant decrease. (* $p < 0.05$, ** $p < 0.01$, *** $p \leq 0.001$) ($n = 6$) (Scale bar = 50 μ m).

Results

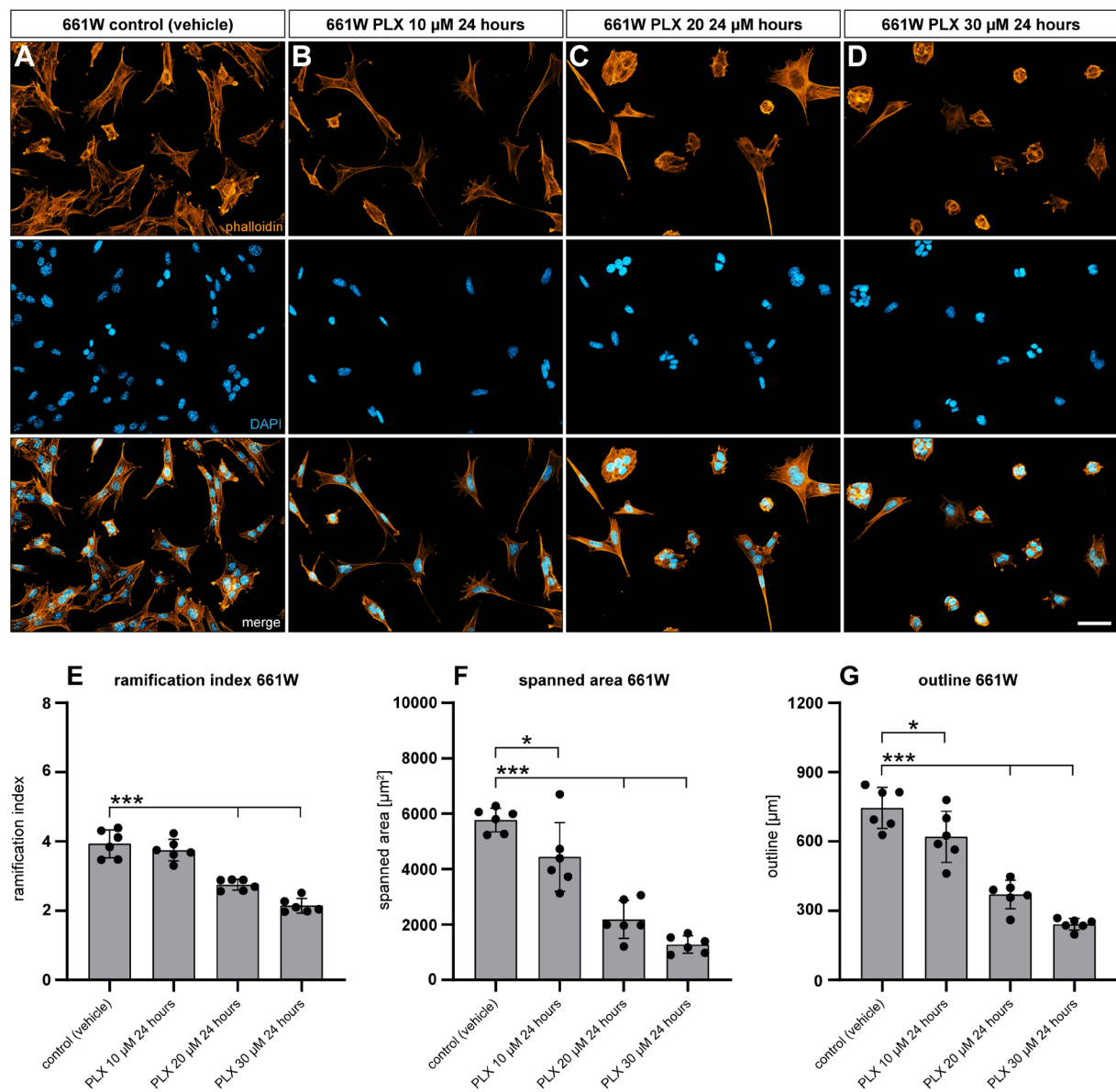


Figure 16 Effect of PLX3397 on morphology in 661W cells. 661W cells were stimulated with PLX3397 at concentration ranging from 10 μ M to 30 μ M in 10 μ M increments for 24 and 48 h. To address cell morphology, phalloidin stainings were performed (A – D). In addition to a visual change in cell morphology, a reduction in cell number could also be observed. In order to best describe the morphology, 3 different parameters were examined in detail (E – G). The same trend applied to all the parameters studied, namely that with increasing PLX3397 concentration, all of them decreased significantly (*p < 0.05, **p < 0.01, ***p ≤ 0.001) (n = 6) (Scale bar = 50 μ m).

Results

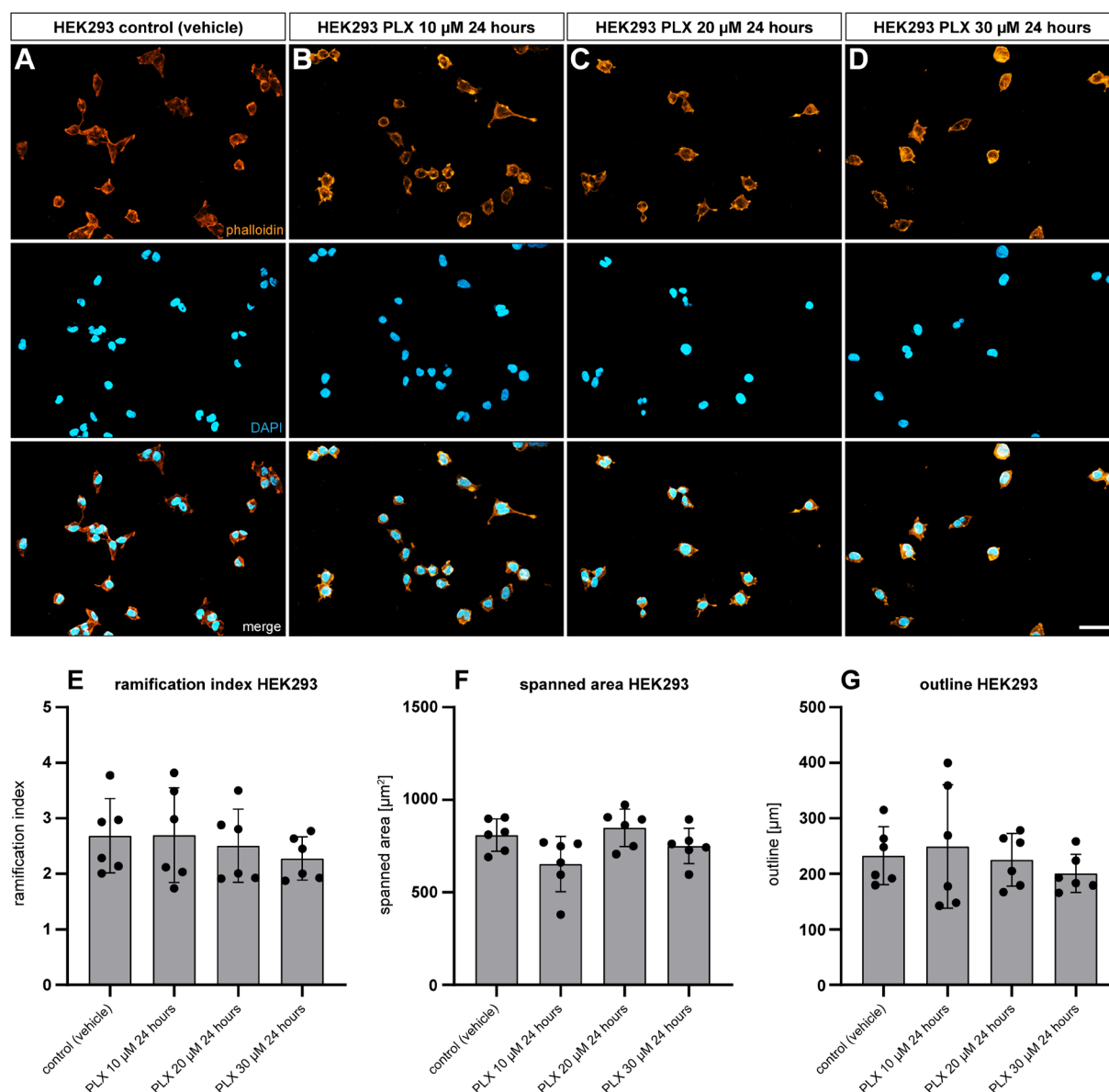


Figure 17 Effect of PLX3397 on morphology in HEK293 cells. HEK293 cells were stimulated with PLX3397 at concentration ranging from 10 μM to 30 μM in 10 μM increments for 24 and 48 h. To address cell morphology, Phalloidin stainings were performed (A – D). Here, for all PLX3397 concentration, HEK293 cells did not appear to be affected in either morphology or cell number. For these reasons, no significant changes in the investigated parameters could be shown (E – G) (*p < 0.05, **p < 0.01, ***p ≤ 0.001) (n = 6) (Scale bar = 50 μm).

3.2 PLX3397 can be detected in the retina after oral administration

To begin, we were interested in determining whether PLX3397 could be detected in the retina following oral dosing. For this, *CX3CR-1^{GFP/-}* reporter mice were fed a diet containing PLX3397 at concentrations of either 150 parts per million (ppm) or 1200 ppm for one week (Figure 18). Subsequently, the concentration of PLX3397 in the retina was determined by LC-MS. The base peak chromatogram displayed each molecule mass, alongside with the charges, that was found in the samples that were analyzed (Figure 18.A). In contrast, the extracted ion chromatogram showed the molecular weight-filtered specific mass of PLX3397, which is 418.105 g per mol. The mass spectra of PLX3397 shown also include the naturally occurring

Results

isotopes, which have weights of 420.105 and 421.105 g per mol, respectively (Figure 18.B). The amount of PLX3397 detected was reflected by the measured intensity. The measured concentrations for 150 ppm or 1200 ppm PLX3397 diet were 39.262 or 379.433 nMol per retina (Figure 18.C). It was shown by BAF *in vivo* imaging that 1200 ppm PLX3397 diet was able to deplete microglia in the retina (Figure 18.L). In addition, SD-OCT scans showed that retinal thickness was significantly reduced when mice received 1200 ppm PLX3397 diet (Figure 18.M; N). Given the absence of a whole cell type, this seems evident. Experiments with 150 ppm of PLX3397 were abandoned since the treatment had no noticeable effects (Figure 18.E; H; K).

3.3 Effect of preventive microglia depletion in the light damaged retina

Reactive microglia are commonly present in retinal degenerative diseases. They can secrete neurotoxic substances and contribute to photoreceptor cell death. However, as a fundamental part of the regulatory immune system they also have supportive effects. In this part of the project, we aimed at studying the effects of preventive microglia depletion in a mouse model of acute retinal degeneration by using PLX3397.

3.3.1 Preventive PLX3397 treatment does not affect the extend of retinal degeneration

For this purpose, experiments were performed on *CX3CR-1^{GFP/-}* reporter mice according to the second experimental setup described in chapter 2.2.5 which is illustrated in Figure 8. Here SD-OCT scans were performed 4 days after 15,000 lux light exposure to determine the effect of PLX3397 treatment on retinal degeneration (Figure 19.A – H). Additionally, the effectiveness of microglia depletion by CSF1R inhibition was checked by BAF *in vivo* imaging. Microglia could not be detected following PLX3397 diet in either nonlight exposed or light exposed retinas, as the BAF images clearly demonstrate (Figure 19.I – L). Moreover, the BAF images showed that the light exposure reactivated the microglia, which could be distinguished by a noticeably larger and amoeboid morphology. The heatmaps already showed by their color change from green to blue that the PLX3397 diet had no effect on the severity of retinal degeneration compared to control diet in light exposed retinas (Figure 19.E – H).

Results

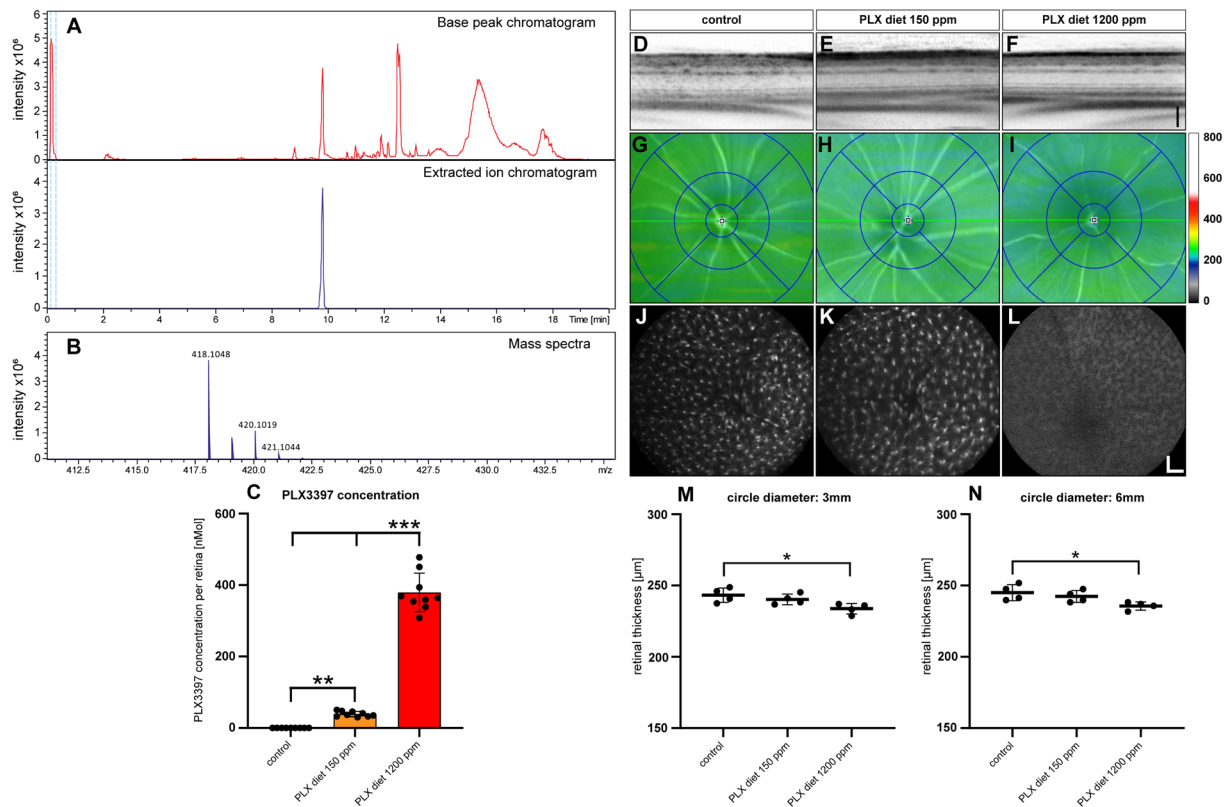


Figure 18 LC-MS determination of PLX3397 in the retina. *CX3CR-1^{GFP/-}* reporter mice received 150 ppm or 1200 ppm PLX3397 diet for one week. The PLX3397 concentration in the retina was subsequently determined by LC-MS. (A-C). The base peak chromatogram showed all molecular masses including charges that were present in the sample. While the extracted ion chromatogram was specifically filtered to the mass of PLX3397 (A). The analyzed mass spectrum of PLX3397 showed the molecular weight including all its common isotopes (B). The amount of detected PLX3397 was reflected by the measured intensity. PLX3397 was detected at a concentration of 39.262 or 379.433 nMol per retina for 150 ppm or 1200 ppm PLX3397 diet (C). Representative scans (D – F) and corresponding heatmaps (G – I) compiled by SD-OCT displaying an overview of the retina. BAF images (J – L) visualize *CX3CR-1^{GFP/-}* microglia in the retina. Here it could be shown that 1200 ppm PLX3397 depleted microglia in the retina. Analyses of retinal thickness for 3 mm and 6 mm section showed that the thickness was significantly reduced when 1200 ppm PLX3397 was fed (M; N) (* $p < 0.05$, ** $p < 0.01$, *** $p \leq 0.001$) ($n = 9$) (Black scale bar = 100 μm ; white scale bar = 200 μm).

SD-OCT scans revealed a significant thinning of the ONL in light exposed retinas, and this thinning was also present in light exposed retinas under conditions of microglia depletion (Figure 19.M; N). It is also crucial to note that, very much like in the previous experiment, the PLX3397 diet alone significantly reduced the retinal thickness.

The cryosections corroborated what the SD-OCT scans had already shown, namely that the absence of microglia following induction of retinal degeneration had no effect on the same (Figure 20). There were no differences between light exposed retinas in the presence or absence of microglia. The thinning of the ONL was equally pronounced in both cases and significantly thinner compared to the control condition (Figure 20.A – D). In addition, reactivation of microglia by light exposure was shown to be successful, as they exhibited an amoeboid phenotype and migrated to the nuclear layers (Figure 20.C). After PLX3397 treatment, no microglia were found in the nuclear layers at any condition (Figure 20.B; D).

Results

The analysis of the flat mounts also demonstrated that the microglia were successfully reactivated after exposure to light (Figure 21.C). Here, too, they exhibit an amoeboid phenotype and congregate increasingly in the SRS. Following PLX3397 treatment, no accumulation of microglia was detected in the SRS or in any other layer independently of experimental condition (Figure 21.B; D).

3.3.2 Absence of microglia triggers astrocytic and Müller cell reactivity

The most prevalent cell type in the CNS are astrocytes, which carry out a multitude of functions including extracellular homeostasis, maintenance and regulatory functions that are implicated in neurogenesis and synaptogenesis. Astrocytes become reactive in the presence of inflammation and damage (Blackburn, Sargsyan et al. 2009, Khakh, Beaumont et al. 2017). The whole thickness of the retina is covered by Müller cells, which surround and contact neuronal cell bodies and processes. Retinal diseases are linked to reactive Müller cells. The ability of retinal neurons to survive may be aided by Müller cell gliosis, which can also accelerate the process of neuronal degeneration (Bringmann and Reichenbach 2001).

Since the expression of glial fibrillary acidic protein (GFAP) is a hallmark of reactive Müller cells and astrocytes including their reactivity, we wanted to investigate in this part of the study how astrocytic and Müller cell reactivity changed in the absence of microglia (Figure 22). Therefore, GFAP stainings were carried out in cryosections. The results showed that already without induced retinal degeneration an increased GFAP expression is detected when microglia have been depleted (Figure 22.B; D). Furthermore, GFAP expression was also increased in light-exposed retinas without PLX3397 treatment (Figure 22.C). This expression was further increased in light-exposed retinas under conditions of microglia depletion (Figure 22.D).

Results

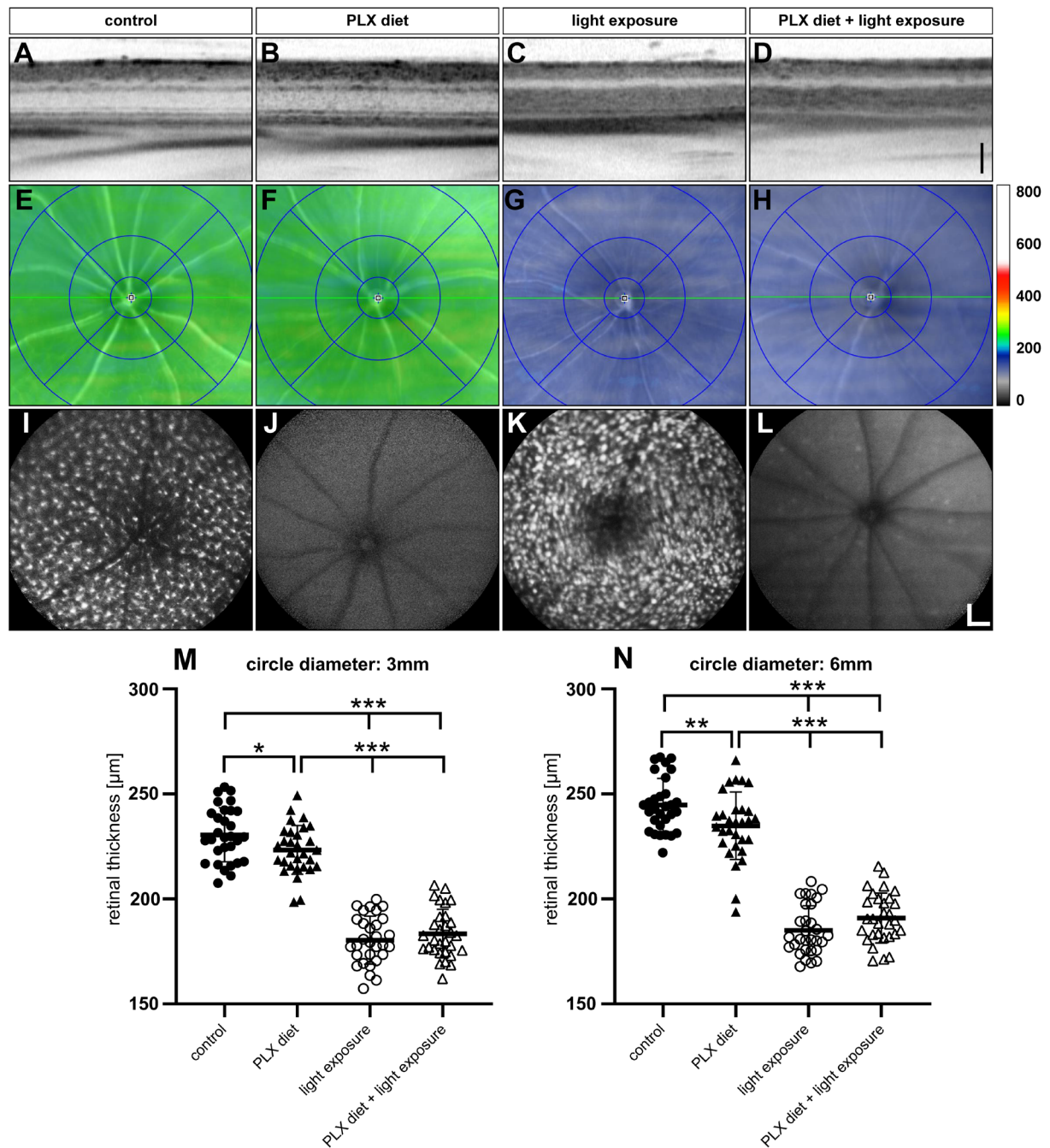


Figure 19 SD-OCT analysis on the effect of preventive microglia depletion on retinal degeneration. *CX3CR-1^{GFP/-}* reporter mice received PLX3397 diet and 15,000 lux light exposure for one hour each alone and in combination. Control animals were neither exposed to light nor received PLX3397 diet. The PLX3397 diet started one week before light exposure and ended 4 days later at the time of analysis. Reflective images of retinal layers showed a thinning of the ONL in light exposed retinas and also in light exposed retinas where microglia were absent (A – D). The color change of the heatmaps showed that the assumption of the retinal thinning in both conditions is well founded (E – H). BAF *in vivo* images showed that microglia were successfully depleted in both the control and light exposed retinas. Furthermore, control and light exposed microglia already exhibited morphological differences (I – L). Microglia depletion could not stop retinal degeneration, according to measurements of retinal thickness. Additionally, it was shown that in the absence of microglia, retinal thickness already decreased without being subjected to induced degeneration (M – N) (*p < 0.05, **p < 0.01, ***p ≤ 0.001) (n = 30) (Black scale bar = 100 μm; white scale bar = 200 μm).

Results

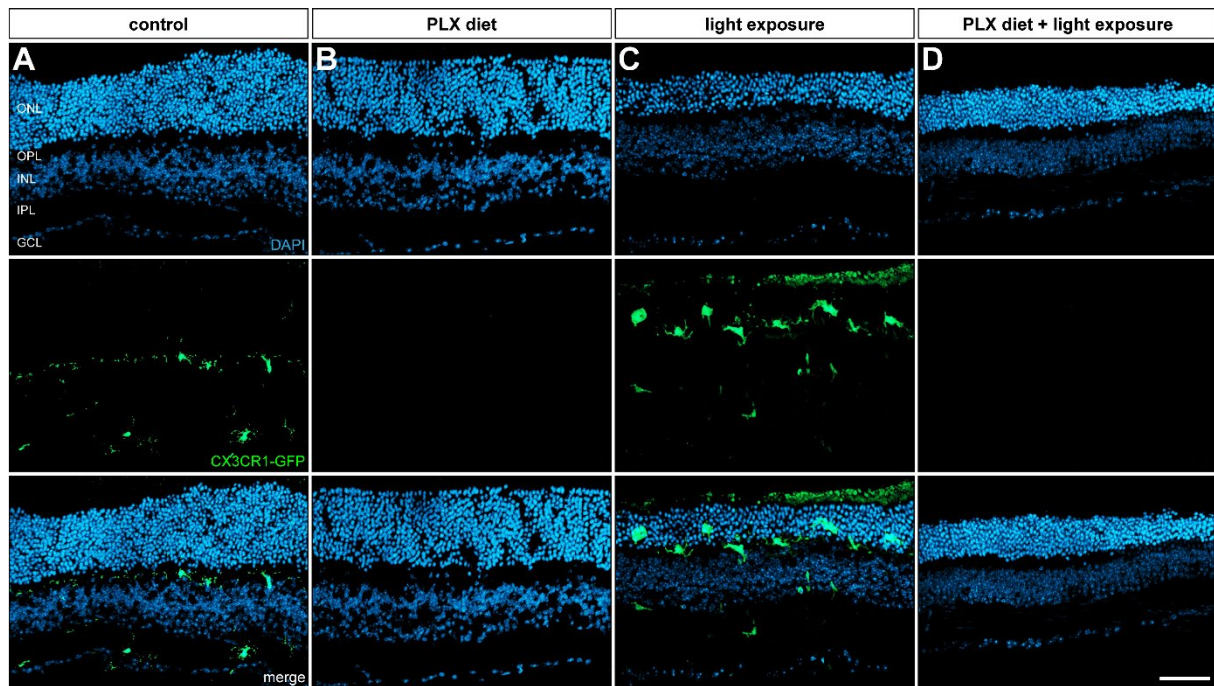


Figure 20 Cryosection analysis on the effect of preventive microglia depletion on retinal degeneration. *CX3CR1^{GFP/-}* reporter mice received PLX3397 diet one week before one hour 15,000 lux light exposure and analysis was carried out in cryosections 4 days after. DAPI containing mounting medium was used for embedding. The absence of microglia could not prevent degeneration of the ONL after light exposure (A – D). Light-induced reactivation of microglia was successful as they exhibited an amoeboid phenotype and migrated into the nuclear layers. This was not the case after PLX3397 diet (Scale bar = 50 μ m).

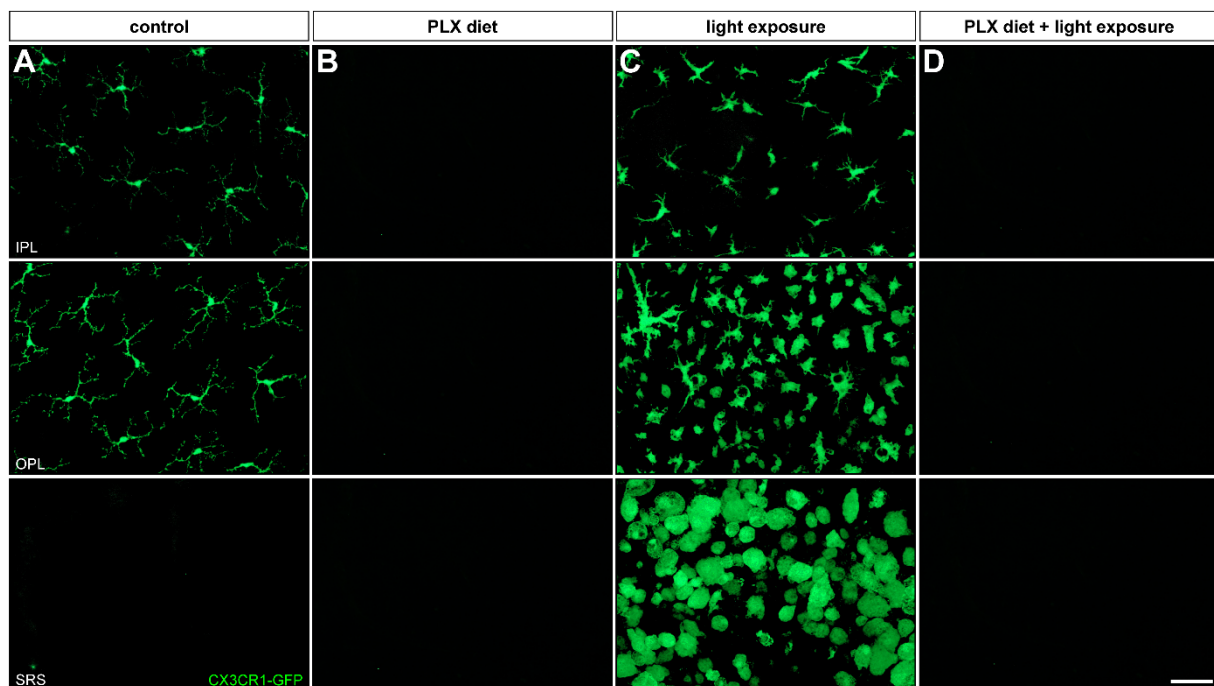


Figure 21 Flat mount analysis on the effect of preventive microglia depletion on retinal degeneration. *CX3CR1^{GFP/-}* reporter mice received PLX3397 diet one week before one hour light exposure and analysis was carried out in flat mounts 4 days after. Microglia successfully reactivated by 15,000 lux light because they took on an amoeboid phenotype (C). Reactivated microglia were also found in the SRS. When PLX3397 was present or under control conditions, microglia were not detected (A; B; D) (Scale bar = 50 μ m).

Results

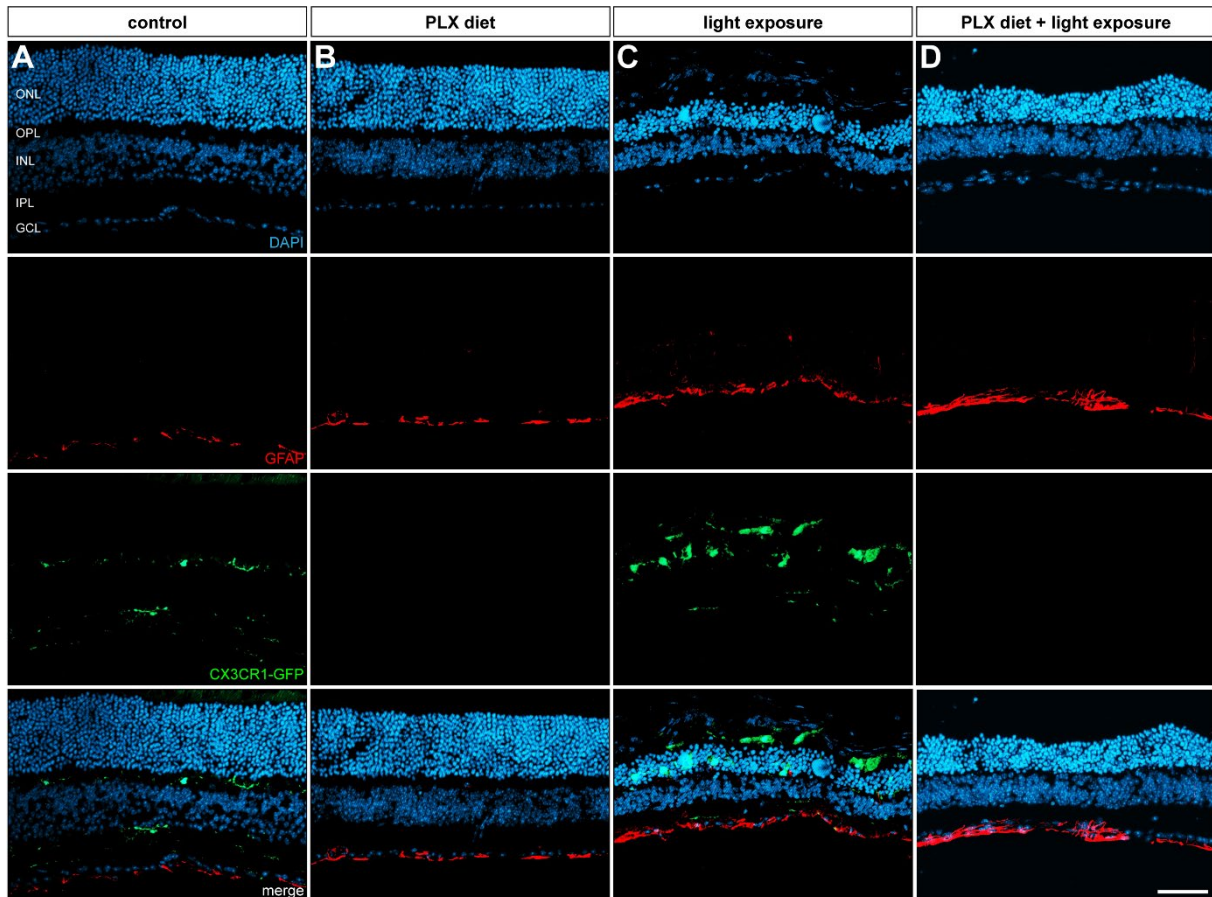


Figure 22 GFAP staining analysis in the context of preventive microglia depletion in retinal degeneration. *CX3CR1^{GFP/-}* reporter mice received PLX3397 diet one week before one hour 15,000 lux light exposure and analysis was carried out in cryosections 4 days after. GFAP stainings were performed in order to investigate astrocytic activity. Only a small amount of GFAP expression could be detected in control condition (A). The absence of microglia increased GFAP expression in astrocytes (B). GFAP expression increased following the reactivation of microglia by light (C). However, when microglia were absent during retinal degeneration, GFAP expression increased even more (D) (Scale bar = 50 μ m).

3.3.3 Absence of microglia cannot prevent photoreceptor cell death

Bleached photoreceptor cells mostly perish in light induced retinal degeneration as a result of overreactive microglia. Here we were interested in whether the mortality rate could be reduced by PLX3397 treatment (Figure 23). It is worth mentioning that the number of photoreceptor cells was unaffected by the chosen PLX3397 concentration. Here, between 820 and 989 photoreceptor cells per 0.15 mm² retina were detected in the control condition and in the condition of microglia depletion (Figure 23.A; B; E). However, a significant decrease in the number of photoreceptor cells could be investigated in retinas that had been exposed to light. Unfortunately, the absence of microglia did not prevent this reduction. In both cases, the numbers vary between 426 and 387 photoreceptor cells per 0.15 mm² retina (Figure 23.C; D; E).

Results

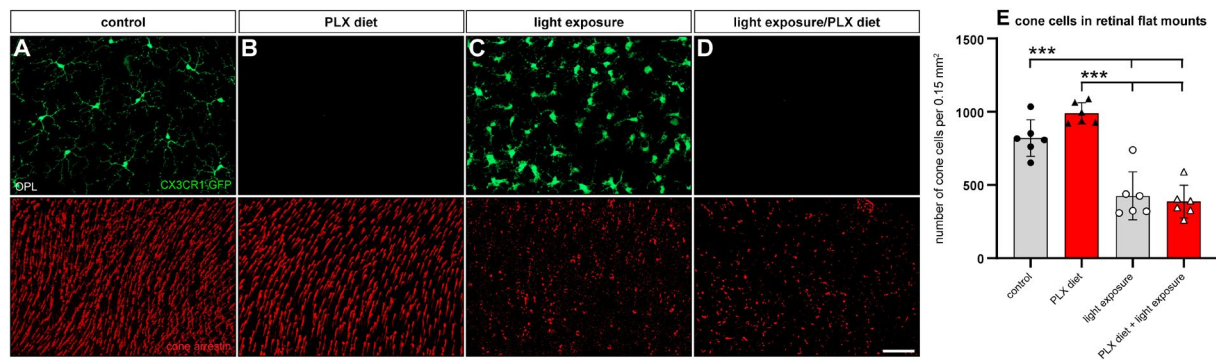


Figure 23 Cone arrestin staining analysis in the context of preventive microglia depletion in retinal degeneration. *CX3CR1^{GFP/-}* reporter mice received PLX3397 diet one week before one hour 15,000 lux light exposure and analysis was carried out in flat mounts 4 days after. Cone arrestin stainings were performed in order to investigate photoreceptor cell death. Here it was shown that in light exposed retinas the number of photoreceptor cells was significantly reduced (C). This was also the case when microglia were depleted during retinal degeneration (D) (* $p < 0.05$, ** $p < 0.01$, *** $p \leq 0.001$) ($n = 6$) (Scale bar = 50 μm).

3.3.4 Absence of microglia increase the amount of TUNEL⁺ cells

When there is damage or degeneration, microglia typically take up phagocytosis and the cleanup of dead cell debris. Here, we aimed to investigate the effects of microglia depletion on dying cells after induced retinal degeneration. TUNEL labeling was used to confirm the quantity of dead cells that were not phagocytosed for this reason (Figure 24). No TUNEL⁺ cells were detected in both control and PLX3397 treated mice (Figure 24.A; B). This also demonstrates that PLX3397 acted very specifically and did not affect or even kill other cells than microglia. 4 days after induced retinal degeneration and in the presence of microglia, a percentage of TUNEL⁺ cells in the ONL of about 38% was detected (Figure 24.C; E). This value increased significantly to about 57% in the absence of microglia (Figure 24.D; E). From this we concluded that even over-reactive microglia in the milieu of an induced damage are necessary in order to remove dead cell debris from the ONL. If they were no longer present, more dead cells accumulate.

Results

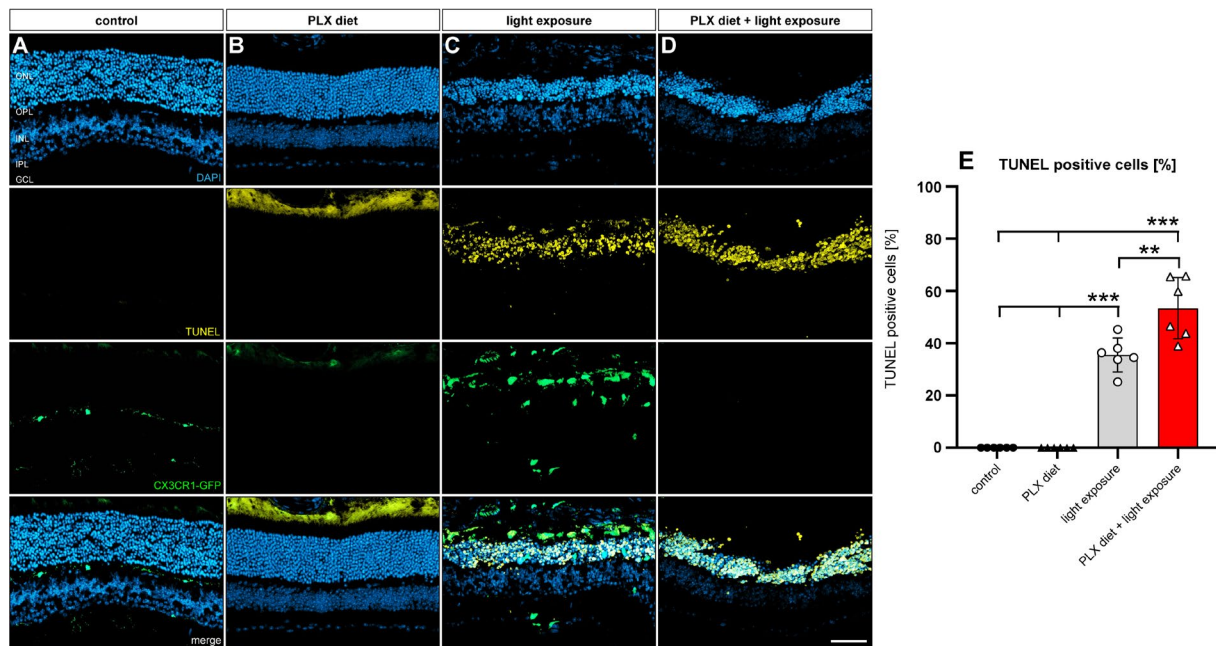


Figure 24 TUNEL staining analysis in the context of preventive microglia depletion in retinal degeneration. *CX3CR1^{GFP/-}* reporter mice received PLX3397 diet one week before one hour 15,000 lux light exposure and analysis was carried out in cryosections 4 days after. TUNEL labelings were performed in order to quantify the extend of retinal degeneration. In neither the control nor the PLX3397 treated mice were any TUNEL⁺ cells found (A; B). In light damaged mice approximately 38% TUNEL⁺ were detected in the ONL (C). This number increased significantly to approximately 57% in the absence of microglia (D) (*p < 0.05, **p < 0.01, ***p ≤ 0.001) (n = 6) (Scale bar = 50 µm).

3.3.5 PLX3397 prevents the expression of pro-inflammatory markers

Since over-reactive microglia are known to express increased proportions of pro-inflammatory markers in models of retinal degeneration, we were interested whether microglia depletion could prevent this or possibly compensates for it by other immune cells. For that reason, microglia activation marker and pro-inflammatory cytokine expression in whole retinal transcripts were determined by qRT-PCR. 4 days after mice were exposed to light with an intensity of 15,000 lux, mRNA expression of the constitutive microglia marker *allograft inflammatory factor 1* (*Aif-1*) was strongly increased and this upregulation was absent in mice fed with PLX3397 (Figure 25.D). Here, the expression level was even below that of the control. The same expression pattern could be shown not only for *Aif-1* but also for the pro-inflammatory cytokines *tumor necrosis factor α* (*Tnf α*) and *Il-1 β* (Figure 25.A; C). Expression of the microglia activation marker *Tspo* was also upregulated after light exposure, and PLX3397 treatment prevented this induction (Figure 25.E). However, it remained slightly elevated compared to the control condition. After exposure to light, expression of the pro-inflammatory cytokines *Il-6* and *Ccl2* were also increased, but this induction could not be completely stopped by PLX3397 treatment (Figure 25.B; F). In contrast to the control condition, it remained significantly elevated. The same trend in the expression of pro-inflammatory markers was also observed in the RPE. This analysis is shown in the supplementary data for a detailed overview (Supplementary figure 1).

Results

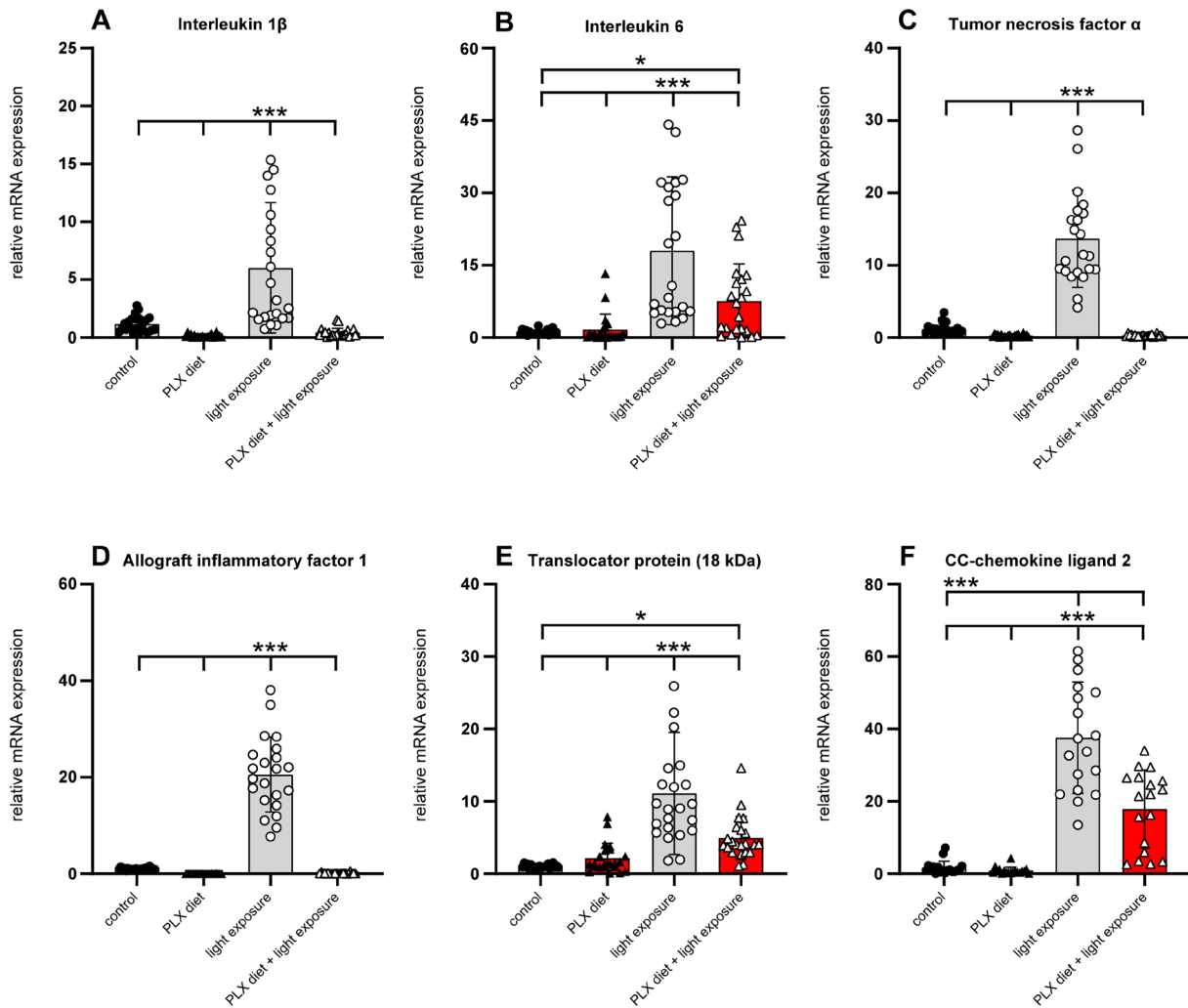


Figure 25 Pro-inflammatory marker expression the context of preventive microglia depletion in retinal degeneration. *CX3CR1^{GFP/-}* reporter mice received PLX3397 diet one week before one hour 15,000 lux light exposure and analysis was carried out 4 days after. Pro-inflammatory marker expression in whole retinal transcripts were determined by using qRT-PCR. *Il-1 β* expression was upregulated in light exposed retinas, whereas this upregulation was absent with PLX3397 treatment. Here, it could be reduced to the level of the control (A). The same expression pattern could also be shown for *Aif-1* and *Tnfa* (C; D). *Il-6* also showed significantly increased expression when retinal degeneration has been induced. The upregulation could be reduced after PLX3397 treatment but was still elevated compared to the control (B). The same expression pattern could be observed for *Tspo* and *Ccl2* (E; F) (* $p < 0.05$, ** $p < 0.01$, *** $p \leq 0.001$) ($n = 22$).

3.4 The nature of retinal microglia repopulation

In the following sections, we wanted to investigate the effects of a curative microglia depletion, which occurs after retinal degeneration had already begun. Here we went one step further and focused on differences in early (immediately after light exposure) or late (7 days after light exposure) microglia depletion. Add to this, the influence of newly repopulated microglia on the progression of retinal degeneration will also be investigated and compared with the naïve microglia. For this reason, the ability of microglia to repopulate back into the plexiform layers after cessation of PLX3397 diet was investigated. This was necessary because previous studies have chosen both a different type of PLX and a different application period. Here, experiments were performed on *CX3CR-1^{GFP/-}* reporter mice according to the third experimental setup described in chapter 2.2.5 which is illustrated in Figure 9.

3.4.1 Microglia repopulate after 7 days with a few changes in morphology

The analysis of retinal flat mounts was performed 4, 7 and 10 days after cessation of the PLX3397 diet. It proved difficult to analyze the data for day 4 after discontinuation of the PLX3397 diet, as the microglia were obviously still in the repopulation phase and therefore could not yet be detected in full numbers. Moreover, they were still migrating back into the plexiform layers, making it difficult to pinpoint their precise location based on morphology and pattern (Figure 26.D). 7 and 10 days after cessation of the PLX3397 diet, microglia were found in the plexiform layers in numbers that were comparable to the control condition (Figure 26.A; B; C). In addition, distinct layers could be determined here based on microglia morphology and pattern (Figure 26.B; C). However, microglia were also detected in a few numbers in the SRS. Six morphological parameters were analyzed in order to describe the phenotype of microglia during the process of repopulation the best possible way. It was done according to the methods described in chapter 2.4.1 and illustrated in figure 11. Since no clear localization of microglia could be assigned 4 days after the stop of PLX3397 diet, only 7 and 10 days after PLX3397 diet were analyzed here. All morphological parameters analyzed for the OPL showed a slight decrease after 7 days of repopulation, which represents a transition from a ramified to an amoeboid morphology. This decrease was restored after 10 days of repopulation. (Figure 26.E – J). From this we conclude that microglia changed their morphology in the course of migration and returned to the initial state after completion of repopulation. The same trend was also observed for the IPL and SRS; this is shown in the supplementary data (Supplementary figure 2 and 3).

Results

The location of microglia as they migrate during repopulation was then further examined by accessing cryosections (Figure 27.A – D). Here, it was demonstrated that the number of microglia in the plexiform layers was significantly decreased 4 days after ceasing the PLX3397 diet. On day 10 this is gradually brought back to the same level as the control (Figure 27.E; F). The INL showed the opposite behavior (Figure 27.H). Here, 4 days after stopping the PLX3397 diet, the number of microglia significantly increased and started to decline after 7 and 10 days. Nevertheless, it still remained slightly elevated compared to the control. The OPL simply displayed an upward trend in the number of microglia, not a significant change. (Figure 27.G). Day 10 after ceasing PLX3397 diet brought it back into line with the control.

3.4.2 Repopulated microglia show altered pro-inflammatory marker expression

In this section of the study, we were interested in how pro- and anti-inflammatory marker expression changed during repopulation of microglia. To this end, we analyzed the mRNA expression of whole retinal transcripts by using qRT-PCR. The expression of the constitutive microglia marker *Aif-1* decreased significantly after four days and completely recovered after 7 days of repopulation (Figure 28.D). This allowed us to assume that the microglia are almost entirely repopulated. After the PLX3397 diet was stopped, expression of the pro-inflammatory cytokine *Il-1 β* was significantly reduced on days 4 and 7, before recovering to control levels on day 10 (Figure 28.A). The expression of *Il-6* was found to be significantly increased throughout the time course of repopulation (Figure 28.B). It also did not return to the control level. The pro-inflammatory marker *Tspo* and the cytokine *Ccl2* showed increased expression as well and they did not returned to control level at day 10 (Figure 28.E; F). In contrast, the expression of *Tnfa* showed no changes in the course of the microglia repopulation (Figure 28.C). The pro-inflammatory marker expression for RPE transcripts are shown in the supplementary data (Supplementary figure 4). Subsequently, the expression of the anti-inflammatory marker *brain-derived neurotrophic factor (Bdnf)*, *nerve growth factor receptor (Ngfr)* and *synaptophysin* were examined. Here no altered expression could be detected at any time point of the repopulation (Figure 28.G – I).

Results

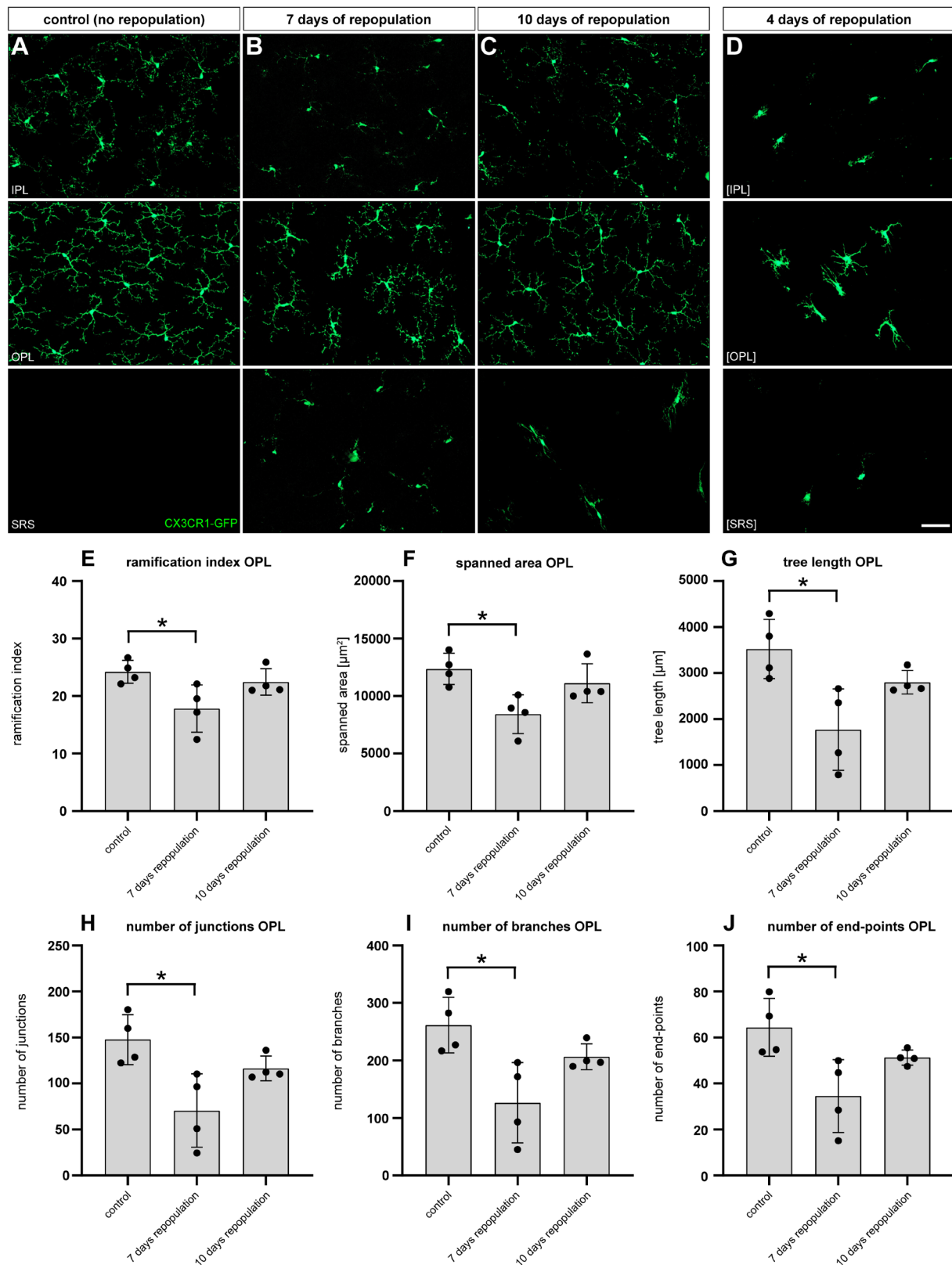


Figure 26 Investigation of microglia repopulation in retinal flat-mounts. *CX3CR1-GFP*^{-/-} reporter mice received PLX3397 diet for one week. Analysis was carried out in flat mounts 4, 7 and 10 days after cessation of PLX3397 diet. After 4 days, the repopulation was still in progress and the microglia were not yet back in full numbers (D). Here it was difficult to determine the exact localization and perform a subsequent analysis. Repopulation of microglia was completed 7 and 10 after PLX3397 diet, respectively (B; C). Nevertheless, minor morphological differences were observed compared to the control, and they recovered at day 10 after PLX3397 cessation (E – J) (* $p < 0.05$, ** $p < 0.01$, *** $p \leq 0.001$) ($n = 4$) (Scale bar = 50 μm).

Results

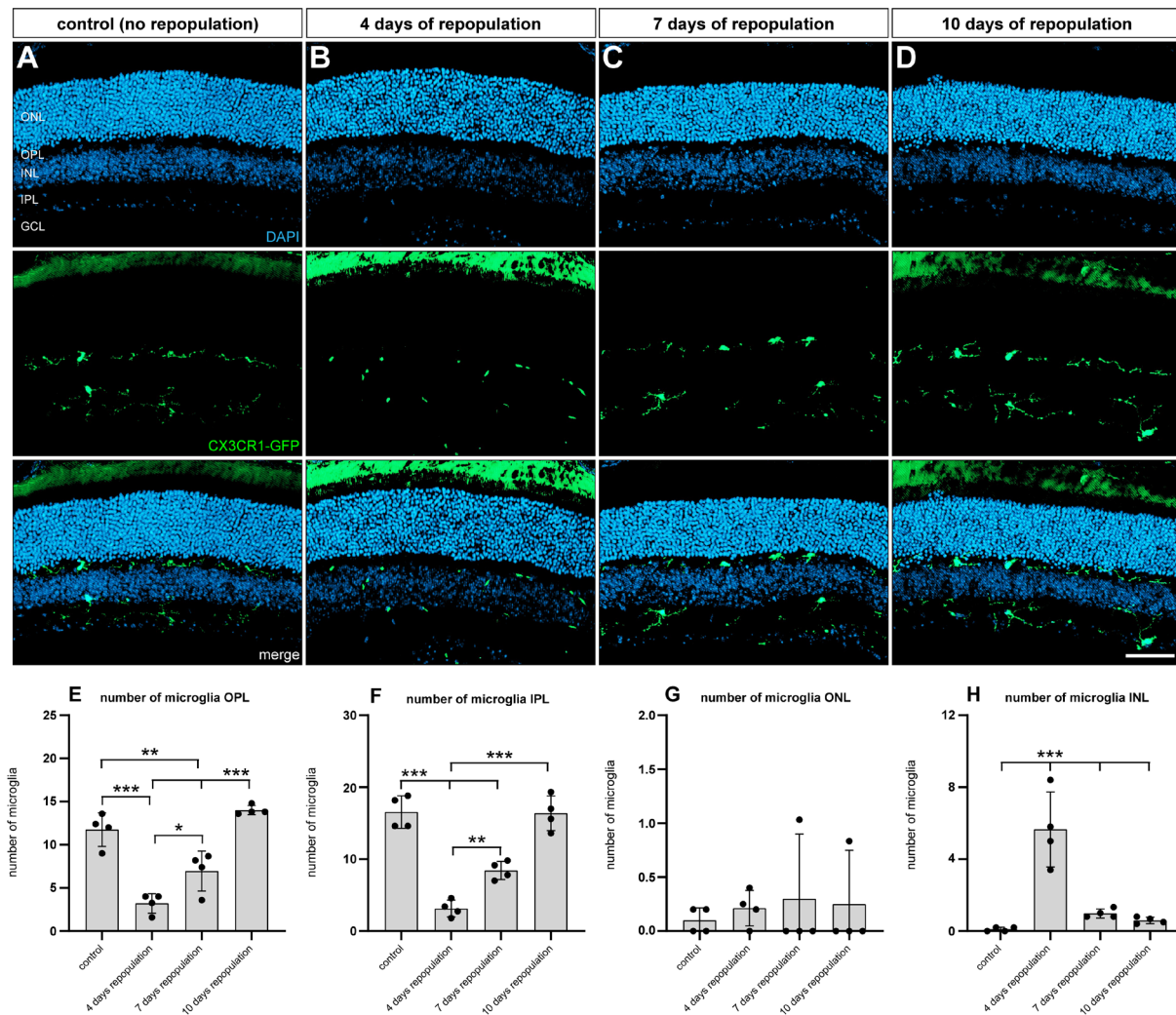


Figure 27 Investigation of microglia repopulation in retinal cryosections. *CX3CR1-GFP*^{-/-} reporter mice received PLX3397 diet for one week. Analysis was carried out in cryosections 4, 7 and 10 days after cessation of PLX3397 diet (A – D). On day 4 after stopping the PLX3397 diet, there were significant less microglia in the plexiform layers (E; F). On day 7 it increased significantly until day 10, when it reached the same level as the control. In the INL, the number of microglia increased significantly after 4 days of repopulation (H). On days 7 and 10, though, it declined to the control level. In the ONL, slight but non-significant increase in microglia numbers was observed, which recovered to the control level on day 10 of repopulation (G) (* $p < 0.05$, ** $p < 0.01$, *** $p \leq 0.001$) ($n = 4$) (Scale bar = 50 μm).

Results

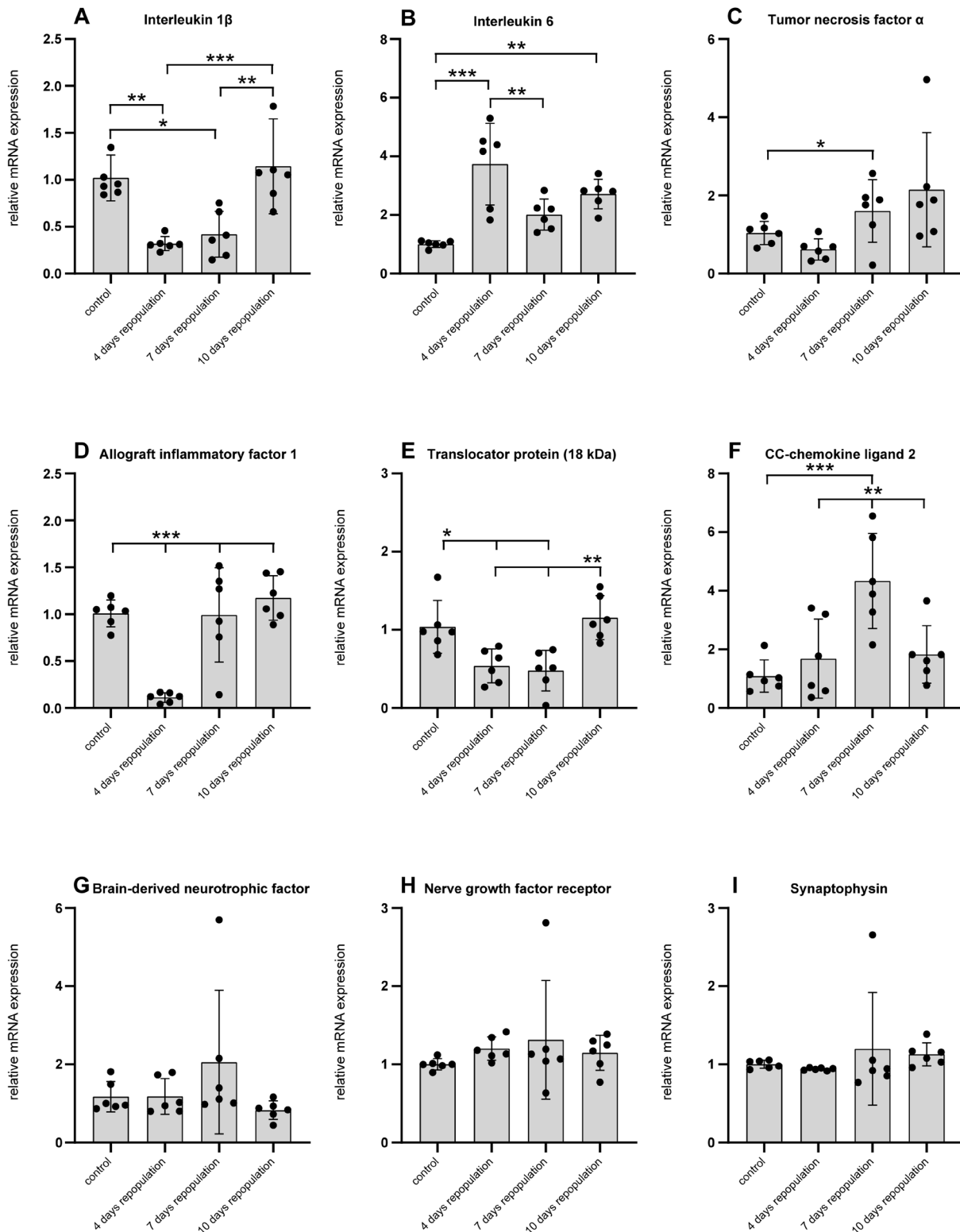


Figure 28 Investigation of pro- and anti-inflammatory marker expression in repopulated microglia. *CX3CR1^{GFP/-}* reporter mice received PLX3397 diet for one week. qRT-PCR of whole retinal transcripts was performed 4, 7 and 10 days after cessation of PLX3397 diet. mRNA expression of the constitutive microglia marker *Aif-1* decreased after 4 days and completely restored after 7 of repopulation (D). Expression of *Il-1 β* was significantly reduced at day 4 and 7 of repopulation and at day 10 again comparable with the control (A). *Il-6* expression was always elevated in repopulated microglia and did not recover to control levels on day 10 (B). The expression of *Tnfa* in repopulated microglia, was increased at day 7 (C). The expression of *Tspo* and *Ccl2* also showed variations, although they recovered to control levels by day 10 after repopulation. Repopulated microglia showed no altered expression in the anti-inflammatory markers under study (G – I) (* $p < 0.05$, ** $p < 0.01$, *** $p \leq 0.001$) (n = 6).

3.5 Progression of retinal degeneration after low intensity light exposure

In the course of curative microglia depletion, we also intended to observe the course over a longer period of time than was the case with the preventive depletion (Chapter 3.3). Among other things, the influence of newly repopulated microglia on the development of retinal degeneration will be examined. Since we knew that the complete repopulation took at least 7 days and the time to deplete microglia completely had to be taken into account, we decided to analyze 14 days after light exposure. Here it was important to mention that for an analysis 14 days after light exposure an intensity of 15,000 lux is much too strong. Therefore, it is reduced to 5,000 lux to expect adequate degeneration over the entire course. Here, we investigated to development of retinal degeneration after low light exposure with an intensity of 5,000 lux. Experiments were performed on *CX3CR-1^{GFP/-}* reporter mice according to the fourth experimental setup described in chapter 2.2.5 which is illustrated in figure 10 in order to investigate the progression of retinal degeneration up to 14 days after low light exposure.

3.5.1 Retinal degeneration reaches its maximum 7 days after light exposure

The analysis of retinal degeneration was performed 4, 7, 10 and 14 days after light exposure with an intensity of 5,000 lux. Here, SD-OCT scans were performed in order to validate the extent of retinal degeneration. Reflective images of the retinal layers showed a gradual decrease in ONL thickness until 7 days after light exposure. From this day until day 14, retinal degeneration remains at the same level (Figure 29.A – E). This was confirmed by the color change of the heatmaps from green to turquoise on day 4 and to blue on days 7, 10 and 14 after light exposure (Figure 29.F – J). Statistical analysis of the data showed a significant decrease to an intermediate degeneration from control to day 4 after light exposure. From day 4 to day 7, a significant reduction to a severe degeneration was detected. From this point on, no further differences were observed. Interestingly, BAF *in vivo* images showed reactivated amoeboid microglia on day four after light exposure (Figure 29.K – O). The state of reactivation gradually transitioned back to a ramified morphology of activated microglia comparable to the control condition by day 14.

3.5.2 Reactivated microglia recover after retinal degeneration has reached its peak

Analysis of the retinal flat mounts revealed that the microglia exhibited an amoeboid phenotype 4 days after light exposure in the layers examined, as BAF *in vivo* images have already demonstrated (Figure 30.B). Additionally, an accumulation of microglia in the SRS could be detected. From day 7 to day 14, it was possible to observe a progressive recovery to the initial ramified state. Furthermore, there was a steady decline in the number of microglia in the SRS

(Figure 30.C – E). However, a few microglia were still present in the SRS on day 14 following light exposure. The evaluation of the six examined morphological parameters in the OPL could clearly confirm what the flat mount images showed (Figure 30.F – K). The evaluated parameters served as a benchmark of the microglia's level of reactivation. A low score indicates the presence of reactivated, amoeboid. A high score, on the other hand, denotes activated microglia with a ramified phenotype. Since all measured parameters showed the same tendency, it could be summarized, that a significant reduction could be observed on day 4, which progressively recovered until day 14 after light exposure where it finally increases to control level. The same trend was also observed for the IPL and SRS; this is shown in the supplementary data (supplementary figure 5 and 6).

Currently, the location of microglia during the whole process of retinal degeneration after low light exposure was taken into account (Figure 31). Here it was seen that on day 4 microglia migrate into the nuclear layers (Figure 31.B; H; I). At the same time, a reduction in the number of microglia in the plexiform layers (mainly the OPL) was observed (Figure 31.B; F; G). Once the degeneration had reached its maximum, a stepwise return to the initial state was seen (Figure 31.C-E). Thus, the microglia migrated back from the nuclear layers (Figure 31.H; I) to the plexiform layers (Figure 31.F; G). The number of microglia in both plexiform layers 14 days after light exposure was found to be at the same level as the control. However, some microglia were still present in the INL 14 days after the onset of retinal degeneration (Figure 31.E; I).

3.5.3 Pro-inflammatory marker expression progressively declines, after retinal degeneration peaks

After studying the morphology and localization of microglia in the course of retinal degeneration after low light exposure, we were interested in how the expression pattern of pro- and anti-inflammatory markers changed throughout the whole course. Because of this, qRT-PCR was used to ascertain the expression of the microglia activation marker in whole retinal transcripts. The entire examined pro-inflammatory marker showed a clear trend toward being massively upregulated on day 4 (Figure 32.A – F). By day 7, the expression levels have already recovered to their initial level and were therefore at the same level as the control. The anti-inflammatory markers investigated here showed no change in their expression over the entire experimental course (Figure 32.G – I).

Based on these findings, it could be shown that microglia that have been reactivated by artificially inducing retinal degeneration migrated to the nuclear layers and exhibited an amoeboid phenotype. They secreted pro-inflammatory and neurotoxic substances. 14 days after low light exposure, they did not remain reactivated in the nuclear layers but migrated back into the plexiform layers and displayed a ramified phenotype again.

Results

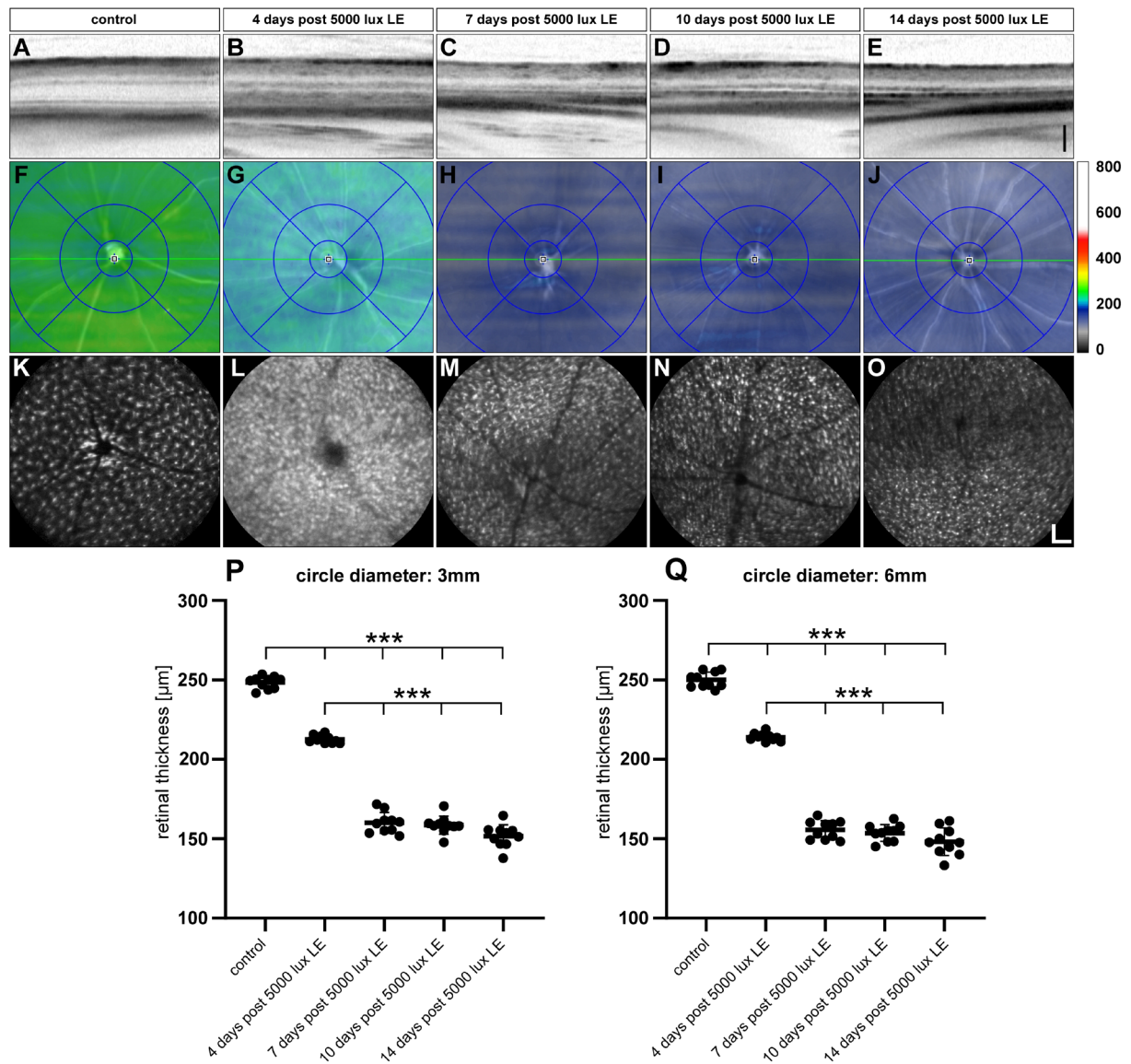


Figure 29 SD-OCT analysis of retinal degeneration after low intensity light exposure. *CX3CR-1^{GFP/-}* reporter mice were exposed to light with an intensity of 5,000 lux for one hour. SD-OCT scans were carried out to quantify the extend of retinal degeneration. Reflective images of retinal layers showed a gradual reduction of ONL thickness up to day 7, from which point no further changes were observed (A – E). This was confirmed by the color change of the heatmaps from green to turquoise and blue (F – J). Statistical analysis of 3 and 6 mm sections showed a stepwise progression of the retinal degeneration from an intermediate to a severe degeneration (P; Q). BAF *in vivo* images showed reactivated and amoeboid microglia on day 4 that reverted to their ramified initial state by day 14 after light exposure (K – O) (* $p < 0.05$, ** $p < 0.01$, *** $p \leq 0.001$) ($n = 10$) (Black scale bar = 100 μm ; white scale bar = 200 μm).

Results

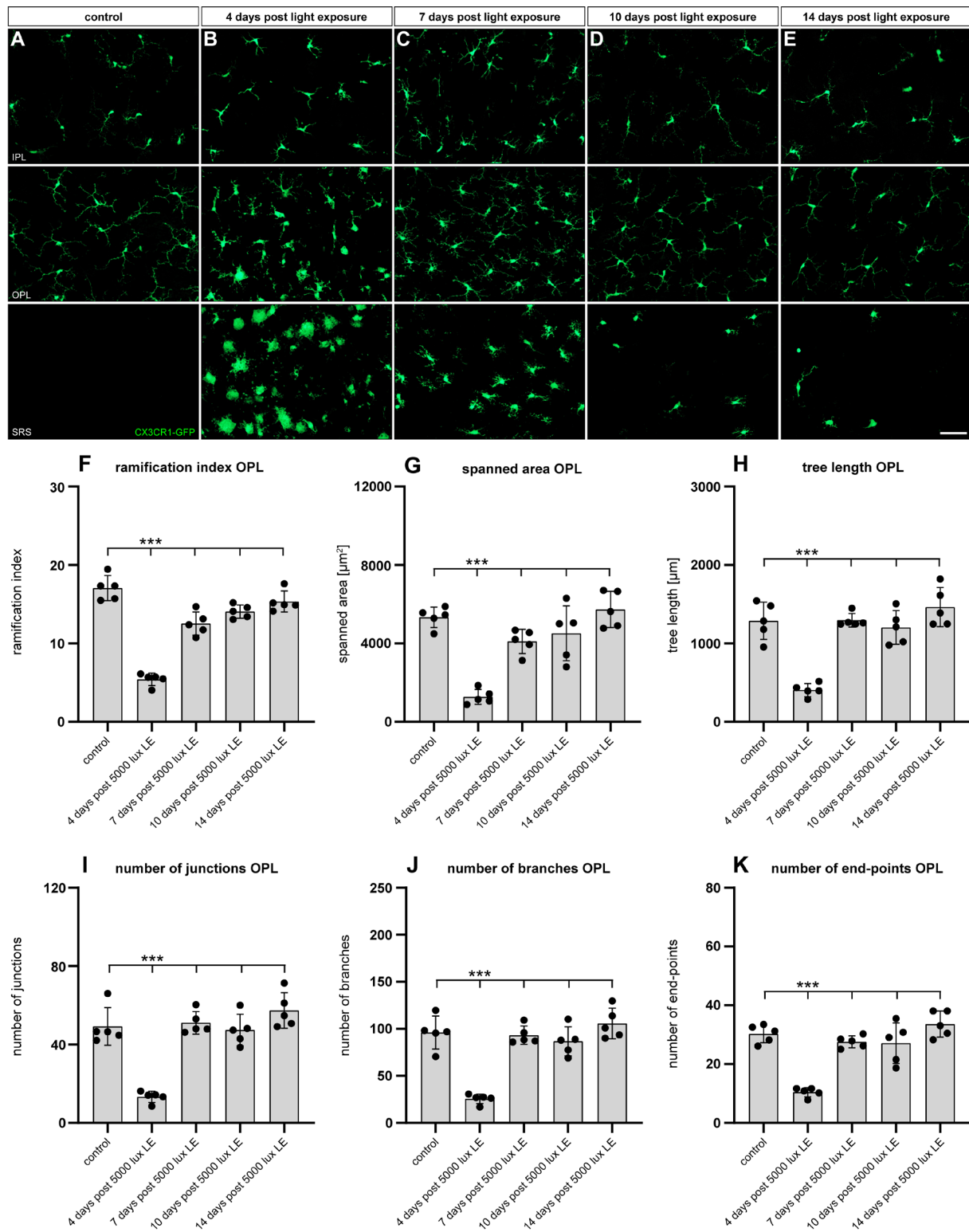


Figure 30 Investigation of microglia morphology after low intensity light exposure in retinal flat mounts. *CX3CR1-GFP*^{-/-} reporter mice were exposed to light with an intensity of 5,000 lux for one hour. Retinal flat mount images were taken at days 4, 7, 10 and 14 after light exposure. It was shown that immediately after induction of retinal degeneration, the reactivated amoeboid microglia gradually returned to their initial state up to 14 days later (A – E). All analyzed morphological parameters showed the same tendency. All parameters are significantly reduced at day 4 and approach to the level of the control at day 7 and 10 until they are comparable to the control at day 14 (F – K). In the SRS, an accumulation of microglia was detected on day 4. This also reduced stepwise until almost the initial state was reached. However, a few microglia still remain in the SRS on day 14 (E) (*p < 0.05, **p < 0.01, ***p ≤ 0.001) (n = 5) (Scale bar = 50 μm).

Results

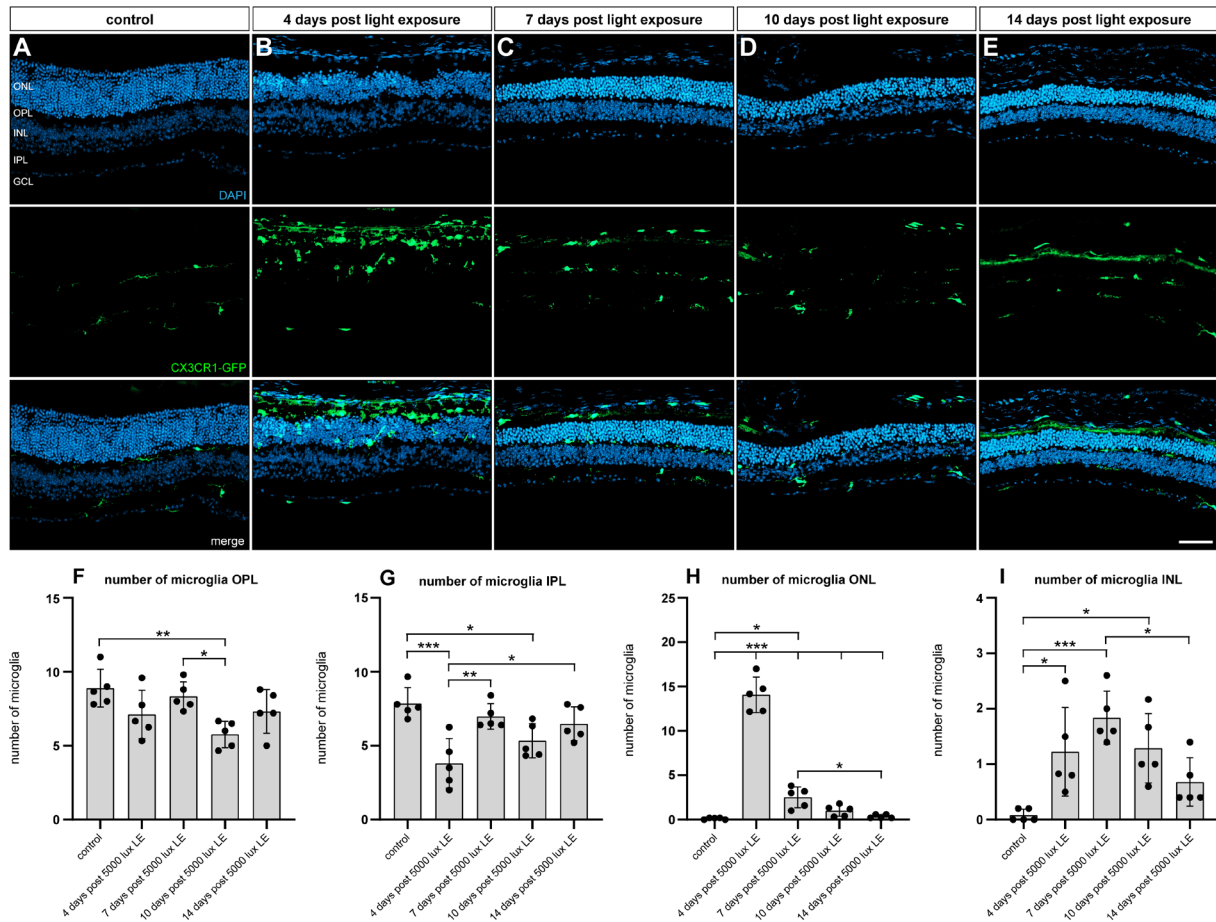


Figure 31 Investigation of microglia location after low intensity light exposure in retinal cryosections. *CX3CR1^{GFP}* reporter mice were exposed to light with an intensity of 5,000 lux for one hour. Retinal cryosection images were taken at days 4, 7, 10 and 14 after light exposure. It has been shown that 4 days after light exposure the microglia migrate from the plexiform layers to the nuclear layers (A – E). When retinal degeneration reached its maximum on day 7, microglia gradually migrated back to the plexiform layers. The enumeration showed that the number of microglia increased significantly on day 4 in both nuclear layers. At the same time, a decrease in the plexiform layers could be determined. In the further course, the numbers recovered again and equalized to the control value (F – I). Only in the INL few microglia remained (* $p < 0.05$, ** $p < 0.01$, *** $p \leq 0.001$) ($n = 5$) (Scale bar = 50 μm).

Results

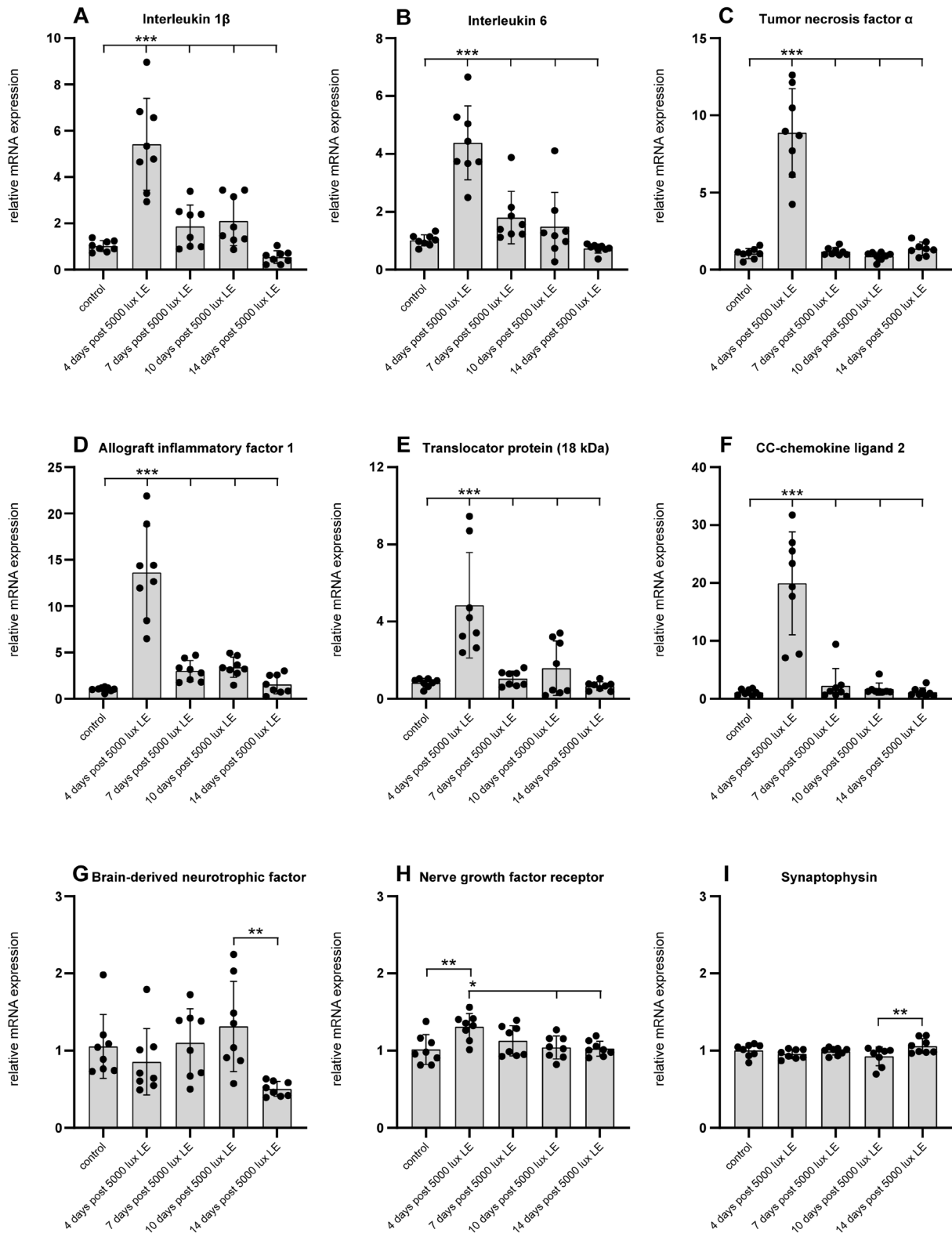


Figure 32 Investigation of pro- and anti-inflammatory markers after low intensity light exposure. *CX3CR-1^{GFP/-}* reporter mice were exposed to light with an intensity of 5,000 lux for one hour. Pro- and anti-inflammatory marker expression in whole retinal transcripts were determined by using qRT-PCR at days 4, 7, 10 and 14 days after light exposure. All pro-inflammatory markers examined were significantly upregulated at day 4 (A – F). From day 7 they were downregulated to their initial level and were comparable to the control. Anti-inflammatory marker expression patterns did not change in any way (G – I) (* $p < 0.05$, ** $p < 0.01$, *** $p \leq 0.001$) ($n = 8$).

3.6 Effect of curative microglia depletion in the light damaged retina

In this part of the study, we addressed the curative depletion of microglia after the induction of retinal degeneration. For that reason, the previous sections enlightened microglia repopulation and the progression of retinal degeneration in a time course of 14 days after low light exposure. This was indispensable since experiments were carried out on *CX3CR-1^{GFP/-}* reporter mice in accordance with the fifth experimental setup outlined in chapter 2.2.5 which is illustrated in Figure 11. Group one served here as a reference for the extent of retinal degeneration, since it received the standard rodent diet for the entire period after light exposure. For the length of the experiment, group two was given the PLX3397 diet in order to study the effects of long-term microglia depletion. To test the efficacy of early and late microglia depletion, respectively, either immediately following induced retinal degeneration or 7 days later, the diets in groups three or four were switched on day 7. Microglia will repopulate in an already damaged environment as a result of early depletion, possibly preventing reactivation.

3.6.1 The timing of microglia depletion has no effect on the extent of retinal degeneration

In order to assess the severity of retinal degeneration, SD-OCT scans were performed 14 days after low light exposure and indicated treatment with PLX3397. Reflective images of the retinal layers showed a massive thinning of the ONL in light exposed retinas (Figure 33.A – E). The heatmaps confirmed by their color change from green to blue that the timing and duration of PLX3397 treatment had no effect on retinal degeneration (Figure 33.F – J). According to the analysis, all experimental settings resulted in a significant reduction in retinal thickness (Figure 33.P; Q). There were no alterations found in retinas that had been exposed to light independent of PLX3397 treatment. Interestingly, the BAF *in vivo* images indicated that there was a difference between, early, no and late microglia depletion when looking at their morphology (Figure 33.K – O). After 14 days, the newly repopulated microglia as a result of early depletion had an amoeboid shape and were reactivated. While the naïve microglia exhibit a ramified morphology and an activated state at the end of the experiment when they were present continuously throughout. No microglia were found in the late depletion scenario.

Results

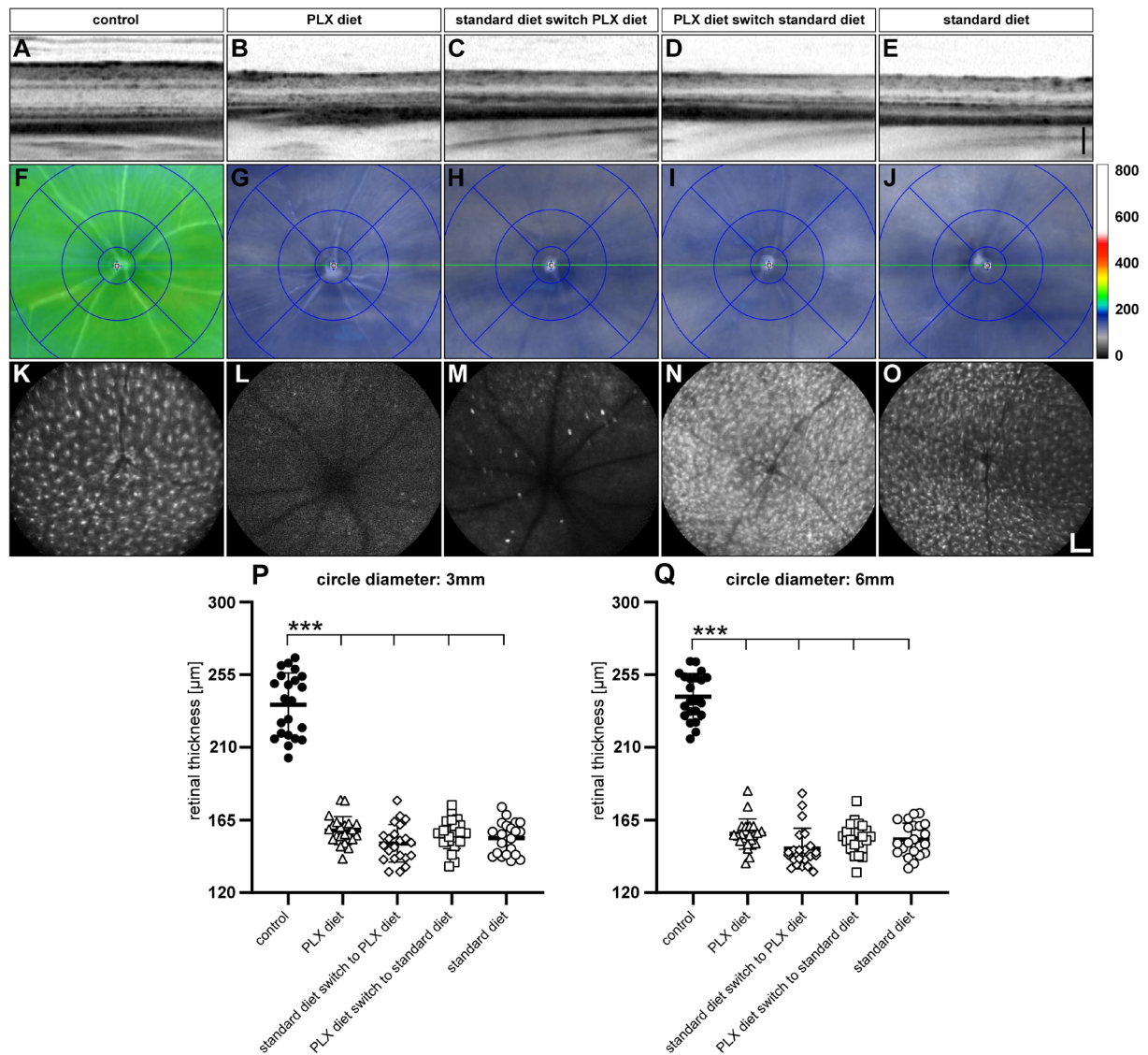


Figure 33 SD-OCT analysis on the effect of curative microglia depletion on retinal degeneration. *CX3CR-1^{GFP/-}* reporter mice received PLX3397 diet as indicated and 5,000 lux light exposure for one hour. SD-OCT scans were carried out to quantify the extend of retinal degeneration. Reflective images of retinal layers showed a massive thinning of the ONL in all experimental conditions (A – E). Heatmaps confirmed by a color change from green to blue that the timing of microglia depletion had no effect on the severity of degeneration (F – J). A significant decrease of retinal thickness could be evaluated from these data (P; Q). BAF *in vivo* images showed an altered morphology according to the different PLX3397 treatments (K – O) (* $p < 0.05$, ** $p < 0.01$, *** $p \leq 0.001$) ($n = 22$) (Black scale bar = 100 μm; white scale bar = 200 μm).

3.6.2 Repopulated microglia are reactivated by a damaged environment

Retinal flat mounts were examined 14 days after low light exposure and indicated PLX3397 treatment in order to thoroughly analyze the morphology. In mice that received the PLX3397 diet for the entire 14 or the final 7 days, no microglia were detected in the examined layers (Figure 34.B; C). Considering the microglia that newly repopulate as a result of early depletion in a damaged environment, it was discovered that they were reactivated and displayed an amoeboid shape (Figure 34.D). Additionally, it was possible to observe a large accumulation of microglia in the SRS. If naïve microglia were present during the whole experimental course of retinal degeneration, they showed up in ramified morphology and activated state (Figure 34.E). Less microglia were found in the SRS. The condition of early microglia depletion with accompanying repopulation, following induced retinal degeneration resulted in a significant reduction in all morphological parameters measured for the OPL (Figure 34.F – K). While in the condition of naïve microglia this decrease was absent and showed no differences to the control condition. The same trend was observed for the IPL and SRS shown in the supplementary data (Supplementary figure 7 and 8). It could be concluded that the newly repopulated microglia were reactivated by the damaged environment in the course of retinal degeneration and took on an amoeboid shape. Naïve microglia that have been present throughout the entire degeneration process were activated and exhibited a ramified morphology at the end.

In order to get a better insight into the localization of microglia, cyosections were examined 14 days after low light exposure and indicated PLX3397 treatment (Figure 35.A – E). The condition of early microglia depletion, showed a significant increase in the number of newly repopulated microglia in both nuclear layers (Figure 35.D; H; I). Naïve microglia that were present throughout the entire experimental period did not show this increase. After early depletion, the number of newly repopulated microglia was significant lower in the OPL (Figure 35.F). Furthermore, there were no differences in numbers between the naïve microglia and the control condition in the OPL. No differences in the IPL's microglia counts could be shown in any of the experimental conditions (Figure 35.G). This unequivocally demonstrated that newly repopulated microglia migrated from the plexiform layers into the nuclear layers towards the damaged areas. In contrast, naïve microglia likely returned to the plexiform layers once the 14 days had passed.

3.6.3 Microglia that removed all cell debris undergo re-ramification and return to the plexiform layers

In order to quantify the extent of retinal degeneration TUNEL stainings were performed to validate the number of dead cells in the ONL following light exposure (Figure 36). TUNEL⁺ cells were massively upregulated in conditions where microglia depletion occurred, regardless of whether they were absent for the entire period or only at the end or beginning of the induced retinal degeneration (Figure 36.B; C; D). Additionally, in persistently depleted microglia, a moderate increase in TUNEL⁺ cells could be seen (Figure 36.B; F). This increase was not significant, though. Roughly, 50% of TUNEL⁺ cells were detected when microglia were depleted for 7 days and 60% were detected with 14 days of depletion (Figure 36.B – D; F). When considering the situation where the naïve microglia persisted throughout the entire process of retinal degeneration this increase was absent. Here, only 10% of the cells were TUNEL⁺. This leads to the conclusion that after the onset of retinal degeneration, naïve microglia were necessitated to remove the cell debris in the ONL and required approximately 14 days to do so. After accomplishing this, they returned to the plexiform layers and reassumed a ramified shape. However, the debris of dead cells still remained in the ONL when microglia were completely or partially absent over time.

3.6.4 Curative microglia depletion and repopulation cannot prevent photoreceptor cell death

In the following, we investigated the effect of curative microglia depletion and repopulation on photoreceptor mortality 14 days after low light exposure. For this purpose, cone arrestin stainings were performed in retinal flat mounts (Figure 37.A – E). Analysis of photoreceptor numbers revealed that no experimental condition could prevent photoreceptor death (Figure 37.F). It made no difference whether microglia were present or absent all the time or in the early or late course of retinal degeneration. Here, all photoreceptor numbers were significantly reduced. In the control, approximately 760 cone arrestin⁺ cells per 0.15 mm² retina could be detected, whereas this number was reduced to 110 per 0.15 mm² in light exposed retinas.

Results

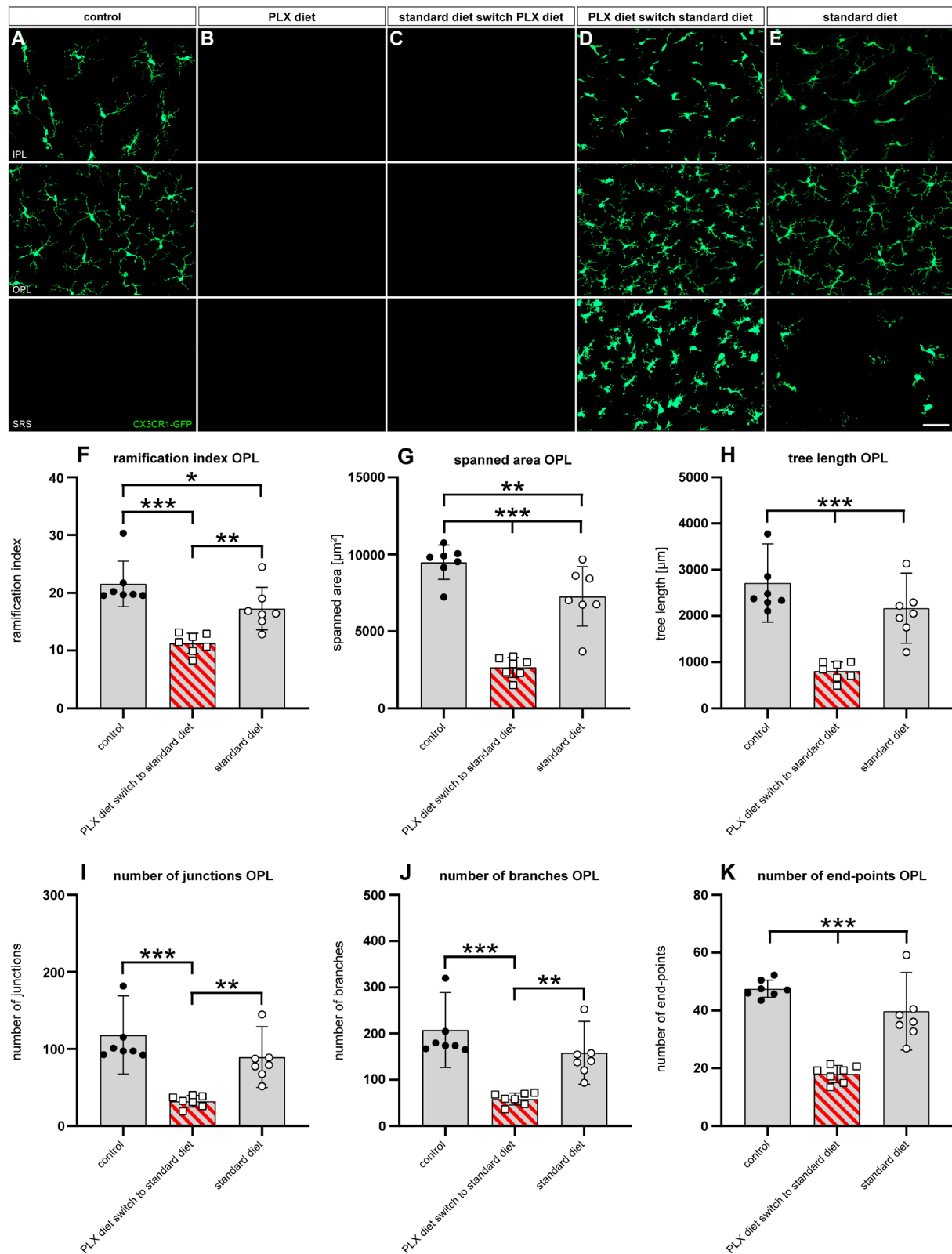
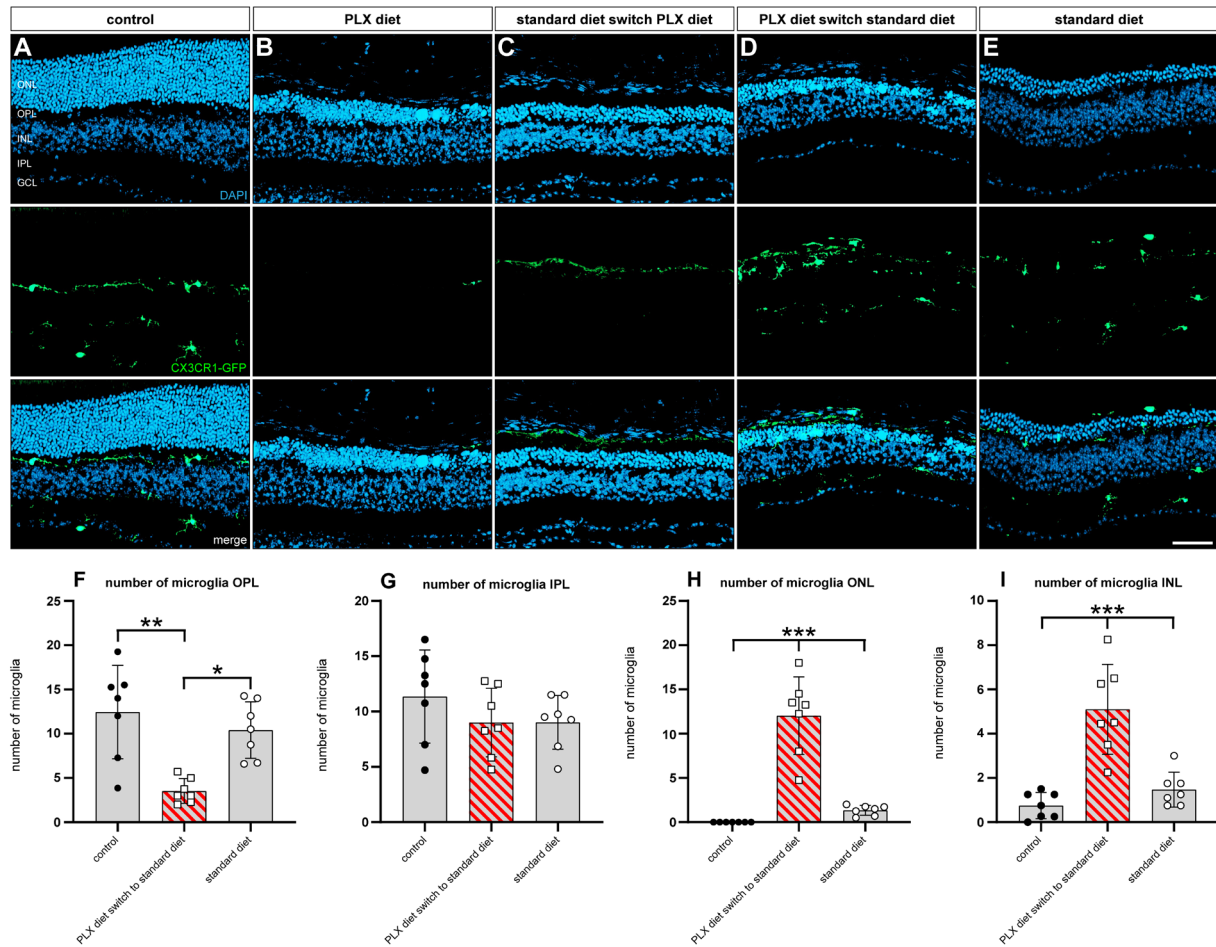


Figure 34 Investigation of microglia morphology in a curative setting of early, late, and no microglia depletion on retinal degeneration. *CX3CR1-GFP⁺* reporter mice received PLX3397 diet as indicated and 5,000 lux light exposure for one hour. Retinal flat mount images were taken 14 days after light exposure. Mice that received constant and late PLX3397 diet no microglia could be detected in the examined layers (B; C). Newly repopulated microglia were reactivated and exhibited an amoeboid morphology (D). Naïve microglia were activated and showed a ramified shape (E). All measured morphological parameters decreased significantly in newly repopulated microglia depletion (F – K). Morphological parameters in naïve microglia were comparable to the control condition (*p < 0.05, **p < 0.01, ***p ≤ 0.001) (n = 7) (Scale bar = 50 μm).

Results



Results

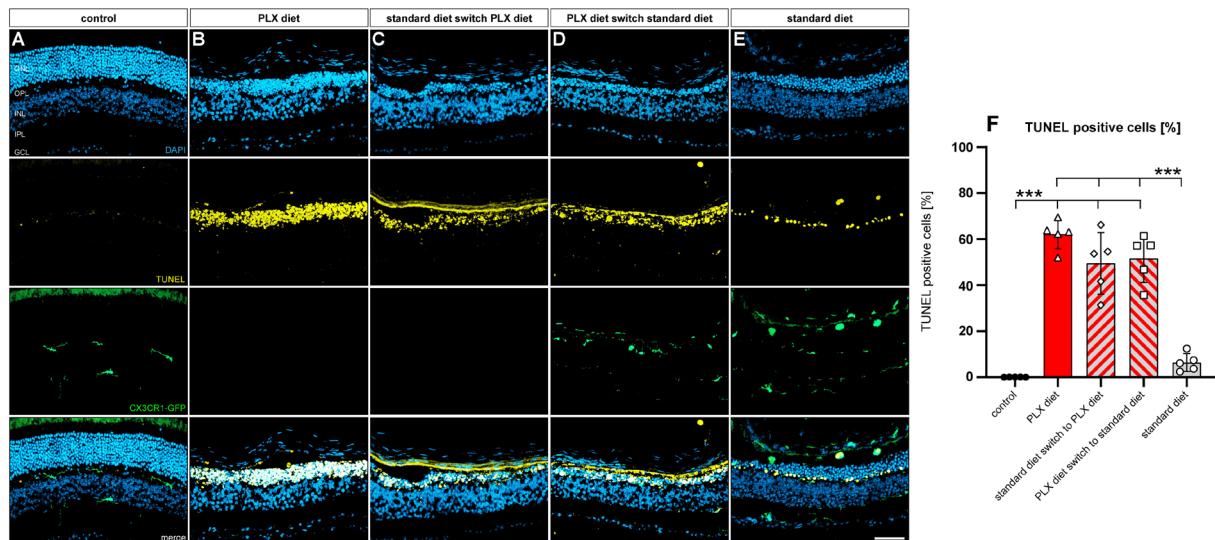


Figure 36 TUNEL staining analysis in a curative setting of early, late, and no microglia depletion on retinal degeneration. *CX3CR1^{GFP/-}* reporter mice received PLX3397 diet as indicated and 5,000 lux light exposure for one hour. TUNEL stainings were carried out in retinal cryosections 14 days after light exposure (A – E). TUNEL⁺ cells were significantly upregulated in conditions of microglia depletion (F). With constantly present microglia throughout the entire course of retinal degeneration, this upregulation could not be detected (* $p < 0.05$, ** $p < 0.01$, *** $p \leq 0.001$) ($n = 5$) (Scale bar = 50 μm).

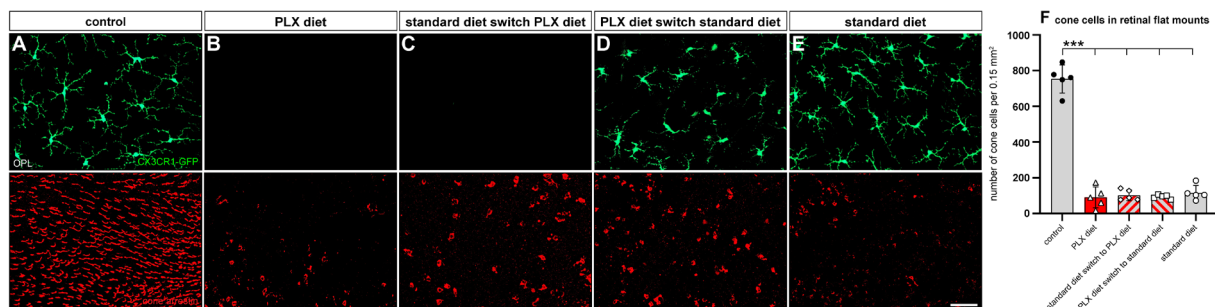


Figure 37 Cone arrestin staining analysis in a curative setting of early, late, and no microglia depletion on retinal degeneration. *CX3CR1^{GFP/-}* reporter mice received PLX3397 diet as indicated and 5,000 lux light exposure for one hour. Cone arrestin stainings were carried out in retinal flat mounts 14 days after light exposure (A – E). Analysis of photoreceptor cell numbers showed a significant reduction in photoreceptor numbers independent of PLX3397 treatment (F) (* $p < 0.05$, ** $p < 0.01$, *** $p \leq 0.001$) ($n = 5$) (Scale bar = 50 μm).

3.6.5 Curative microglia depletion and repopulation triggers astrocytic and Müller cell reactivity

Next, we were interested in how astrocyte and Müller cell reactivity changed 14 days after low light exposure with indicated PLX3397 treatment. Therefore, GFAP stainings were performed in retinal cyrosections (Figure 38). It was observed that GFAP expression with stress fiber formation were both considerably elevated following 7 days of microglia depletion independent of the timing (Figure 38.C; D). Microglia depletion throughout the entire experimental course also showed an increase in GFAP expression, although the formation of stress fibers was not as prominent (Figure 38.B). GFAP expression was marginally elevated relative to the control condition if microglia were present during the entire course of retinal degeneration (Figure 38.E). Stress fiber formation was not detected in this experimental condition. It could be concluded that the complete or partial absence of microglia enhanced astrocytic and Müller cell reactivity.

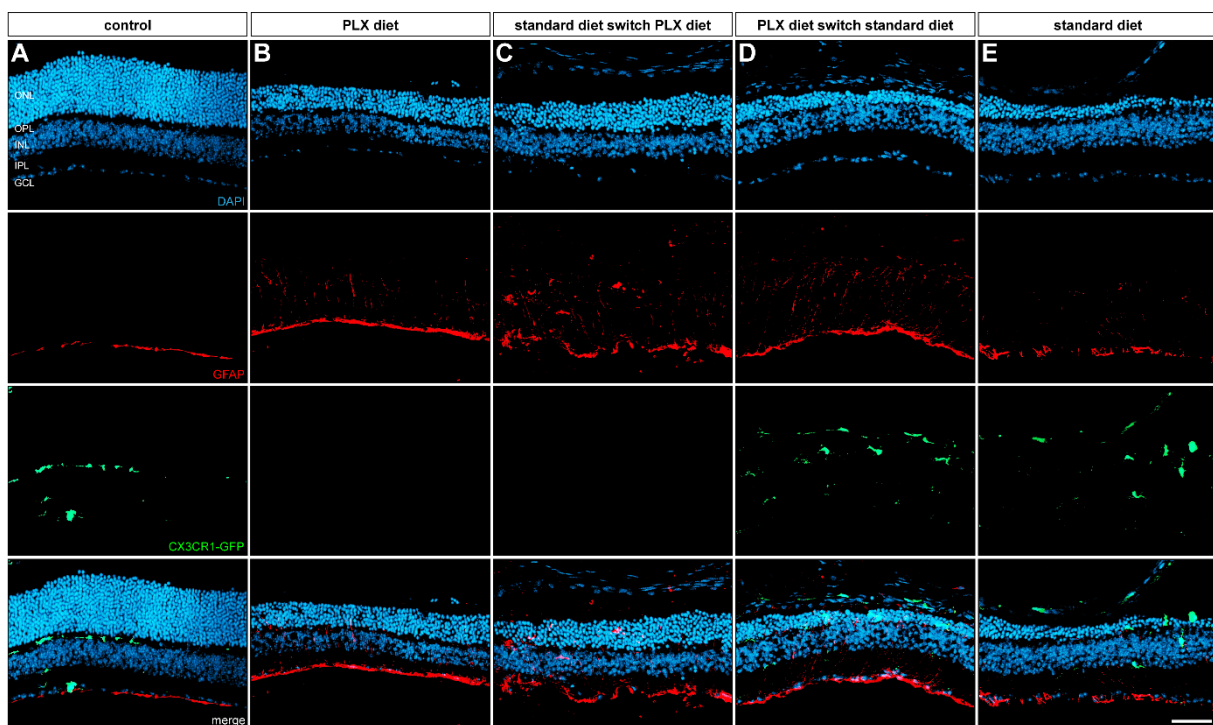


Figure 38 GFAP staining analysis in a curative setting of early, late, and no microglia depletion on retinal degeneration. *CX3CR1*^{GFP/-} reporter mice received PLX3397 diet as indicated and 5,000 lux light exposure for one hour. GFAP stainings were carried out in retinal flat mounts 14 days after light exposure. GFAP expression and stress fiber formation were elevated relative to the control in the course of 7 days of early or late microglia depletion after low light exposure (C; D). Were microglia constantly depleted during retinal degeneration an increased GFAP expression and stress fiber formation could also be observed (B). An upregulation of GFAP expression was not as prominent as in the other groups when no microglia depletion occurred (E). No stress fibers were detected here (Scale bar = 50 μ m).

3.6.6 Repopulated microglia show increased pro-inflammatory marker expression

Finally, we were interested in how pro- and anti-inflammatory marker expression was affected in relation to the timing of microglia depletion after low light exposure. In this context, we additionally wanted to provide insights into the differences between naïve and newly repopulated microglia. For that reason, qRT-PCR was used to examine the expression of the microglia activation marker in whole retinal transcripts. Here, the trend was mirrored by all the pro inflammatory markers that have been examined (Figure 39.A – F). These were significantly upregulated in newly repopulated microglia as a result of early depletion. Such an increase was averted by late and continuous depletion during the whole experimental period. Furthermore, naïve microglia that were present throughout the entire course of retinal degeneration were also found to lack a significant increase in pro-inflammatory marker expression. In these three situations, the expression level was similar to that of the control. Again, the only exceptions were *Il-6* and *Ccl2*. As already shown in the preventive setup, both pro-inflammatory cytokines were significantly increased even in the absence of microglia. The same trend was also observed for the RPE, seen in the supplementary figure 9. The anti-inflammatory markers studied showed no changes in expression levels in any of the experimental conditions (Figure 39.G – I).

Results

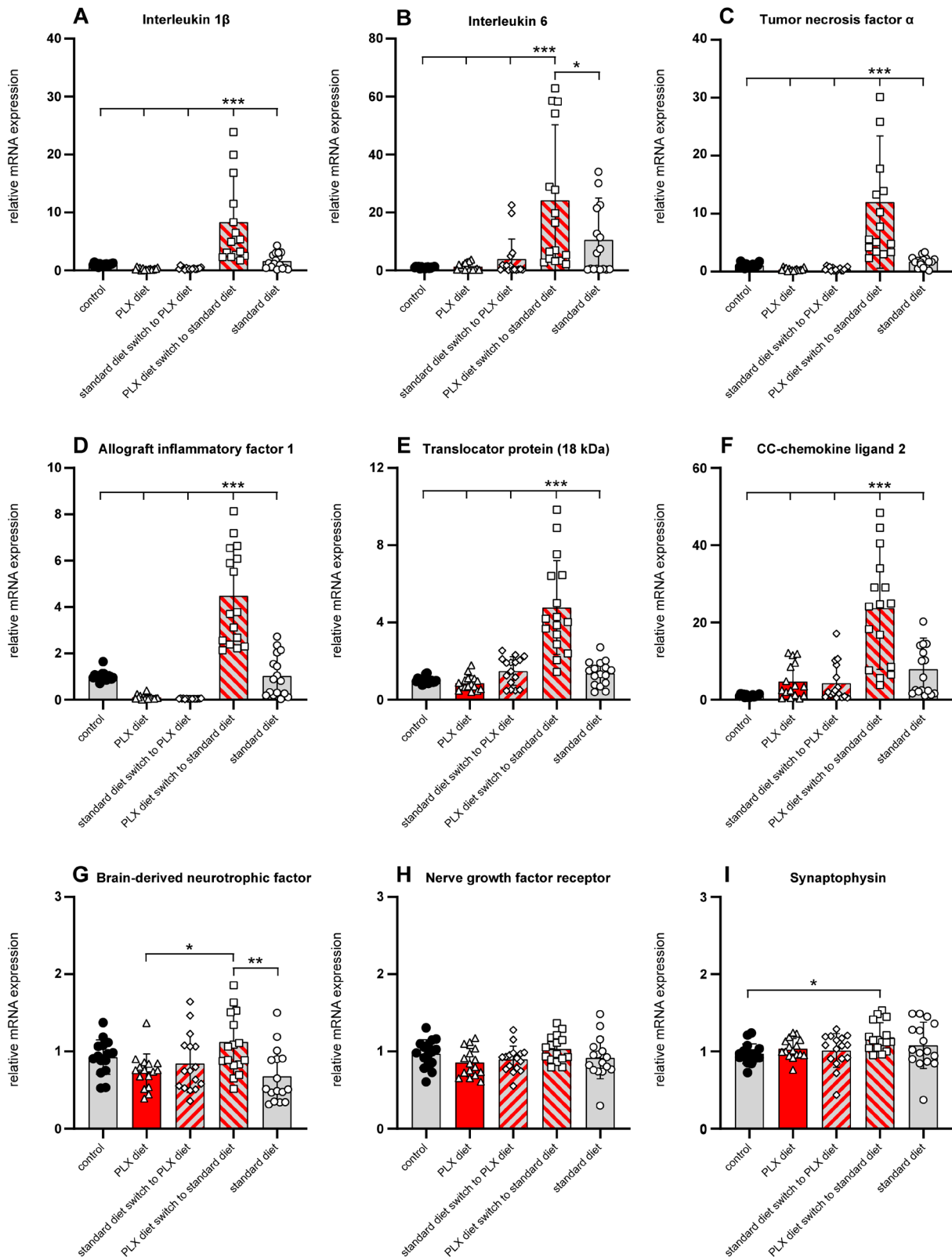


Figure 39 Investigation of pro- and anti-inflammatory cytokines in a curative setting of early, late, and no microglia depletion on retinal degeneration. *CX3CR1^{GFP/-}* reporter mice received PLX3397 diet as indicated and 5.000 lux light exposure for one hour. Pro- and anti-inflammatory cytokine expression in whole retinal transcripts were determined by using qRT-PCR 14 days after light exposure. The expression of pro-inflammatory markers significantly increased in newly repopulated microglia, which is associated with early depletion (A – F). The anti-inflammatory cytokines showed no difference (G – I) (* $p < 0.05$, ** $p < 0.01$, *** $p \leq 0.001$) ($n = 16$).

3.7 Effects of microglia depletion in a model of acute retinal degeneration

In summary, PLX3397 was shown to affect both murine BV-2 microglial cells and 661W photoreceptor cells in their morphology and viability. However, the effects on BV-2 cells were much more pronounced and were achieved at lower concentrations than in 661W cells. Furthermore, retinal microglia were efficiently depleted with PLX3397 under control and light damage conditions. The preventive microglia depletion model could stop over-expression of pro-inflammatory markers in a setting of induced retinal degeneration. However, the extend of retinal degeneration could not be reduced when microglia were absent after light damage. In this context, the mortality rate of cone-photoreceptors could not be rescued with PLX3397 treatment. Additionally, it could be demonstrated that dead cell debris accumulated in the ONL under the condition of complete microglia depletion since these could not be phagocytosed. Moreover, within all situations, the absence of microglia increased the expression of GFAP, indicating increased astrocyte and Müller cell reactivity. Microglia completely repopulated within 7 days after cessation of PLX3397 diet. However, repopulated microglia differed from the naïve microglia in terms of both morphology and the expression of pro-inflammatory markers, which were again comparable to the naïve microglia at day 10. Retinal degeneration had reached its maximum on day 7 after low light exposure. Microglia also showed a gradual decrease in pro-inflammatory marker expression as well as a transition from the reactivated amoeboid to the activated ramified isoform throughout the course of retinal degeneration. The curative microglia depletion model indicated that within 14 days of low light exposure, microglia that were constantly present had eliminated most of the dead photoreceptor debris from the nuclear layers. Since there were no further pro-inflammatory triggers, they migrated back into the plexiform layers. Because of this, only a few TUNEL⁺ cells were detected at this time, and pro-inflammatory marker expression was no longer upregulated. For this reason, microglia did not exhibit an amoeboid but a ramified shape. Additionally, a reduced astrocytic and Müller cell reactivity could be shown. Considering the newly repopulated microglia, it was shown that their reactivity could not be dampened in any case. As they repopulate into a damaged environment, they were immediately reactivated, took on an amoeboid shape and migrated into the nuclear layers. Therefore, the pro-inflammatory marker expression was also significantly increased. Moreover, 7 days seemed to be insufficient to remove the dead photoreceptor debris, as a significantly increased number of TUNEL⁺ cells could be detected. Additionally, an increased astrocyte activity and Müller cell reactivity with confining formation of stress fibers could be shown when microglia were continuously depleted or for 7 days. For these reasons, we draw the conclusion that a number of factors, in addition to over-reactive microglia contribute to retinal degeneration. In actuality, it was demonstrated that microglia depletion and newly repopulated microglia did not rescue the extend of retinal degeneration.

4. Discussion

Reactive microglia are commonly present in retinal degenerative diseases like AMD. They secrete neurotoxic substances and phagocytose stressed but healthy photoreceptors. Therefore, they contribute to retinal degeneration and vision loss. Here, we demonstrated that depletion of microglia with the CSF1R inhibitor PLX3397 could not prevent photoreceptor cell death. Even newly repopulated microglia could not stop retinal degeneration.

4.1 PLX3397 allows specific and rapid depletion of microglia populations

Microglia depletion paradigms have considerably assisted research efforts to pinpoint the functions that microglia perform in the central nervous system. A powerful and adjustable strategy for eliminating microglia is CSF1R inhibition with PLX3397. Although this procedure is surgically noninvasive, treatment depends on peripheral delivery of a tiny chemical, which has the potential to cause off-target effects (Green, Crapser et al. 2020). The analysis of metabolic activity is frequently used to evaluate the viability of cells in order to ascertain the effects, including possible side effects or potency of test compounds (Braissant, Astasov-Frauenhoffer et al. 2020). The measurement of dead cells or free-floating DNA, which leaks into the surrounding culture medium upon loss of membrane integrity, accesses the cytotoxicity of test compounds (Riss, Niles et al. 2004). Together, these two parameters offer a reliable characterization of the potency and off-target effects of PLX3397 on various cell lines.

Murine BV-2 microglia cells were an excellent choice to test the efficacy or potency of PLX3397 *in vitro*. Since they highly express CSF1R, the IC_{50} for metabolic activity and the EC_{50} for cell mortality were reached at the lowest concentrations of the cell lines tested here. Morphological changes were also observed at the lowest concentrations of all cell lines used. CSF1R belongs to the class of the type III protein tyrosine kinase (PTK) receptors (Stanley and Chitu 2014). The platelet-derived growth factor receptors (PDGFR), which are expressed in photoreceptors, also belong to this class. PTK receptors are all characterized by an intracellular kinase domain and five extracellular immune globulin (Ig)-like domains (Figure 5) (Heldin and Lennartsson 2013). This leads to the assumption that PLX3397 probably has off-target effects. Therefore, the effect of PLX3397 on 661W photoreceptors was tested *in vitro*. The experiments performed here showed that very high IC_{50} and EC_{50} values were reached for both metabolic activity and cell mortality. These were significantly higher than those of BV-2 cells were and only slightly lower than the highest PLX3397 concentration used. Only the morphology of the 661W photoreceptors was visibly affected at lower concentrations. However, experiments unequivocally showed that PLX3397 causes persistent PDGFR blockage (Patwardhan, Surriga et al. 2014). Since the PTK receptors are expressed on different cell types and thus probably have other functions that do not affect metabolic activity or cell mortality. In adult

mice, CSF1R strongly influences the survival of cells expressing this receptor, so blocking its signaling will most likely lead to a reduction in metabolic activity and an increase in cell mortality. PDGFR on the other hand affects intestinal fluid pressure, prevents formation of edema and is involved in wound healing (Patwardhan, Surriga et al. 2014). Therefore, metabolic activity and cell mortality associated with blockage of PDGFR signaling in 661W photoreceptors cannot be assumed to be affected in the same way as it is in BV-2 cells when CSF1R signaling is blocked. This is also supported by our *in vivo* experiments, as no TUNEL⁺ cells could be detected in the ONL after PLX3397 treatment without inducing retinal degeneration. In consideration of this, photoreceptors or any other cell type do not die *in vivo* upon supplementation of the selected PLX3397 concentration. The phagocytosis of dead cell debris in order to avoid TUNEL labeling can also be excluded, since microglia are absent here. Due to the lack of expression of CSF1R or any other PDGF family receptor (Cömert et al, unpublished), HEK293 cells showed the highest values in reaching the IC₅₀ and EC₅₀ for metabolic activity and cell mortality. During the course of PLX3397 treatment, the morphology did not change either. CSF1R inhibition provides control over the dynamics of microglia populations, achieving rapid and sustained depletion without triggering significant off-target effects, compensating mechanisms or pro-inflammatory cytokine storms. Consequently, the usage of PLX3397 represents a chance to ascertain whether and how microglia have an impact on retinal degenerative diseases. Our data are excellently supported by some *ex vivo* experiments in which PLX3397 treatment did not show remarkable effects on other CNS related cell types following long-term oral administration (Liu, Given et al. 2019).

Subsequent delivery of CSF1R inhibitors *in vivo* leads to a regulated cell death in microglia. This form of cell death is apoptosis that is characterized by the activation of the caspase signaling pathway and the identification of TUNEL⁺ cells (Matsudaira and Prinz 2022). Microglia are the main cells in charge of removing cell debris, although they are not likely to phagocytose the debris of their congeneric relatives. However, we and other researchers have discovered that fast microglia depletion with PLX3397 does not cause significant deposition of microglia debris or noticeable inflammatory responses (Huang, Xu et al. 2018, Zhan, Krabbe et al. 2019). This observation may be explained by the fact that astrocytes in the brain and retina are primarily responsible for phagocytosing microglia waste within hours. In astrocytes, RUBICON dependent LC3-associated phagocytosis, a type of non-canonical autophagy, serves to eliminate microglia debris so fast (Zhou, Li et al. 2022). Therefore, we could not detect any TUNEL⁺ after microglia depletion without inducing retinal degeneration.

4.2 Microglia show content dependent and region-specific responses

Despite extensive research and new progress, the function of microglia in both neurological diseases and the healthy CNS remains subject to discussion. It has been discovered that both normal aging and the development of neurodegenerative diseases are correlated with microglial reactivation or priming to pro-inflammatory signals (Perry and Holmes 2014, Norden, Muccigrosso et al. 2015). Several neurological diseases, including AMD, are linked to microglial reactivation following pro-inflammatory stimuli (Crews, Lawrimore et al. 2017, Fonken, Frank et al. 2018, Rashid, Akhtar-Schaefer et al. 2019). Our results have shown that microglia depletion and consequent lack of most pro-inflammatory markers (except those related to astrocytes) had no effect on light-induced retinal degeneration or photoreceptor loss. Here, we could even show that dead cell debris accumulated in the ONL due to lack of phagocytosis. However, there is also a large number of disagreements over the potential protective or harmful effects of microglia depletion in neuro-degenerative diseases, which are probably caused by a variety of reasons, including differences in the methods implemented to deplete microglia and the disease models used in those studies. The hypothesis that different effects of microglia depletion depend on the CNS compartment may also be supported by the fact that the retinal microglia were more sensitive to CSF1R blockage compared to brain microglia (Church, Rodriguez et al. 2022). Microglia were found to protect against neuronal damage following cerebral artery occlusion. When microglia were selectively depleted from the brain, spreading depolarization of neurons after artery occlusion was significantly reduced, which was linked to neuronal death and neuronal network activity was dysregulated (Szalay, Martinecz et al. 2016). The expression of pro-inflammatory markers was decreased by microglia depletion during acute ethanol withdrawal after binge, while induction of anti-inflammatory genes was boosted (Walter and Crews 2017). This counteracted the harmful effect of alcohol treatment. In our study, we could also show a reduced expression of microglia related pro-inflammatory markers. However, this could not rescue the photoreceptors from dying. In contrast, we did not detect increased expression of anti-inflammatory genes after microglia depletion. In the retinal environment, it has been shown that microglia reactivated by intravenous LPS stimulation contributed to the breakdown of the BRB accompanied by accumulation of sub-retinal fluid and a robust release of pro-inflammatory cytokines (Kokona, Ebnetter et al. 2018). Microglia depletion with PLX5622 prevented BRB breakdown and reduced cytokine levels in the retina. In intracerebral hemorrhage (IHC) mouse models, microglia depletion seemed to be neuroprotective because of decreased lesion size, cerebral edema and neurodeficiencies. Furthermore, leukocyte infiltration was reduced and the integrity of the BBB was preserved by microglia elimination (Li, Li et al. 2017).

In contrast, it had been shown that in ischemia models, the number of infiltrating leukocytes was greatly increased after microglia depletion. Here, the integrity of the BBB was reduced

(Jin, Shi et al. 2017). According to studies, acute microglia depletion caused gray matter microgliosis, neuronal death in the somatosensory cortex with a dysregulated type 1 interferon activation phenotype and ataxia-like behavior (Rubino, Mayo et al. 2018). These findings add to earlier research that had shown neurodegeneration in layer V cortex because of microglia depletion during embryonic and early postnatal development (Ueno, Fujita et al. 2013, Miyamoto, Wake et al. 2016). In the initial stages of mouse hepatitis virus treatment, the lack of microglia enhanced infection rates and mortality. The expression of MHC II on invading macrophages decreased because of the depletion of microglia. Because MHC II is necessary for cluster of differentiation (CD) 4 T cell activation, this declined in MHC II in the brains was likely a factor in the reduced virus-specific CD4⁺ T cell response seen in the absence of microglia (Wheeler, Sariol et al. 2018). However, in an explanation of their findings, most studies referred to the cross-talk between microglia and diverse cell types, which included Müller cells, astrocytes, endothelial cells, pericytes, and ganglion cells. Microglia can alter the characteristics of neuronal membranes and synaptic connections by releasing soluble signaling molecules and physically interacting with synaptic components (Tremblay, Lowery et al. 2010, Schafer, Lehrman et al. 2012, Ferrini, Trang et al. 2013, Lewitus, Konefal et al. 2016). Regardless of the disease model itself or the method of microglia depletion, one answer to the controversial results can probably be found in the microglia themselves. It is likely that the mature microglia populations in the CNS exhibits heterogeneity, according to gene expression analysis and immunohistochemistry studies (Lawson, Perry et al. 1990, de Haas, Boddeke et al. 2008, Grabert, Michoel et al. 2016). Nevertheless, a common set of molecular markers and functional responsibilities are shared by all microglia. However, significant variations in the transcriptome of microglia in different brain regions were identified, supporting the idea that these cells have region-specific phenotypes and functional states (Hanisch and Kettenmann 2007). Throughout various brain regions, microglia exhibit significant heterogeneity in density and branching complexity (De Biase, Schuebel et al. 2017). Different pathological stimuli can also cause different morphologic changes in microglia with confining functional alterations (Hanisch and Kettenmann 2007). Depending on the target, participating receptors, and environment, microglia responses may result in the release of different components. Phagocytosis and the release of pro-inflammatory mediators took place when brain microglia were challenged by bacterial invasion (Häusler, Prinz et al. 2002). Microglia in the brain, on the other hand, released anti-inflammatory mediators while clearing away myelin debris or dead cells (Magnus, Chan et al. 2001). In our experiments performed here, retinal microglia were stimulated by light damaged and stressed photoreceptors. Therefore, in this context, since both the stimulus and the region of microglia differ from the experiments described above, the outcome after depletion may be completely different. However, in our experiments we could also not show that the expression of anti-inflammatory markers was increased after

or during phagocytosis. From these observations, it can be concluded that microglia responses can change depending on the stimulus's context and intensity. They are flexible and stimulus-dependent. Moreover, stimuli compete for dominating impact over the actions of microglia.

4.3 Astrocytes might contribute to retinal degeneration

Astrocytes make up approximately 50% of the CNS's total volume and are the most prevalent cell type in the CNS. Similar to microglia, astrocytes are both friend and foe in degenerative diseases. On one hand, astrocytes have strong pro-inflammatory capabilities because they actively contribute to the secretion of pro-inflammatory markers such as *Ccl2*, *Il-1 β* or *Il-6* at the stage of CNS injury (Colombo and Farina 2016). This could also be confirmed by our results, as pro-inflammatory markers such as *Ccl2* and *Il-6* were still significantly elevated in the absence of microglia after induction of retinal degeneration compared with control. However, the expression was highest in the presence of microglia. Thus, we demonstrated that the levels of secreted pro-inflammatory markers originated in both astrocytes and microglia. Additionally, astrocytes are regarded as amateur antigen-presenting cells, which probably lead to the recruitment of T cells (Constantinescu, Tani et al. 2005, Kimelberg 2010). These reactive T cells might also contribute to the degeneration of stressed but healthy cells in an inflammatory environment. On the other hand, astrocytes can release TGF- β , which gives them the capacity to induce scar tissue formation and limit inflammation (Sofroniew 2015). Astrocyte scar boundaries possibly act as functional barriers that control and limit the entry of inflammatory cells into the CNS through contact and diffusion-mediated mechanisms. In brain ischemia models, PLX3397 treatment significantly increased astrocyte reactivity by substantially up-regulating *iNos* levels and other pro-inflammatory mediators (Jin, Shi et al. 2017). Furthermore, it was demonstrated that isolated oxygen-glucose deprivation treated astrocyte conditioned medium accelerated neuronal death as evidenced by an increase in the number of TUNEL⁺ cells and lactate dehydrogenase (LDH) release. These results show that microglia may be essential for neuron-astrocyte interaction in ischemic brain injury and that the neuroprotective benefit of microglia may derive from its inhibitory effect on the astrocyte response (Szalay, Martinecz et al. 2016, Jin, Shi et al. 2017). In line with these studies, we also found increased astrocyte activity together with the formation of stress fibers in conditions of microglia depletion, which probably contribute to retinal degeneration after light exposure. Thus, we can conclude that after microglia perish, astrocytes are likely to come into play. However, they are unable to compensate for the phagocytotic activity of microglia, which was presumably reflected in increased TUNEL⁺ cell numbers.

4.4 Müller cells might contribute to retinal degeneration

Previous studies have shown that Müller cells can also contribute to retinal degeneration. Neurons receive trophic compounds from Müller cells, which also eliminate metabolic waste (Poitry, Poitry-Yamate et al. 2000). Photoreceptors preferentially take up lactate produced by the metabolism of glucose by Müller cells as a source of energy for their oxidative metabolism (Poitry-Yamate, Poitry et al. 1995). Müller cells are therefore necessary for retinal neurons to survive. Selective Müller cell death results in photoreceptor apoptosis and retinal degeneration (Dubois-Dauphin, Poitry-Yamate et al. 2000). By quickly absorbing released neurotransmitters and by giving neurons neurotransmitter precursors, Müller cells play a direct and indirect role in the neuronal communication and degeneration process within the retina (Rauen and Wiessner 2000).

Müller cell reactivity is characterized by response to a pathogenic stimulus. These response is shown as an upregulation of the intermediate filaments vimentin, and, in particular, GFAP. Vimentin is typically found in astrocytes and Müller cells, whereas GFAP is only seen in astrocytes in a healthy retina (Schnitzer 1988, Okada, Matsumura et al. 1990). Both varieties of intermediate filaments are highly expressed in reactive Müller cells. As the expression of GFAP by Müller cells is an early non-specific but highly sensitive indicator of a wide variety of retinal diseases, the presence of an intraretinal pathological process can be reliably determined by detecting GFAP expression in Müller cells (Osborne, Block et al. 1991, Osborne and Larsen 1996). For example, Photoreceptor degeneration and photoreceptor degeneration in light-induced photoreceptor degeneration have both been linked to an up-regulation of GFAP (Grosche, Härtig et al. 1995, de Raad, Szczesny et al. 1996). Additionally, Müller cell hypertrophy has been linked to a number of disorders, including retinal detachment and retinal light-damage (Erickson, Guérin et al. 1990, Grosche, Grimm et al. 1997). Müller cells express iNOS when they are in a diseased state (Kobayashi, Kuroiwa et al. 2000). The etiology of diabetic retinopathy and ischemia and infectious processes may be impacted by Müller cells' NO production (Goureau, Hicks et al. 1994). NO can increase retinal blood flow when there is hypoxia or hypoglycemia. Although the NO that activated Müller cells release is not toxic to the Müller cells themselves, it may cause the death of neuronal cells (Roth 1997).

4.5 Microglia develop tolerance to repeated or persistent inflammatory stimuli

In this study we investigated the progression of retinal degeneration and the response of microglia after low light exposure over a long period of time. We found that pro-inflammatory response of microglia was at its peak 4 days after light exposure. Here, the highest expression of pro-inflammatory markers was observed and microglia showed a reactivated and amoeboid phenotype. From day 7 to day 14 after light exposure, the expression of pro-inflammatory

markers gradually decreased to control levels. The morphology also changed to an activated and ramified phenotype. The same observations were made after repeated LPS injections. Pro-inflammatory marker analysis of whole retinal transcripts showed a significant increase after the first LPS injection. Nevertheless, this increase was only temporary, as only basic fibroblast growth factor and vascular cell adhesion molecule 1 were increased after 4 repeated LPS injections, while the levels of other pro-inflammatory markers were unchanged from those found in the retinas of mice that had not been challenged (Kokona, Ebner et al. 2018). So-called endotoxin tolerance may be brought on by repeated LPS injections (Wendeln, Degenhardt et al. 2018). Due to receptor desensitization and the downregulation of inflammatory marker gene production, microglia are hypothesized to become hyporesponsive to LPS. Pretreatment of murine microglia with LPS inhibited phosphorylation of the extracellular signal-regulated kinases that are correlated to reactivate microglia in the presence of inflammatory stimuli (Medvedev, Kopydlowski et al. 2000). Furthermore, a downregulation of the transcription factors nuclear factor κ B (NF- κ B) and activator protein 1 (AP-1) in response to subsequent LPS stimulation was observed. In this perspective, it has also been demonstrated that repeated LPS priming of peripheral blood mononuclear cells reduced the expression of the costimulatory molecule CD8 and MHC II (Wolk, Döcke et al. 2000). Additionally, it demonstrates that repetitive LPS stimulation decreases the immune response of microglia. Although the method of microglia stimulation used in our experiments differed from that induced by LPS, we were able to demonstrate attenuation of microglia reactivity after long-term low-light damage. Therefore, we can conclude that not only the presentation of LPS but also degenerating photoreceptors lead to endotoxin tolerance in microglia. The following can be deduced, that any kind of inflammatory stimulus triggers a tolerance in microglia as long as they are repeated often enough or persist for a long time.

4.6 Microenvironment influences the response of repopulated microglia to stimuli

Microglia repopulate after depletion from a resident pool of depletion resistant microglia and from peripherally invading macrophages that can develop a microglia like characteristic (Lund, Pieber et al. 2018). Repopulation experiments with PLX5622 revealed that retinal microglia had two separate niches in which they thrived, they shared a single developmental lineage. These niches' microglia varied in their reliance on *Il-34* and functional role in processing visual information. Microglia from both pools migrated to the subretinal space during certain retinal degeneration models (O'Koren, Yu et al. 2019). This microglial infiltration involved transcriptional reprogramming of the microglia, which is characterized by downregulation of homeostatic checkpoint gene expression and elevation of injury-responsive gene expression. This transition is linked to the RPE defense against related damage. According to another

study, diabetic mice treated with PLX5622 showed increased microglial ramification index following repopulation along with increased cellular branches as contrasted to amoeboid shaped microglia in diabetic controls (Church, Rodriguez et al. 2022). Transcriptomic research, which supported these findings, showed a decrease for gene clusters associated with microglial reactivation, suggesting that these changes in microglia morphology are related to transcriptional reprogramming. This resulted in reduced pathogenic angiogenesis, vascular damage and neuronal cell loss in diabetic retinas. Some other study found that after ethanol treatment, repopulated microglia expressed increased anti-inflammatory cytokines, microglial inhibitory signals and growth factors like *Il-10*, *Bdnf* and *Ngfr* (Coleman, Zou et al. 2020). This was coupled to an attenuated induction of pro-inflammatory markers. Hence, we predicted that the repopulation of microglia in the light-exposed retina would provide new and unprimed microglia, which probably protect from retinal degeneration.

In contrast to the studies mentioned here, we could not confirm that priming of microglia was prevented in the model we used. The newly repopulated microglia were directly reactivated by the degenerative and damaged environment. This was reflected in a significant decrease of the ramification index towards an amoeboid form. Moreover, the expression of pro-inflammatory markers was strongly increased compared to control or naïve microglia. Additionally, in contrast to the naïve microglia, the newly repopulated microglia were not able to phagocytose the dead cell debris in the ONL, as we could detect a significantly increased number of TUNEL⁺ cells. We also did not detect increased expression of anti-inflammatory growth factors in repopulated microglia, which might have contributed to protection against retinal degeneration. Our results are probably supported and explained by a study in which repopulated microglia were challenged with LPS and compared to repopulated microglia in the normal aged CNS. Evidence was found that aging-related increases in intracellular lipofuscin accumulation and CD68⁺ lysosome size could be reversed by microglial repopulation (O'Neil, Witcher et al. 2018). A gene profile that distinguished aging microglia from disease-related microglia was also discovered by micro-specific RNA sequencing. Microglial repopulation affected on third of these genes. Even with this partial reversal of the aged microglial transcriptome, LPS treatment continued to cause increased disease behavior in repopulated microglia and CNS inflammation in aged mice. Here, we have proof that the diseased or damaged CNS microenvironment may be a factor for microglial priming. The fact that the diseased microenvironment remained unchanged by microglial renewal and presumably influences repopulating microglia is another pertinent subject of consideration. The inflammatory fingerprint of the diseased, aging CNS is retained throughout the CNS and across species (López-Otín, Blasco et al. 2013). Hence, the continued presence of an inflammatory or damaged milieu in the aged CNS may be the reason why microglial repopulation failed to alter age-associated aggravation of disease behavior and neuroinflammation after LPS

challenge or light-induced retinal degeneration in mice. Notwithstanding the intermediated RNA expression profile mentioned above, the repopulation of microglia had no impact on the two thirds of genes that are differently regulated with aging. Pro inflammatory cytokine *IL-1 β* and MHC II component *H2-Eb1*, which are related with disease-associated microglia priming were unaffected genes (Frank, Barrientos et al. 2006, Henry, Huang et al. 2009). Despite the reversal of one third of the genes, pathway analysis indicated that repopulation had minimal advantages. For instance, age-associated increases in NF- κ B signaling, reactive oxygen species (ROS) generation by macrophages, and augmented interferon (Ifn) γ , *Ifn α* , *Il-1 β* and Tnf signaling in microglia were all consistent with differential gene expression (von Bernhardt, Eugén-von Bernhardt et al. 2015). Overall, microglia repopulation reduces intracellular lipid deposition associated with aging, but only partially restores the dysfunctional microglia transcriptome.

Astrocytic and Müller cell reactivity-related genes, such as GFAP were unaffected by the repopulation of microglia, which usually become upregulated in diseased conditions. Here we could confirm that GFAP expression was upregulated when microglia repopulated in the light damaged retina and in any other setting of microglia absence. It is crucial to note that these results are different from a recent study that claimed microglia repopulation restored disease-associated dysregulation in genes linked to astrocyte reactivity. Repopulated microglia in diabetic retinopathy induced astrocytes to release metalloproteases, increase tight junction proteins, and upregulated junctional adhesion molecules (Church, Rodriguez et al. 2022). Furthermore, the synthesis of neurotrophic factors by astrocytes contributes to both vascular protection and neuroprotection. In contrast to advanced age, where degenerative diseases gradually affected the CNS, the advantage of microglial repopulation may be more significant in circumstances with regionally or temporally circumscribed damage. For example, persistent microgliosis, leukocyte infiltration and pro-inflammatory gene expression were all alleviated by microglia repopulation after inducible hippocampal injury and neuron death (Rice, Pham et al. 2017). These findings support the idea that whether forced microglial repopulation is sufficient to change responses to subsequent stimuli depends on the context. Our results suggest that the microenvironment has a significant impact on the establishment of the pro-inflammatory characteristic of microglia in the context of retinal degeneration. According to our study, the effects of age or disease on the microenvironment are likely to affect the repopulation of microglia in a way that restores their initial impaired phenotype.

4.7 Microglia depletion does not reduce the extend of light-induced retinal degeneration

Microglia have been considered a major causal element in photoreceptor degeneration due to their frequent release of pro-inflammatory markers, production of nitric oxide and ROS. A detrimental role for microglia was revealed in numerous experimental settings where microglia depletion reduced photoreceptor mortality. Microglial recruitment into the photoreceptor layer was dramatically increased in *CX3CR1*-deficient rd10 mice and was linked to accelerated photoreceptor apoptosis and atrophy comparatively to *CX3CR1*-sufficient rd10 littermates (Zabel, Zhao et al. 2016). Increased phagosome numbers and a faster rate of phagocytosis of fluorescent beads and photoreceptor debris were observed in *CX3CR1* deficient microglia, suggesting that *CX3CR1* signaling in microglia controls the phagocytic clearance of stressed photoreceptors. Noteworthy microglial activation markers and enhanced expression of pro-inflammatory cytokines were linked to retinal microglia with *CX3CR1* deficiency. The morphological and functional improvement of photoreceptor degeneration after genetic depletion of retinal microglia provides evidence of the microglial contribution to rod photoreceptor death. The vitronectin receptor antagonist cyclic arginine-glycine-aspartate (cRGD) also improved the morphological and functional characteristics of degeneration by molecularly inhibiting microglial phagocytosis (Zhao, Zabel et al. 2015).

In contrast, we could show that both strong light exposure and low light exposure led to reactivation of microglia and degeneration of photoreceptors. However, it made no difference whether the microglia were depleted before or after the light exposure. Both in the presence and in the absence of microglia, the number of photoreceptors was significantly reduced, although the expression of microglia-related pro-inflammatory markers was significantly reduced. Furthermore, we observed an increased number of TUNEL⁺ cells in the conditions of microglia depletion due to the lack of phagocytosis. As a result, microglia were not necessary for light-induced retinal degeneration, and they seemed to have a general positive impact on the retinal degeneration. These findings suggest that photoreceptors exist on the margin between function and cell survival and dysfunction and death, and that practically any flaw may sway them in the direction of cell death (Wright, Chakarova et al. 2010). Light exposure is the most obvious cause of photoreceptor degradation. Most photoreceptor cell death occurs at wavelengths about 500 nm, which are similar to the absorption spectrum of rhodopsin (Noell, Walker et al. 1966). There is mounting evidence that light damage to photoreceptors necessitates the release of all-trans retinal from light-activated rhodopsin. All-trans retinal photoexcitation produces singlet oxygen and may result in photo-oxidative damage, which kills the photoreceptor cells without any participation of microglia (Sun and Nathans 2001, Travis, Golczak et al. 2007). Similar results were observed in a mouse model of retinal detachment. Here, retinal detachment caused a fast reactivation of microglia, which then migrated into the damaged area and formed close associations with invading macrophages. Increased disease

Discussion

severity and a reduction in macrophage infiltration are the outcomes of retinal microglia depletion, indicating that microglia are important in controlling inflammation in the retina (Okunuki, Mukai et al. 2018). This pattern was also seen in prion-induced retinal degeneration, where microglia depletion with PLX5622 caused photoreceptor degeneration to start much earlier (Striebel, Race et al. 2019). At the terminal stage of prion-induced retinal degeneration, Iba1⁺ cells were primarily identified as microglia in untreated mice, whereas in PLX5622 treated mice, Iba1⁺ cells were reduced and an increased number of monocytes and few regenerating microglia were found. It appears that both cell types phagocytosed damaged photoreceptors. The clearance of partially degraded photoreceptors to prevent bystander cell damage is one possible strategy by which microglia may extend photoreceptor survival.

5. Conclusion

In summary, we could show that microglia depletion reduced the expression of pro-inflammatory markers in a model light induced retinal degeneration. However, the absence of microglia could not prevent the extend of retinal degeneration. On the contrary, we could observe that in the course of missing phagocytosis dead cell debris accumulated in the ONL. This cell debris could still release cytotoxic substances that could affect the living cells in the vicinity and lead them to cell death. In conditions of microglia depletion, astrocytic and Müller cell reactivity was upregulated, which also might contribute to the process of retinal degeneration. Through their interactions with astrocytes or Müller cells, microglia control their reactivity and attenuate the damaging effect on viable cells in an inflammatory environment. Thus, we can conclude that microglia depletion to reduce or stop retinal degeneration is not desirable because the loss of positive effects outweighs the loss of negative effects. Furthermore, we demonstrated that the reactivity of microglia could not be reduced by forced renewal through repopulation. The repopulation of microglia in a diseased condition is likely to be impacted by the microenvironment, making it impossible to maintain unprimed and activated microglia. Summing everything up, we believe that microglia modulation may be a potential therapeutic approach to prevent retinal degeneration rather than depletion and repopulation. Microglia should be modified in a way that keeps both their capacity for phagocytosis and their beneficial effects on other cells. Nonetheless, their over-reactivity and damaging effects on living cells should be controlled.

6. References

- Abou-Kheir, W., B. Isaac, H. Yamaguchi and D. Cox (2008). "Membrane targeting of WAVE2 is not sufficient for WAVE2-dependent actin polymerization: a role for IRSp53 in mediating the interaction between Rac and WAVE2." J Cell Sci **121**(Pt 3): 379-390.
- Ajami, B., J. L. Bennett, C. Krieger, W. Tetzlaff and F. M. Rossi (2007). "Local self-renewal can sustain CNS microglia maintenance and function throughout adult life." Nat Neurosci **10**(12): 1538-1543.
- Alliot, F., I. Godin and B. Pessac (1999). "Microglia derive from progenitors, originating from the yolk sac, and which proliferate in the brain." Brain Res Dev Brain Res **117**(2): 145-152.
- Anderson, D. H., M. J. Radeke, N. B. Gallo, E. A. Chapin, P. T. Johnson, C. R. Curletti, L. S. Hancox, J. Hu, J. N. Ebright, G. Malek, M. A. Hauser, C. B. Rickman, D. Bok, G. S. Hageman and L. V. Johnson (2010). "The pivotal role of the complement system in aging and age-related macular degeneration: hypothesis re-visited." Prog Retin Eye Res **29**(2): 95-112.
- Andriessen, E. M., A. M. Wilson, G. Mawambo, A. Dejda, K. Miloudi, F. Sennlaub and P. Sapieha (2016). "Gut microbiota influences pathological angiogenesis in obesity-driven choroidal neovascularization." EMBO Mol Med **8**(12): 1366-1379.
- Antonietta Ajmone-Cat, M., M. Lavinia Salvatori, R. De Simone, M. Mancini, S. Biagioni, A. Bernardo, E. Cacci and L. Minghetti (2012). "Docosahexaenoic acid modulates inflammatory and antineurogenic functions of activated microglial cells." J Neurosci Res **90**(3): 575-587.
- Arshavsky, V. Y., T. D. Lamb and E. N. Pugh, Jr. (2002). "G proteins and phototransduction." Annu Rev Physiol **64**: 153-187.
- Ashwell, K. (1990). "Microglia and cell death in the developing mouse cerebellum." Brain Res Dev Brain Res **55**(2): 219-230.
- Askew, K., K. Li, A. Olmos-Alonso, F. Garcia-Moreno, Y. Liang, P. Richardson, T. Tipton, M. A. Chapman, K. Riecken, S. Beccari, A. Sierra, Z. Molnár, M. S. Cragg, O. Garaschuk, V. H. Perry and D. Gomez-Nicola (2017). "Coupled Proliferation and Apoptosis Maintain the Rapid Turnover of Microglia in the Adult Brain." Cell Rep **18**(2): 391-405.
- Augood, C. A., J. R. Vingerling, P. T. de Jong, U. Chakravarthy, J. Seland, G. Soubrane, L. Tomazzoli, F. Topouzis, G. Bentham, M. Rahu, J. Vioque, I. S. Young and A. E. Fletcher (2006). "Prevalence of age-related maculopathy in older Europeans: the European Eye Study (EUREYE)." Arch Ophthalmol **124**(4): 529-535.
- Bader, J. E., R. T. Enos, K. T. Velázquez, M. S. Carson, A. T. Sougiannis, O. P. McGuinness, C. M. Robinson and E. A. Murphy (2019). "Repeated clodronate-liposome treatment results in neutrophilia and is not effective in limiting obesity-linked metabolic impairments." Am J Physiol Endocrinol Metab **316**(3): E358-e372.
- Bazan, N. G., J. M. Calandria and C. N. Serhan (2010). "Rescue and repair during photoreceptor cell renewal mediated by docosahexaenoic acid-derived neuroprotectin D1." J Lipid Res **51**(8): 2018-2031.
- Beckmann, N., E. Giorgetti, A. Neuhaus, S. Zurbrugg, N. Accart, P. Smith, J. Perdoux, L. Perrot, M. Nash, S. Desrayaud, P. Wipfli, W. Friauff and D. R. Shimshek (2018). "Brain region-specific enhancement of remyelination and prevention of demyelination by the CSF1R kinase inhibitor BLZ945." Acta Neuropathol Commun **6**(1): 9.

References

- Bessis, A., C. Béchade, D. Bernard and A. Roumier (2007). "Microglial control of neuronal death and synaptic properties." Glia **55**(3): 233-238.
- Blackburn, D., S. Sargsyan, P. N. Monk and P. J. Shaw (2009). "Astrocyte function and role in motor neuron disease: a future therapeutic target?" Glia **57**(12): 1251-1264.
- Blasi, E., R. Barluzzi, V. Bocchini, R. Mazzolla and F. Bistoni (1990). "Immortalization of murine microglial cells by a v-raf/v-myc carrying retrovirus." J Neuroimmunol **27**(2-3): 229-237.
- Bonifer, C. and D. A. Hume (2008). "The transcriptional regulation of the Colony-Stimulating Factor 1 Receptor (csf1r) gene during hematopoiesis." Front Biosci **13**: 549-560.
- Bourgin, C., R. P. Bourette, S. Arnaud, Y. Liu, L. R. Rohrschneider and G. Mouchiroud (2002). "Induced expression and association of the Mona/Gads adapter and Gab3 scaffolding protein during monocyte/macrophage differentiation." Mol Cell Biol **22**(11): 3744-3756.
- Braissant, O., M. Astasov-Frauenhoffer, T. Waltimo and G. Bonkat (2020). "A Review of Methods to Determine Viability, Vitality, and Metabolic Rates in Microbiology." Front Microbiol **11**: 547458.
- Bressler, S. B., B. Muñoz, S. D. Solomon and S. K. West (2008). "Racial differences in the prevalence of age-related macular degeneration: the Salisbury Eye Evaluation (SEE) Project." Arch Ophthalmol **126**(2): 241-245.
- Bringmann, A. and A. Reichenbach (2001). "Role of Muller cells in retinal degenerations." Front Biosci **6**: E72-92.
- Bruttger, J., K. Karraam, S. Wörtge, T. Regen, F. Marini, N. Hoppmann, M. Klein, T. Blank, S. Yona, Y. Wolf, M. Mack, E. Pinteaux, W. Müller, F. Zipp, H. Binder, T. Bopp, M. Prinz, S. Jung and A. Waisman (2015). "Genetic Cell Ablation Reveals Clusters of Local Self-Renewing Microglia in the Mammalian Central Nervous System." Immunity **43**(1): 92-106.
- Buch, T., F. L. Heppner, C. Tertilt, T. J. Heinen, M. Kremer, F. T. Wunderlich, S. Jung and A. Waisman (2005). "A Cre-inducible diphtheria toxin receptor mediates cell lineage ablation after toxin administration." Nat Methods **2**(6): 419-426.
- Butovsky, O., M. P. Jedrychowski, C. S. Moore, R. Cialic, A. J. Lanser, G. Gabriely, T. Koeglspenger, B. Dake, P. M. Wu, C. E. Doykan, Z. Fanek, L. Liu, Z. Chen, J. D. Rothstein, R. M. Ransohoff, S. P. Gygi, J. P. Antel and H. L. Weiner (2014). "Identification of a unique TGF- β -dependent molecular and functional signature in microglia." Nature Neuroscience **17**(1): 131-143.
- Buttgereit, A., I. Lelios, X. Yu, M. Vrohligs, N. R. Krakoski, E. L. Gautier, R. Nishinakamura, B. Becher and M. Greter (2016). "Sall1 is a transcriptional regulator defining microglia identity and function." Nat Immunol **17**(12): 1397-1406.
- Cammer, M., J. C. Gevrey, M. Lorenz, A. Dovas, J. Condeelis and D. Cox (2009). "The mechanism of CSF-1-induced Wiskott-Aldrich syndrome protein activation in vivo: a role for phosphatidylinositol 3-kinase and Cdc42." J Biol Chem **284**(35): 23302-23311.
- Cardona, A. E., E. P. Pioro, M. E. Sasse, V. Kostenko, S. M. Cardona, I. M. Dijkstra, D. Huang, G. Kidd, S. Dombrowski, R. Dutta, J. C. Lee, D. N. Cook, S. Jung, S. A. Lira, D. R. Littman and R. M. Ransohoff (2006). "Control of microglial neurotoxicity by the fractalkine receptor." Nat Neurosci **9**(7): 917-924.

References

- Cecchini, M. G., M. G. Dominguez, S. Mocci, A. Wetterwald, R. Felix, H. Fleisch, O. Chisholm, W. Hofstetter, J. W. Pollard and E. R. Stanley (1994). "Role of colony stimulating factor-1 in the establishment and regulation of tissue macrophages during postnatal development of the mouse." Development **120**(6): 1357-1372.
- Chader, G. J. and A. Taylor (2013). "Preface: The aging eye: normal changes, age-related diseases, and sight-saving approaches." Invest Ophthalmol Vis Sci **54**(14): Orsf1-4.
- Chan, W. Y., S. Kohsaka and P. Rezaie (2007). "The origin and cell lineage of microglia: new concepts." Brain Res Rev **53**(2): 344-354.
- Chang, K. H., Y. R. Wu, Y. C. Chen, H. C. Wu and C. M. Chen (2019). "Association between CSF1 and CSF1R Polymorphisms and Parkinson's Disease in Taiwan." J Clin Med **8**(10).
- Chang, M., J. A. Hamilton, G. M. Scholz, P. Masendycz, S. L. Macaulay and C. L. Elsegood (2009). "Phosphatidylinositol-3 kinase and phospholipase C enhance CSF-1-dependent macrophage survival by controlling glucose uptake." Cell Signal **21**(9): 1361-1369.
- Chen, X., H. Liu, P. J. Focia, A. H.-R. Shim and X. He (2008). "Structure of macrophage colony stimulating factor bound to FMS: Diverse signaling assemblies of class III receptor tyrosine kinases." Proceedings of the National Academy of Sciences **105**(47): 18267-18272.
- Cherepanoff, S., P. McMenamin, M. C. Gillies, E. Kettle and S. H. Sarks (2010). "Bruch's membrane and choroidal macrophages in early and advanced age-related macular degeneration." Br J Ophthalmol **94**(7): 918-925.
- Chitu, V. and E. R. Stanley (2017). "Regulation of Embryonic and Postnatal Development by the CSF-1 Receptor." Curr Top Dev Biol **123**: 229-275.
- Cho, M. S., S. J. Kim, S. Y. Ku, J. H. Park, H. Lee, D. H. Yoo, U. C. Park, S. A. Song, Y. M. Choi and H. G. Yu (2012). "Generation of retinal pigment epithelial cells from human embryonic stem cell-derived spherical neural masses." Stem Cell Res **9**(2): 101-109.
- Church, K. A., D. Rodriguez, D. Vanegas, I. L. Gutierrez, S. M. Cardona, J. L. M. Madrigal, T. Kaur and A. E. Cardona (2022). "Models of microglia depletion and replenishment elicit protective effects to alleviate vascular and neuronal damage in the diabetic murine retina." Journal of Neuroinflammation **19**(1): 300.
- Church, K. A., D. Rodriguez, D. Vanegas, I. L. Gutierrez, S. M. Cardona, J. L. M. Madrigal, T. Kaur and A. E. Cardona (2022). "Models of microglia depletion and replenishment elicit protective effects to alleviate vascular and neuronal damage in the diabetic murine retina." J Neuroinflammation **19**(1): 300.
- Coleman, L. G., J. Zou and F. T. Crews (2020). "Microglial depletion and repopulation in brain slice culture normalizes sensitized proinflammatory signaling." Journal of Neuroinflammation **17**(1): 27.
- Colombo, E. and C. Farina (2016). "Astrocytes: Key Regulators of Neuroinflammation." Trends Immunol **37**(9): 608-620.
- Combadière, C., C. Feumi, W. Raoul, N. Keller, M. Rodéro, A. Pézard, S. Lavalette, M. Houssier, L. Jonet, E. Picard, P. Debré, M. Sirinyan, P. Deterre, T. Ferroukhi, S. Y. Cohen, D. Chauvaud, J. C. Jeanny, S. Chemtob, F. Behar-Cohen and F. Sennlaub (2007). "CX3CR1-dependent subretinal microglia cell accumulation is associated with cardinal features of age-related macular degeneration." J Clin Invest **117**(10): 2920-2928.

References

- Constantinescu, C. S., M. Tani, R. M. Ransohoff, M. Wysocka, B. Hilliard, T. Fujioka, S. Murphy, P. J. Tighe, J. Das Sarma, G. Trinchieri and A. Rostami (2005). "Astrocytes as antigen-presenting cells: expression of IL-12/IL-23." J Neurochem **95**(2): 331-340.
- Coussens, L., C. Van Beveren, D. Smith, E. Chen, R. L. Mitchell, C. M. Isacke, I. M. Verma and A. Ullrich (1986). "Structural alteration of viral homologue of receptor proto-oncogene fms at carboxyl terminus." Nature **320**(6059): 277-280.
- Crews, F. T., C. J. Lawrimore, T. J. Walter and L. G. Coleman, Jr. (2017). "The role of neuroimmune signaling in alcoholism." Neuropharmacology **122**: 56-73.
- Cronk, J. C., A. J. Filiano, A. Louveau, I. Marin, R. Marsh, E. Ji, D. H. Goldman, I. Smirnov, N. Geraci, S. Acton, C. C. Overall and J. Kipnis (2018). "Peripherally derived macrophages can engraft the brain independent of irradiation and maintain an identity distinct from microglia." J Exp Med **215**(6): 1627-1647.
- Cunha-Vaz, J. (2007). "Characterization and relevance of different diabetic retinopathy phenotypes." Dev Ophthalmol **39**: 13-30.
- Curcio, C. A., M. Johnson, J. D. Huang and M. Rudolf (2009). "Aging, age-related macular degeneration, and the response-to-retention of apolipoprotein B-containing lipoproteins." Prog Retin Eye Res **28**(6): 393-422.
- D'Orazio, T. J. and J. Y. Niederkorn (1998). "A novel role for TGF-beta and IL-10 in the induction of immune privilege." J Immunol **160**(5): 2089-2098.
- Dai, X. M., X. H. Zong, V. Sylvestre and E. R. Stanley (2004). "Incomplete restoration of colony-stimulating factor 1 (CSF-1) function in CSF-1-deficient Csf1op/Csf1op mice by transgenic expression of cell surface CSF-1." Blood **103**(3): 1114-1123.
- Damani, M. R., L. Zhao, A. M. Fontainhas, J. Amaral, R. N. Fariss and W. T. Wong (2011). "Age-related alterations in the dynamic behavior of microglia." Aging Cell **10**(2): 263-276.
- Dauffy, J., G. Mouchiroud and R. P. Bourette (2006). "The interferon-inducible gene, Ifi204, is transcriptionally activated in response to M-CSF, and its expression favors macrophage differentiation in myeloid progenitor cells." J Leukoc Biol **79**(1): 173-183.
- De Biase, L. M., K. E. Schuebel, Z. H. Fufeld, K. Jair, I. A. Hawes, R. Cimbrow, H. Y. Zhang, Q. R. Liu, H. Shen, Z. X. Xi, D. Goldman and A. Bonci (2017). "Local Cues Establish and Maintain Region-Specific Phenotypes of Basal Ganglia Microglia." Neuron **95**(2): 341-356.e346.
- de Haas, A. H., H. W. Boddeke and K. Biber (2008). "Region-specific expression of immunoregulatory proteins on microglia in the healthy CNS." Glia **56**(8): 888-894.
- de Raad, S., P. J. Szczesny, K. Munz and C. E. Remé (1996). "Light damage in the rat retina: glial fibrillary acidic protein accumulates in Müller cells in correlation with photoreceptor damage." Ophthalmic Res **28**(2): 99-107.
- DeAngelis, M. M., L. A. Owen, M. A. Morrison, D. J. Morgan, M. Li, A. Shakoor, A. Vitale, S. Iyengar, D. Stambolian, I. K. Kim and L. A. Farrer (2017). "Genetics of age-related macular degeneration (AMD)." Hum Mol Genet **26**(R1): R45-r50.
- Dick, A. D., D. Carter, M. Robertson, C. Broderick, E. Hughes, J. V. Forrester and J. Liversidge (2003). "Control of myeloid activity during retinal inflammation." J Leukoc Biol **74**(2): 161-166.

References

- Dick, A. D., A. L. Ford, J. V. Forrester and J. D. Sedgwick (1995). "Flow cytometric identification of a minority population of MHC class II positive cells in the normal rat retina distinct from CD45lowCD11b/c+CD4low parenchymal microglia." Br J Ophthalmol **79**(9): 834-840.
- Dornstaeder, B., M. Suh, S. Kuny, F. Gaillard, I. M. Macdonald, M. T. Clandinin and Y. Sauvé (2012). "Dietary docosahexaenoic acid supplementation prevents age-related functional losses and A2E accumulation in the retina." Invest Ophthalmol Vis Sci **53**(4): 2256-2265.
- Dubois-Dauphin, M., C. Poitry-Yamate, F. de Bilbao, A. K. Julliard, F. Jourdan and G. Donati (2000). "Early postnatal Müller cell death leads to retinal but not optic nerve degeneration in NSE-Hu-Bcl-2 transgenic mice." Neuroscience **95**(1): 9-21.
- Ebert, S., T. Schoeberl, Y. Walczak, K. Stoecker, T. Stempfl, C. Moehle, B. H. Weber and T. Langmann (2008). "Chondroitin sulfate disaccharide stimulates microglia to adopt a novel regulatory phenotype." J Leukoc Biol **84**(3): 736-740.
- Ebert, S., Y. Walczak, C. Remé and T. Langmann (2012). "Microglial activation and transcriptomic changes in the blue light-exposed mouse retina." Adv Exp Med Biol **723**: 619-632.
- Elegheert, J., A. Desfosses, A. V. Shkumatov, X. Wu, N. Bracke, K. Verstraete, K. Van Craenenbroeck, B. R. Brooks, D. I. Svergun, B. Vergauwen, I. Gutsche and S. N. Savvides (2011). "Extracellular complexes of the hematopoietic human and mouse CSF-1 receptor are driven by common assembly principles." Structure **19**(12): 1762-1772.
- Elmore, M. R., R. J. Lee, B. L. West and K. N. Green (2015). "Characterizing newly repopulated microglia in the adult mouse: impacts on animal behavior, cell morphology, and neuroinflammation." PLoS One **10**(4): e0122912.
- Elmore, M. R., A. R. Najafi, M. A. Koike, N. N. Dagher, E. E. Spangenberg, R. A. Rice, M. Kitazawa, B. Matusow, H. Nguyen, B. L. West and K. N. Green (2014). "Colony-stimulating factor 1 receptor signaling is necessary for microglia viability, unmasking a microglia progenitor cell in the adult brain." Neuron **82**(2): 380-397.
- Erblich, B., L. Zhu, A. M. Etgen, K. Dobrenis and J. W. Pollard (2011). "Absence of colony stimulation factor-1 receptor results in loss of microglia, disrupted brain development and olfactory deficits." PLoS One **6**(10): e26317.
- Erickson, P. A., C. J. Guérin and S. K. Fisher (1990). "Tritiated uridine labeling of the retina: changes after retinal detachment." Exp Eye Res **51**(2): 153-158.
- Felix, J., J. Elegheert, I. Gutsche, A. V. Shkumatov, Y. Wen, N. Bracke, E. Pannecoucke, I. Vandenberghe, B. Devreese, D. I. Svergun, E. Pauwels, B. Vergauwen and S. N. Savvides (2013). "Human IL-34 and CSF-1 establish structurally similar extracellular assemblies with their common hematopoietic receptor." Structure **21**(4): 528-539.
- Ferreira, R., T. Santos, L. Cortes, S. Cochaud, F. Agasse, A. P. Silva, S. Xapelli and J. O. Malva (2012). "Neuropeptide Y inhibits interleukin-1 beta-induced microglia motility." J Neurochem **120**(1): 93-105.
- Ferrini, F., T. Trang, T. A. Mattioli, S. Laffray, T. Del'Guidice, L. E. Lorenzo, A. Castonguay, N. Doyon, W. Zhang, A. G. Godin, D. Mohr, S. Beggs, K. Vandal, J. M. Beaulieu, C. M. Cahill, M. W. Salter and Y. De Koninck (2013). "Morphine hyperalgesia gated through microglia-mediated disruption of neuronal Cl⁻ homeostasis." Nat Neurosci **16**(2): 183-192.

References

- Ferris, F. L., 3rd, S. L. Fine and L. Hyman (1984). "Age-related macular degeneration and blindness due to neovascular maculopathy." Arch Ophthalmol **102**(11): 1640-1642.
- Fonken, L. K., M. G. Frank, A. D. Gaudet and S. F. Maier (2018). "Stress and aging act through common mechanisms to elicit neuroinflammatory priming." Brain Behav Immun **73**: 133-148.
- Frank, M. G., R. M. Barrientos, J. C. Biedenkapp, J. W. Rudy, L. R. Watkins and S. F. Maier (2006). "mRNA up-regulation of MHC II and pivotal pro-inflammatory genes in normal brain aging." Neurobiol Aging **27**(5): 717-722.
- Franze, K., J. Grosche, S. N. Skatchkov, S. Schinkinger, C. Foja, D. Schild, O. Uckermann, K. Travis, A. Reichenbach and J. Guck (2007). "Muller cells are living optical fibers in the vertebrate retina." Proc Natl Acad Sci U S A **104**(20): 8287-8292.
- Fritsche, L. G., R. N. Fariss, D. Stambolian, G. R. Abecasis, C. A. Curcio and A. Swaroop (2014). "Age-related macular degeneration: genetics and biology coming together." Annu Rev Genomics Hum Genet **15**: 151-171.
- Fuhrmann, M., T. Bittner, C. K. Jung, S. Burgold, R. M. Page, G. Mitteregger, C. Haass, F. M. LaFerla, H. Kretschmar and J. Herms (2010). "Microglial Cx3cr1 knockout prevents neuron loss in a mouse model of Alzheimer's disease." Nat Neurosci **13**(4): 411-413.
- Gass, J. D. (1967). "Pathogenesis of disciform detachment of the neuroepithelium." Am J Ophthalmol **63**(3): Suppl:1-139.
- Geerlings, M. J., E. K. de Jong and A. I. den Hollander (2017). "The complement system in age-related macular degeneration: A review of rare genetic variants and implications for personalized treatment." Mol Immunol **84**: 65-76.
- Gelderblom, H. and M. V. de Sande (2020). "Pexidartinib: first approved systemic therapy for patients with tenosynovial giant cell tumor." Future Oncol **16**(29): 2345-2356.
- Ginhoux, F., M. Greter, M. Leboeuf, S. Nandi, P. See, S. Gokhan, M. F. Mehler, S. J. Conway, L. G. Ng, E. R. Stanley, I. M. Samokhvalov and M. Merad (2010). "Fate mapping analysis reveals that adult microglia derive from primitive macrophages." Science **330**(6005): 841-845.
- Goureau, O., D. Hicks, Y. Courtois and Y. De Kozak (1994). "Induction and regulation of nitric oxide synthase in retinal Müller glial cells." J Neurochem **63**(1): 310-317.
- Grabert, K., T. Michoel, M. H. Karavolos, S. Clohisey, J. K. Baillie, M. P. Stevens, T. C. Freeman, K. M. Summers and B. W. McColl (2016). "Microglial brain region-dependent diversity and selective regional sensitivities to aging." Nat Neurosci **19**(3): 504-516.
- Grasset, M. F., S. Gobert-Gosse, G. Mouchiroud and R. P. Bourette (2010). "Macrophage differentiation of myeloid progenitor cells in response to M-CSF is regulated by the dual-specificity phosphatase DUSP5." J Leukoc Biol **87**(1): 127-135.
- Grathwohl, S. A., R. E. Kälin, T. Bolmont, S. Prokop, G. Winkelmann, S. A. Kaeser, J. Odenthal, R. Radde, T. Eldh, S. Gandy, A. Aguzzi, M. Staufenbiel, P. M. Mathews, H. Wolburg, F. L. Heppner and M. Jucker (2009). "Formation and maintenance of Alzheimer's disease beta-amyloid plaques in the absence of microglia." Nat Neurosci **12**(11): 1361-1363.
- Green, K. N., J. D. Crapser and L. A. Hohsfield (2020). "To Kill a Microglia: A Case for CSF1R Inhibitors." Trends Immunol **41**(9): 771-784.
- Grimm, C. and C. E. Remé (2013). "Light damage as a model of retinal degeneration." Methods Mol Biol **935**: 87-97.

References

- Gritsch, S., J. Lu, S. Thilemann, S. Wörtge, W. Möbius, J. Bruttger, K. Karram, T. Ruhwedel, M. Blanfeld, D. Vardeh, A. Waisman, K. A. Nave and R. Künér (2014). "Oligodendrocyte ablation triggers central pain independently of innate or adaptive immune responses in mice." Nat Commun **5**: 5472.
- Grosche, J., D. Grimm, N. Clemens and A. Reichenbach (1997). "Retinal light damage vs. normal aging of rats: altered morphology, intermediate filament expression, and nuclear organization of Müller (glial) cells." J Hirnforsch **38**(4): 459-470.
- Grosche, J., W. Härtig and A. Reichenbach (1995). "Expression of glial fibrillary acidic protein (GFAP), glutamine synthetase (GS), and Bcl-2 protooncogene protein by Müller (glial) cells in retinal light damage of rats." Neurosci Lett **185**(2): 119-122.
- Guilbert, L. J. and E. R. Stanley (1980). "Specific interaction of murine colony-stimulating factor with mononuclear phagocytic cells." J Cell Biol **85**(1): 153-159.
- Gupta, N., K. E. Brown and A. H. Milam (2003). "Activated microglia in human retinitis pigmentosa, late-onset retinal degeneration, and age-related macular degeneration." Exp Eye Res **76**(4): 463-471.
- Hageman, G. S., D. H. Anderson, L. V. Johnson, L. S. Hancox, A. J. Taiber, L. I. Hardisty, J. L. Hageman, H. A. Stockman, J. D. Borchardt, K. M. Gehrs, R. J. Smith, G. Silvestri, S. R. Russell, C. C. Klaver, I. Barbazetto, S. Chang, L. A. Yannuzzi, G. R. Barile, J. C. Merriam, R. T. Smith, A. K. Olsh, J. Bergeron, J. Zernant, J. E. Merriam, B. Gold, M. Dean and R. Allikmets (2005). "A common haplotype in the complement regulatory gene factor H (HF1/CFH) predisposes individuals to age-related macular degeneration." Proc Natl Acad Sci U S A **102**(20): 7227-7232.
- Haines, J. L., M. A. Hauser, S. Schmidt, W. K. Scott, L. M. Olson, P. Gallins, K. L. Spencer, S. Y. Kwan, M. Noureddine, J. R. Gilbert, N. Schnetz-Boutaud, A. Agarwal, E. A. Postel and M. A. Pericak-Vance (2005). "Complement factor H variant increases the risk of age-related macular degeneration." Science **308**(5720): 419-421.
- Hammond, C. J., A. R. Webster, H. Snieder, A. C. Bird, C. E. Gilbert and T. D. Spector (2002). "Genetic influence on early age-related maculopathy: a twin study." Ophthalmology **109**(4): 730-736.
- Hampe, A., B. M. Shamon, M. Gobet, C. J. Sherr and F. Galibert (1989). "Nucleotide sequence and structural organization of the human FMS proto-oncogene." Oncogene Res **4**(1): 9-17.
- Hanisch, U.-K. and H. Kettenmann (2007). "Microglia: active sensor and versatile effector cells in the normal and pathologic brain." Nature Neuroscience **10**(11): 1387-1394.
- Harada, C., T. Harada, H. M. Quah, F. Maekawa, K. Yoshida, S. Ohno, K. Wada, L. F. Parada and K. Tanaka (2003). "Potential role of glial cell line-derived neurotrophic factor receptors in Müller glial cells during light-induced retinal degeneration." Neuroscience **122**(1): 229-235.
- Häusler, K. G., M. Prinz, C. Nolte, J. R. Weber, R. R. Schumann, H. Kettenmann and U. K. Hanisch (2002). "Interferon-gamma differentially modulates the release of cytokines and chemokines in lipopolysaccharide- and pneumococcal cell wall-stimulated mouse microglia and macrophages." Eur J Neurosci **16**(11): 2113-2122.
- Heesterbeek, T. J., L. Lorés-Motta, C. B. Hoyng, Y. T. E. Lechanteur and A. I. den Hollander (2020). "Risk factors for progression of age-related macular degeneration." Ophthalmic Physiol Opt **40**(2): 140-170.

References

- Heldin, C. H. and J. Lennartsson (2013). "Structural and functional properties of platelet-derived growth factor and stem cell factor receptors." Cold Spring Harb Perspect Biol **5**(8): a009100.
- Henry, C. J., Y. Huang, A. M. Wynne and J. P. Godbout (2009). "Peripheral lipopolysaccharide (LPS) challenge promotes microglial hyperactivity in aged mice that is associated with exaggerated induction of both pro-inflammatory IL-1 β and anti-inflammatory IL-10 cytokines." Brain Behav Immun **23**(3): 309-317.
- Heppner, F. L., M. Greter, D. Marino, J. Falsig, G. Raivich, N. Hövelmeyer, A. Waisman, T. Rüllicke, M. Prinz, J. Priller, B. Becher and A. Aguzzi (2005). "Experimental autoimmune encephalomyelitis repressed by microglial paralysis." Nat Med **11**(2): 146-152.
- Hilla, A. M., H. Diekmann and D. Fischer (2017). "Microglia Are Irrelevant for Neuronal Degeneration and Axon Regeneration after Acute Injury." J Neurosci **37**(25): 6113-6124.
- Hillmer, A. T., D. Holden, K. Fowles, N. Nabulsi, B. L. West, R. E. Carson and K. P. Cosgrove (2017). "Microglial depletion and activation: A [(11)C]PBR28 PET study in nonhuman primates." EJNMMI Res **7**(1): 59.
- Himes, S. R., H. Tagoh, N. Goonetilleke, T. Sasmono, D. Oceandy, R. Clark, C. Bonifer and D. A. Hume (2001). "A highly conserved c-fms gene intronic element controls macrophage-specific and regulated expression." J Leukoc Biol **70**(5): 812-820.
- Hoek, R. M., S. R. Ruuls, C. A. Murphy, G. J. Wright, R. Goddard, S. M. Zurawski, B. Blom, M. E. Homola, W. J. Streit, M. H. Brown, A. N. Barclay and J. D. Sedgwick (2000). "Down-regulation of the macrophage lineage through interaction with OX2 (CD200)." Science **290**(5497): 1768-1771.
- Horst, C. J., L. V. Johnson and J. C. Besharse (1990). "Transmembrane assemblage of the photoreceptor connecting cilium and motile cilium transition zone contain a common immunologic epitope." Cell Motil Cytoskeleton **17**(4): 329-344.
- Hu, B., S. Duan, Z. Wang, X. Li, Y. Zhou, X. Zhang, Y. W. Zhang, H. Xu and H. Zheng (2021). "Insights Into the Role of CSF1R in the Central Nervous System and Neurological Disorders." Front Aging Neurosci **13**: 789834.
- Huang, Y., Z. Xu, S. Xiong, G. Qin, F. Sun, J. Yang, T. F. Yuan, L. Zhao, K. Wang, Y. X. Liang, L. Fu, T. Wu, K. F. So, Y. Rao and B. Peng (2018). "Dual extra-retinal origins of microglia in the model of retinal microglia repopulation." Cell Discov **4**: 9.
- Huang, Y., Z. Xu, S. Xiong, F. Sun, G. Qin, G. Hu, J. Wang, L. Zhao, Y.-X. Liang, T. Wu, Z. Lu, M. S. Humayun, K.-F. So, Y. Pan, N. Li, T.-F. Yuan, Y. Rao and B. Peng (2018). "Repopulated microglia are solely derived from the proliferation of residual microglia after acute depletion." Nature Neuroscience **21**(4): 530-540.
- Hume, D. A., S. J. Monkley and B. J. Wainwright (1995). "Detection of c-fms protooncogene in early mouse embryos by whole mount in situ hybridization indicates roles for macrophages in tissue remodelling." Br J Haematol **90**(4): 939-942.
- Hume, D. A., V. H. Perry and S. Gordon (1983). "Immunohistochemical localization of a macrophage-specific antigen in developing mouse retina: phagocytosis of dying neurons and differentiation of microglial cells to form a regular array in the plexiform layers." J Cell Biol **97**(1): 253-257.

References

- Hwang, S. J., B. Choi, S. S. Kang, J. H. Chang, Y. G. Kim, Y. H. Chung, D. H. Sohn, M. W. So, C. K. Lee, W. H. Robinson and E. J. Chang (2012). "Interleukin-34 produced by human fibroblast-like synovial cells in rheumatoid arthritis supports osteoclastogenesis." Arthritis Res Ther **14**(1): R14.
- Jager, R. D., W. F. Mieler and J. W. Miller (2008). "Age-related macular degeneration." N Engl J Med **358**(24): 2606-2617.
- Jin, W. N., S. X. Shi, Z. Li, M. Li, K. Wood, R. J. Gonzales and Q. Liu (2017). "Depletion of microglia exacerbates postischemic inflammation and brain injury." J Cereb Blood Flow Metab **37**(6): 2224-2236.
- Joly, S., M. Francke, E. Ulbricht, S. Beck, M. Seeliger, P. Hirrlinger, J. Hirrlinger, K. S. Lang, M. Zinkernagel, B. Odermatt, M. Samardzija, A. Reichenbach, C. Grimm and C. E. Remé (2009). "Cooperative phagocytes: resident microglia and bone marrow immigrants remove dead photoreceptors in retinal lesions." Am J Pathol **174**(6): 2310-2323.
- Joly, S., C. Lange, M. Thiersch, M. Samardzija and C. Grimm (2008). "Leukemia inhibitory factor extends the lifespan of injured photoreceptors in vivo." J Neurosci **28**(51): 13765-13774.
- Jung, S., J. Aliberti, P. Graemmel, M. J. Sunshine, G. W. Kreutzberg, A. Sher and D. R. Littman (2000). "Analysis of fractalkine receptor CX(3)CR1 function by targeted deletion and green fluorescent protein reporter gene insertion." Mol Cell Biol **20**(11): 4106-4114.
- Kaiser, T. and G. Feng (2019). "Tmem119-EGFP and Tmem119-CreERT2 Transgenic Mice for Labeling and Manipulating Microglia." eNeuro **6**(4).
- Kanda, A., W. Chen, M. Othman, K. E. Branham, M. Brooks, R. Khanna, S. He, R. Lyons, G. R. Abecasis and A. Swaroop (2007). "A variant of mitochondrial protein LOC387715/ARMS2, not HTRA1, is strongly associated with age-related macular degeneration." Proc Natl Acad Sci U S A **104**(41): 16227-16232.
- Karlstetter, M., R. Scholz, M. Rutar, W. T. Wong, J. M. Provis and T. Langmann (2015). "Retinal microglia: just bystander or target for therapy?" Prog Retin Eye Res **45**: 30-57.
- Kautzman, A. G., P. W. Keeley, M. M. Nahmou, G. Luna, S. K. Fisher and B. E. Reese (2018). "Sox2 regulates astrocytic and vascular development in the retina." Glia **66**(3): 623-636.
- Kettenmann, H., U. K. Hanisch, M. Noda and A. Verkhratsky (2011). "Physiology of microglia." Physiol Rev **91**(2): 461-553.
- Khakh, B. S., V. Beaumont, R. Cachope, I. Munoz-Sanjuan, S. A. Goldman and R. Grantyn (2017). "Unravelling and Exploiting Astrocyte Dysfunction in Huntington's Disease." Trends Neurosci **40**(7): 422-437.
- Kheir, W. A., J. C. Gevrey, H. Yamaguchi, B. Isaac and D. Cox (2005). "A WAVE2-Abi1 complex mediates CSF-1-induced F-actin-rich membrane protrusions and migration in macrophages." J Cell Sci **118**(Pt 22): 5369-5379.
- Kierdorf, K., D. Erny, T. Goldmann, V. Sander, C. Schulz, E. G. Perdiguero, P. Wieghofer, A. Heinrich, P. Riemke, C. Hölscher, D. N. Müller, B. Luckow, T. Brouwer, K. Debowski, G. Fritz, G. Opdenakker, A. Diefenbach, K. Biber, M. Heikenwalder, F. Geissmann, F. Rosenbauer and M. Prinz (2013). "Microglia emerge from erythromyeloid precursors via Pu.1- and Irf8-dependent pathways." Nat Neurosci **16**(3): 273-280.

References

- Kimelberg, H. K. (2010). "Functions of mature mammalian astrocytes: a current view." Neuroscientist **16**(1): 79-106.
- Klein, R., B. E. Klein, M. D. Knudtson, T. Y. Wong, M. F. Cotch, K. Liu, G. Burke, M. F. Saad and D. R. Jacobs, Jr. (2006). "Prevalence of age-related macular degeneration in 4 racial/ethnic groups in the multi-ethnic study of atherosclerosis." Ophthalmology **113**(3): 373-380.
- Klein, R. J., C. Zeiss, E. Y. Chew, J. Y. Tsai, R. S. Sackler, C. Haynes, A. K. Henning, J. P. SanGiovanni, S. M. Mane, S. T. Mayne, M. B. Bracken, F. L. Ferris, J. Ott, C. Barnstable and J. Hoh (2005). "Complement factor H polymorphism in age-related macular degeneration." Science **308**(5720): 385-389.
- Kobayashi, M., T. Kuroiwa, R. Shimokawa, R. Okeda and T. Tokoro (2000). "Nitric oxide synthase expression in ischemic rat retinas." Jpn J Ophthalmol **44**(3): 235-244.
- Kokona, D., A. Ebnetter, P. Escher and M. S. Zinkernagel (2018). "Colony-stimulating factor 1 receptor inhibition prevents disruption of the blood-retina barrier during chronic inflammation." Journal of Neuroinflammation **15**(1): 340.
- Krady, J. K., A. Basu, C. M. Allen, Y. Xu, K. F. LaNoue, T. W. Gardner and S. W. Levison (2005). "Minocycline reduces proinflammatory cytokine expression, microglial activation, and caspase-3 activation in a rodent model of diabetic retinopathy." Diabetes **54**(5): 1559-1565.
- Krady, J. K., H. W. Lin, C. M. Liberto, A. Basu, S. G. Kremlev and S. W. Levison (2008). "Ciliary neurotrophic factor and interleukin-6 differentially activate microglia." J Neurosci Res **86**(7): 1538-1547.
- Kreutzberg, G. W. (1996). "Microglia: a sensor for pathological events in the CNS." Trends Neurosci **19**(8): 312-318.
- Lambert, N. G., H. ElShelmani, M. K. Singh, F. C. Mansergh, M. A. Wride, M. Padilla, D. Keegan, R. E. Hogg and B. K. Ambati (2016). "Risk factors and biomarkers of age-related macular degeneration." Prog Retin Eye Res **54**: 64-102.
- Langmann, T. (2007). "Microglia activation in retinal degeneration." Journal of Leukocyte Biology **81**(6): 1345-1351.
- Lawson, L. J., V. H. Perry, P. Dri and S. Gordon (1990). "Heterogeneity in the distribution and morphology of microglia in the normal adult mouse brain." Neuroscience **39**(1): 151-170.
- Lee, A. W. and D. J. States (2000). "Both src-dependent and -independent mechanisms mediate phosphatidylinositol 3-kinase regulation of colony-stimulating factor 1-activated mitogen-activated protein kinases in myeloid progenitors." Mol Cell Biol **20**(18): 6779-6798.
- Lewitus, G. M., S. C. Konefal, A. D. Greenhalgh, H. Pribiag, K. Augereau and D. Stellwagen (2016). "Microglial TNF- α Suppresses Cocaine-Induced Plasticity and Behavioral Sensitization." Neuron **90**(3): 483-491.
- Li, M., Z. Li, H. Ren, W. N. Jin, K. Wood, Q. Liu, K. N. Sheth and F. D. Shi (2017). "Colony stimulating factor 1 receptor inhibition eliminates microglia and attenuates brain injury after intracerebral hemorrhage." J Cereb Blood Flow Metab **37**(7): 2383-2395.
- Li, Z. H., N. G. Dulyaninova, R. P. House, S. C. Almo and A. R. Bresnick (2010). "S100A4 regulates macrophage chemotaxis." Mol Biol Cell **21**(15): 2598-2610.
- Li, Z. H., A. Spektor, O. Varlamova and A. R. Bresnick (2003). "Mts1 regulates the assembly of nonmuscle myosin-IIA." Biochemistry **42**(48): 14258-14266.

References

- Liu, H., C. Leo, X. Chen, B. R. Wong, L. T. Williams, H. Lin and X. He (2012). "The mechanism of shared but distinct CSF-1R signaling by the non-homologous cytokines IL-34 and CSF-1." Biochim Biophys Acta **1824**(7): 938-945.
- Liu, Y., K. S. Given, E. L. Dickson, G. P. Owens, W. B. Macklin and J. L. Bennett (2019). "Concentration-dependent effects of CSF1R inhibitors on oligodendrocyte progenitor cells ex vivo and in vivo." Exp Neurol **318**: 32-41.
- Locatelli, G., S. Wörtge, T. Buch, B. Ingold, F. Frommer, B. Sobottka, M. Krüger, K. Karram, C. Bühlmann, I. Bechmann, F. L. Heppner, A. Waisman and B. Becher (2012). "Primary oligodendrocyte death does not elicit anti-CNS immunity." Nat Neurosci **15**(4): 543-550.
- López-Otín, C., M. A. Blasco, L. Partridge, M. Serrano and G. Kroemer (2013). "The hallmarks of aging." Cell **153**(6): 1194-1217.
- Lund, H., M. Pieber, R. Parsa, J. Han, D. Grommisch, E. Ewing, L. Kular, M. Needhamsen, A. Espinosa, E. Nilsson, A. K. Överby, O. Butovsky, M. Jagodic, X.-M. Zhang and R. A. Harris (2018). "Competitive repopulation of an empty microglial niche yields functionally distinct subsets of microglia-like cells." Nature Communications **9**(1): 4845.
- Ma, W., S. Coon, L. Zhao, R. N. Fariss and W. T. Wong (2013). "A2E accumulation influences retinal microglial activation and complement regulation." Neurobiol Aging **34**(3): 943-960.
- Ma, X., W. Y. Lin, Y. Chen, S. Stawicki, K. Mukhyala, Y. Wu, F. Martin, J. F. Bazan and M. A. Starovasnik (2012). "Structural basis for the dual recognition of helical cytokines IL-34 and CSF-1 by CSF-1R." Structure **20**(4): 676-687.
- MacDonald, K. P., V. Rowe, H. M. Bofinger, R. Thomas, T. Sasmono, D. A. Hume and G. R. Hill (2005). "The colony-stimulating factor 1 receptor is expressed on dendritic cells during differentiation and regulates their expansion." J Immunol **175**(3): 1399-1405.
- Madeira, M. H., R. Boia, P. F. Santos, A. F. Ambrósio and A. R. Santiago (2015). "Contribution of microglia-mediated neuroinflammation to retinal degenerative diseases." Mediators Inflamm **2015**: 673090.
- Magnus, T., A. Chan, O. Grauer, K. V. Toyka and R. Gold (2001). "Microglial phagocytosis of apoptotic inflammatory T cells leads to down-regulation of microglial immune activation." J Immunol **167**(9): 5004-5010.
- Mancini, A., A. Koch, A. D. Whetton and T. Tamura (2004). "The M-CSF receptor substrate and interacting protein FMIP is governed in its subcellular localization by protein kinase C-mediated phosphorylation, and thereby potentiates M-CSF-mediated differentiation." Oncogene **23**(39): 6581-6589.
- Masland, R. H. (2001). "The fundamental plan of the retina." Nature Neuroscience **4**(9): 877-886.
- Matsudaira, T. and M. Prinz (2022). "Life and death of microglia: Mechanisms governing microglial states and fates." Immunol Lett **245**: 51-60.
- McKercher, S. R., B. E. Torbett, K. L. Anderson, G. W. Henkel, D. J. Vestal, H. Baribault, M. Klemsz, A. J. Feeney, G. E. Wu, C. J. Paige and R. A. Maki (1996). "Targeted disruption of the PU.1 gene results in multiple hematopoietic abnormalities." Embo j **15**(20): 5647-5658.

References

- Medvedev, A. E., K. M. Kopydlowski and S. N. Vogel (2000). "Inhibition of Lipopolysaccharide-Induced Signal Transduction in Endotoxin-Tolerized Mouse Macrophages: Dysregulation of Cytokine, Chemokine, and Toll-Like Receptor 2 and 4 Gene Expression1." The Journal of Immunology **164**(11): 5564-5574.
- Meng, S., Z. Chen, T. Munoz-Antonia and J. Wu (2005). "Participation of both Gab1 and Gab2 in the activation of the ERK/MAPK pathway by epidermal growth factor." Biochem J **391**(Pt 1): 143-151.
- Merry, T. L., A. E. S. Brooks, S. W. Masson, S. E. Adams, J. K. Jaiswal, S. M. F. Jamieson and P. R. Shepherd (2020). "The CSF1 receptor inhibitor pexidartinib (PLX3397) reduces tissue macrophage levels without affecting glucose homeostasis in mice." Int J Obes (Lond) **44**(1): 245-253.
- Mezey, E., K. J. Chandross, G. Harta, R. A. Maki and S. R. McKercher (2000). "Turning blood into brain: cells bearing neuronal antigens generated in vivo from bone marrow." Science **290**(5497): 1779-1782.
- Michaelson, M. D., P. L. Bieri, M. F. Mehler, H. Xu, J. C. Arezzo, J. W. Pollard and J. A. Kessler (1996). "CSF-1 deficiency in mice results in abnormal brain development." Development **122**(9): 2661-2672.
- Milligan, C. E., T. J. Cunningham and P. Levitt (1991). "Differential immunochemical markers reveal the normal distribution of brain macrophages and microglia in the developing rat brain." J Comp Neurol **314**(1): 125-135.
- Miyamoto, A., H. Wake, A. W. Ishikawa, K. Eto, K. Shibata, H. Murakoshi, S. Koizumi, A. J. Moorhouse, Y. Yoshimura and J. Nabekura (2016). "Microglia contact induces synapse formation in developing somatosensory cortex." Nature Communications **7**(1): 12540.
- Moiseyev, G., Y. Chen, Y. Takahashi, B. X. Wu and J. X. Ma (2005). "RPE65 is the isomerohydrolase in the retinoid visual cycle." Proc Natl Acad Sci U S A **102**(35): 12413-12418.
- Mok, S., R. C. Koya, C. Tsui, J. Xu, L. Robert, L. Wu, T. Graeber, B. L. West, G. Bollag and A. Ribas (2014). "Inhibition of CSF-1 receptor improves the antitumor efficacy of adoptive cell transfer immunotherapy." Cancer Res **74**(1): 153-161.
- Morris, B., F. Imrie, A. M. Armbricht and B. Dhillon (2007). "Age-related macular degeneration and recent developments: new hope for old eyes?" Postgrad Med J **83**(979): 301-307.
- Muñiz, A., W. A. Greene, M. L. Plamper, J. H. Choi, A. J. Johnson, A. T. Tsin and H. C. Wang (2014). "Retinoid uptake, processing, and secretion in human iPS-RPE support the visual cycle." Invest Ophthalmol Vis Sci **55**(1): 198-209.
- Muniz, A., E. T. Villazana-Espinoza, A. L. Hatch, S. G. Trevino, D. M. Allen and A. T. Tsin (2007). "A novel cone visual cycle in the cone-dominated retina." Exp Eye Res **85**(2): 175-184.
- Munugalavadla, V., J. Borneo, D. A. Ingram and R. Kapur (2005). "p85alpha subunit of class IA PI-3 kinase is crucial for macrophage growth and migration." Blood **106**(1): 103-109.
- Nandi, S., S. Gokhan, X. M. Dai, S. Wei, G. Enikolopov, H. Lin, M. F. Mehler and E. R. Stanley (2012). "The CSF-1 receptor ligands IL-34 and CSF-1 exhibit distinct developmental brain expression patterns and regulate neural progenitor cell maintenance and maturation." Dev Biol **367**(2): 100-113.

References

- Neal, M. L., S. M. Fleming, K. M. Budge, A. M. Boyle, C. Kim, G. Alam, E. E. Beier, L. J. Wu and J. R. Richardson (2020). "Pharmacological inhibition of CSF1R by GW2580 reduces microglial proliferation and is protective against neuroinflammation and dopaminergic neurodegeneration." Faseb j **34**(1): 1679-1694.
- Newman, A. M., N. B. Gallo, L. S. Hancox, N. J. Miller, C. M. Radeke, M. A. Maloney, J. B. Cooper, G. S. Hageman, D. H. Anderson, L. V. Johnson and M. J. Radeke (2012). "Systems-level analysis of age-related macular degeneration reveals global biomarkers and phenotype-specific functional networks." Genome Medicine **4**(2): 16.
- Nimmerjahn, A., F. Kirchhoff and F. Helmchen (2005). "Resting microglial cells are highly dynamic surveillants of brain parenchyma in vivo." Science **308**(5726): 1314-1318.
- Nishida, K., Y. Yoshida, M. Itoh, T. Fukada, T. Ohtani, T. Shirogane, T. Atsumi, M. Takahashi-Tezuka, K. Ishihara, M. Hibi and T. Hirano (1999). "Gab-family adapter proteins act downstream of cytokine and growth factor receptors and T- and B-cell antigen receptors." Blood **93**(6): 1809-1816.
- Noell, W. K., V. S. Walker, B. S. Kang and S. Berman (1966). "Retinal damage by light in rats." Invest Ophthalmol **5**(5): 450-473.
- Norden, D. M., M. M. Muccigrosso and J. P. Godbout (2015). "Microglial priming and enhanced reactivity to secondary insult in aging, and traumatic CNS injury, and neurodegenerative disease." Neuropharmacology **96**(Pt A): 29-41.
- O'Koren, E. G., C. Yu, M. Klingeborn, A. Y. W. Wong, C. L. Prigge, R. Mathew, J. Kalnitsky, R. A. Msallam, A. Silvin, J. N. Kay, C. Bowes Rickman, V. Y. Arshavsky, F. Ginhoux, M. Merad and D. R. Saban (2019). "Microglial Function Is Distinct in Different Anatomical Locations during Retinal Homeostasis and Degeneration." Immunity **50**(3): 723-737.e727.
- O'Neil, S. M., K. G. Witcher, D. B. McKim and J. P. Godbout (2018). "Forced turnover of aged microglia induces an intermediate phenotype but does not rebalance CNS environmental cues driving priming to immune challenge." Acta Neuropathol Commun **6**(1): 129.
- Okada, M., M. Matsumura, N. Ogino and Y. Honda (1990). "Müller cells in detached human retina express glial fibrillary acidic protein and vimentin." Graefes Arch Clin Exp Ophthalmol **228**(5): 467-474.
- Okunuki, Y., R. Mukai, E. A. Pearsall, G. Klokman, D. Husain, D. H. Park, E. Korobkina, H. L. Weiner, O. Butovsky, B. R. Ksander, J. W. Miller and K. M. Connor (2018). "Microglia inhibit photoreceptor cell death and regulate immune cell infiltration in response to retinal detachment." Proc Natl Acad Sci U S A **115**(27): E6264-e6273.
- Osborne, N. N., F. Block and K. H. Sontag (1991). "Reduction of ocular blood flow results in glial fibrillary acidic protein (GFAP) expression in rat retinal Müller cells." Vis Neurosci **7**(6): 637-639.
- Osborne, N. N. and A. K. Larsen (1996). "Antigens associated with specific retinal cells are affected by ischaemia caused by raised intraocular pressure: effect of glutamate antagonists." Neurochem Int **29**(3): 263-270.
- Ovchinnikov, D. A., C. E. DeBats, D. P. Sester, M. J. Sweet and D. A. Hume (2010). "A conserved distal segment of the mouse CSF-1 receptor promoter is required for maximal expression of a reporter gene in macrophages and osteoclasts of transgenic mice." J Leukoc Biol **87**(5): 815-822.

References

- Paglinawan, R., U. Malipiero, R. Schlapbach, K. Frei, W. Reith and A. Fontana (2003). "TGFbeta directs gene expression of activated microglia to an anti-inflammatory phenotype strongly focusing on chemokine genes and cell migratory genes." Glia **44**(3): 219-231.
- Paolicelli, R. C., G. Bolasco, F. Pagani, L. Maggi, M. Scianni, P. Panzanelli, M. Giustetto, T. A. Ferreira, E. Guiducci, L. Dumas, D. Ragozzino and C. T. Gross (2011). "Synaptic pruning by microglia is necessary for normal brain development." Science **333**(6048): 1456-1458.
- Papakonstanti, E. A., O. Zwaenepoel, A. Bilancio, E. Burns, G. E. Nock, B. Houseman, K. Shokat, A. J. Ridley and B. Vanhaesebroeck (2008). "Distinct roles of class IA PI3K isoforms in primary and immortalised macrophages." Journal of Cell Science **121**(24): 4124-4133.
- Parkhurst, C. N., G. Yang, I. Ninan, J. N. Savas, J. R. Yates, 3rd, J. J. Lafaille, B. L. Hempstead, D. R. Littman and W. B. Gan (2013). "Microglia promote learning-dependent synapse formation through brain-derived neurotrophic factor." Cell **155**(7): 1596-1609.
- Patwardhan, P. P., O. Surriga, M. J. Beckman, E. de Stanchina, R. P. Dematteo, W. D. Tap and G. K. Schwartz (2014). "Sustained inhibition of receptor tyrosine kinases and macrophage depletion by PLX3397 and rapamycin as a potential new approach for the treatment of MPNSTs." Clin Cancer Res **20**(12): 3146-3158.
- Perry, V. H. and S. Gordon (1988). "Macrophages and microglia in the nervous system." Trends Neurosci **11**(6): 273-277.
- Perry, V. H. and C. Holmes (2014). "Microglial priming in neurodegenerative disease." Nat Rev Neurol **10**(4): 217-224.
- Pixley, F. J. and E. R. Stanley (2004). "CSF-1 regulation of the wandering macrophage: complexity in action." Trends Cell Biol **14**(11): 628-638.
- Poitry-Yamate, C. L., S. Poitry and M. Tsacopoulos (1995). "Lactate released by Müller glial cells is metabolized by photoreceptors from mammalian retina." J Neurosci **15**(7 Pt 2): 5179-5191.
- Poitry, S., C. Poitry-Yamate, J. Ueberfeld, P. R. MacLeish and M. Tsacopoulos (2000). "Mechanisms of glutamate metabolic signaling in retinal glial (Müller) cells." J Neurosci **20**(5): 1809-1821.
- Provis, J. M. (2001). "Development of the primate retinal vasculature." Prog Retin Eye Res **20**(6): 799-821.
- Purves, D. Vision. Handbook of Neuroscience for the Behavioral Sciences.
- Rashid, K., I. Akhtar-Schaefer and T. Langmann (2019). "Microglia in Retinal Degeneration." Frontiers in Immunology **10**.
- Rauen, T. and M. Wiessner (2000). "Fine tuning of glutamate uptake and degradation in glial cells: common transcriptional regulation of GLAST1 and GS." Neurochem Int **37**(2-3): 179-189.
- Réu, P., A. Khosravi, S. Bernard, J. E. Mold, M. Salehpour, K. Alkass, S. Perl, J. Tisdale, G. Possnert, H. Druid and J. Frisén (2017). "The Lifespan and Turnover of Microglia in the Human Brain." Cell Rep **20**(4): 779-784.

References

- Rice, R. A., J. Pham, R. J. Lee, A. R. Najafi, B. L. West and K. N. Green (2017). "Microglial repopulation resolves inflammation and promotes brain recovery after injury." Glia **65**(6): 931-944.
- Rice, R. A., E. E. Spangenberg, H. Yamate-Morgan, R. J. Lee, R. P. Arora, M. X. Hernandez, A. J. Tenner, B. L. West and K. N. Green (2015). "Elimination of Microglia Improves Functional Outcomes Following Extensive Neuronal Loss in the Hippocampus." J Neurosci **35**(27): 9977-9989.
- Riss, T., A. Niles, R. Moravec, N. Karassina and J. Vidugiriene (2004). Cytotoxicity Assays: In Vitro Methods to Measure Dead Cells. Assay Guidance Manual. S. Markossian, A. Grossman, K. Brimacombe et al. Bethesda (MD), Eli Lilly & Company and the National Center for Advancing Translational Sciences.
- Rohde, C. M., J. Schrum and A. W. Lee (2004). "A juxtamembrane tyrosine in the colony stimulating factor-1 receptor regulates ligand-induced Src association, receptor kinase function, and down-regulation." J Biol Chem **279**(42): 43448-43461.
- Rönnstrand, L. (2004). "Signal transduction via the stem cell factor receptor/c-Kit." Cell Mol Life Sci **61**(19-20): 2535-2548.
- Roth, S. (1997). "Role of nitric oxide in retinal cell death." Clin Neurosci **4**(5): 216-223.
- Rothwell, V. M. and L. R. Rohrschneider (1987). "Murine c-fms cDNA: cloning, sequence analysis and retroviral expression." Oncogene Res **1**(4): 311-324.
- Roumier, A., C. Béchade, J. C. Poncer, K. H. Smalla, E. Tomasello, E. Vivier, E. D. Gundelfinger, A. Triller and A. Bessis (2004). "Impaired synaptic function in the microglial KARAP/DAP12-deficient mouse." J Neurosci **24**(50): 11421-11428.
- Rubino, S. J., L. Mayo, I. Wimmer, V. Siedler, F. Brunner, S. Hametner, A. Madi, A. Lanser, T. Moreira, D. Donnelly, L. Cox, R. M. Rezende, O. Butovsky, H. Lassmann and H. L. Weiner (2018). "Acute microglia ablation induces neurodegeneration in the somatosensory system." Nat Commun **9**(1): 4578.
- Sakurai, K., A. Onishi, H. Imai, O. Chisaka, Y. Ueda, J. Usukura, K. Nakatani and Y. Shichida (2007). "Physiological properties of rod photoreceptor cells in green-sensitive cone pigment knock-in mice." J Gen Physiol **130**(1): 21-40.
- Sampaio, N. G., W. Yu, D. Cox, J. Wyckoff, J. Condeelis, E. R. Stanley and F. J. Pixley (2011). "Phosphorylation of CSF-1R Y721 mediates its association with PI3K to regulate macrophage motility and enhancement of tumor cell invasion." J Cell Sci **124**(Pt 12): 2021-2031.
- Santos, A. M., R. Calvente, M. Tassi, M. C. Carrasco, D. Martín-Oliva, J. L. Marín-Teva, J. Navascués and M. A. Cuadros (2008). "Embryonic and postnatal development of microglial cells in the mouse retina." J Comp Neurol **506**(2): 224-239.
- Sarrazin, S., N. Mossadegh-Keller, T. Fukao, A. Aziz, F. Mourcin, L. Vanhille, L. Kelly Modis, P. Kastner, S. Chan, E. Duprez, C. Otto and M. H. Sieweke (2009). "MafB restricts M-CSF-dependent myeloid commitment divisions of hematopoietic stem cells." Cell **138**(2): 300-313.
- Sasmono, R. T., D. Oceandy, J. W. Pollard, W. Tong, P. Pavli, B. J. Wainwright, M. C. Ostrowski, S. R. Himes and D. A. Hume (2003). "A macrophage colony-stimulating factor receptor-green fluorescent protein transgene is expressed throughout the mononuclear phagocyte system of the mouse." Blood **101**(3): 1155-1163.

References

- Schafer, D. P., E. K. Lehrman, A. G. Kautzman, R. Koyama, A. R. Mardinly, R. Yamasaki, R. M. Ransohoff, M. E. Greenberg, B. A. Barres and B. Stevens (2012). "Microglia sculpt postnatal neural circuits in an activity and complement-dependent manner." Neuron **74**(4): 691-705.
- Schnitzer, J. (1988). "Immunocytochemical studies on the development of astrocytes, Müller (glial) cells, and oligodendrocytes in the rabbit retina." Brain Res Dev Brain Res **44**(1): 59-72.
- Scott, E. W., M. C. Simon, J. Anastasi and H. Singh (1994). "Requirement of transcription factor PU.1 in the development of multiple hematopoietic lineages." Science **265**(5178): 1573-1577.
- Seddon, J. M., U. A. Ajani and B. D. Mitchell (1997). "Familial aggregation of age-related maculopathy." Am J Ophthalmol **123**(2): 199-206.
- Seddon, J. M., J. Cote, W. F. Page, S. H. Aggen and M. C. Neale (2005). "The US twin study of age-related macular degeneration: relative roles of genetic and environmental influences." Arch Ophthalmol **123**(3): 321-327.
- Sherr, C. J., C. W. Rettenmier, R. Sacca, M. F. Roussel, A. T. Look and E. R. Stanley (1985). "The c-fms proto-oncogene product is related to the receptor for the mononuclear phagocyte growth factor, CSF-1." Cell **41**(3): 665-676.
- Shull, M. M., I. Ormsby, A. B. Kier, S. Pawlowski, R. J. Diebold, M. Yin, R. Allen, C. Sidman, G. Proetzel, D. Calvin and et al. (1992). "Targeted disruption of the mouse transforming growth factor-beta 1 gene results in multifocal inflammatory disease." Nature **359**(6397): 693-699.
- Sliney, D. H. (2016). "What is light? The visible spectrum and beyond." Eye **30**(2): 222-229.
- Sofroniew, M. V. (2015). "Astrocyte barriers to neurotoxic inflammation." Nat Rev Neurosci **16**(5): 249-263.
- Spangenberg, E., P. L. Severson, L. A. Hohsfield, J. Crapser, J. Zhang, E. A. Burton, Y. Zhang, W. Spevak, J. Lin, N. Y. Phan, G. Habets, A. Rymar, G. Tsang, J. Walters, M. Nespi, P. Singh, S. Broome, P. Ibrahim, C. Zhang, G. Bollag, B. L. West and K. N. Green (2019). "Sustained microglial depletion with CSF1R inhibitor impairs parenchymal plaque development in an Alzheimer's disease model." Nature Communications **10**(1): 3758.
- Spangenberg, E. E., R. J. Lee, A. R. Najafi, R. A. Rice, M. R. Elmore, M. Blurton-Jones, B. L. West and K. N. Green (2016). "Eliminating microglia in Alzheimer's mice prevents neuronal loss without modulating amyloid- β pathology." Brain **139**(Pt 4): 1265-1281.
- Stanley, E. R. and V. Chitu (2014). "CSF-1 receptor signaling in myeloid cells." Cold Spring Harb Perspect Biol **6**(6).
- Strauss, O. (2005). "The Retinal Pigment Epithelium in Visual Function." Physiological Reviews **85**(3): 845-881.
- Striebel, J. F., B. Race, K. Williams, J. A. Carroll, M. Klingeborn and B. Chesebro (2019). "Microglia are not required for prion-induced retinal photoreceptor degeneration." Acta Neuropathol Commun **7**(1): 48.
- Sun, H. and J. Nathans (2001). "ABCR, the ATP-binding cassette transporter responsible for Stargardt macular dystrophy, is an efficient target of all-trans-retinal-mediated photooxidative damage in vitro. Implications for retinal disease." J Biol Chem **276**(15): 11766-11774.

References

- Sunness, J. S., G. S. Rubin, C. A. Applegate, N. M. Bressler, M. J. Marsh, B. S. Hawkins and D. Haselwood (1997). "Visual function abnormalities and prognosis in eyes with age-related geographic atrophy of the macula and good visual acuity." Ophthalmology **104**(10): 1677-1691.
- Suzu, S., M. Hiyoshi, Y. Yoshidomi, H. Harada, M. Takeya, F. Kimura, K. Motoyoshi and S. Okada (2007). "M-CSF-mediated macrophage differentiation but not proliferation is correlated with increased and prolonged ERK activation." J Cell Physiol **212**(2): 519-525.
- Szalay, G., B. Martinecz, N. Lénárt, Z. Környei, B. Orsolits, L. Judák, E. Császár, R. Fekete, B. L. West, G. Katona, B. Rózsa and Á. Dénes (2016). "Microglia protect against brain injury and their selective elimination dysregulates neuronal network activity after stroke." Nat Commun **7**: 11499.
- Tahmasebi, F., P. Pasbakhsh, K. Mortezaee, S. Madadi, S. Barati and I. R. Kashani (2019). "Effect of the CSF1R inhibitor PLX3397 on remyelination of corpus callosum in a cuprizone-induced demyelination mouse model." J Cell Biochem **120**(6): 10576-10586.
- Tang, J. and T. S. Kern (2011). "Inflammation in diabetic retinopathy." Prog Retin Eye Res **30**(5): 343-358.
- Tap, W. D., Z. A. Wainberg, S. P. Anthony, P. N. Ibrahim, C. Zhang, J. H. Healey, B. Chmielowski, A. P. Staddon, A. L. Cohn, G. I. Shapiro, V. L. Keedy, A. S. Singh, I. Puzanov, E. L. Kwak, A. J. Wagner, D. D. Von Hoff, G. J. Weiss, R. K. Ramanathan, J. Zhang, G. Habets, Y. Zhang, E. A. Burton, G. Visor, L. Sanftner, P. Severson, H. Nguyen, M. J. Kim, A. Marimuthu, G. Tsang, R. Shellooe, C. Gee, B. L. West, P. Hirth, K. Nolop, M. van de Rijn, H. H. Hsu, C. Peterfy, P. S. Lin, S. Tong-Starksen and G. Bollag (2015). "Structure-Guided Blockade of CSF1R Kinase in Tenosynovial Giant-Cell Tumor." N Engl J Med **373**(5): 428-437.
- Thanos, S., J. Kacza, J. Seeger and J. Mey (1994). "Old dyes for new scopes: the phagocytosis-dependent long-term fluorescence labelling of microglial cells in vivo." Trends Neurosci **17**(5): 177-182.
- Thanos, S., C. Pavlidis, J. Mey and H. J. Thiel (1992). "Specific transcellular staining of microglia in the adult rat after traumatic degeneration of carbocyanine-filled retinal ganglion cells." Exp Eye Res **55**(1): 101-117.
- Tian, Y., H. Shen, L. Xia and J. Lu (2013). "Elevated serum and synovial fluid levels of interleukin-34 in rheumatoid arthritis: possible association with disease progression via interleukin-17 production." J Interferon Cytokine Res **33**(7): 398-401.
- Travis, G. H., M. Golczak, A. R. Moise and K. Palczewski (2007). "Diseases caused by defects in the visual cycle: retinoids as potential therapeutic agents." Annu Rev Pharmacol Toxicol **47**: 469-512.
- Tremblay, M., R. L. Lowery and A. K. Majewska (2010). "Microglial interactions with synapses are modulated by visual experience." PLoS Biol **8**(11): e1000527.
- Truett, G. E., P. Heeger, R. L. Mynatt, A. A. Truett, J. A. Walker and M. L. Warman (2000). "Preparation of PCR-quality mouse genomic DNA with hot sodium hydroxide and tris (HotSHOT)." Biotechniques **29**(1): 52, 54.
- Tushinski, R. J. and E. R. Stanley (1983). "The regulation of macrophage protein turnover by a colony stimulating factor (CSF-1)." J Cell Physiol **116**(1): 67-75.

References

- Ueno, M., Y. Fujita, T. Tanaka, Y. Nakamura, J. Kikuta, M. Ishii and T. Yamashita (2013). "Layer V cortical neurons require microglial support for survival during postnatal development." Nature Neuroscience **16**(5): 543-551.
- VanNewkirk, M. R., M. B. Nanjan, J. J. Wang, P. Mitchell, H. R. Taylor and C. A. McCarty (2000). "The prevalence of age-related maculopathy: the visual impairment project." Ophthalmology **107**(8): 1593-1600.
- Varga, Z. M., J. Wegner and M. Westerfield (1999). "Anterior movement of ventral diencephalic precursors separates the primordial eye field in the neural plate and requires cyclops." Development **126**(24): 5533-5546.
- Varvel, N. H., S. A. Grathwohl, F. Baumann, C. Liebig, A. Bosch, B. Brawek, D. R. Thal, I. F. Charo, F. L. Heppner, A. Aguzzi, O. Garaschuk, R. M. Ransohoff and M. Jucker (2012). "Microglial repopulation model reveals a robust homeostatic process for replacing CNS myeloid cells." Proc Natl Acad Sci U S A **109**(44): 18150-18155.
- Velilla, S., J. J. García-Medina, A. García-Layana, R. Dolz-Marco, S. Pons-Vázquez, M. D. Pinazo-Durán, F. Gómez-Ulla, J. F. Arévalo, M. Díaz-Llopis and R. Gallego-Pinazo (2013). "Smoking and age-related macular degeneration: review and update." J Ophthalmol **2013**: 895147.
- von Bernhardt, R., L. Eugénin-von Bernhardt and J. Eugénin (2015). "Microglial cell dysregulation in brain aging and neurodegeneration." Front Aging Neurosci **7**: 124.
- Waisman, A., F. Ginhoux, M. Greter and J. Bruttger (2015). "Homeostasis of Microglia in the Adult Brain: Review of Novel Microglia Depletion Systems." Trends Immunol **36**(10): 625-636.
- Walter, T. J. and F. T. Crews (2017). "Microglial depletion alters the brain neuroimmune response to acute binge ethanol withdrawal." Journal of Neuroinflammation **14**(1): 86.
- Wang, Y. and H. Neumann (2010). "Alleviation of neurotoxicity by microglial human Siglec-11." J Neurosci **30**(9): 3482-3488.
- Wei, S., S. Nandi, V. Chitu, Y. G. Yeung, W. Yu, M. Huang, L. T. Williams, H. Lin and E. R. Stanley (2010). "Functional overlap but differential expression of CSF-1 and IL-34 in their CSF-1 receptor-mediated regulation of myeloid cells." J Leukoc Biol **88**(3): 495-505.
- Wendeln, A. C., K. Degenhardt, L. Kaurani, M. Gertig, T. Ulas, G. Jain, J. Wagner, L. M. Häslér, K. Wild, A. Skodras, T. Blank, O. Staszewski, M. Datta, T. P. Centeno, V. Capece, M. R. Islam, C. Kerimoglu, M. Staufenbiel, J. L. Schultze, M. Beyer, M. Prinz, M. Jucker, A. Fischer and J. J. Neher (2018). "Innate immune memory in the brain shapes neurological disease hallmarks." Nature **556**(7701): 332-338.
- Wenzel, A., C. Grimm, M. Samardzija and C. E. Remé (2005). "Molecular mechanisms of light-induced photoreceptor apoptosis and neuroprotection for retinal degeneration." Prog Retin Eye Res **24**(2): 275-306.
- Wheeler, D. L., A. Sariol, D. K. Meyerholz and S. Perlman (2018). "Microglia are required for protection against lethal coronavirus encephalitis in mice." J Clin Invest **128**(3): 931-943.
- Wiktor-Jedrzejczak, W., A. Bartocci, A. W. Ferrante, Jr., A. Ahmed-Ansari, K. W. Sell, J. W. Pollard and E. R. Stanley (1990). "Total absence of colony-stimulating factor 1 in the macrophage-deficient osteopetrotic (op/op) mouse." Proc Natl Acad Sci U S A **87**(12): 4828-4832.

References

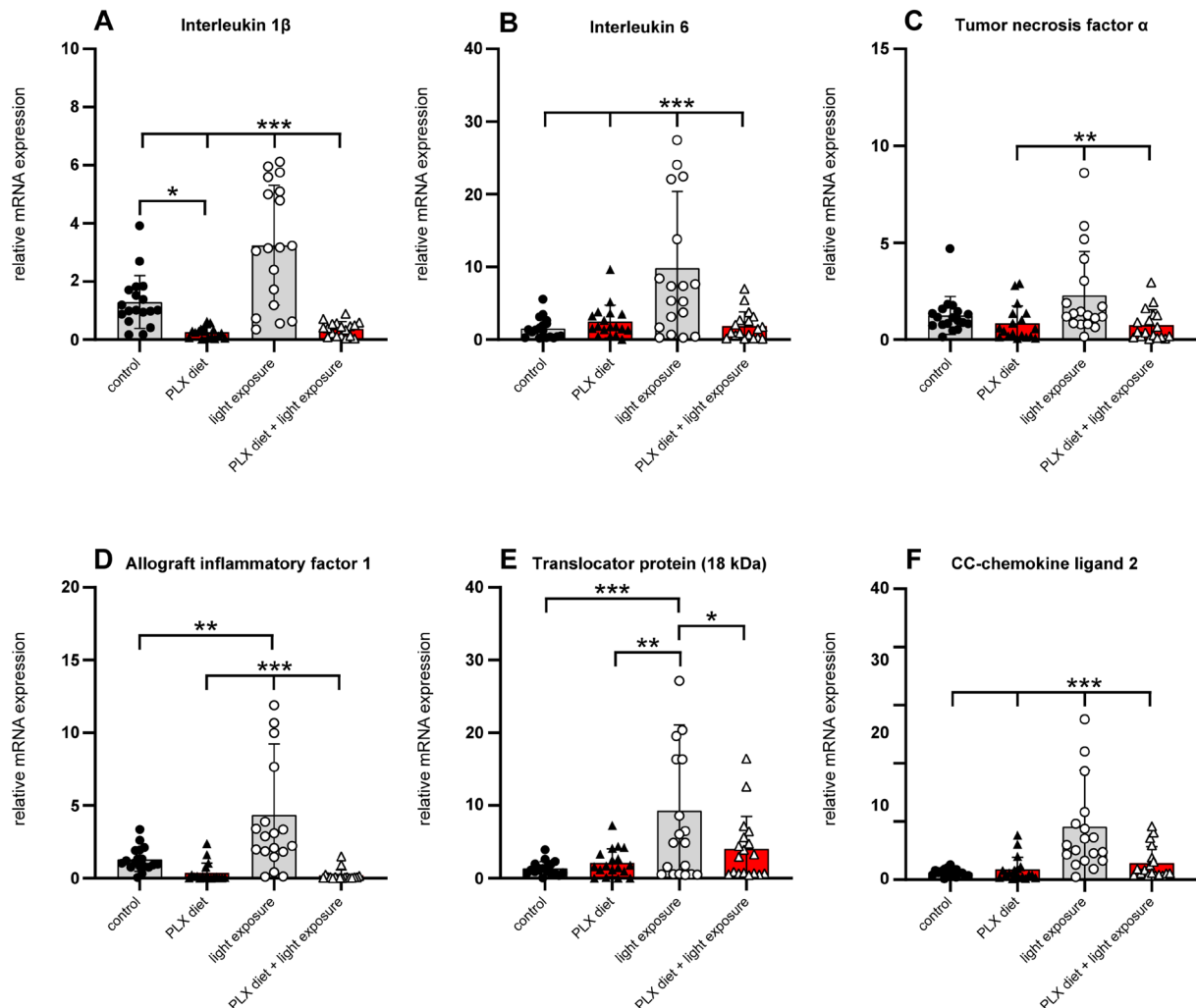
- Wiktor-Jedrzejczak, W., M. Z. Ratajczak, A. Ptasznik, K. W. Sell, A. Ahmed-Ansari and W. Ostertag (1992). "CSF-1 deficiency in the op/op mouse has differential effects on macrophage populations and differentiation stages." Exp Hematol **20**(8): 1004-1010.
- Wilhelmsen, K., K. R. Mesa, J. Lucero, F. Xu and J. Hellman (2012). "ERK5 protein promotes, whereas MEK1 protein differentially regulates, the Toll-like receptor 2 protein-dependent activation of human endothelial cells and monocytes." J Biol Chem **287**(32): 26478-26494.
- Wilhelmsen, K. and P. van der Geer (2004). "Phorbol 12-myristate 13-acetate-induced release of the colony-stimulating factor 1 receptor cytoplasmic domain into the cytosol involves two separate cleavage events." Mol Cell Biol **24**(1): 454-464.
- Wolk, K., W. D. Döcke, V. von Baehr, H. D. Volk and R. Sabat (2000). "Impaired antigen presentation by human monocytes during endotoxin tolerance." Blood **96**(1): 218-223.
- Wright, A. F., C. F. Chakarova, M. M. Abd El-Aziz and S. S. Bhattacharya (2010). "Photoreceptor degeneration: genetic and mechanistic dissection of a complex trait." Nat Rev Genet **11**(4): 273-284.
- Wright, G. J., M. J. Puklavec, A. C. Willis, R. M. Hoek, J. D. Sedgwick, M. H. Brown and A. N. Barclay (2000). "Lymphoid/neuronal cell surface OX2 glycoprotein recognizes a novel receptor on macrophages implicated in the control of their function." Immunity **13**(2): 233-242.
- Xiong, Y., D. Song, Y. Cai, W. Yu, Y. G. Yeung and E. R. Stanley (2011). "A CSF-1 receptor phosphotyrosine 559 signaling pathway regulates receptor ubiquitination and tyrosine phosphorylation." J Biol Chem **286**(2): 952-960.
- Xu, H., M. Chen, E. J. Mayer, J. V. Forrester and A. D. Dick (2007). "Turnover of resident retinal microglia in the normal adult mouse." Glia **55**(11): 1189-1198.
- Yang, L., J. H. Kim, K. D. Kovacs, J. G. Arroyo and D. F. Chen (2009). "Minocycline inhibition of photoreceptor degeneration." Arch Ophthalmol **127**(11): 1475-1480.
- Yoshida, H., S. Hayashi, T. Kunisada, M. Ogawa, S. Nishikawa, H. Okamura, T. Sudo, L. D. Shultz and S. Nishikawa (1990). "The murine mutation osteopetrosis is in the coding region of the macrophage colony stimulating factor gene." Nature **345**(6274): 442-444.
- Yu, W., J. Chen, Y. Xiong, F. J. Pixley, X. M. Dai, Y. G. Yeung and E. R. Stanley (2008). "CSF-1 receptor structure/function in MacCsf1r-/- macrophages: regulation of proliferation, differentiation, and morphology." J Leukoc Biol **84**(3): 852-863.
- Zabel, M. K., L. Zhao, Y. Zhang, S. R. Gonzalez, W. Ma, X. Wang, R. N. Fariss and W. T. Wong (2016). "Microglial phagocytosis and activation underlying photoreceptor degeneration is regulated by CX3CL1-CX3CR1 signaling in a mouse model of retinitis pigmentosa." Glia **64**(9): 1479-1491.
- Zhan, L., G. Krabbe, F. Du, I. Jones, M. C. Reichert, M. Telpoukhovskaia, L. Kodama, C. Wang, S. H. Cho, F. Sayed, Y. Li, D. Le, Y. Zhou, Y. Shen, B. West and L. Gan (2019). "Proximal recolonization by self-renewing microglia re-establishes microglial homeostasis in the adult mouse brain." PLoS Biol **17**(2): e3000134.
- Zhao, L., W. Ma, R. N. Fariss and W. T. Wong (2011). "Minocycline attenuates photoreceptor degeneration in a mouse model of subretinal hemorrhage microglial: inhibition as a potential therapeutic strategy." Am J Pathol **179**(3): 1265-1277.

References

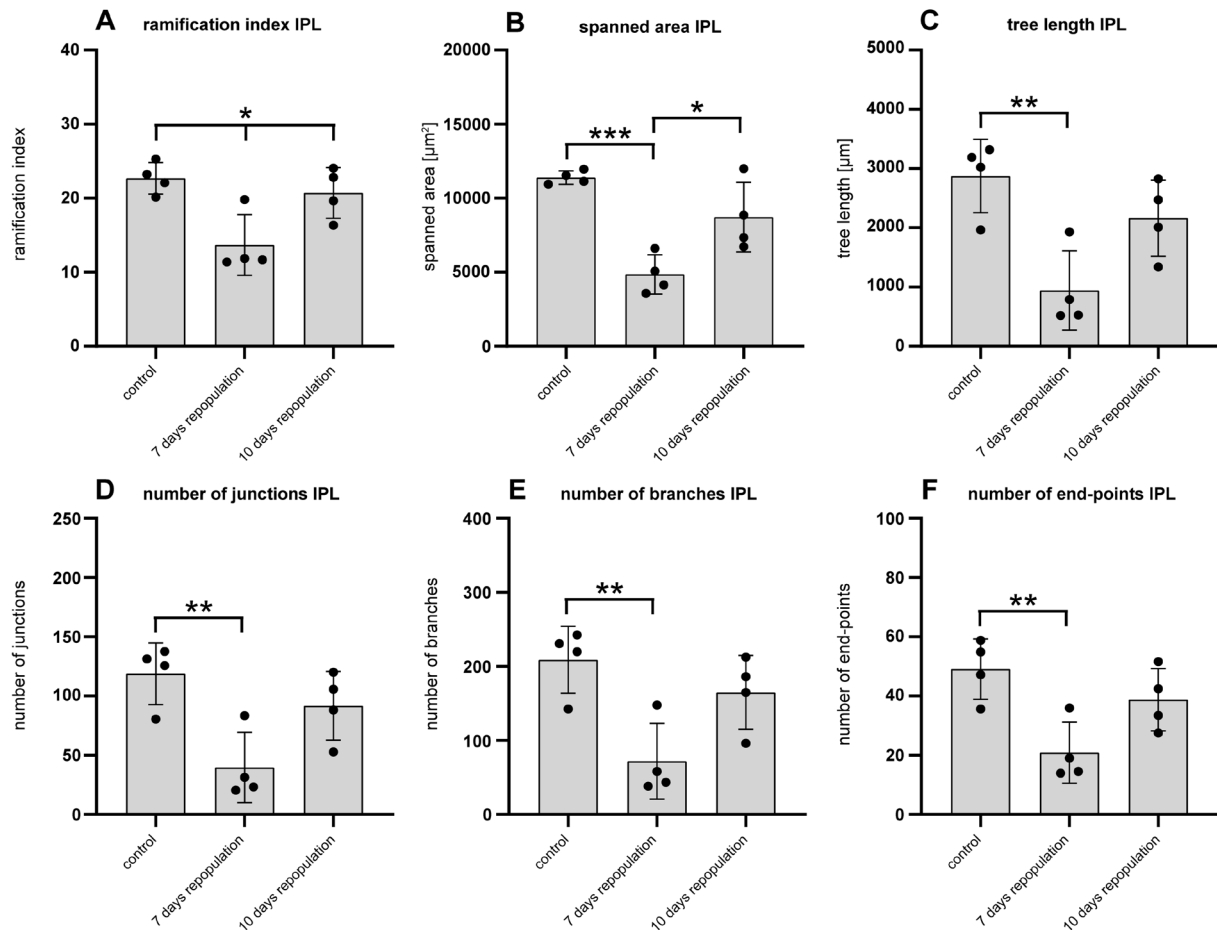
Zhao, L., M. K. Zabel, X. Wang, W. Ma, P. Shah, R. N. Fariss, H. Qian, C. N. Parkhurst, W. B. Gan and W. T. Wong (2015). "Microglial phagocytosis of living photoreceptors contributes to inherited retinal degeneration." EMBO Mol Med **7**(9): 1179-1197.

Zhou, T., Y. Li, X. Li, F. Zeng, Y. Rao, Y. He, Y. Wang, M. Liu, D. Li, Z. Xu, X. Zhou, S. Du, F. Niu, J. Peng, X. Mei, S.-J. Ji, Y. Shu, W. Lu, F. Guo, T. Wu, T.-F. Yuan, Y. Mao and B. Peng (2022). "Microglial debris is cleared by astrocytes via C4b-facilitated phagocytosis and degraded via RUBICON-dependent noncanonical autophagy in mice." Nature Communications **13**(1): 6233.

7. Attachments

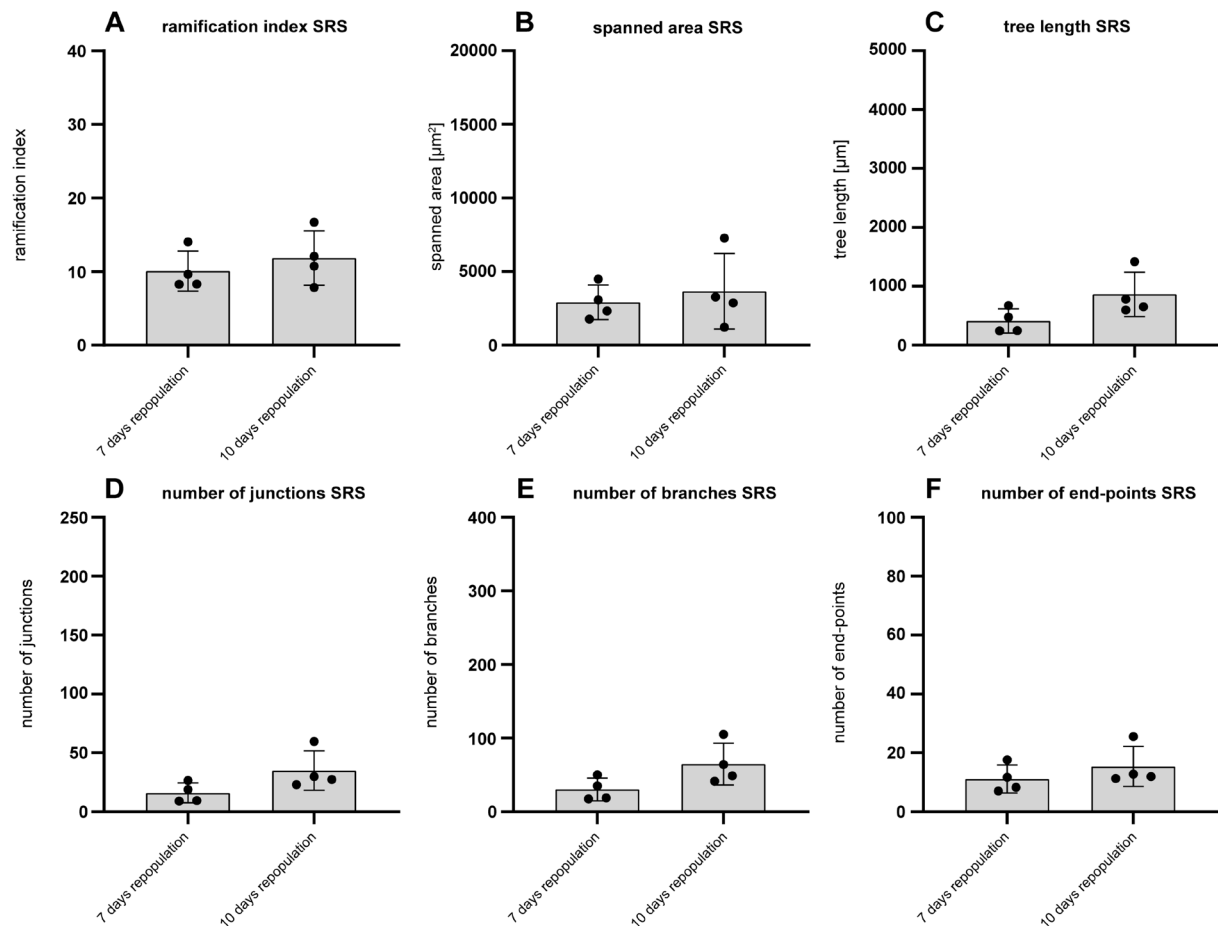


Supplementary figure 1 Pro-inflammatory marker expression in the context of preventive microglia depletion in retinal degeneration. *CX3CR-1^{GFP}* reporter mice received PLX3397 diet one week before one hour 15,000 lux light exposure and analysis was carried out 4 days after. Pro-inflammatory marker expression in whole RPE transcripts were determined by using qRT-PCR. *Il-1 β* expression was upregulated in light exposed RPE's, whereas this upregulation was absent with PLX3397 treatment. Here, it could be reduced below the level of the control (A). The same expression pattern could also be shown for *Aif1* and *Tnfa* (C; D). *Il-6* also showed significantly increased expression when retinal degeneration has been induced. The upregulation could be reduced after PLX3397 treatment and was comparable to the control (B). The same expression pattern could be observed for *Tspo* and *Ccl2* (E; F) (* $p < 0.05$, ** $p < 0.01$, *** $p \leq 0.001$) (n = 18).

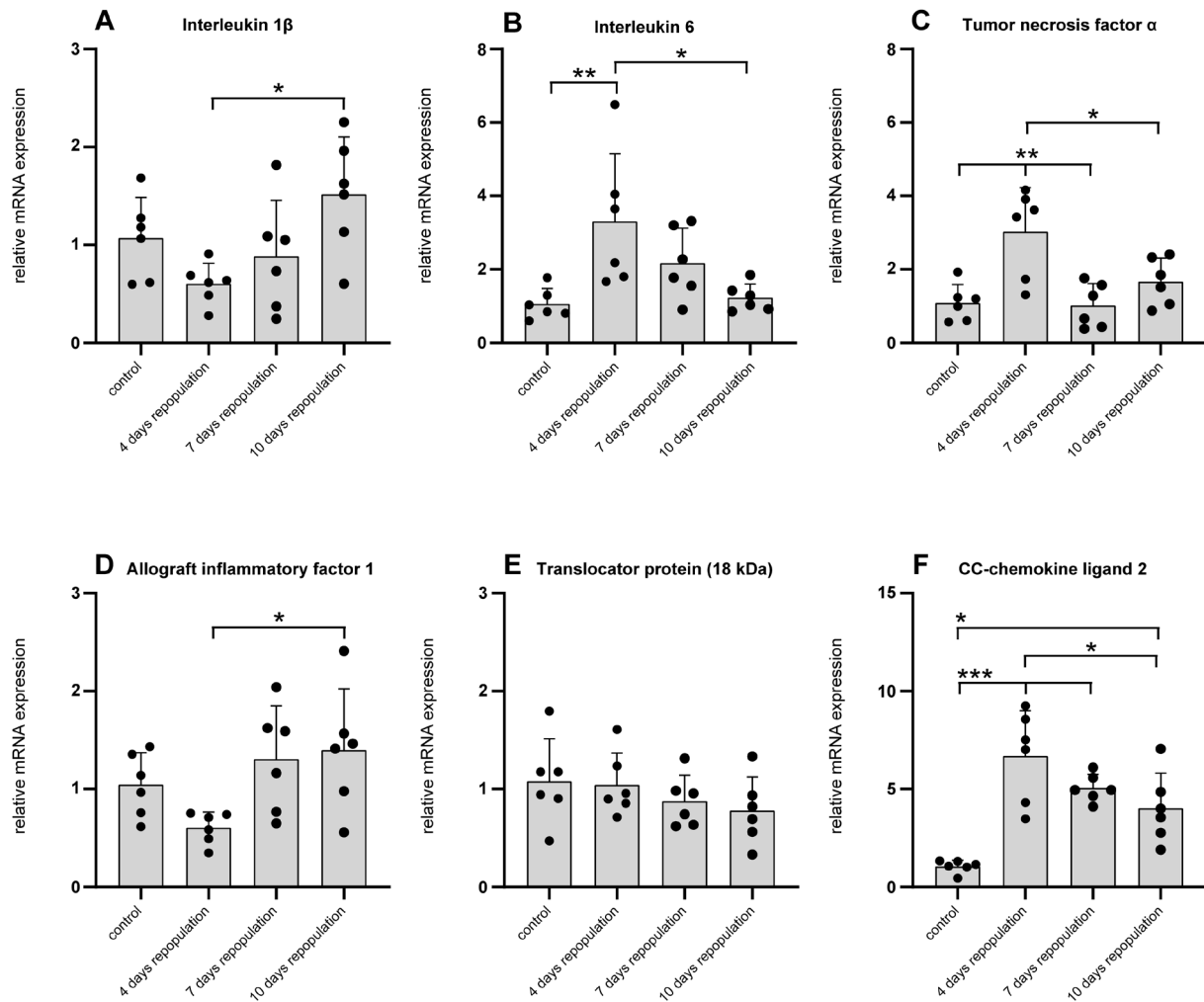


Supplementary figure 2 Investigation of microglia repopulation in retinal flat-mounts. *CX3CR-1^{GFP/-}* reporter mice received PLX3397 diet for one week. Analysis was carried out in flat mounts 4, 7 and 10 days after cessation of PLX3397 diet. After 4 days, the repopulation was still in progress and the microglia were not yet back in full numbers. Here it was difficult to determine the exact localization and perform a subsequent analysis. Repopulation of microglia was completed 7 and 10 after PLX3397 diet, respectively. Nevertheless, minor morphological differences were observed compared to the control, and they recovered at day 10 after PLX3397 cessation (A – F) (* $p < 0.05$, ** $p < 0.01$, *** $p \leq 0.001$) ($n = 4$).

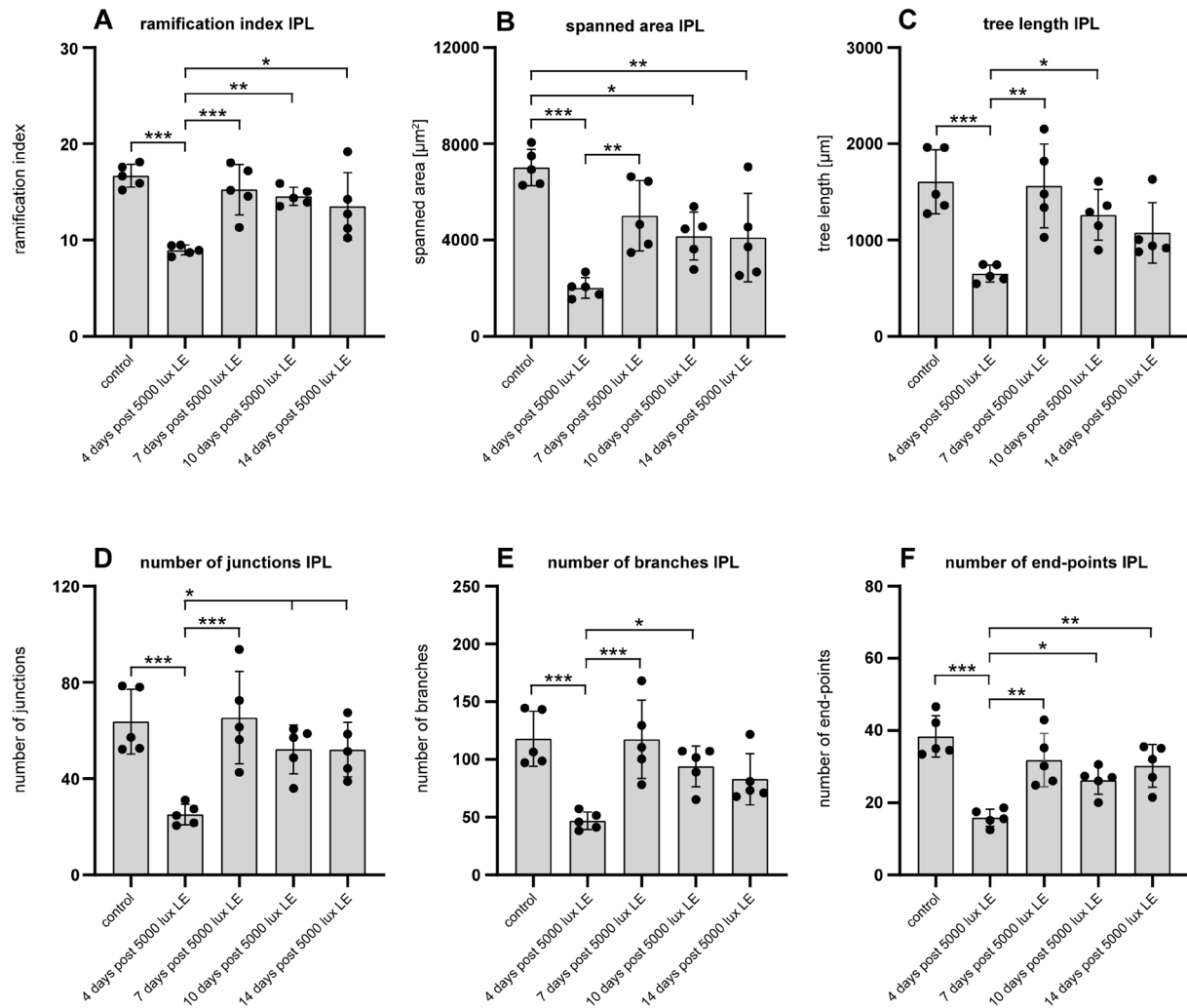
Attachments



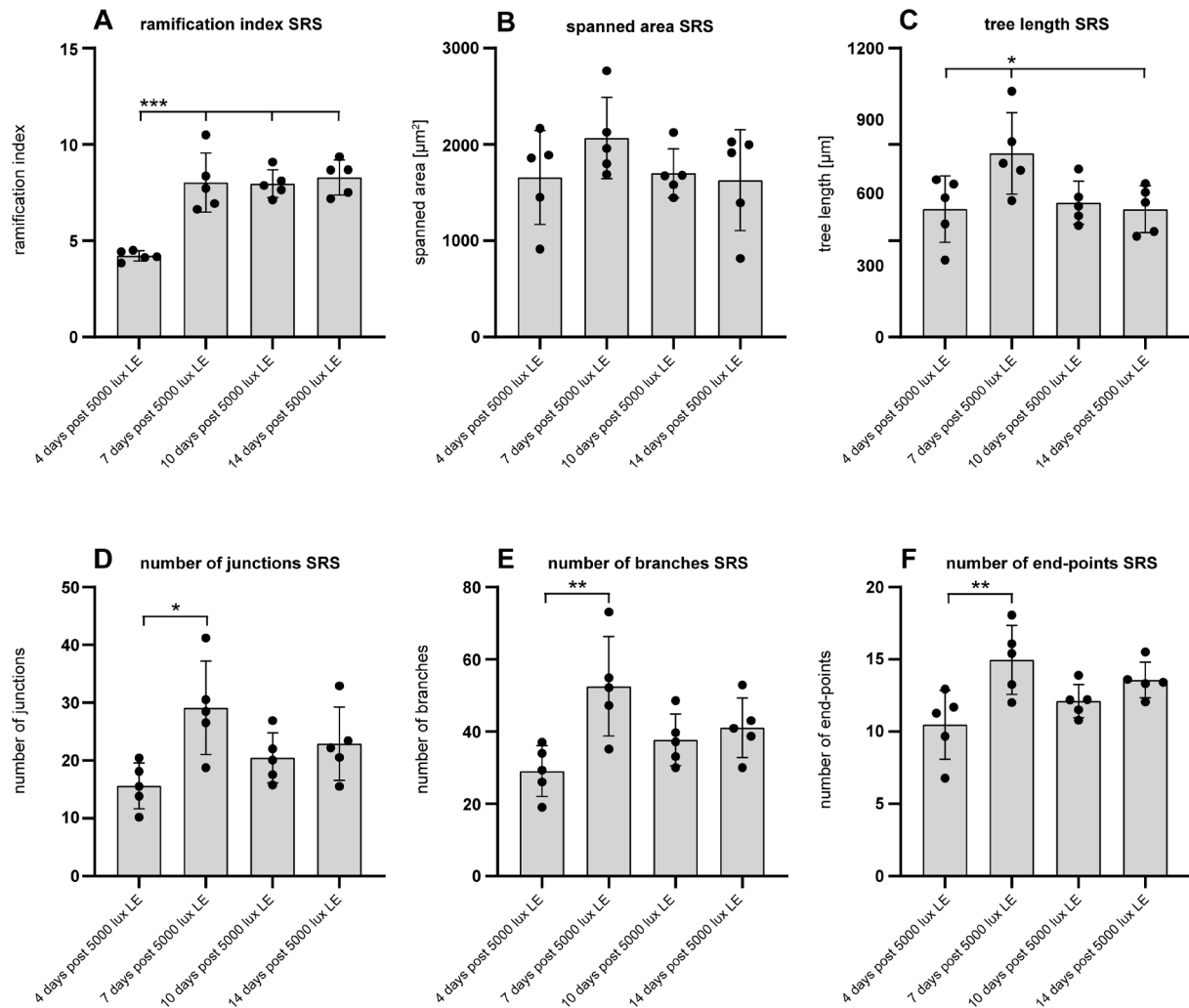
Supplementary figure 3 Investigation of microglia repopulation in retinal flat-mounts. *CX3CR-1^{GFP/+}* reporter mice received PLX3397 diet for one week. Analysis was carried out in flat mounts 4, 7 and 10 days after cessation of PLX3397 diet. After 4 days, the repopulation was still in progress and the microglia were not yet back in full numbers. Here it was difficult to determine the exact localization and perform a subsequent analysis. Repopulation of microglia was completed 7 and 10 after PLX3397 diet, respectively. Nevertheless, minor morphological differences were observed compared to the control, and they recovered at day 10 after PLX3397 cessation (A – F) (* $p < 0.05$, ** $p < 0.01$, *** $p \leq 0.001$) ($n = 4$).



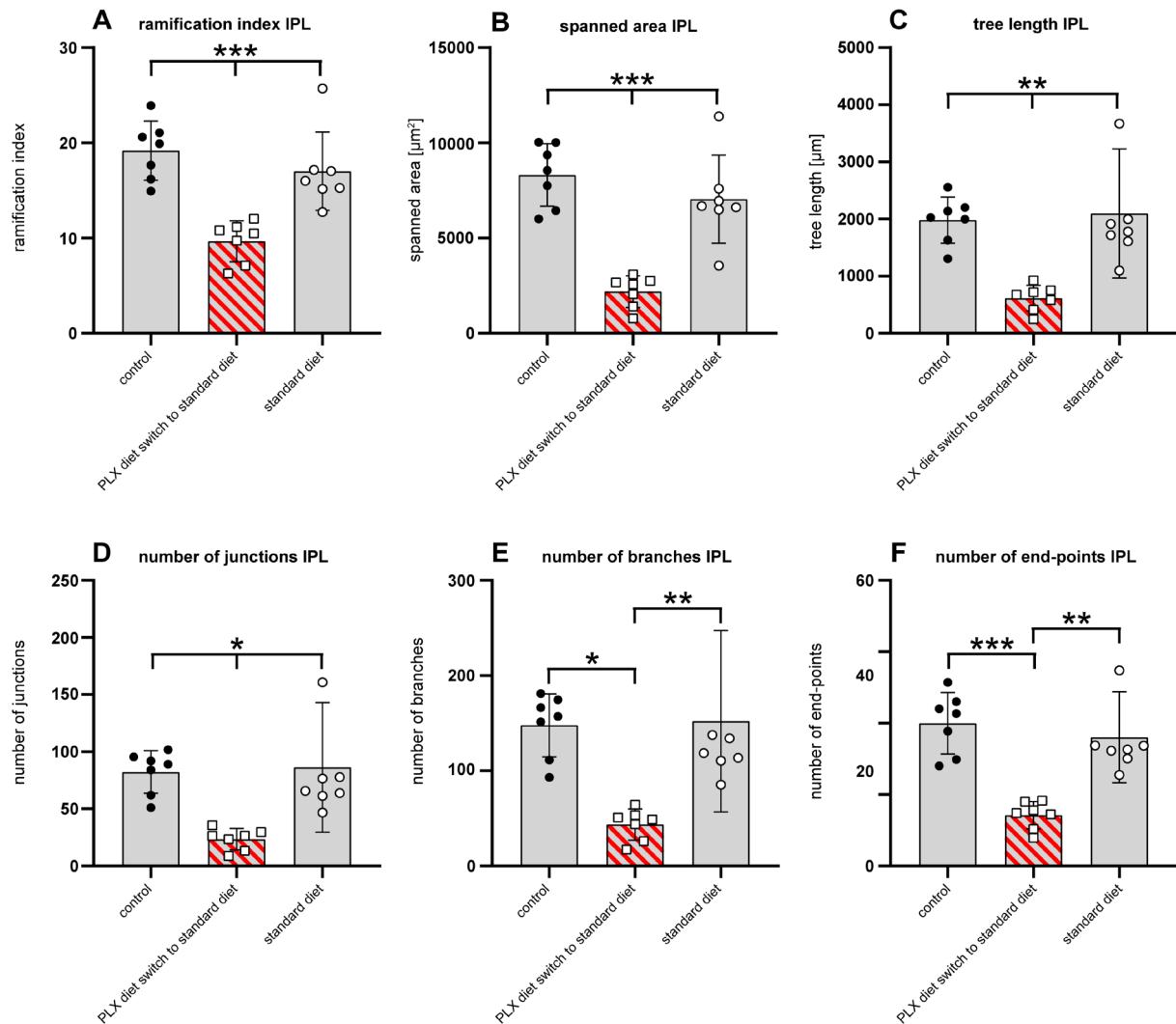
Supplementary figure 4 Investigation of pro- and anti-inflammatory marker expression in repopulated microglia. *CX3CR1^{GFP/-}* reporter mice received PLX3397 diet for one week. qRT-PCR of whole RPE transcripts was performed 4, 7 and 10 days after cessation of PLX3397 diet. mRNA expression of the constitutive microglia marker *Aif-1* decreased after 4 days and completely restored after 7 of repopulation (D). Expression of *Il-1 β* was significantly reduced at day 4 and at day 7 and 10 again comparable with the control (A). *Il-6* expression was elevated in repopulated microglia at days 4 and 7 and did recover to control levels on day 10 (B). The expression of *Tnfa* in repopulated microglia, was increased at day 4 (C). The expression of TSPO (E) did not show any changes and *Ccl2* was always upregulated (F) (* $p < 0.05$, ** $p < 0.01$, *** $p \leq 0.001$) ($n = 6$).



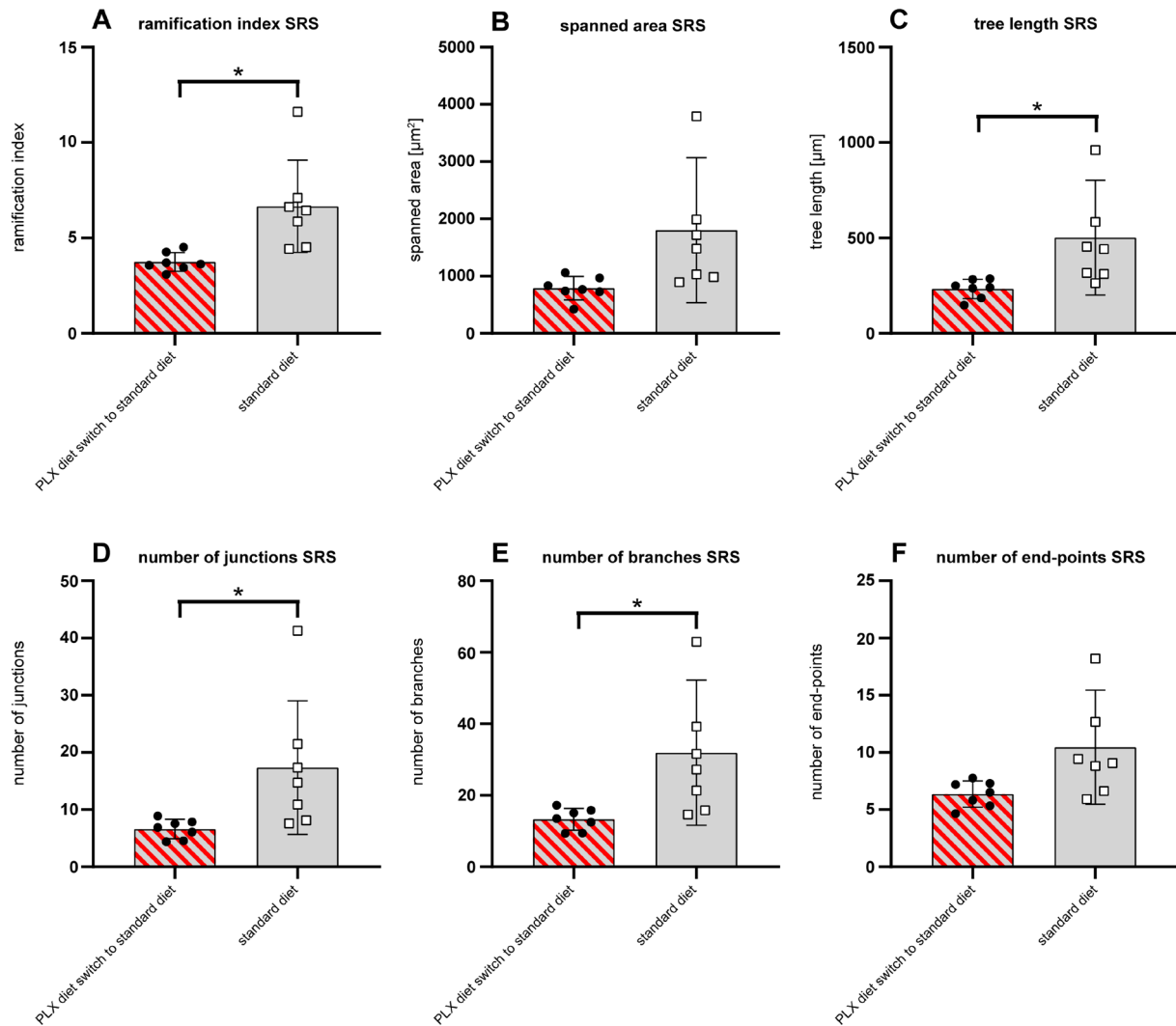
Supplementary figure 5 Investigation of microglia morphology after low intensity light exposure in retinal flat mounts. *CX3CR-1^{GFP/+}* reporter were exposed to light with an intensity of 5,000 lux for one hour. Retinal flat mount images were taken at days 4, 7, 10 and 14 after light exposure. It was shown that immediately after induction of retinal degeneration, the reactivated amoeboid microglia gradually returned to their initial state up to 14 days later. All analyzed morphological parameters showed the same tendency. All parameters were significantly reduced at day 4 and approached to the level of the control at day 7 and 10 until they were comparable to the control at day 14 (A – F) (* $p < 0.05$, ** $p < 0.01$, *** $p \leq 0.001$) ($n = 5$).



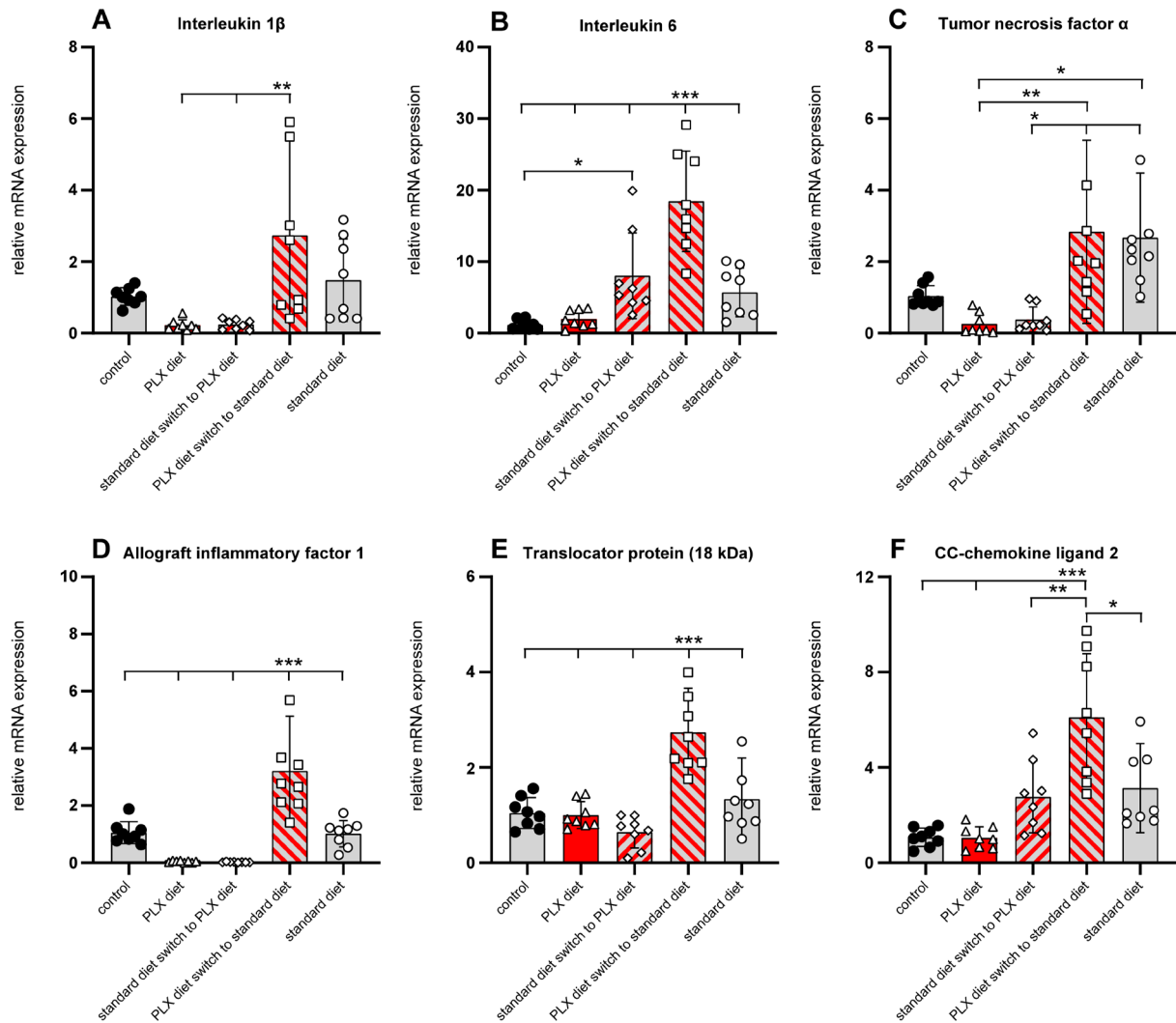
Supplementary figure 6 Investigation of microglia morphology after low intensity light exposure in retinal flat mounts. *CX3CR-1^{GFP/+}* reporter were exposed to light with an intensity of 5,000 lux for one hour. Retinal flat mount images were taken at days 4, 7, 10 and 14 after light exposure. It was shown that immediately after induction of retinal degeneration, the reactivated amoeboid microglia gradually returned to their initial state up to 14 days later. In the control, no microglia could be detected in the SRS. All parameters were slightly reduced at day 4 and approached to the level highest level at day 7 and decreased again until day 14 (A – F). However, the values of the morphological parameters at day 14 were still higher compared to day 4. In the SRS, an accumulation of microglia was detected on day 4. This also reduced stepwise until almost the initial state was reached. However, a few microglia still remained in the SRS on day 14 (* $p < 0.05$, ** $p < 0.01$, *** $p \leq 0.001$) ($n = 5$).



Supplementary figure 7 Investigation of microglia morphology in a curative setting of early, late, and no microglia depletion on retinal degeneration. *CX3CR1^{GFP/+}* reporter mice received PLX3397 diet as indicated and 5,000 lux light exposure for one hour. Retinal flat mount images were taken 14 days after light exposure. Mice that received constant and late PLX3397 diet no microglia could be detected in the examined layers. Repopulated microglia were reactivated and exhibited an amoeboid morphology. Constantly present microglia were activated and showed a ramified shape. All measured morphological parameters decreased significantly in the condition of early microglia depletion (A – F). Morphological parameters in constantly present microglia were comparable to the control condition (*p < 0.05, **p < 0.01, ***p ≤ 0.001) (n = 7).



Supplementary figure 8 Investigation of microglia morphology in a curative setting of early, late, and no microglia depletion on retinal degeneration. *CX3CR-1^{GFP/-}* reporter mice received PLX3397 diet as indicated and 5,000 lux light exposure for one hour. Retinal flat mount images were taken 14 days after light exposure. Mice that received constant and late PLX3397 diet no microglia could be detected in the examined layers. Repopulated microglia were reactivated and exhibited an amoeboid morphology. Constantly present microglia were activated and showed a ramified shape. All measured morphological parameters decreased significantly in the condition of early microglia depletion (A – F). Morphological parameters in constantly present microglia recovered at day 14 (* $p < 0.05$, ** $p < 0.01$, *** $p \leq 0.001$) ($n = 7$).



Supplementary figure 9 Investigation of pro- and anti-inflammatory markers in a curative setting of early, late, and no microglia depletion on retinal degeneration. *CX3CR1^{GFP}* reporter mice received PLX3397 diet as indicated and 5,000 lux light exposure for one hour. Pro- and anti-inflammatory marker expression in whole RPE transcripts were determined by using qRT-PCR 14 days after light exposure. The expression of pro-inflammatory markers was significantly increased in newly repopulated microglia, which was associated with early depletion (A – F). Constantly present microglia showed a reduced expression but in some cases it was still slightly elevated compared to the control (B; C; E; F) (*p < 0.05, **p < 0.01, ***p ≤ 0.001) (n = 8).

8. Acknowledgements

My greatest appreciation and respect go to my supervisor, Prof. Dr. Thomas Langmann, for his unwavering support throughout my studies, vast knowledge, enlightening conversations, and guidance in research and writing. My thanks also go to Prof. Dr. Elena Rugarli and Prof. Dr. Christian Pallasch for taking over the position as tutors and examiners. The Pro-Retina foundation deserves a special mention for providing financial support that allowed for the completion of this doctoral thesis.

I also want to convey my gratitude to Dr. Anne Wolf for her encouraging advice, lively discussions, constructive feedback of my work, and entertaining yet educational annotations on my studies.

I wish to express my heartfelt thankfulness to Mandy Hector for being the best office fellow I could imagine, for assisting me with some of my computer's obstinate issues, and for always brightening my spirits when I was in one of my "phases".

Moreover, I want to appreciate technician team member Eva Scheiffert for helping with experimental setup, rigging, and support when a device did not function as it should. I would also like to thank our secretary Anja Volkmann for her active support, without whom I would never have found my way through the jungle of bureaucracy.

My humblest, tis my desire to express my admiration and gratitude towards Urbi Kinuthia, who through his sagacious discourse, hath deftly broadened not only my scientific knowledge but also the horizons of my mind.

Special thanks goes out to all of my fellow lab members, Dr. Sarva Kehani, Dr. Verena Behnke, Dr. Mona Tabel, Anna Gröger, Carolin Peters, Julia Hofmann, and Justus Dick, for their insightful comments of my scientific performance and for offering me a great time in the lab.

Finally yet importantly, I would like to thank my family and friends, without whom I would never have gotten through this time so well. You have always had the appropriate words to pick me back up morally when I have lost my motivation. In difficult times, you always managed to give me a little change to get through them. Special thanks to my parents and grandparents to whom I dedicate this work. I love you all!

9. Eidesstattliche Erklärung

Ich versichere, dass ich die von mir vorgelegte Dissertation selbstständig angefertigt, die benutzten Quellen und Hilfsmittel vollständig angegeben und die Stellen der Arbeit - einschließlich Tabellen, Karten und Abbildungen -, die anderen Werken im Wortlaut oder dem Sinn nach entnommen sind, in jedem Einzelfall als Entlehnung kenntlich gemacht habe; dass diese Dissertation noch keiner anderen Fakultät oder Universität zur Prüfung vorgelegen hat; dass sie - abgesehen von unten angegebenen Teilpublikationen - noch nicht veröffentlicht worden ist sowie, dass ich eine solche Veröffentlichung vor Abschluss des Promotionsverfahrens nicht vornehmen werde. Die Bestimmungen dieser Promotionsordnung sind mir bekannt. Die von mir vorgelegte Dissertation ist von Prof. Dr. Thomas Langmann betreut worden.

Ich versichere, dass ich alle Angaben wahrheitsgemäß nach bestem Wissen und Gewissen gemacht habe und verpflichte mich, jedmögliche, die obigen Angaben betreffenden Veränderungen, dem Promotionsausschuss unverzüglich mitzuteilen.

.....

Datum

.....

Unterschrift

10. Curriculum Vitae

Nils Laudenberg
Hölderlinstraße 60
50858 Köln
nils.laudenberg@gmx.net

Educational history

- | | |
|-------------|---|
| 2019 – 2023 | PhD Student of the IPMM
Colony stimulating factor 1 receptor (CSF1R) blockade of microglia reactivity in the light-damage model of retinal degeneration. Lab of Prof. Dr. Thomas Langmann, University of Cologne. |
| 2016 – 2019 | Master of Science in Neuroscience
Co-modulation effect of two antagonistic neuromodulators on the activity of a chain of coupled oscillators. Lab of PD Dr. Carmen Smarandache-Wellmann, University of Cologne. |
| 2012 – 2015 | Bachelor of Science in Biology
Expression pattern and RNAi knock out of the muscle excess gene 3 (MEX3) in nematodes. Lab of PD Dr. Michael Kroiher, University of Cologne. |
| 2011 | High-School Diploma (Abitur)
Johann-Gottfried Herder Gymnasium, Cologne |

Work experience

Internship at the CECAD center Cologne: I investigated the relevance of the Protein Sec22b and its influence and responsibility for the vesicle traffic from the Golgi apparatus to the endoplasmatic reticulum.

Internship at the Max-Planck Institute for Plant Breeding Research Cologne: I performed research work at plant-microbe interactions; including analysis of the importance of bacterial presence for plant development. I also investigated how far bacterial presence prevents the plant from infection of a plant pathogen called *Fusarium oxysporum*.

Internship at the Sleep-Laboratory Severins Kloster Cologne: Here I have taken over the complete patient care overnight. This includes attaching the sensors to the patients and monitoring them overnight. As these night shifts were carried out alone, I had to make quick, focused and safe judgments for the patients in the event of complications in order not to jeopardize the course of the sleep monitoring. Every abnormality had to be documented and the evaluation of the data received was evaluated by me the next day and handed over to the senior physician.

Scientific conferences

13th Göttingen Meeting of the German Neuroscience Society, Göttingen, Germany (2019). Poster presentation.

1st Bonn-Cologne Neuroscience Symposium, Bonn, Germany (2019). Poster presentation.

15th Pro Retina Research-Colloquium, Online Platform Wonder, (2021). Poster Presentation.

16th Pro Retina Research-Colloquium, Potsdam, Germany (2022). Poster Presentation.

IPMM Days, Cologne, Germany (2022). Oral presentation.

Swiss Eye Research Meeting (SERM), Neuchatel, Switzerland (2023). Oral presentation.

Supervising and teaching

I took over a part of the teaching in the Neuroscience and Biological Sciences program by supervising the modules Retinal Immunology and Neuronal Networks: From experiment to Presentation. I also have experience in tutoring students, as I was allowed to train two individual students during my time as a student. This included planning and supervising their experiments as well as reviewing and grading their work.

Supervisor of the MD student Melis Cansu Cömert for two years.

Supervisor of the internship student Aurélie Fail for two month.

Research related career development and workshops

In order to improve my skills in data analysis and presentation, as well as to enhance my general skills that benefit my scientific work, I participated in several workshops. I participated in an **Adobe Illustrator workshop** to improve my skills in creating scientific illustrations and figures, which go beyond the basic level. Since I work with living mice, it is important to handle the animals carefully and with respect, therefore I participated in the workshop **ethics and theory of Science**. In order to get exact knowledge regarding the statistical analysis of my data and beyond, I participated in a **statistic workshop** that covered about all aspects of data analysis. I also attended a course on **scientific writing** to hone my skills in this area.

Languages

German: native speaker

English: fluent

References

Prof. Dr. Thomas Langmann, University of Cologne, Experimental Immunology of the Eye,
Joseph-Stelzmann Straße 9, 50931 Cologne, (0221) 478-7324,
thomas.langmann@uk-koeln.de

Other references available upon request.